frontiers | Research Topics

Molecular mechanisms of neuropsychiatric diseases

Edited by
Nashat Abumaria, Melanie Grubisha and Mónica Isa Moreira-Rodrigues

Published in
Frontiers in Molecular Neuroscience

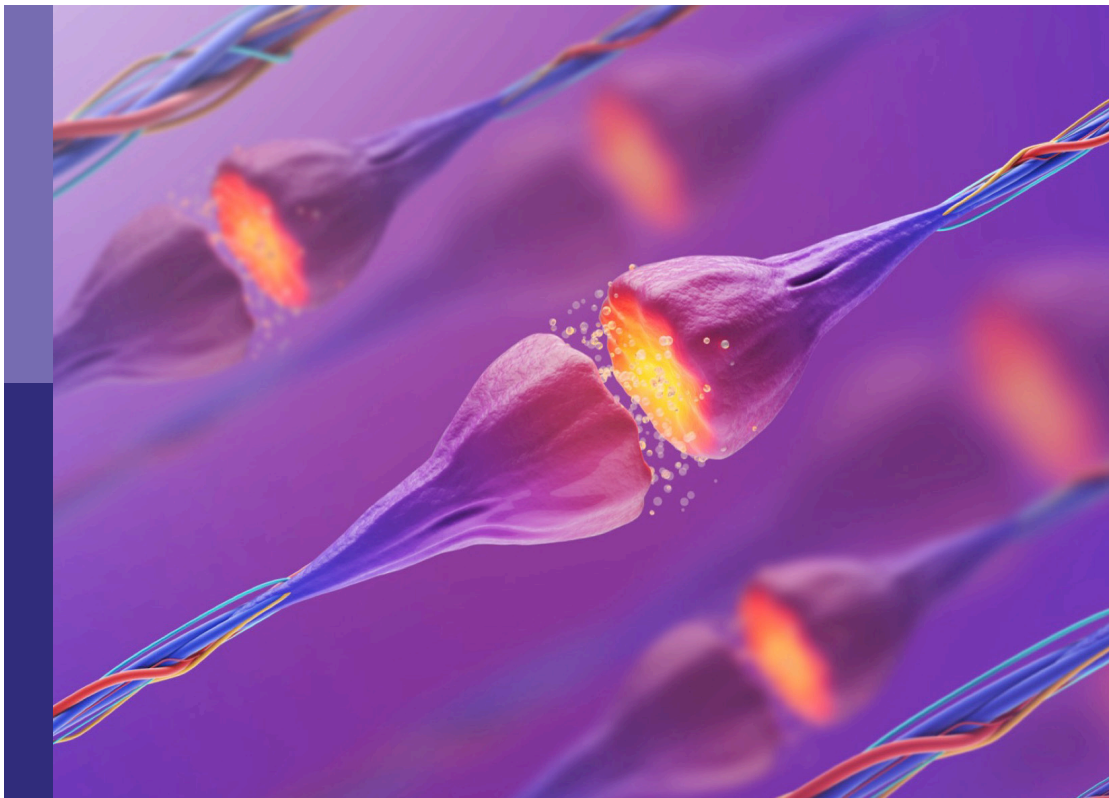

ISSN 1664-8714
ISBN 978-2-83251-118-3
DOI 10.3389/978-2-83251-118-3

About Frontiers

Frontiers is more than just an open access publisher of scholarly articles: it is a pioneering approach to the world of academia, radically improving the way scholarly research is managed. The grand vision of Frontiers is a world where all people have an equal opportunity to seek, share and generate knowledge. Frontiers provides immediate and permanent online open access to all its publications, but this alone is not enough to realize our grand goals.

Frontiers journal series

The Frontiers journal series is a multi-tier and interdisciplinary set of open-access, online journals, promising a paradigm shift from the current review, selection and dissemination processes in academic publishing. All Frontiers journals are driven by researchers for researchers; therefore, they constitute a service to the scholarly community. At the same time, the *Frontiers journal series* operates on a revolutionary invention, the tiered publishing system, initially addressing specific communities of scholars, and gradually climbing up to broader public understanding, thus serving the interests of the lay society, too.

Dedication to quality

Each Frontiers article is a landmark of the highest quality, thanks to genuinely collaborative interactions between authors and review editors, who include some of the world's best academicians. Research must be certified by peers before entering a stream of knowledge that may eventually reach the public - and shape society; therefore, Frontiers only applies the most rigorous and unbiased reviews. Frontiers revolutionizes research publishing by freely delivering the most outstanding research, evaluated with no bias from both the academic and social point of view. By applying the most advanced information technologies, Frontiers is catapulting scholarly publishing into a new generation.

What are Frontiers Research Topics?

Frontiers Research Topics are very popular trademarks of the *Frontiers journals series*: they are collections of at least ten articles, all centered on a particular subject. With their unique mix of varied contributions from Original Research to Review Articles, Frontiers Research Topics unify the most influential researchers, the latest key findings and historical advances in a hot research area.

Find out more on how to host your own Frontiers Research Topic or contribute to one as an author by contacting the Frontiers editorial office: frontiersin.org/about/contact

Molecular mechanisms of neuropsychiatric diseases

Topic editors

Nashat Abumaria — Fudan University, China

Melanie Grubisha — University of Pittsburgh, United States

Mónica Isa Moreira-Rodrigues — Universidade do Porto, Portugal

Citation

Abumaria, N., Grubisha, M., Moreira-Rodrigues, M. I., eds. (2023). *Molecular mechanisms of neuropsychiatric diseases*. Lausanne: Frontiers Media SA.

doi: 10.3389/978-2-83251-118-3

Table of contents

frontiers | Frontiers in Molecular Neuroscience

TYPE Editorial
PUBLISHED 08 December 2022
DOI 10.3389/fnmol.2022.1102296

OPEN ACCESS

EDITED AND REVIEWED BY
Detlev Boison,
Rutgers, The State University of New Jersey, United States

*CORRESPONDENCE
Mónica Moreira-Rodrigues
mirodrigues@icbas.up.pt
Melanie J. Grubisha
grubisham@upmc.edu

†These authors have contributed equally to this work and share senior authorship

SPECIALTY SECTION
This article was submitted to Brain Disease Mechanisms, a section of the journal Frontiers in Molecular Neuroscience

RECEIVED 18 November 2022
ACCEPTED 23 November 2022
PUBLISHED 08 December 2022

CITATION
Moreira-Rodrigues M and Grubisha MJ (2022) Editorial: Molecular mechanisms of neuropsychiatric diseases.
Front. Mol. Neurosci. 15:1102296.
doi: 10.3389/fnmol.2022.1102296

Editorial: Molecular mechanisms of neuropsychiatric diseases

Mónica Moreira-Rodrigues[1]*† and Melanie J. Grubisha[2]*†

[1]Laboratory of General Physiology and Center for Drug Discovery and Innovative Medicines (MedInUP), Department of Immuno-physiology and Pharmacology, School of Medicine and Biomedical Sciences (ICBAS), University of Porto (UP), Porto, Portugal, [2]Department of Psychiatry, University of Pittsburgh, Pittsburgh, PA, United States

KEYWORDS

neuropsychiatric disorders, molecular mechanisms, depression, schizophrenia, post-traumatic stress disorder, intellectual development disorder, catatonia

Editorial on the Research Topic
Molecular mechanisms of neuropsychiatric diseases

Neuropsychiatric disorders, such as depression, schizophrenia, bipolar disorder, obsessive compulsive disorder, post-traumatic stress disorder (PTSD), autism spectrum disorder and others are estimated to impair millions of individuals globally. Despite the high global prevalence, much remains unknown about the underlying molecular mechanisms that lead to these and other neuropsychiatric diseases. The likelihood of developing these disorders may depend on a variety of genetic, developmental and environmental factors. The molecular alterations produced by these factors may contribute to both disease onset or the persistence of a specific pathology. Identifying the molecular mechanisms of a disease will increase our understanding of the underlying pathophysiology and ultimately lead to the rational design of targeted treatments. The goal of this Research Topic was to explore fundamental molecular mechanisms underlying neuropsychiatric diseases, and how these mechanisms may be exploited for potential therapeutic benefit.

A longstanding challenge in the elucidation of molecular mechanisms underlying neuropsychiatric disease has been the initial paucity of anatomical and/or molecular findings. Distinguished American neurologist Dr. Fred Plum once referred to schizophrenia as "the graveyard of neuropathologists." This Topic features multiple papers that serve to tackle this and other challenges and link clinical entities to anatomical and molecular abnormalities.

Ren et al. showed that schizophrenia patients with auditory verbal hallucinations exhibit a decrease in cortical thickness in orbitofrontal cortices, which was negatively correlated with severity of these symptoms. Seeking to discover molecular aberrations in a depression-relevant model, Chen et al. employed a large-scale-omics approach to achieve metabolic profiling in the olfactory bulb of a chronic mild stress mouse model. They discovered an abnormal metabolism of the tryptophan pathway in the olfactory bulb, which may mediate the occurrence of a depression-like phenotype in a chronic mild stress model. On the other way, Martinho, Oliveira et al. sought to identify specific molecular abnormalities underlying contextual fear memory relevant to

PTSD, and that modulating this system can reverse fear-related phenotypic changes. In Martinho, Oliveira et al., they found that epinephrine may be involved in the persistence of traumatic memories in PTSD, possibly through enhancement of the expression of *Nr4a2* and *Nr4a3* genes in the hippocampus. The persistence of contextual traumatic memories may contribute to anxiety-like behavior and resistance of traumatic memory extinction in a PTSD rodent model. In a follow-up study, Martinho, Correia et al. showed that nepicastat, a highly potent central and peripheral DBH (dopamine beta-hydroxylase) inhibitor that is effective in modulating the sympathetic nervous system, decreases the persistence of traumatic memories and anxiety-like behavior in this model, which may have direct translational potential in the treatment of PTSD.

Linking anatomical and phenotypic findings to genetic underpinnings has proved to be another challenge, yet one the field has fearlessly embraced. Although the high complexity of neuronal and cortical structure is regulated by a myriad of genes, Parnell et al. devised a clever strategy to reduce the genetic complexity to a single mutation in a relevant gene to better understand its specific contribution to both normal and abnormal neuronal architecture. Using the E1577K point mutation in Kalirin-7, Parnell et al. showed that in contrast to wild type Kalirin-7, the E1577K mutant failed to drive dendritic arborization, spine density, and NMDAR activity within spines, alongside a robust reduction in Kalirin-7 RAC1 guanine exchange factor activity. Similarly, Che et al. identified a splicing variant and a novel frameshift variant of the BCL11B gene, thus suggesting that an aberrant translation of this gene may lead to an intellectual development disorder. Fujii et al. used a FRET-based approach to understand the impact of CAMK2A (Ca^{2+}/calmodulin dependent protein kinase II alpha) gene mutation in patients' phenotype. Han et al. discovered a novel missense single nucleotide polymorphism, rs61753730 (Q152E), located in the fourth exon of the frizzled class receptor 6 gene (FZD6), which they demonstrate impacts depressive-like symptoms of Fzd6-knockin mice. These findings contribute to our understanding of the genetic underpinnings of both normal and abnormal neurodevelopment, thus paving the way for future targeted therapeutics.

Finally, it is imperative that we continue to integrate the field's existing cellular and molecular knowledge with clinical observations. In this Topic, Ariza-Salamanca et al. highlighted molecular and cellular mechanisms leading to catatonia, which had previously been described as a purely clinical syndrome. In a similar vein, Grubisha et al. reviewed post-translational modifications in human post-mortem brain tissues of neuropsychiatric diseases. Translational momentum is fueled by this bench-to-bedside viewpoint, with one constantly informing and advancing the other.

In conclusion, through multiple innovative approaches, this Research Topic advanced our knowledge in understanding molecular mechanisms underlying several neuropsychiatric disorders. The papers herein integrate anatomical, cellular, molecular, and genetic findings in work that will ultimately advance the field toward elucidation of novel therapeutic targets and inform future rational drug design.

Author contributions

All authors listed have made a substantial, direct, and intellectual contribution to the work and approved it for publication.

Funding

MM-R scientific work was supported by Foundation for Science and Technology (FCT, project UIDB/04308/2020 and UIDP/04308/2020).

Acknowledgments

We thank all the contributors and reviewers who have participated in this Research Topic.

Conflict of interest

The authors declare that the research was conducted in the absence of any commercial or financial relationships that could be construed as a potential conflict of interest.

Publisher's note

frontiers in Molecular Neuroscience

ORIGINAL RESEARCH
published: 26 October 2020
doi: 10.3389/fnmol.2020.588802

Epinephrine May Contribute to the Persistence of Traumatic Memories in a Post-traumatic Stress Disorder Animal Model

Raquel Martinho[1,2], *Ana Oliveira*[1,2], *Gabriela Correia*[1,2], *Márcia Marques*[1,2], *Rafaela Seixas*[1,2], *Paula Serrão*[2,3] *and Mónica Moreira-Rodrigues*[1,2]*

[1]*Laboratory of General Physiology, Institute of Biomedical Sciences Abel Salazar, University of Porto (ICBAS/UP), Porto, Portugal,* [2]*Center for Drug Discovery and Innovative Medicines, University of Porto (MedInUP), Porto, Portugal,* [3]*Department of Pharmacology and Therapeutics, Faculty of Medicine, University of Porto (FMUP), Porto, Portugal*

The importance of catecholamines in post-traumatic stress disorder (PTSD) still needs to be explored. We aimed to evaluate epinephrine's (EPI) causal role and molecular mechanism for the persistence of PTSD traumatic memories. Wild-type (WT) and EPI-deficient mice (phenylethanolamine-*N*-methyltransferase-knockout mice, Pnmt-KO) were induced with PTSD and behavioral tests were performed. Some Pnmt-KO mice were administered with EPI or vehicle. Catecholamines were quantified by HPLC-ED. *Nr4a1*, *Nr4a2*, and *Nr4a3* mRNA expression were evaluated by real-time PCR in hippocampus samples. It was observed an increase in EPI and freezing behavior, and a decrease in open arm entries in the elevated plus-maze test and time spent in the light in the light–dark test in WT mice in the PTSD-induction group compared to control. After induction of PTSD, Pnmt-KO mice showed a decrease in freezing, as well as an increase in open arm entries and transitions between compartments compared to WT. After PTSD induction, Pnmt-KO mice administered with EPI showed an increase in freezing compared with the vehicle. On day 0 of PTSD induction, it was observed an increase in mRNA expression of *Nr4a2* and *Nr4a3* genes in the hippocampus of WT mice compared to control, contrary to Pnmt-KO mice. In conclusion, our data suggest that EPI may be involved in the persistence of traumatic memories in PTSD, possibly through enhancement of the expression of *Nr4a2* and *Nr4a3* genes in the hippocampus. Peripheral administration of EPI restored contextual traumatic memories in Pnmt-KO mice, which suggests a causal role for EPI. The persistence of contextual traumatic memories may contribute to anxiety-like behavior and resistance of traumatic memory extinction in this PTSD mice model.

Keywords: epinephrine, norepinephrine, post-traumatic stress disorder, epinephrine deficient mice, phenylethanolamine-*N*-methyltransferase-knockout mice, hippocampus, Nr4a transcription factors

OPEN ACCESS

Edited by:
Arturo Gabriel Romano, University of Buenos Aires, Argentina

Reviewed by:
Michael Ziegler, University of California, San Diego, United States
Natasa Spasojevic, University of Belgrade, Serbia

***Correspondence:**
Mónica Moreira-Rodrigues
mirodrigues@icbas.up.pt

Received: *29 July 2020*
Accepted: *22 September 2020*
Published: *26 October 2020*

Citation:
Martinho R, Oliveira A, Correia G, Marques M, Seixas R, Serrão P and Moreira-Rodrigues M (2020) Epinephrine May Contribute to the Persistence of Traumatic Memories in a Post-traumatic Stress Disorder Animal Model. Front. Mol. Neurosci. 13:588802. doi: 10.3389/fnmol.2020.588802

INTRODUCTION

The autonomic nervous system mobilizes the body's resources under stress and induces the "freeze, fight or flight" response, important for survival and adaptation in nature. To maintain homeostasis, the sympathetic nervous system is constantly being activated (Lipov, 2014). However, in some circumstances, stress may cause pathology, as is the case for post-traumatic stress disorder (PTSD) and other anxiety disorders (Crawley, 1981; Crawley et al., 1984; Maercker et al., 2013).

Patients with PTSD usually have three major features: re-experience the stressful event, attempt to avoid reminders of the trauma, and a state of hyperarousal, such as increased hypervigilance and startle response (van der Kolk, 2000; Pole, 2007; Pitman et al., 2012; American Psychiatric Association, 2013; Yehuda et al., 2015). Although these symptoms are common after the traumatic event, they abnormally persist in individuals with PTSD. This disorder can thus be seen, in part, as a failure to recover from the normal reaction to the trauma (Yehuda et al., 1992). Therefore, patients with PTSD show deficits in the extinction of emotional memories and have persistent severe anxiety (Lissek et al., 2005; Inslicht et al., 2013).

Some studies have suggested that epinephrine (EPI) is an important hormone for long-term memory consolidation in human and animal subjects (Cahill and Alkire, 2003; Dornelles et al., 2007). Moreover, we also have shown in previous studies that mice deficient in EPI (phenylethanolamine-*N*-methyltransferase-knockout, Pnmt-KO mice) have reduced contextual fear learning (Toth et al., 2013; Alves et al., 2016). It has been documented in PTSD patients an increase of stress hormones in urine, namely EPI and norepinephrine (NE; Yehuda et al., 1992; Lemieux and Coe, 1995; Pitman and Delahanty, 2005). The increase of stress hormones can facilitate the strengthening of traumatic memories (Pitman, 1989; Pitman and Delahanty, 2005), but the action mechanism of these catecholamines in PTSD mice models needs to be explored.

Several animal models have been developed using different types of traumatic events to study PTSD in humans (Pynoos et al., 1996). The PTSD animal model that we have selected is centered on the concept that exposure to foot shocks displays the pathophysiological process and the core symptomatology of PTSD, including freezing and anxiety-like behavior (Li et al., 2006; Zhang et al., 2012; Verma et al., 2016).

Nr4a is a subfamily of orphan nuclear receptors genes. These genes encode for three transcription factors, namely *Nr4a1*, *Nr4a2*, and *Nr4a3*, which mediate several cellular responses (Hazel et al., 1988; Law et al., 1992; Ohkura et al., 1996). Besides their involvement in physiologic processes such as energy metabolism, inflammatory responses, and hypothalamic-pituitary-adrenal axis regulation (Wilson et al., 1993; Honkaniemi et al., 1994; Murphy and Conneely, 1997; Maira et al., 1999), these genes have been implicated in contextual fear memory formation (Liu et al., 1994; Woronicz et al., 1994; Fernandez et al., 2000; Pei et al., 2006; Rojas et al., 2007; Hawk and Abel, 2011; Oliveira et al., 2018). Previous studies showed that contextual fear conditioning induces *Nr4a* genes transcription in the hippocampus, a brain structure involved in the acquisition of contextual fear conditioning in response to stress stimuli (von Hertzen and Giese, 2005; Hawk et al., 2012; Mizuno et al., 2012; Oliveira et al., 2018). Thus, the study of *Nr4a* genes expression in this model may be relevant. The present study aimed to understand the influence of EPI in the persistence of PTSD traumatic memories and possible molecular mechanisms.

MATERIALS AND METHODS

Animals

All animal care and experimental protocols were carried out following European Directive number 2010/63/EU, transposed to Portuguese legislation by Directive Law 113/2013 and 1/2019, and approved by the Organism Responsible for Animal Welfare in Faculty of Medicine of University of Porto and National Authority for Animal Health. The Pnmt-KO mice ($Pnmt^{-/-}$) were produced by the insertion of the Cre-recombinase gene into the locus encoding for the Pnmt enzyme, which results in EPI's deficiency in homozygous ($Pnmt^{-/-}$). Pnmt-KO mice were first generated in C57BL/6 mice (Ebert et al., 2004) and these mice were fully bred in 129x1/SvJ background. Steven N. Ebert kindly provided a couple of Pnmt-KO ($Pnmt^{-/-}$) and heterozygous ($Pnmt^{+/-}$) mice and they were bred in our conventional vivarium. Regarding breeding, 1 male and 2 females of heterozygous ($Pnmt^{+/-}$) mice siblings were placed together for mating. Pups were weaned 21 days after birth, males and females were separated, and placed in individual cages. Genotypes at the Pnmt locus were identified by polymerase chain reaction (PCR) of ear DNA, as described before (Ebert et al., 2004). From heterozygous couples ($Pnmt^{+/-}$) we selected wild-type (WT) female and WT male mice ($Pnmt^{+/+}$) or Pnmt-KO female and Pnmt-KO male mice ($Pnmt^{-/-}$), which were siblings, and were placed in the same cage to breed WT ($Pnmt^{+/+}$) or Pnmt-KO ($Pnmt^{-/-}$) mice, respectively. WT (n = 45) and Pnmt-KO (n = 41) female mice (8–12 weeks old) were kept under controlled environmental conditions (12 h light/dark cycle, room temperature 23 ± 1°C, humidity 50%, autoclaved drinking water, mice diet 4RF25/I and 4RF21/A; Mucedola, Porto, Portugal) in the same room and housed with the respective litter. When female rodents are placed in small groups and share a recirculated air supply it is observed a synchrony of their ovarian cycles, which is mediated by pheromones (McClintock, 1978; Schank and McClintock, 1992). During the 5 days of habituation before experiments, all mice were handled once daily with gloved hands for 2 min. Also, all experimental groups in a protocol were performed on the same day, not more than 2 h apart. Therefore, the step of measuring the estrous cycle for each individual was waived.

PTSD Mice Model

As previously described (Li et al., 2006; Zhang et al., 2012; Verma et al., 2016), mice were exposed to an aversive procedure consisting of two training sessions (day 0 and day 1). For the training sessions, we used a clear Plexiglass chamber with a

metal grid floor, wired to a stimulus generator. On these days, the mice had a 2-min habituation period and then they were then submitted to 15 electric shocks (intensity, 0.8 mA; duration, 10 s; the interval between sessions, 10 s), during a total time of 5 min. After training, the mice were re-exposed on days 2 and 7 to the aversive context. Re-exposure consisted of introducing the mice in the same chamber, without applying foot shocks, for 5 min. Control mice were placed in the same chamber and during the same amount of time and days as the other mice (days 0, 1, 2, and 7), but did not receive the electric shocks. The mice's behavior was recorded with a digital video camera Sony HDR-CX405 (Sony Corporation, Japan). Freezing was defined as the absence of movement except for respiration for at least 3 s (Valentinuzzi et al., 1998). The percentage of accumulated freezing time was then calculated. Vocalization response was defined as the audible vocalization and jump response was defined as the removal of at least three paws from the grid floor in response to the shock (Rocinholi et al., 1997). All quantifications were performed manually and blinded. In the first protocol, WT mice were induced with PTSD (PTSD-induction group) or not (control group) until day 7. Then, urine, plasma, and adrenal gland were collected for catecholamines evaluation by HPLC-ED (**Figure 1A**). In the second protocol, freezing behavior was evaluated in WT and Pnmt-KO mice (PTSD-induction group or control group) on days 2 and 7. Afterward, elevated plus maze (day 8), light–dark transition (day 9), and open field (day 10) tests were conducted (**Figure 1A**). At the end of protocols mice were anesthetized (ketamine, 100 mg/kg and xylazine, 10 mg/kg; i.p.), and blood and left adrenal glands were collected (**Figure 1A**). In the third protocol, EPI (0.1 mg/kg, i.p., 3 min; Lee et al., 2001) or vehicle (0.9% NaCl) were administered to Pnmt-KO mice (PTSD-induction group) on days 0, 1, 2, and 7 and freezing behavior was evaluated (**Figure 1B**). In the fourth protocol, the same procedure was repeated just on day 0 with WT and Pnmt-KO mice (PTSD-induction group or control group) and the hippocampus was collected for real-time PCR (qPCR; **Figure 1A**).

Metabolic Studies

WT mice were placed in metabolic cages (Tecniplast, Buguggiate-VA, Italy) for 24-h urine collection on day 7 for later determination of catecholamines, as previously described (Moreira-Rodrigues et al., 2007b, 2010, 2012). Twenty-four hours food and water intake and feces weight were evaluated.

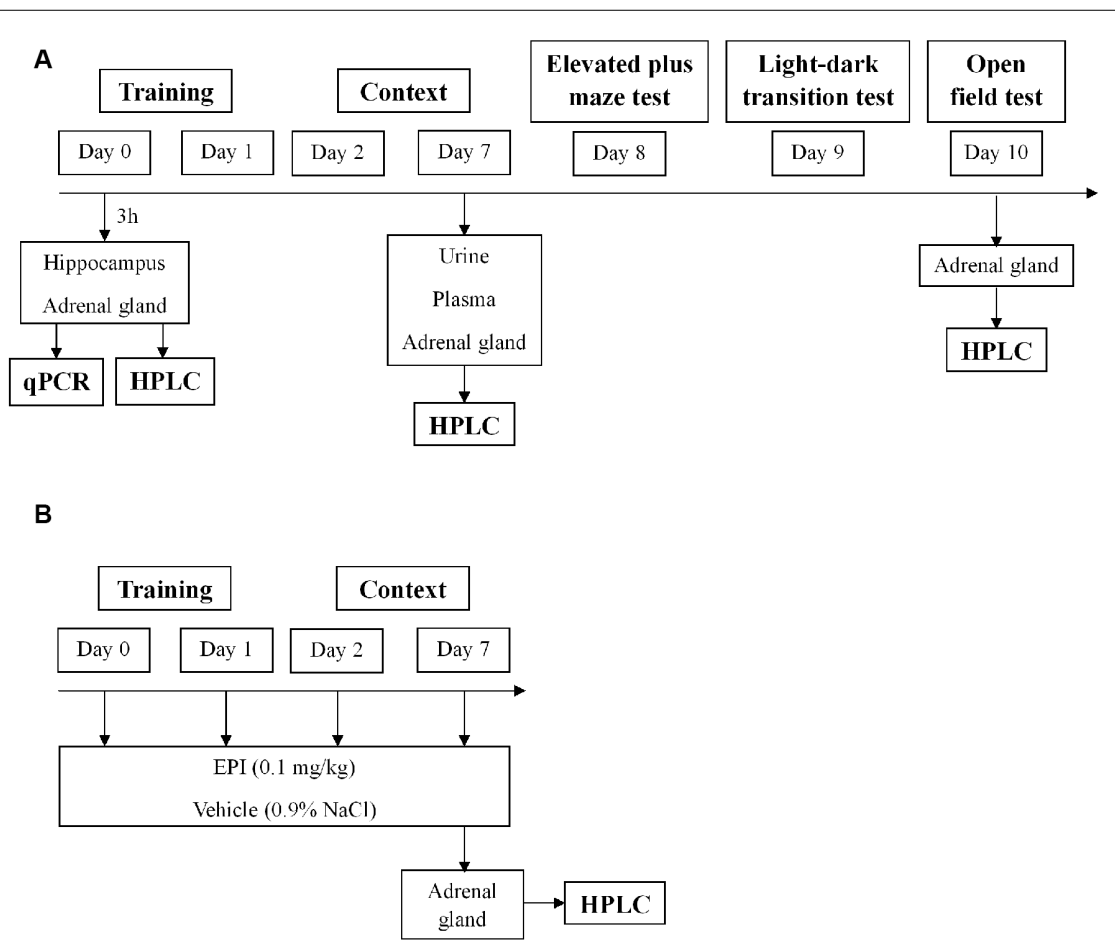

FIGURE 1 | Schematic representation of behavioral protocols, experimental design, treatments, and sample collection. **(A)** Results in **Figures 2**–**7**, **9**; **(B)** results in **Figure 8**. HPLC, high-performance liquid chromatography; qPCR, real-time polymerase chain reaction.

The urine vials for catecholamines quantification contained 60 µl of hydrochloric acid (6 mol/l) to avoid spontaneous oxidation of the amines and its derivatives. All urine samples were frozen at −80°C until further use.

Quantification of Catecholamines

The left adrenal gland was collected and emerged in perchloric acid 0.2 M overnight, at 4°C, and kept under −80°C until further use. Afterward, the adrenal glands supernatant was centrifuged for 2 min (2,700× *g* and 4°C) and diluted. Blood was also collected by left ventricle puncture to a heparinized tube, then the samples were centrifuged (1,000× *g*, 15 min, 4°C) and kept at −80°C until further use. The catecholamines present in plasma and urine were concentrated by the alumina method, as previously described (Moreira-Rodrigues et al., 2007b, 2010, 2012, 2014). Catecholamines in the adrenal gland, plasma, and urine samples were separated by reverse-phase high-performance liquid chromatography (HPLC) and quantified by electrochemical detection. The detection limit was between 350 fmol and 1,000 fmol.

Other Behavioral Testing

Elevated Plus Maze Test

Eight days after PTSD induction, an elevated plus-maze test was conducted as previously described (Pellow et al., 1985; Popovitz et al., 2019). Briefly, the apparatus consisted of two open arms (40 × 10 cm) alternating at right angles with two arms enclosed by 20 cm high walls. The four arms delimited a central area of 5 cm^2. The whole apparatus was placed 60 cm above the floor. The test began by placing the animal in the center with its head facing a closed arm. The visits in open and closed arms and total arm entries for 5 min were recorded with a digital video camera Sony HDR-CX405 (Sony Corporation, Japan), analyzed manually and blinded, and a four paws criterion was used for arm entries (Li et al., 2006).

Light–Dark Transition Test

Nine days after PTSD induction, the light–dark transition test was carried out as previously described (Li et al., 2006). The apparatus consisted of a wooden chamber subdivided into a dark (50 × 20 × 25 cm) and a light compartment (50 × 30 × 25 cm). The compartments were connected by a small divider (10 × 10 cm). Each animal was placed into the light compartment facing the opposite wall to the entry. The latency of the first entry into the dark compartment, the time spent in each compartment, and the number of transitions between compartments were recorded with a digital video camera Sony HDR-CX405 (Sony Corporation, Japan) for 5 min and analyzed manually and blinded.

Open Field Test

Ten days after PTSD induction, the open field test was conducted as described before (Zhang et al., 2012; Inoue et al., 2018). The open field wooden chamber (50 × 50 × 30 cm) had black lines on the floor delineating twelve peripheral squares (12.5 × 12.5 cm) and a central square (25 × 25 cm). Each animal was placed in the corner of the arena and locomotor activity was recorded for 10 min with a digital video camera Sony HDR-CX405 (Sony Corporation, Japan). The total distance traveled was analyzed using ToxTrac ver 2.84 (open source software freely available at sourceforge.net/projects/toxtrac, Rodriguez et al., 2017, 2018; Henry et al., 2019). The number of squares crossed, entries in the center, and feces were analyzed manually and blinded.

RNA Isolation and Relative Quantification of mRNA Expression

qPCR was performed in hippocampus samples collected 3 h after day 0 of PTSD induction, as previously described (Moreira-Rodrigues et al., 2007a; Mendes et al., 2018; Oliveira et al., 2018). Total RNA isolation was carried out with the illustra^{TM} RNAspin Mini RNA Isolation Kit (GE Healthcare Life Sciences, Buckinghamshire, UK). The membrane desalting step of the kit created a chemical environment for efficient on-column DNase I digest and thus the isolated total RNA was free of genomic DNA. The concentration and purity of the isolated RNA were measured using the NanoDrop 2000 spectrophotometer (Thermo Fisher Scientific, Waltham, MA, USA). Reverse transcription was performed in a T100^{TM} Thermal Cycler (Bio-Rad, Hercules, CA, USA) using a Reverse Transcription kit (NZY First-Strand cDNA Synthesis Kit NZYTech—Genes and Enzymes, Lisbon, Portugal). qPCR reactions were carried out in StepOne^{TM} real-time PCR System (Applied BioSystems, Waltham, MA, USA). Gene-specific primers (10 µM), Maxima SYBR Green qPCR Master Mix (Thermo Fisher Scientific, Waltham, MA, USA), and Nuclease-free H_2O (Thermo Fisher Scientific, Waltham, MA, USA) were mixed and cDNA was added (1:20). As negative controls, a no template control and a minus reverse transcriptase control were used. The cycling parameters were as follows: denaturation at 95°C for 30 s, annealing at 60°C for 1 min, and extension at 60°C for 1 min (40 cycles). Gene-specific primers and the size of amplified DNA fragments are in **Table 1**. Results of mRNA quantification are expressed in an arbitrary unit (AU) after normalization for Glyceraldehyde 3-phosphate dehydrogenase (GAPDH).

Drugs

(-)-epinephrine (EPI) and perchloric acid were purchased from Sigma–Aldrich (St. Louis, MO, USA). Ketamine (Imalgene 1000, Merial, Lisbon, Portugal) and xylazine (Rompum 2%, Bayer, Lisbon, Portugal) were purchased from Agrofauna (Vila Nova de Gaia, Portugal).

TABLE 1 | Primers used in gene expression analysis.

Gene	Primer (5′→ 3′)	Size (bp)
Nr4a1	F: AAAATCCCTGGCTTCATTGAG	102
	R: TTTAGATCGGTATGCCAGGCG	
Nr4a2	F: CGGTTTCAGAAGTGCCTAGC	214
	R: TTGCCTGGAACCTGGAATAG	
Nr4a3	F: GTGGCTCGACTCCATTAAAGAC	144
	R: GTGCATAGCTCCTCCACTCTCT	
Gapdh	F: CCATCACCATCTTCCAGGAG	322
	R: GCATGGACTGTGGTCATGAG	

Nr4, Nuclear receptor 4; Gapdh, Glyceraldehyde 3-phosphate dehydrogenase; F, forward primer; and R, reverse primer.

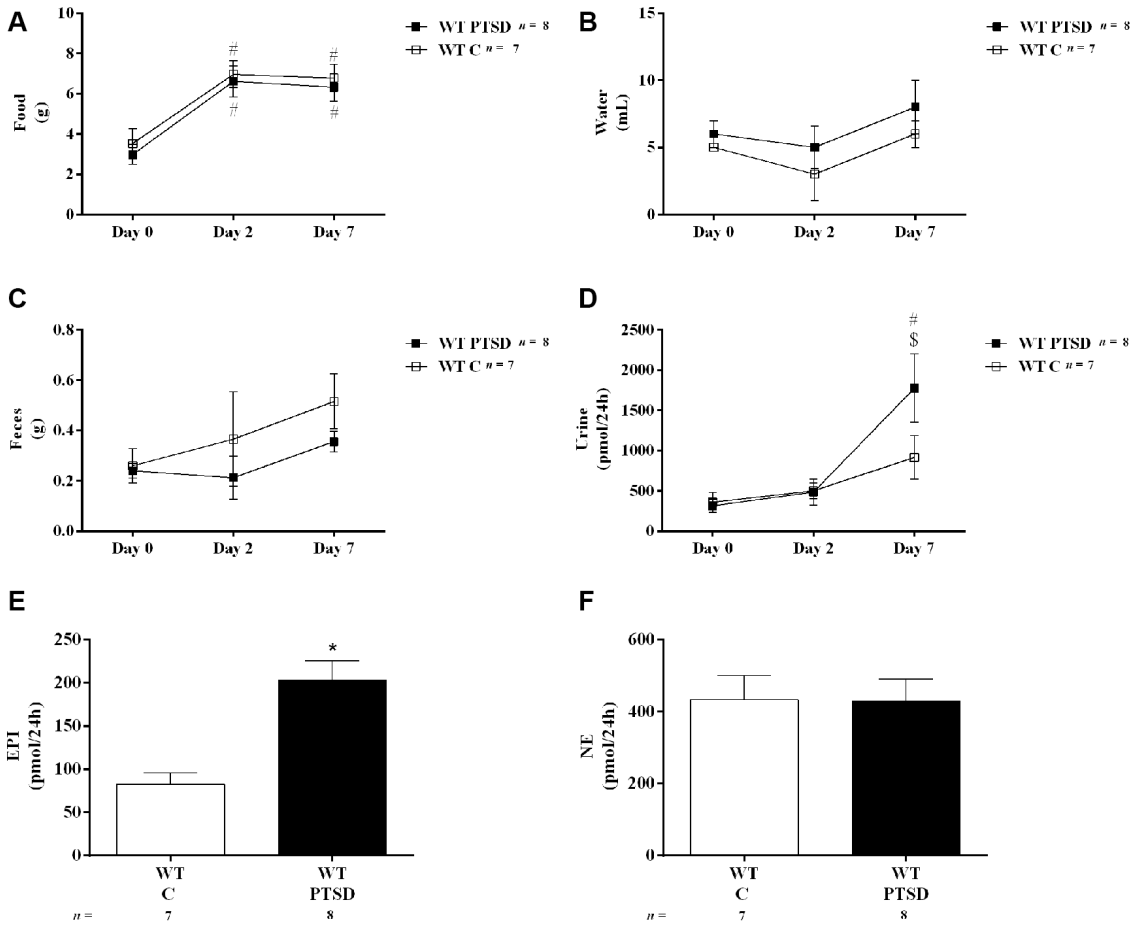

FIGURE 2 | Twenty-four hours **(A)** food and **(B)** water intake, **(C)** feces weight, **(D)** urine volume, and urinary **(E)** epinephrine (EPI) and **(F)** norepinephrine (NE) quantity in 24 h of wild-type (WT) mice in the post-traumatic stress disorder (PTSD) induction group or control group (WT C) on day 7 of PTSD induction. Values are means ± standard error of the means (SEM) of 7–8 mice per group. WT C, WT control mice, placed in the same chamber during the same amount of time and days as the other mice but were not induced with PTSD; WT PTSD, WT mice in the PTSD-induction group. #Significantly different from correspondent values on day 0 of respective group ($p < 0.05$). $Significantly different from correspondent values on day 2 of the respective group ($p < 0.05$). *Significantly different from correspondent values in WT control mice ($p < 0.05$).

Statistics

All results were presented as means ± standard error of the means (SEM). For parameters measured during metabolic studies (two groups; WT mice in the PTSD-induction group and WT control mice; **Figure 2**). Two-way analysis of variance (ANOVA) repeated measures followed by Tukey's *post hoc* test was performed using pathology as "between-subjects factor" and time as "within-subjects factor" (repeated measure). For the catecholamines concentration results (two groups; WT mice in the PTSD-induction group and WT control mice; **Figures 2**, **3**) an unpaired *t*-test was used to determine group differences. For vocalization and jump responses (four groups; WT and Pnmt-KO in the PTSD groups or controls; **Figure 4**). Two-way ANOVA followed by Tukey's *post hoc* test was performed where the main effect of genotype, pathology, and genotype × pathology interaction was evaluated. Also, for vocalization and jump responses (two groups; Pnmt-KO in the PTSD group administered with EPI or vehicle; **Figure 8**), an unpaired *t*-test was used to determine group differences. For freezing behavior (four groups; WT and Pnmt-KO in the PTSD groups or controls; **Figure 4**). Three-way ANOVA repeated measures followed by Tukey's *post hoc* test was performed using genotype and pathology as "between-subjects factor," and time as "within-subjects factor" (repeated measure). Also, for freezing behavior (two groups; Pnmt-KO in the PTSD group administered with EPI or vehicle; **Figure 8**). Two-way ANOVA repeated measures followed by Sidak's *post hoc* test was performed using treatment as "between-subjects factor" and time as "within-subjects factor" (repeated measure). Furthermore, for elevated plus maze test, light–dark transition test, open field test, and qPCR results (four groups; WT and Pnmt-KO in the PTSD groups or controls; **Figures 5**–**7**, **9**). Two-way ANOVA followed by Tukey's *post hoc* test was performed and the main effect of genotype, pathology, and genotype × pathology interaction

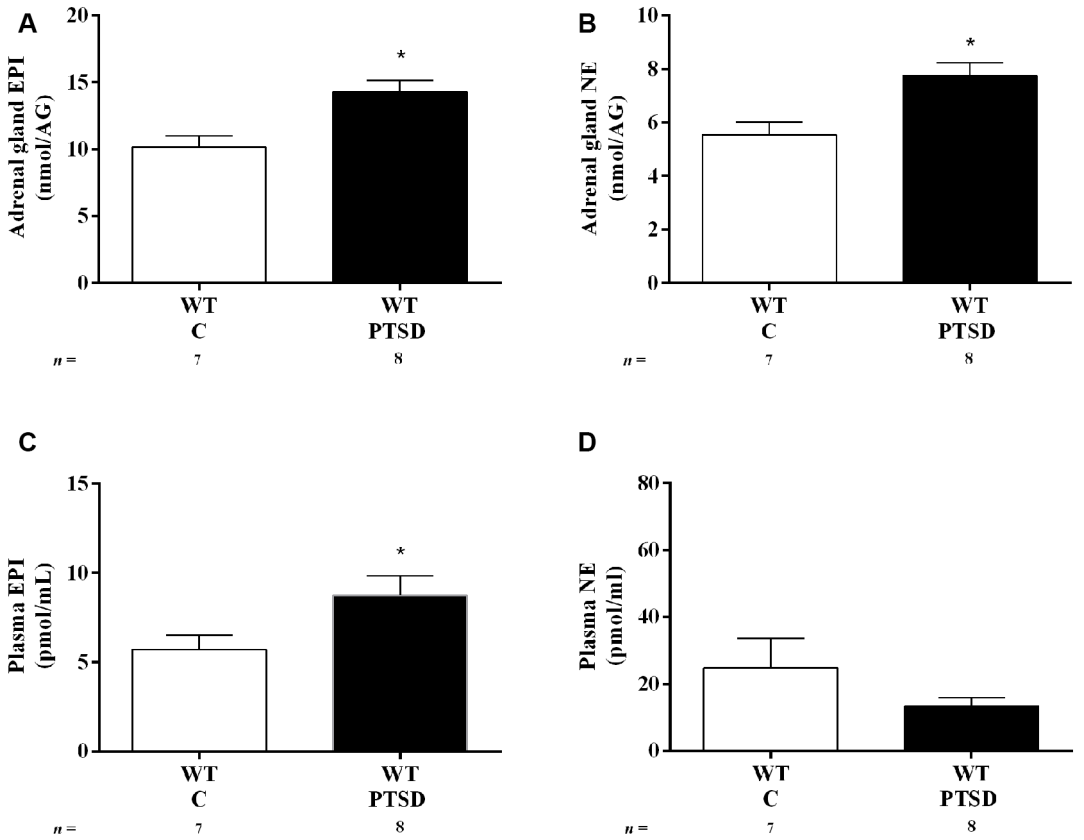

FIGURE 3 | Concentration of **(A,C)** epinephrine (EPI) and **(B,D)** norepinephrine (NE) in **(A,B)** adrenal gland and **(C,D)** plasma of WT mice in the PTSD induction group or control group (WT C) on day 7 of PTSD induction. Values are means ± SEM of 7–8 mice per group. WT C, WT control mice, placed in the same chamber during the same amount of time and days as the other mice but were not induced with PTSD; WT PTSD, WT mice in the PTSD-induction group. *Significantly different from correspondent values in WT control mice ($p < 0.05$).

was evaluated. Effect sizes were estimated by calculating Cohen's d test for pairwise comparisons and partial eta squared (η_p^2) for ANOVA. The correlations were evaluated by calculating Pearson's correlation coefficient r. The statistically significant difference was set at $p < 0.05$.

RESULTS

EPI Increases After PTSD Induction

To evaluate catecholamines levels in this PTSD mice model, WT mice were put in metabolic cages. In both WT mice in the PTSD-induction and control groups, food intake was significantly increased in both days 2 and 7 when compared to day 0 (**Figure 2A**). However, no statistically significant differences were observed between these groups in food intake (**Figure 2A**) during the 7 days of PTSD induction. Also, no significant differences were observed in water intake (**Figure 2B**) and feces weight (**Figure 2C**) between groups. Also, 24-h urine volume was significantly increased in WT mice in the PTSD-induction group on day 7 when compared to day 2 and day 0, which was not observed in WT control mice (**Figure 2D**). However, no statistically significant differences in 24-h urine volume were observed between these groups of mice. Furthermore, EPI in 24-h urine was significantly increased in WT mice 7 days after induction of PTSD when compared to WT control mice (**Figure 2E**). Also, there was a statistically significant increase of EPI (**Figure 3A**) and NE (**Figure 3B**) in the adrenal gland, and of EPI in plasma (**Figure 3C**) of WT mice in the PTSD-induction group when compared to WT control mice. Moreover, significantly strong positive correlations were observed between EPI in adrenal gland and urine ($r = 0.6615$, $p < 0.05$), and between EPI in plasma and urine ($r = 0.5076$, $p < 0.05$). On the other hand, no statistically significant differences were observed in NE in urine (**Figure 2F**) and plasma (**Figure 3D**) between these groups. EPI was vestigial in the adrenal glands of Pnmt-KO mice. Details of statistical data are in **Supplementary Data 1.1**.

EPI-Deficient Mice Have Less Freezing After PTSD Induction Than WT

On days 0 and 1 of the PTSD induction model, it was observed a significant increase in vocalization response in WT

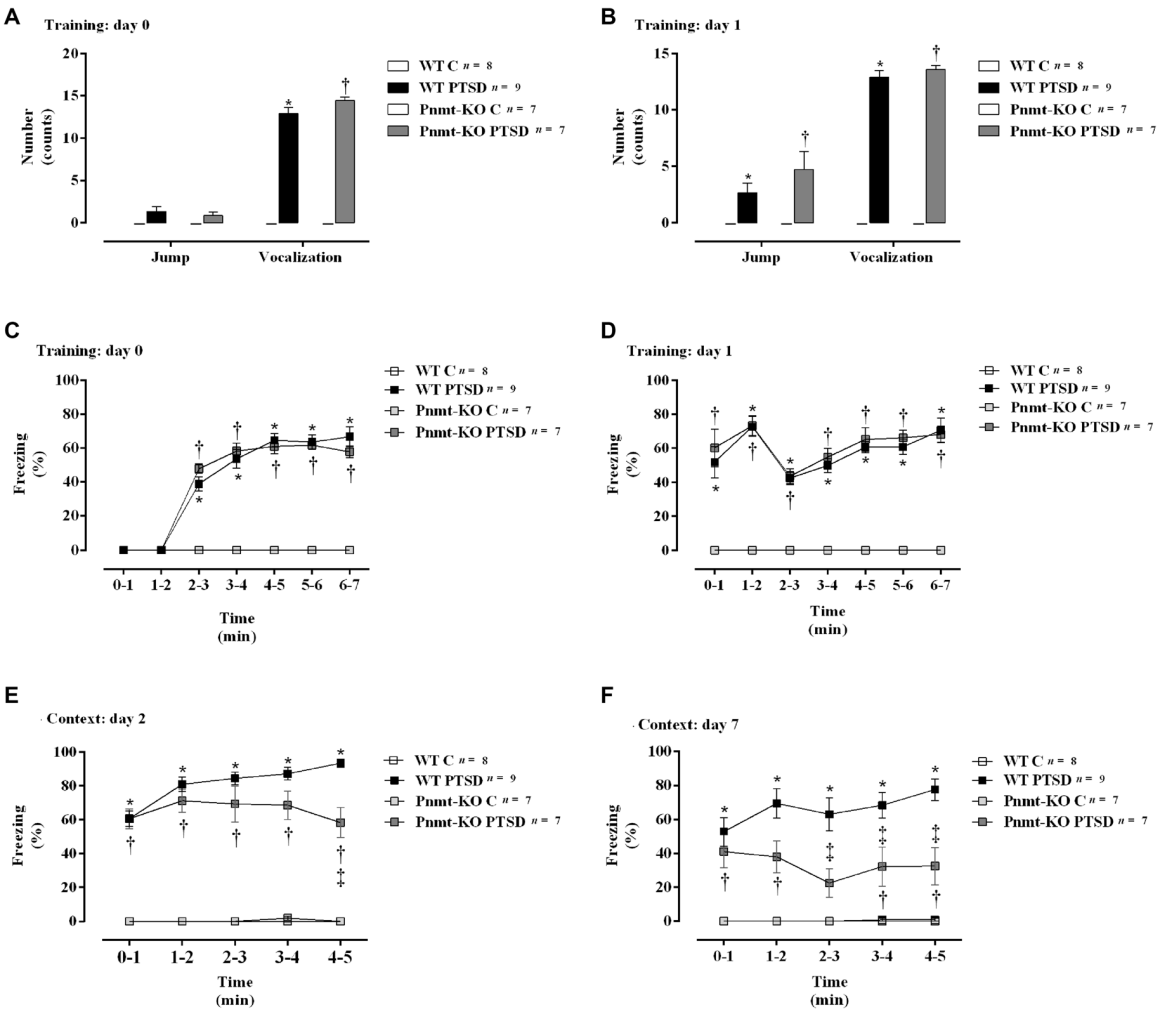

FIGURE 4 | (A,B) Shock responsivity on training sessions (days 0 and 1) and **(C–F)** freezing behavior during induction of PTSD. Freezing on **(C)** day 0, **(D)** day 1, **(E)** day 2, and **(F)** day 7 in WT and phenylethanolamine-*N*-methyltransferase-knockout (Pnmt-KO) mice in the PTSD-induction group or not (control, WT C and Pnmt-KO C). Values are means ± SEM of 7–9 mice per group. C, control mice, placed in the same chamber during the same amount of time and days as the other mice but were not induced with PTSD; WT C, WT control mice; WT PTSD, WT mice in the PTSD-induction group; Pnmt-KO C, Pnmt-KO control mice; Pnmt-KO PTSD, Pnmt-KO mice in the PTSD-induction group. *Significantly different from correspondent values in WT control mice ($p < 0.05$). †Significantly different from correspondent values in Pnmt-KO control mice ($p < 0.05$). ‡Significantly different from correspondent values in WT mice with similar pathology ($p < 0.05$).

mice in the PTSD-induction group compared to WT control (**Figures 4A,B**). Moreover, no statistically significant differences in shock responsivity (vocalization and jump; **Figures 4A,B**) were observed between WT and Pnmt-KO mice in the PTSD-induction groups. Also, it was observed a significant increase in freezing behavior during training days 0 and 1 in WT mice in the PTSD-induction group compared to control (**Figures 4C,D**). No statistically significant differences in freezing behavior were observed between WT and Pnmt-KO mice PTSD-induction groups during training days 0 and 1 (**Figures 4C,D**).

Furthermore, after re-exposure to the aversive context, it was observed a higher freezing response in WT mice in the PTSD-induction group compared to control, on days 2 and 7 (**Figures 4E,F**). Moreover, significantly strong positive correlations were observed between contextual freezing on day 7 and EPI in adrenal gland ($r = 0.4959$, $p < 0.05$), plasma ($r = 0.4001$, $p < 0.05$), and urine ($r = 0.5825$, $p < 0.05$). Also, Pnmt-KO mice in the PTSD-induction group showed a significant decrease in freezing behavior compared to WT mice PTSD-induction group on days 2 and 7 (**Figures 4E,F**). Details of statistical data are in **Supplementary Data 1.2**.

EPI-Deficient Mice Have Less Anxiety After PTSD Induction Than WT

In the elevated plus-maze test (day 8), the open arms entries (**Figure 5A**) and the total number of arm entries (**Figure 5B**) were significantly decreased in WT mice in the PTSD-induction group when compared to WT control. Also, the open arms entries were significantly

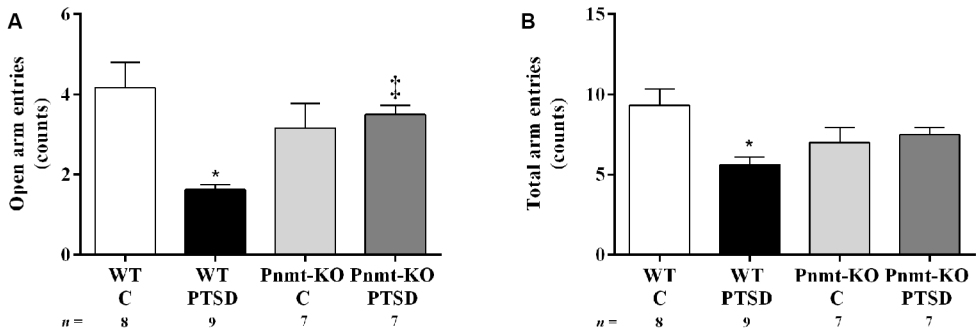

FIGURE 5 | Elevated-plus maze test results in WT and phenylethanolamine-*N*-methyltransferase-knockout (Pnmt-KO) mice in the PTSD induction group or control group (WT C and Pnmt-KO C) 8 days after PTSD induction. The number of **(A)** open arm entries and **(B)** total arm entries. Values are means ± SEM of 7–9 mice per group. C, control mice, placed in the same chamber during the same amount of time and days as the other mice but were not induced with PTSD; WT C, WT control mice; WT PTSD, WT mice in the PTSD-induction group; Pnmt-KO C, Pnmt-KO control mice; Pnmt-KO PTSD, Pnmt-KO mice in the PTSD-induction group. *Significantly different from correspondent values in WT control mice ($p < 0.05$). ‡Significantly different from correspondent values in WT mice with similar pathology ($p < 0.05$).

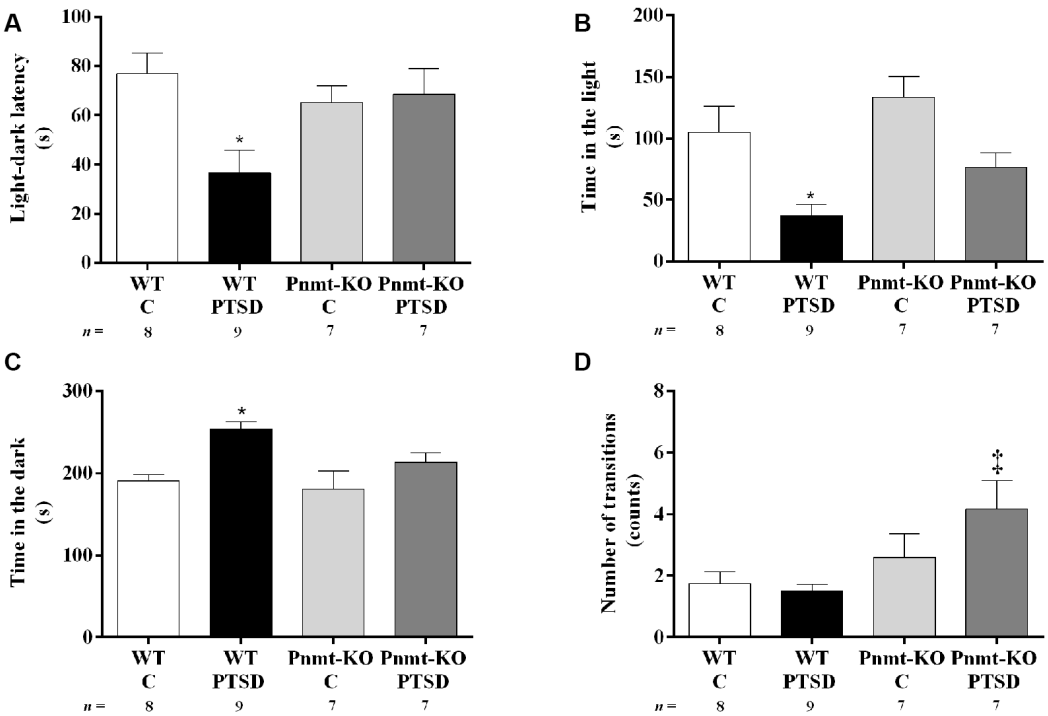

FIGURE 6 | Light–dark transition test results in WT and phenylethanolamine-*N*-methyltransferase-knockout (Pnmt-KO) mice in the PTSD induction group or control group (WT C and Pnmt-KO C) 9 days after PTSD induction. **(A)** Latency to enter the dark compartment, time spent in the **(B)** dark, **(C)** light compartment, and **(D)** the total number of transitions between compartments. Values are means ± SEM of 7–9 mice per group. C, control mice, placed in the same chamber during the same amount of time and days as the other mice but were not induced with PTSD; WT C, WT control mice; WT PTSD, WT mice in the PTSD-induction group; Pnmt-KO C, Pnmt-KO control mice; Pnmt-KO PTSD, Pnmt-KO mice in the PTSD-induction group. *Significantly different from correspondent values in WT control mice ($p < 0.05$). ‡Significantly different from correspondent values in WT mice with similar pathology ($p < 0.05$).

increased in Pnmt-KO mice when compared to WT mice in the PTSD-induction groups (**Figure 5A**). In WT mice in the PTSD-induction group, significantly strong negative correlations were observed between contextual freezing on day 7 and open arms entries ($r = -0.6263$, $p < 0.05$), and total number of arm entries ($r = -0.6440$, $p < 0.05$). In other groups, no correlations were observed ($p > 0.05$).

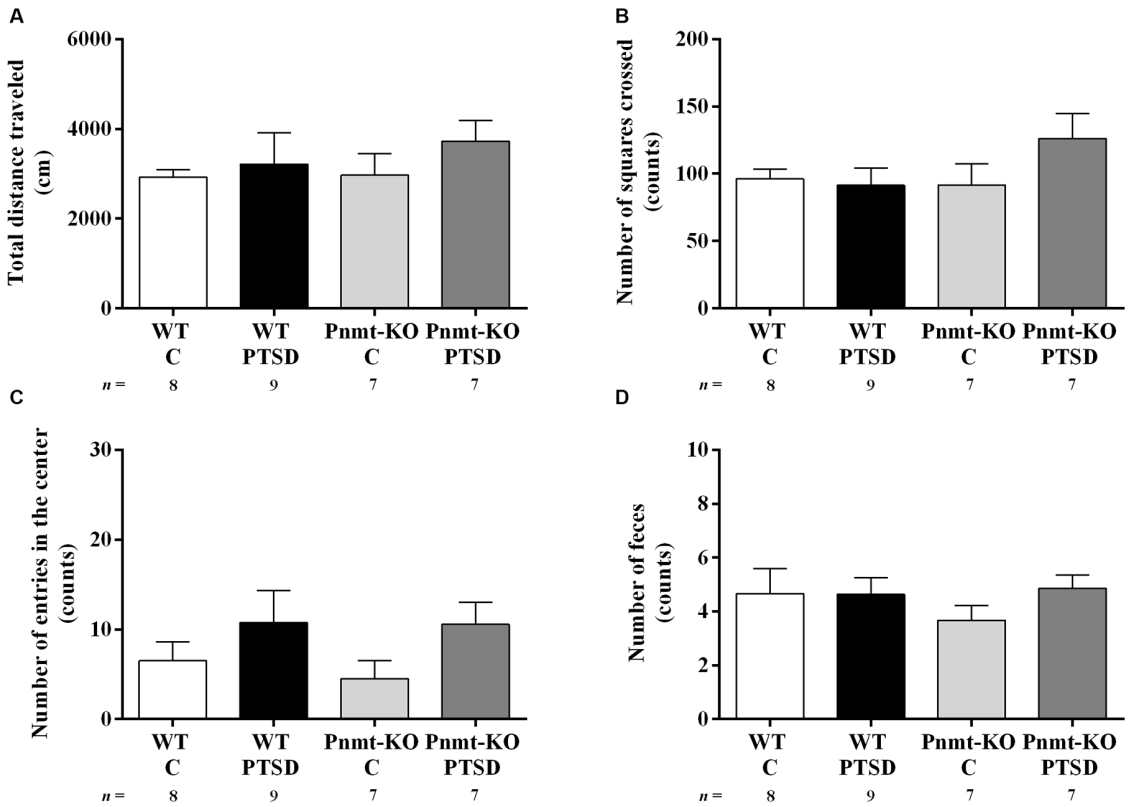

FIGURE 7 | Open field test results in WT and phenylethanolamine-*N*-methyltransferase-knockout (Pnmt-KO) mice in the PTSD induction group or control group (WT C and Pnmt-KO C) 10 days after PTSD induction. **(A)** Total distance traveled and the number of **(B)** squares crossed, **(C)** entries in the center, and **(D)** feces. Values are means ± SEM of 7–9 mice per group. C, control mice, placed in the same chamber during the same amount of time and days as the other mice but were not induced with PTSD; WT C, WT control mice; WT PTSD, WT mice in the PTSD-induction group; Pnmt-KO C, Pnmt-KO control mice; Pnmt-KO PTSD, Pnmt-KO mice in the PTSD-induction group.

In the light–dark transition test (day 9), WT mice in the PTSD-induction group exhibited a significant decrease in the latency to escape from the light to the dark compartment (**Figure 6A**) and in the time spent in the light compartment (**Figure 6B**) compared to WT control, and also a significant increase in the time spent in the dark compartment in this group (**Figure 6C**). No significant differences were observed in these parameters in Pnmt-KO mice. Also, it was observed a significant increase in the total number of transitions between compartments in Pnmt-KO mice when compared to WT mice in the PTSD-induction groups (**Figure 6D**). Details of statistical data are in **Supplementary Data 1.3**.

PTSD Induction Did Not Affect Spontaneous Locomotor Activity

In the open field test (day 10) no statistically significant differences were observed in the total distance traveled (**Figure 7A**), number of squares crossed (**Figure 7B**), entries in the center (**Figure 7C**), and feces (**Figure 7D**) between groups. Also, in all groups, no correlations were observed between contextual freezing on day 7 and open-field parameters.

Peripheral EPI may be Involved in the Persistence of Traumatic Memories in PTSD

On days 0 and 1 of PTSD induction model, no statistically significant differences were observed in vocalization and jump responses, and in freezing behavior between Pnmt-KO mice administered with EPI or vehicle in the PTSD-induction groups (**Figures 8A–D**). Also, it was observed a significant increase in freezing behavior in Pnmt-KO mice administered with EPI after 7 days of PTSD induction compared to Pnmt-KO mice administered with vehicle (**Figures 8E,F**). Details of statistical data are in **Supplementary Data 1.4**.

EPI Appears to Contribute for the Persistence of Traumatic Memories in PTSD by Influencing Nr4a Genes Expression in the Hippocampus

It was observed a significant increase in mRNA expression of *Nr4a2* and *Nr4a3* genes in the hippocampus in the WT mice PTSD-induction group compared to WT control, which was

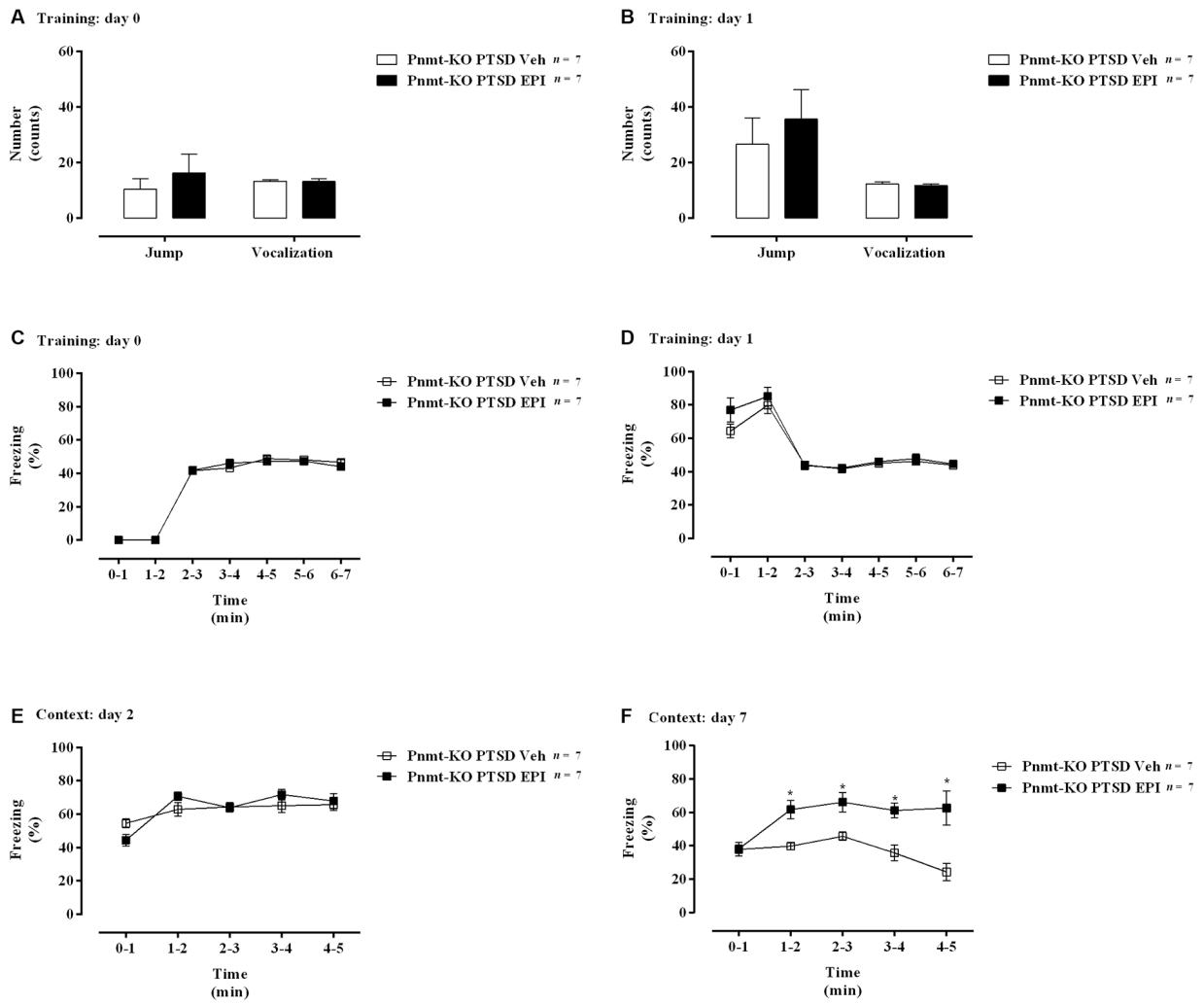

FIGURE 8 | (A,B) Shock responsivity on training sessions and **(C–F)** freezing behavior during the induction of PTSD. Freezing on **(C)** day 0, **(D)** day 1, **(E)** day 2, and **(F)** day 7 in phenylethanolamine-*N*-methyltransferase-knockout (Pnmt-KO) mice in the PTSD-induction group administered with epinephrine (EPI) or vehicle (Veh). Values are means ± SEM of 7 mice per group. Pnmt KO PTSD EPI, Pnmt-KO mice in the PTSD-induction group administered with epinephrine. Pnmt-KO PTSD Veh, Pnmt-KO mice in the PTSD-induction group administered with the vehicle. *Significantly different from correspondent values in Pnmt-KO mice in the PTSD-induction group administered with vehicle ($p < 0.05$).

not observed in Pnmt-KO mice. No significant differences were observed between WT and Pnmt-KO control mice regarding mRNA expression of *Nr4a* family genes. Details of statistical data are in **Supplementary Data 1.5**.

DISCUSSION

PTSD is one of the most common anxiety disorders that can develop after exposure to exceptionally horrifying or threatening events. However, the propensity to develop anxiety disorders also depends on genetic and environmental factors (Sartori et al., 2011). Women have 2 to 3 times higher risk of developing PTSD compared to men. Also, the lifetime prevalence of PTSD is about 10–12% in women and 5–6% in men (Tolin and Foa, 2006; Christiansen and Hansen, 2015; Olff, 2017). Therefore, in this study, we decided to use female mice.

Reconsolidation is capable of continuously alter the strength of memories during our lifetime (Lee, 2008) and may be regulated by adrenergic activity (Przybyslawski et al., 1999). PTSD-related memory is a maladaptive fear memory, which is decontextualized and leads to an intrusive recollection of the trauma in safe environments (Foa et al., 1989; Desmedt et al., 2015). Thus, we decided to apply a validated PTSD mice model (Li et al., 2006; Zhang et al., 2012; Verma et al., 2016) to study the influence of EPI in PTSD.

Animals experiencing a traumatic event, such as multiple foot shocks, rapidly form a strong phobia when a mild aversive experience occurs (Fanselow et al., 1993). This phenomenon may correspond to the emergence of phobias

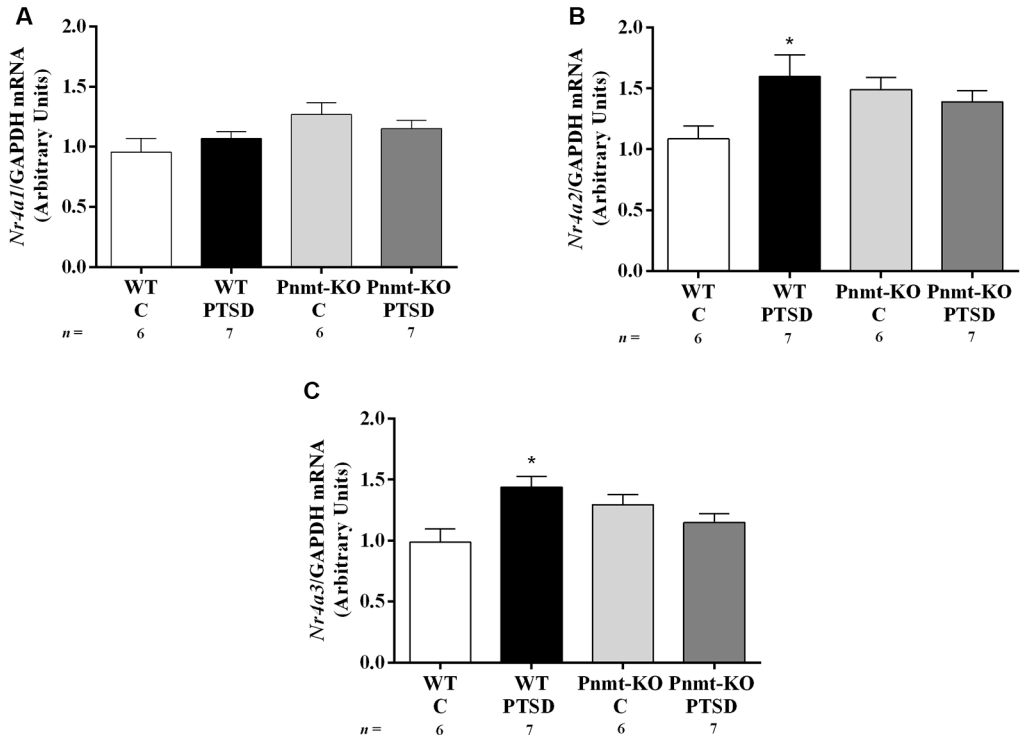

FIGURE 9 | Hippocampus mRNA expression of **(A)** *Nr4a1*, **(B)** *Nr4a2*, and **(C)** *Nr4a3* in WT and phenylethanolamine-*N*-methyltransferase-knockout (Pnmt-KO) mice in the PTSD induction group or control group (WT C and Pnmt-KO C) after day 0 of PTSD induction. Values are means ± SEM of 6–7 mice per group. Results of mRNA are expressed as arbitrary units (AUs) after normalization for Glyceraldehyde 3-phosphate dehydrogenase (GAPDH). C, control mice, placed in the same chamber during the same amount of time and days as the other mice but were not induced with PTSD; WT C, WT control mice; WT PTSD, WT mice in the PTSD-induction group; Pnmt-KO C, Pnmt-KO control mice; Pnmt-KO PTSD, Pnmt-KO mice in the PTSD-induction group. *Significantly different from correspondent values in WT control mice ($p < 0.05$).

in PTSD patients (Rau et al., 2005). The administration of multiple foot shocks in this PTSD model has been confirmed to mimic the traumatic event. Moreover, contextual reminders in this PTSD animal model parallel the exposure to contextual cues present throughout an aversive stressful situation (Li et al., 2006; Zhang et al., 2012; Verma et al., 2016). This may perhaps induce the re-experiencing of the traumatic event (Gisquet-Verrier et al., 2004), which seems to be analogous to the behavioral changes seen in PTSD patients. Based on previous studies, the freezing response upon re-exposure to the shock context in this model is a measure of conditioned associative fear memory, reflecting the response to trauma-related cues as a symptom of PTSD (Siegmund and Wotjak, 2007).

Recent studies have established a relationship between stress hormones and PTSD (Shalev et al., 2008; Porhomayon et al., 2014). It has been documented in PTSD patients an increase of stress hormones, namely catecholamines, such as dopamine, NE, and EPI in urine (Yehuda et al., 1992; Lemieux and Coe, 1995). In accordance, EPI was increased in the adrenal gland, plasma, and urine of WT mice in the PTSD-induction group when compared to control and significantly strong positive correlations were observed between EPI in adrenal gland and urine, and between EPI in plasma and urine. No differences were observed in the food and water intake between WT mice in the PTSD-induction group and control. Therefore, the metabolic activity of these animals was not different and thus, tyrosine (precursor of NE and EPI in the catecholamine biosynthesis pathway) ingestion, which may come from the diet (Wurtman and Fernstrom, 1975; Aquilani et al., 2003), did not seem altered. Also, NE in the adrenal gland was increased in WT mice in the PTSD-induction group compared to control, which is the precursor of EPI. Consequently, the observed increase in urine EPI appears to be due to the raise of this catecholamine production in WT mice in the PTSD-induction group. On the other hand, EPI in Pnmt-KO mice was vestigial in the adrenal gland because these animals do not produce EPI, as previously shown (Ebert et al., 2004; Moreira-Rodrigues et al., 2014; Alves et al., 2016).

In the PTSD mice model used, WT mice showed an elevated freezing response and avoidance to the context associated with the aversive foot shock indicating that the aversive foot shocks followed by repeated reminders are a consistent and long-lasting animal model for PTSD, as previously shown (Li et al., 2006; Zhang et al., 2012). The absence of differences in freezing, vocalization, and jump responses in both training

days (days 0 and 1) between WT and Pnmt-KO mice in the PTSD-induction group suggests that pain perception of the foot shock and acquisition of contextual fear memories were not affected by genotype (absence of EPI). Besides, pain perception and acquisition were also not affected by EPI administration.

We have previously shown that EPI strengthens contextual fear learning by acting in peripheral β_2-adrenoceptors. In this study (Alves et al., 2016), we used a fear conditioning test which is a test to evaluate emotional learning and fear memory but does not induce an anxiety disorder. On the other hand, now we report the induction of PTSD in mice (Pynoos et al., 1996; Pawlyk et al., 2005; Louvart et al., 2006; Bali and Jaggi, 2015), an anxiety disorder, with a more intense traumatic stimulus (days 0 and 1) followed by exposure to repeated situational reminders (days 2 and 7), which induces an increase in the anxiety response (at least until day 10). In this PTSD mice model, we observed significantly strong positive correlations between contextual freezing on day 7 and EPI in the adrenal gland, plasma, and urine.

We show that the release of EPI may be important for the formation and persistence of traumatic memories in PTSD since freezing behavior in EPI-deficient mice (Pnmt-KO) after re-exposition to the context was lower than in WT mice in the PTSD-induction groups. Moreover, EPI peripheral administration restored traumatic contextual memory in EPI-deficient mice (Pnmt-KO) on day 7 of PTSD induction, which suggests a causal role for EPI. Therefore, peripheral EPI appears to strengthen contextual traumatic memories in PTSD. EPI or vehicle was given on days 0, 1, 2, and 7 since EPI has a short half-life (3- to 5-min; Khan, 2006). It remains unanswered if the pre-treatment with EPI only on days 0 and 1 (traumatic stimulus) is sufficient to influence behavior on day 7 in Pnmt-KO mice. On the other hand, we have previously reported that Pnmt-KO mice appear to have a decrease in β_2-adrenoceptor vasodilating effects (Bao et al., 2007; Moreira-Rodrigues et al., 2014). In fact, at rest, Pnmt-KO mice blood pressure was shown to be a little higher than in WT animals (Mendes et al., 2016), and during stress, such as acute exercise, Pnmt-KO mice were shown to have significantly increased blood pressure (Bao et al., 2007). Therefore, we cannot exclude a possible increase in blood pressure during stress to influence behavior.

EPI is a hydrophilic hormone and thus does not cross the blood-brain barrier (Weil-Malherbe et al., 1959). On the other hand, the administration of EPI directly to the brain does not seem to be physiologic. Also, Pnmt has very little expression and enzymatic activity in the brain (Ho et al., 1974; Lew et al., 1977; Mefford, 1987), however, we cannot exclude that epinephrine neurons may ascend to the hippocampus. One of the most common hypotheses is that glucose may mediate EPI's action in the central nervous system (Morris et al., 2013). We have already suggested that after a fear event, EPI is released from the adrenal gland to the bloodstream. Afterward, EPI may act in β_2-adrenoceptors inducing liver cells to release a transient glucose surge into the blood which may be a mediator in the central nervous system strengthening contextual fear memories (Alves et al., 2016; Oliveira et al., 2018).

The elevated plus-maze is described as a method for assessing anxiety-like responses of rodents (Pellow et al., 1985). This test is based on the natural tendency of animals to avoid open and elevated places, as well as on their natural exploratory behavior in novel environments (Zhang et al., 2012). Also, in the light–dark transition test, the time spent in the light is a good index of anxiety-like behavior (anxiogenic activity; Takao and Miyakawa, 2006). We performed behavioral tests consisting of the elevated plus-maze, light–dark transition, and open field with a 24-h interval between each test. Our findings are consistent with previous results suggesting that WT mice in the PTSD-induction group exhibit an anxiogenic-like behavior (Li et al., 2006; Zhang et al., 2012) since it was shown an elevated freezing response associated with a decrease in the number of open arms entries and time spent in the light compartment in these mice. A significantly strong negative correlation was observed between contextual freezing on day 7 and open arms entries in WT mice in the PTSD-induction group. Crawley (1981) and Crawley et al. (1984) have previously described an increased number of transitions between compartments as a key index of anxiolytic action. Thus, EPI-deficient Pnmt-KO mice seem to present lower anxiety levels than WT mice in the PTSD-induction groups, since they showed a decrease in freezing behavior and an increase in the number of open arms entries and transitions between compartments.

Furthermore, in the open field test, no significant differences were observed in the total distance traveled, number of squares crossed, and entries in the center, and in all groups, no correlations were observed between contextual freezing on day 7 and open-field parameters. These results are following a previous study which showed that foot shocks associated with situational reminders did not affect the locomotor activity of male mice in an open field test performed 3–6 weeks after the first foot shock of the PTSD mice model (Pynoos et al., 1996). Thus, this seems to support the idea that the aversive procedure did not affect the animals' spontaneous locomotor activity (Li et al., 2006; Zhang et al., 2012). Also, Toth et al. (2013) have previously shown that Pnmt-KO mice did not show any alteration in spontaneous locomotor activity compared to WT mice, which is in agreement with our results.

Taking into consideration the contextual traumatic memory that arises from PTSD induction, we decided to investigate the hippocampal gene transcription to further understand the molecular basis of this pathology. It is known that the hippocampus is a brain structure involved in the formation of contextual fear memories and also that to form long-term memories there is a requirement for new gene transcription and protein synthesis (Flexner et al., 1963; Phillips and LeDoux, 1992). *Nr4a* genes are considered to be immediate early genes because their expression can be rapidly induced by different stimuli (Morgan and Curran, 1989). Previous studies showed *Nr4a* subfamily genes expression in the hippocampus to be upregulated after training of fear conditioning procedure

contributing to contextual memory consolidation on the next day (von Hertzen and Giese, 2005; Hawk and Abel, 2011; Hawk et al., 2012). Also, we have already shown that glucose may be a mediator of EPI in the central nervous system and could be important to induce the expression of the *Nr4a* family genes involved in contextual fear memories (Oliveira et al., 2018). The NR4A transcription factors induce the expression of several target genes, such as the brain-derived neurotrophic factor (*Bdnf*) gene suggested to play an important role in hippocampus-dependent contextual fear memory (Mizuno et al., 2012). Another gene target is proto-oncogene c-Rel which seems to be necessary for learning and consolidation of hippocampal-dependent memory (Ahn et al., 2008).

Three hours after day 0 of PTSD model induction we show an increase in *Nr4a2* and *Nr4a3* mRNA expression in the hippocampus of WT mice in the PTSD-induction group in comparison to control. Since WT mice in the PTSD-induction group exhibited higher freezing response after contextual exposure, these results suggest that *Nr4a2* and *Nr4a3* hippocampal mRNA expression might be involved in the consolidation of traumatic memories in PTSD on day 2. Moreover, *Nr4a1*, *Nr4a2*, and *Nr4a3* mRNA expression was not altered in the Pnmt-KO mice PTSD-induction group in comparison to control and this may contribute to lower contextual traumatic memory observed in these mice 2 days after PTSD induction. Since *Nr4a* subfamily genes are immediate early genes, they are more prone to change their expression only a few hours after the stimulus and afterward return to baseline levels (Morgan and Curran, 1989; von Hertzen and Giese, 2005; Hawk and Abel, 2011; Hawk et al., 2012). However, it remains unanswered if exposure to repeated situational reminders (days 2 and 7) is a sufficient stimulus to increase *Nr4a* subfamily genes expression again on day 2 and day 7. On day 7 of the PTSD induction model, WT mice maintained a high freezing response after contextual exposure, contrary to Pnmt-KO mice. Therefore, EPI seems to enhance the persistence of traumatic memories which may contribute to the dysfunction of these memories' extinction. This is in agreement with what is observed in patients with PTSD which show deficits in the extinction of traumatic memories (Lissek et al., 2005; Inslicht et al., 2013).

In conclusion, the decrease of freezing behavior presented by mice lacking endogenous EPI (Pnmt-KO mice) supports the idea that EPI may be required to the formation and persistence of contextual traumatic memories in PTSD through enhancement of the expression of *Nr4a2* and *Nr4a3* genes in the hippocampus. Peripheral administration of EPI restored traumatic memories in Pnmt-KO mice, which suggests a causal role for EPI. The persistence of contextual traumatic memories may contribute to anxiety-like behavior and resistance of traumatic memory extinction in this PTSD mice model.

DATA AVAILABILITY STATEMENT

The raw data supporting the conclusions of this article will be made available by the authors, without undue reservation.

ETHICS STATEMENT

The animal study was reviewed and approved by Organism Responsible for Animal Welfare in Faculty of Medicine of University of Porto and National Authority for Animal Health.

AUTHOR CONTRIBUTIONS

MM-R and RM conceived the study. RM performed most of the experiences and respective statistical analysis. AO, GC, MM, RS, and PS performed some experiences and respective statistical analysis. RM and MM-R reviewed the statistical analysis, interpreted results, and wrote the manuscript. All authors contributed to the article and approved the submitted version.

FUNDING

This work was partially supported by Foundation for Science and Technology (FCT) (project UIDB/04308/2020); RM and AO were in receipt of PhD studentships from FCT (SFRH/BD/133860/2017 and SFRH/BD/138984/2018, respectively).

ACKNOWLEDGMENTS

We thank Sónia Soares, Diogo Silva and António Carlos Ferreira for their technical support.

SUPPLEMENTARY MATERIAL

The Supplementary Material for this article can be found online at: https://www.frontiersin.org/articles/10.3389/fnmol.2020.588802/full#supplementary-material.

REFERENCES

Ahn, H. J., Hernandez, C. M., Levenson, J. M., Lubin, F. D., Liou, H. C., and Sweatt, J. D. (2008). c-Rel, an NF-kappaB family transcription factor, is required for hippocampal long-term synaptic plasticity and memory formation. *Learn. Mem.* 15, 539–549. doi: 10.1101/lm.866408

Alves, E., Lukoyanov, N., Serrao, P., Moura, D., and Moreira-Rodrigues, M. (2016). Epinephrine increases contextual learning through activation of peripheral β2-adrenoceptors. *Psychopharmacology* 233, 2099–2108. doi: 10.1007/s00213-016-4254-5

Aquilani, R., Iadarola, P., Boschi, F., Pistarini, C., Arcidiaco, P., and Contardi, A. (2003). Reduced plasma levels of tyrosine, precursor of brain catecholamines and of essential amino acids in patients with severe traumatic brain injury after rehabilitation. *Arch. Phys. Med. Rehabil.* 84, 1258–1265. doi: 10.1016/s0003-9993(03)00148-5

American Psychiatric Association. (2013). *Diagnostic and Statistical Manual of Mental Disorders: DSM-5*. 5th Edn. Washington, DC: American Psychiatric Association.

Bali, A., and Jaggi, A. S. (2015). Electric foot shock stress: a useful tool in neuropsychiatric studies. *Rev. Neurosci.* 26, 655–677. doi: 10.1515/revneuro-2015-0015

Bao, X., Lu, C. M., Liu, F., Gu, Y., Dalton, N. D., Zhu, B. Q., et al. (2007). Epinephrine is required for normal cardiovascular responses to stress in the phenylethanolamine *N*-methyltransferase knockout mouse. *Circulation* 116, 1024–1031. doi: 10.1161/CIRCULATIONAHA.107.696005

Cahill, L., and Alkire, M. T. (2003). Epinephrine enhancement of human memory consolidation: interaction with arousal at encoding. *Neurobiol. Learn. Mem.* 79, 194–198. doi: 10.1016/s1074-7427(02)00036-9

Christiansen, D. M., and Hansen, M. (2015). Accounting for sex differences in PTSD: a multi-variable mediation model. *Eur. J. Psychotraumatol.* 6:26068. doi: 10.3402/ejpt.v6.26068

Crawley, J. N. (1981). Neuropharmacologic specificity of a simple animal model for the behavioral actions of benzodiazepines. *Pharmacol. Biochem. Behav.* 15, 695–699. doi: 10.1016/0091-3057(81)90007-1

Crawley, J. N., Skolnick, P., and Paul, S. M. (1984). Absence of intrinsic antagonist actions of benzodiazepine antagonists on an exploratory model of anxiety in the mouse. *Neuropharmacology* 23, 531–537. doi: 10.1016/0028-3908(84)90026-1

Desmedt, A., Marighetto, A., and Piazza, P. V. (2015). Abnormal fear memory as a model for posttraumatic stress disorder. *Biol. Psychiatry* 78, 290–297. doi: 10.1016/j.biopsych.2015.06.017

Dornelles, A., de Lima, M. N. M., Grazziotin, M., Presti-Torres, J., Garcia, V. A., Scalco, F. S., et al. (2007). Adrenergic enhancement of consolidation of object recognition memory. *Neurobiol. Learn. Mem.* 88, 137–142. doi: 10.1016/j.nlm.2007.01.005

Ebert, S. N., Rong, Q., Boe, S., Thompson, R. P., Grinberg, A., and Pfeifer, K. (2004). Targeted insertion of the Cre-recombinase gene at the phenylethanolamine *N*-methyltransferase locus: a new model for studying the developmental distribution of adrenergic cells. *Dev. Dyn.* 231, 849–858. doi: 10.1002/dvdy.20188

Fanselow, M. S., DeCola, J. P., and Young, S. L. (1993). Mechanisms responsible for reduced contextual conditioning with massed unsignaled unconditional stimuli. *J. Exp. Psychol. Anim. Behav. Process.* 19, 121–137.

Fernandez, P. M., Brunel, F., Jimenez, M. A., Saez, J. M., Cereghini, S., and Zakin, M. M. (2000). Nuclear receptors Nor1 and NGFI-B/Nur77 play similar, albeit distinct, roles in the hypothalamo-pituitary-adrenal axis. *Endocrinology* 141, 2392–2400. doi: 10.1210/endo.141.7.7562

Flexner, J. B., Flexner, L. B., and Stellar, E. (1963). Memory in mice as affected by intracerebral puromycin. *Science* 141, 57–59. doi: 10.1126/science.141.3575.57

Foa, E. B., Steketee, G., and Rothbaum, B. O. (1989). Behavioral/cognitive conceptualizations of post-traumatic stress disorder. *Behav. Ther.* 20, 155–176. doi: 10.1016/s0005-7894(89)80067-x

Gisquet-Verrier, P., Botreau, F., Venero, C., and Sandi, C. (2004). Exposure to retrieval cues improves retention performance and induces changes in ACTH and corticosterone release. *Psychoneuroendocrinology* 29, 529–556. doi: 10.1016/s0306-4530(03)00085-4

Hawk, J. D., and Abel, T. (2011). The role of NR4A transcription factors in memory formation. *Brain Res. Bull.* 85, 21–29. doi: 10.1016/j.brainresbull.2011.02.001

Hawk, J. D., Bookout, A. L., Poplawski, S. G., Bridi, M., Rao, A. J., Sulewski, M. E., et al. (2012). NR4A nuclear receptors support memory enhancement by histone deacetylase inhibitors. *J. Clin. Invest.* 122, 3593–3602. doi: 10.1172/JCI64145

Hazel, T. G., Nathans, D., and Lau, L. F. (1988). A gene inducible by serum growth factors encodes a member of the steroid and thyroid hormone receptor superfamily. *Proc. Natl. Acad. Sci.* 85, 8444–8448. doi: 10.1073/pnas.85.22.8444

Henry, J., Rodriguez, A., and Wlodkowic, D. (2019). Impact of digital video analytics on accuracy of chemobehavioural phenotyping in aquatic toxicology. *PeerJ* 7:e7367. doi: 10.7717/peerj.7367

Ho, T., Fuxe, K., Goldstein, M., and Johansson, O. (1974). Immunohistochemical evidence for the existence of adrenaline neurons in the rat brain. *Brain Res.* 66, 235–251.

Honkaniemi, J., Kononen, J., Kainu, T., Pyykonen, I., and Pelto-Huikko, M. (1994). Induction of multiple immediate early genes in rat hypothalamic paraventricular nucleus after stress. *Brain Res. Mol. Brain Res.* 25, 234–241. doi: 10.1016/0169-328x(94)90158-9

Inoue, R., Talukdar, G., Takao, K., Miyakawa, T., and Mori, H. (2018). Dissociated role of D-serine in extinction during consolidation vs. reconsolidation of context conditioned fear. *Front. Mol. Neurosci.* 11:161. doi: 10.3389/fnmol.2018.00161

Inslicht, S. S., Metzler, T. J., Garcia, N. M., Pineles, S. L., Milad, M. R., Orr, S. P., et al. (2013). Sex differences in fear conditioning in posttraumatic stress disorder. *J. Psychiatr. Res.* 47, 64–71. doi: 10.1016/j.jpsychires.2012.08.027

Khan, M. G. (2006). "Cardiopulmonary resuscitation (CPR)," in *Encyclopedia of Heart Diseases*, ed. M. Gabriel Khan (Burlington, MA: Academic Press), 215–222.

Law, S. W., Conneely, O. M., DeMayo, F. J., and O'Malley, B. W. (1992). Identification of a new brain-specific transcription factor, NURR1. *Mol. Endocrinol.* 6, 2129–2135. doi: 10.1210/mend.6.12.1491694

Lee, J. L. (2008). Memory reconsolidation mediates the strengthening of memories by additional learning. *Nat. Neurosci.* 11, 1264–1266. doi: 10.1038/nn.2205

Lee, H. J., Berger, S. Y., Stiedl, O., Spiess, J., and Kim, J. J. (2001). Post-training injections of catecholaminergic drugs do not modulate fear conditioning in rats and mice. *Neurosci. Lett.* 303, 123–126. doi: 10.1016/s0304-3940(01)01733-5

Lemieux, A. M., and Coe, C. L. (1995). Abuse-related posttraumatic stress disorder: evidence for chronic neuroendocrine activation in women. *Psychosom. Med.* 57, 105–115. doi: 10.1097/00006842-199503000-00002

Lew, J. Y., Matsumoto, Y., Pearson, J., Goldstein, M., Hokfelt, T., and Fuxe, K. (1977). Localization and characterization of phenylethanolamine *N*-methyl transferase in the brain of various mammalian species. *Brain Res.* 119, 199–210. doi: 10.1016/0006-8993(77)90100-7

Li, S., Murakami, Y., Wang, M., Maeda, K., and Matsumoto, K. (2006). The effects of chronic valproate and diazepam in a mouse model of posttraumatic stress disorder. *Pharmacol. Biochem. Behav.* 85, 324–331. doi: 10.1016/j.pbb.2006.08.015

Lipov, E. (2014). Post traumatic stress disorder (PTSD) as an over activation of sympathetic nervous system: an alternative view. *Trauma Treat.* 3, 1–3. doi: 10.4172/2167-1222.1000181

Lissek, S., Powers, A. S., McClure, E. B., Phelps, E. A., Woldehawariat, G., Grillon, C., et al. (2005). Classical fear conditioning in the anxiety disorders: a meta-analysis. *Behav. Res. Ther.* 43, 1391–1424. doi: 10.1016/j.brat.2004.10.007

Liu, Z.-G., Smith, S. W., McLaughlin, K. A., Schwartz, L. M., and Osborne, B. A. (1994). Apoptotic signals delivered through the T-cell receptor of a T-cell hybrid require the immediate-early gene Nur77. *Nature* 367, 281–284. doi: 10.1038/367281a0

Louvart, H., Maccari, S., Lesage, J., Léonhardt, M., Dickes-Coopman, A., and Darnaudéry, M. (2006). Effects of a single footshock followed by situational reminders on HPA axis and behaviour in the aversive context in male and female rats. *Psychoneuroendocrinology* 31, 92–99. doi: 10.1016/j.psyneuen.2005.05.014

Maercker, A., Brewin, C. R., Bryant, R. A., Cloitre, M., van Ommeren, M., Jones, L. M., et al. (2013). Diagnosis and classification of disorders specifically associated with stress: proposals for ICD-11. *World Psychiatry* 12, 198–206. doi: 10.1002/wps.20057

Maira, M., Martens, C., Philips, A., and Drouin, J. (1999). Heterodimerization between members of the Nur subfamily of orphan nuclear receptors as a novel mechanism for gene activation. *Mol. Cell Biol.* 19, 7549–7557. doi: 10.1128/mcb.19.11.7549

McClintock, M. K. (1978). Estrous synchrony and its mediation by airborne chemical communication (*Rattus norvegicus*). *Horm. Behav.* 10, 264–275. doi: 10.1016/0018-506x(78)90071-5

Mefford, I. N. (1987). Are there epinephrine neurons in rat brain? *Brain Res. Rev.* 12, 383–395.

Mendes, P., Martinho, R., Leite, S., Leite-Moreira, A., Lourenco, A., and Moreira-Rodrigues, M. (2016). Exercise-induced hypertension and cardiac hypertrophy in epinephrine-deficient mice. *J. Hypertens.* 34:e98. doi: 10.1097/01.hjh.0000491586.92904.fb

Mendes, P., Martinho, R., Leite, S., Maia-Moço, L., Leite-Moreira, A. F., Lourenço, A. P., et al. (2018). Chronic exercise induces pathological left ventricular hypertrophy in adrenaline-deficient mice. *Int. J. Cardiol.* 253, 113–119. doi: 10.1016/j.ijcard.2017.10.014

Mizuno, K., Dempster, E., Mill, J., and Giese, K. P. (2012). Long-lasting regulation of hippocampal Bdnf gene transcription after contextual fear conditioning. *Genes Brain Behav.* 11, 651–659. doi: 10.1111/j.1601-183X.2012.00805.x

Moreira-Rodrigues, M., Graca, A. L., Ferreira, M., Afonso, J., Serrao, P., Morato, M., et al. (2014). Attenuated aortic vasodilation and sympathetic

prejunctional facilitation in epinephrine-deficient mice: selective impairment of beta2-adrenoceptor responses. *J. Pharmacol. Exp. Ther.* 351, 243–249. doi: 10.1124/jpet.114.217281

Moreira-Rodrigues, M., Quelhas-Santos, J., Roncon-Albuquerque, R., Serrao, P., Leite-Moreira, A., Sampaio-Maia, B., et al. (2012). Blunted renal dopaminergic system in a mouse model of diet-induced obesity. *Exp. Biol. Med.* 237, 949–955. doi: 10.1258/ebm.2012.012077

Moreira-Rodrigues, M., Quelhas-Santos, J., Serrão, P., Fernandes-Cerqueira, C., Sampaio-Maia, B., and Pestana, M. (2010). Glycaemic control with insulin prevents the reduced renal dopamine D1 receptor expression and function in streptozotocin-induced diabetes. *Nephrol. Dial. Transplant.* 25, 2945–2953. doi: 10.1093/ndt/gfq150

Moreira-Rodrigues, M., Roncon-Albuquerque, R. Jr., Henriques-Coelho, T., Lourenco, A. P., Sampaio-Maia, B., Santos, J., et al. (2007a). Cardiac remodeling and dysfunction in nephrotic syndrome. *Kidney Int.* 71, 1240–1248. doi: 10.1038/sj.ki.5002204

Moreira-Rodrigues, M., Sampaio-Maia, B., Moura, M., and Pestana, M. (2007b). Renal dopaminergic system activity in uninephrectomized rats up to 26 weeks after surgery. *Am. J. Nephrol.* 27, 232–239. doi: 10.1159/000101368

Morgan, J. I., and Curran, T. (1989). Stimulus-transcription coupling in neurons: role of cellular immediate-early genes. *Trends Neurosci.* 12, 459–462. doi: 10.1016/0166-2236(89)90096-9

Morris, K. A., Li, S., Bui, D. D., and Gold, P. E. (2013). Glucose attenuates impairments in memory and CREB activation produced by an α4β2 but not an α7 nicotinic receptor antagonist. *Neuropharmacology* 67, 233–242. doi: 10.1016/j.neuropharm.2012.11.008

Murphy, E. P., and Conneely, O. M. (1997). Neuroendocrine regulation of the hypothalamic pituitary adrenal axis by the nurr1/nur77 subfamily of nuclear receptors. *Mol. Endocrinol.* 11, 39–47.

Ohkura, N., Ito, M., Tsukada, T., Sasaki, K., Yamaguchi, K., and Miki, K. (1996). Structure, mapping and expression of a human NOR-1 gene, the third member of the Nur77/NGFI-B family. *Biochim. Biophys. Acta* 1308, 205–214. doi: 10.1016/0167-4781(96)00101-7

Olff, M. (2017). Sex and gender differences in post-traumatic stress disorder: an update. *Eur. J. Psychotraumatol.* 8:1351204. doi: 10.1080/20008198.2017.1351204

Oliveira, A., Martinho, R., Serrão, P., and Moreira-Rodrigues, M. (2018). Epinephrine released during traumatic events may strengthen contextual fear memory through increased hippocampus mRNA expression of Nr4a transcription factors. *Front. Mol. Neurosci.* 11:334. doi: 10.3389/fnmol.2018.00334

Pawlyk, A. C., Jha, S. K., Brennan, F. X., Morrison, A. R., and Ross, R. J. (2005). A rodent model of sleep disturbances in posttraumatic stress disorder: the role of context after fear conditioning. *Biol. Psychiatry* 57, 268–277. doi: 10.1016/j.biopsych.2004.11.008

Pei, L., Waki, H., Vaitheesvaran, B., Wilpitz, D. C., Kurland, I. J., and Tontonoz, P. (2006). NR4A orphan nuclear receptors are transcriptional regulators of hepatic glucose metabolism. *Nat. Med.* 12, 1048–1055. doi: 10.1038/nm1471

Pellow, S., Chopin, P., File, S. E., and Briley, M. (1985). Validation of open:closed arm entries in an elevated plus-maze as a measure of anxiety in the rat. *J. Neurosci. Methods* 14, 149–167. doi: 10.1016/0165-0270(85)90031-7

Phillips, R. G., and LeDoux, J. E. (1992). Differential contribution of amygdala and hippocampus to cued and contextual fear conditioning. *Behav. Neurosci.* 106, 274–285. doi: 10.1037//0735-7044.106.2.274

Pitman, R. K. (1989). Post-traumatic stress disorder, hormones and memory. *Biol. Psychiatry* 26, 221–223. doi: 10.1016/0006-3223(89)90033-4

Pitman, R. K., and Delahanty, D. L. (2005). Conceptually driven pharmacologic approaches to acute trauma. *CNS Spectr.* 10, 99–106. doi: 10.1017/s109285290001943x

Pitman, R. K., Rasmusson, A. M., Koenen, K. C., Shin, L. M., Orr, S. P., Gilbertson, M. W., et al. (2012). Biological studies of post-traumatic stress disorder. *Nat. Rev. Neurosci.* 13, 769–787. doi: 10.1038/nrn3339

Pole, N. (2007). The psychophysiology of posttraumatic stress disorder: a meta-analysis. *Psychol. Bull.* 133, 725–746. doi: 10.1037/0033-2909.133.5.725

Popovitz, J., Mysore, S. P., and Adwanikar, H. (2019). Long-term effects of traumatic brain injury on anxiety-like behaviors in mice: behavioral and neural correlates. *Front. Behav. Neurosci.* 13:6. doi: 10.3389/fnbeh.2019.00006

Porhomayon, J., Kolesnikov, S., and Nader, N. D. (2014). The impact of stress hormones on post-traumatic stress disorders symptoms and memory in cardiac surgery patients. *J. Cardiovasc. Thorac. Res.* 6, 79–84. doi: 10.5681/jcvtr.2014.018

Przybyslawski, J., Roullet, P., and Sara, S. J. (1999). Attenuation of emotional and nonemotional memories after their reactivation: role of beta adrenergic receptors. *J. Neurosci.* 19, 6623–6628. doi: 10.1523/JNEUROSCI.19-15-06623.1999

Pynoos, R. S., Ritzmann, R. F., Steinberg, A. M., Goenjian, A., and Prisecaru, I. (1996). A behavioral animal model of posttraumatic stress disorder featuring repeated exposure to situational reminders. *Biol. Psychiatry* 39, 129–134. doi: 10.1016/0006-3223(95)00088-7

Rau, V., DeCola, J. P., and Fanselow, M. S. (2005). Stress-induced enhancement of fear learning: an animal model of posttraumatic stress disorder. *Neurosci. Biobehav. Rev.* 29, 1207–1223. doi: 10.1016/j.neubiorev.2005.04.010

Rocinholi, L. F., Almeida, S. S., and De-Oliveira, L. M. (1997). Response threshold to aversive stimuli in stimulated early protein-malnourished rats. *Braz. J. Med. Biol. Res.* 30, 407–413. doi: 10.1590/s0100-879x1997000300016

Rodriguez, A., Zhang, H., Klaminder, J., Brodin, T., and Andersson, M. (2017). ToxId: an efficient algorithm to solve occlusions when tracking multiple animals. *Sci. Rep.* 7:14774. doi: 10.1038/s41598-017-15104-2

Rodriguez, A., Zhang, H., Klaminder, J., Brodin, T., Andersson, P. L., and Andersson, M. (2018). ToxTrac: a fast and robust software for tracking organisms. *Methods Ecol. Evol.* 9, 460–464. doi: 10.1111/2041-210x.12874

Rojas, P., Joodmardi, E., Hong, Y., Perlmann, T., and Ogren, S. O. (2007). Adult mice with reduced Nurr1 expression: an animal model for schizophrenia. *Mol. Psychiatry* 12, 756–766. doi: 10.1038/sj.mp.4001993

Sartori, S. B., Hauschild, M., Bunck, M., Gaburro, S., Landgraf, R., and Singewald, N. (2011). Enhanced fear expression in a psychopathological mouse model of trait anxiety: pharmacological interventions. *PLoS One* 6:e16849. doi: 10.1371/journal.pone.0016849

Schank, J. C., and McClintock, M. K. (1992). A coupled-oscillator model of ovarian-cycle synchrony among female rats. *J. Theor. Biol.* 157, 317–362. doi: 10.1016/s0022-5193(05)80614-9

Shalev, A. Y., Videlock, E. J., Peleg, T., Segman, R., Pitman, R. K., and Yehuda, R. (2008). Stress hormones and post-traumatic stress disorder in civilian trauma victims: a longitudinal study. Part I: HPA axis responses. *Int. J. Neuropsychopharmacol.* 11, 365–372. doi: 10.1017/S1461145707008127

Siegmund, A., and Wotjak, C. T. (2007). A mouse model of posttraumatic stress disorder that distinguishes between conditioned and sensitised fear. *J. Psychiatr. Res.* 41, 848–860. doi: 10.1016/j.jpsychires.2006.07.017

Takao, K., and Miyakawa, T. (2006). Light/dark transition test for mice. *J. Vis. Exp.* 1:104. doi: 10.3791/104

Tolin, D. F., and Foa, E. B. (2006). Sex differences in trauma and posttraumatic stress disorder: a quantitative review of 25 years of research. *Psychol. Bull.* 132, 959–992. doi: 10.1037/0033-2909.132.6.959

Toth, M., Ziegler, M., Sun, P., Gresack, J., and Risbrough, V. (2013). Impaired conditioned fear response and startle reactivity in epinephrine-deficient mice. *Behav. Pharmacol.* 24, 1–9. doi: 10.1097/FBP.0b013e32835cf408

Valentinuzzi, V. S., Kolker, D. E., Vitaterna, M. H., Shimomura, K., Whiteley, A., Low-Zeddies, S., et al. (1998). Automated measurement of mouse freezing behavior and its use for quantitative trait locus analysis of contextual fear conditioning in (BALB/cJ × C57BL/6J)F_2 mice. *Learn. Mem.* 5, 391–403.

van der Kolk, B. (2000). Posttraumatic stress disorder and the nature of trauma. *Dialogues Clin. Neurosci.* 2, 7–22.

Verma, M., Bali, A., Singh, N., and Jaggi, A. S. (2016). Investigating the role of nisoldipine in foot-shock-induced post-traumatic stress disorder in mice. *Fundam. Clin. Pharmacol.* 30, 128–136. doi: 10.1111/fcp.12174

von Hertzen, L. S. J., and Giese, K. P. (2005). Memory reconsolidation engages only a subset of immediate-early genes induced during consolidation. *J. Neurosci.* 25, 1935–1942. doi: 10.1523/JNEUROSCI.4707-04.2005

Weil-Malherbe, H., Axelrod, J., and Tomchick, R. (1959). Blood-brain barrier for adrenaline. *Science* 129, 1226–1227. doi: 10.1126/science.129.3357.1226

Wilson, T. E., Mouw, A. R., Weaver, C. A., Milbrandt, J., and Parker, K. L. (1993). The orphan nuclear receptor NGFI-B regulates expression of the gene encoding steroid 21-hydroxylase. *Mol. Cell. Biol.* 13, 861–868. doi: 10.1128/mcb.13.2.861

Woronicz, J. D., Calnan, B., Ngo, V. U., and Winoto, A. (1994). Requirement for the orphan steroid receptor Nur77 in apoptosis of T-cell hybridomas. *Nature* 367, 277–281. doi: 10.1038/367277a0

Wurtman, R. J., and Fernstrom, J. D. (1975). Control of brain monoamine synthesis by diet and plasma amino acids. *Am. J. Clin. Nutr.* 28, 638–647. doi: 10.1093/ajcn/28.6.638

Yehuda, R., Hoge, C. W., McFarlane, A. C., Vermetten, E., Lanius, R. A., Nievergelt, C. M., et al. (2015). Post-traumatic stress disorder. *Nat. Rev. Dis. Prim.* 1:15057. doi: 10.1038/nrdp.2015.57

Yehuda, R., Southwick, S., Giller, E. L., Ma, X., and Mason, J. W. (1992). Urinary catecholamine excretion and severity of PTSD symptoms in Vietnam combat veterans. *J. Nerv. Ment. Dis.* 180, 321–325. doi: 10.1097/00005053-199205000-00006

Zhang, L.-M., Yao, J.-Z., Li, Y., Li, K., Chen, H.-X., Zhang, Y.-Z., et al. (2012). Anxiolytic effects of flavonoids in animal models of posttraumatic stress disorder. *Evid. Based Complement. Alternat. Med.* 2012:623753. doi: 10.1155/2012/623753

Conflict of Interest: The authors declare that the research was conducted in the absence of any commercial or financial relationships that could be construed as a potential conflict of interest.

frontiers in Molecular Neuroscience

MINI REVIEW
published: 16 July 2021
doi: 10.3389/fnmol.2021.689495

Investigating Post-translational Modifications in Neuropsychiatric Disease: The Next Frontier in Human Post-mortem Brain Research

*Melanie J. Grubisha[1], Robert A. Sweet[1] and Matthew L. MacDonald[1,2]**

[1] Department of Psychiatry, University of Pittsburgh, Pittsburgh, PA, United States, [2] Biomedical Mass Spectrometry Center, University of Pittsburgh, Pittsburgh, PA, United States

Gene expression and translation have been extensively studied in human post-mortem brain tissue from subjects with psychiatric disease. Post-translational modifications (PTMs) have received less attention despite their implication by unbiased genetic studies and importance in regulating neuronal and circuit function. Here we review the rationale for studying PTMs in psychiatric disease, recent findings in human post-mortem tissue, the required controls for these types of studies, and highlight the emerging mass spectrometry approaches transforming this research direction.

Keywords: proteomics, post-translational modification, schizophrenia, psychiatric disease, autism, post-mortem brain

OPEN ACCESS

Edited by:
Verena Tretter,
Medical University of Vienna, Austria

Reviewed by:
Stephen D. Ginsberg,
Nathan Kline Institute for Psychiatric Research, United States
Jose F. Maya-Vetencourt,
Italian Institute of Technology (IIT), Italy

***Correspondence:**
Matthew L. MacDonald
macdonaldml@upmc.edu

Specialty section:
This article was submitted to Brain Disease Mechanisms, a section of the journal Frontiers in Molecular Neuroscience

Received: *01 April 2021*
Accepted: *18 June 2021*
Published: *16 July 2021*

Citation:
Grubisha MJ, Sweet RA and MacDonald ML (2021) Investigating Post-translational Modifications in Neuropsychiatric Disease: The Next Frontier in Human Post-mortem Brain Research. Front. Mol. Neurosci. 14:689495. doi: 10.3389/fnmol.2021.689495

INTRODUCTION

Psychiatric disease imparts a substantial burden on the global population. For example, depression (Liu et al., 2020), schizophrenia (Charlson et al., 2018), bipolar disorder (Ferrari et al., 2016), and autism spectrum disorder (Baxter et al., 2015) are estimated to collectively impair the lives of over 350 million individuals across the globe, with limited treatment options and a relatively small number of compounds in FDA trials (O'Brien et al., 2014). Thus, psychiatric disease is deservedly the focus of intense scientific study. Psychiatric disorders have varying levels of heritability (Brainstorm et al., 2018) and genome wide association studies (GWAS) have identified risk loci for some, such as schizophrenia (Schizophrenia Working Group of the Psychiatric Genomics Consortium, 2014) and autism spectrum disorder (Grove et al., 2019). Studies in live patients [e.g., TMS, EEG (Vittala et al., 2020), and fMRI (Chen et al., 2011; Birur et al., 2017; Lau et al., 2019)] and of post-mortem brain tissue have found distinct impairments in discreet brain areas (Minzenberg et al., 2009), circuits (Eggan et al., 2012; Glausier et al., 2014; Lewis and Glausier, 2016), and cellular structures (Somerville et al., 2011; Shelton et al., 2015; Glausier et al., 2017; MacDonald et al., 2017; Uranova et al., 2018; McKinney et al., 2019) that could plausibly underlie disease symptoms. For example, individuals with schizophrenia display impairments in working memory tasks (Minzenberg et al., 2009), which are associated with altered activation of the dorsolateral prefrontal cortex (Minzenberg et al., 2009)

as well as impairments in the processing of auditory sensory information (Javitt et al., 1995, 1997, 2000; Rabinowicz et al., 2000) which are associated with altered event-related potentials localized to the primary auditory cortex (Javitt et al., 1996; Lewis and Sweet, 2009). Alterations in dendritic spine density have been reproducibly observed in layer 3 of both the dorsolateral prefrontal cortex (Glantz and Lewis, 2000; Kolluri et al., 2005) and primary auditory cortex (Sweet et al., 2009; Shelton et al., 2015; MacDonald et al., 2017; McKinney et al., 2019) and are believed to contribute to the observed impairments in working memory and auditory sensory processing. It is important to note that the limited studies that have investigated layer 5 in a cortical region did not observe decreased spine density (Kolluri et al., 2005). Additionally, studies a have also not found a concurrent decrease in presynaptic boutons in layer 3 of cortical regions (Moyer et al., 2013). Thus, synaptic alterations in cortical regions in schizophrenia are limited to specific layers and structures. Interesting, subcortical regions appear to have distinct pathologies. For example, while the hippocampus displays similar decreases in dendritic spine density (Rosoklija et al., 2000), it displays different activity alterations and GABA cell pathology (Heckers and Konradi, 2015). Thus, it is essential to investigate the molecular pathology of individual brain areas, layers, cell types, and cellular structures. Alterations in dendritic spines have also been observed in bipolar disorder (Konopaske et al., 2014) and autism spectrum disorder (Martinez-Cerdeno, 2017).

While many areas of research benefit greatly from the use of animal models, polygenetic psychiatric disorders are difficult, if not impossible to model in animals, complicating the investigation of disease etiology. In an effort to elucidate the molecular mechanisms driving these structural and functional impairments the field has turned to transcriptomic and proteomic analyses of human post-mortem brain tissue to quantify disease associated differences in transcripts (Hernandez et al., 2021) and proteins (Martins-de-Souza, 2012; Focking et al., 2015; MacDonald et al., 2019b), providing many valuable insights into disease pathology.

More recently, multi-omics analyses, grounded in GWAS, have identified quantitative trait loci (QTLs) for common risk variants associated with gene expression (eQTLs) (Gandal et al., 2018) and protein levels (pQTLs) (Robins et al., 2019). eQTL studies have started to provide insight into the biological effects of common risk loci. To date at least one human brain pQTL study has been published, finding that only a subset of pQTLs were also eQTLs (Robins et al., 2019), highlighting the disconnect between the transcriptome and the proteome. Several groups are currently pursuing well powered proteomic investigations of the human brain, suggesting that additional proteogenomic studies will further map associations between common variants and protein expression in psychiatric disease. While these studies are powerful, they fail to capture the more dynamic aspects of the proteome, such as post-translational modifications (PTMs), that are among the final mediators of cell and circuit activity, and are difficult, if not impossible, to infer from the transcript or protein levels.

Post-translational modifications have been studied in neurological disorders, most notably Tau hyperphosphorylation in Tauopathies such as Alzheimer's disease (Avila, 2006; Neddens et al., 2018), but they have received less attention in psychiatric disease and their study in human post-mortem brain tissue is often viewed with skepticism. This skepticism is not entirely unwarranted, as many PTMs are highly dynamic. However, many are stable post-mortem and, as PTMs regulate protein activity, this information is likely more valuable than protein levels alone. Here we review the rationale for studying PTMs in psychiatric disease, recent findings in human post-mortem brain tissue, the common pitfalls and required controls for these types of studies, and highlight the emerging mass spectrometry approaches transforming this research direction.

PTMs ARE IMPLICATED IN PSYCHIATRIC DISEASE

Unbiased genetic analyses firmly implicate PTMs in the etiology of a number of psychiatric diseases. The most recent report from The Schizophrenia Working Group of the Psychiatric Genomics Consortium et al. (2020) identified 130 genes with common non-coding variation associated with schizophrenia, including seven protein kinases/phosphatases (AKT3, MOB4, DCLK3, PTPRK, PAK6, FHIT, and MAPK3), a proteasome subunit (PSMA4), and a ubiquitin ligase (PJA1) (The Schizophrenia Working Group of the Psychiatric Genomics Consortium et al., 2020). Similarly, of the 209 genes currently implicated in Autism Spectrum Disorder with high confidence (as currently defined by SFARI), 16 are kinases/phosphatases (BCKDK, BRSK2, CASK, CDKL5, CSNK2A1, DMPK, DYRK1A, PPP2R5D, PPP1R9B, PPP5C, PTEN, PTK7, PTPN11, TAOK1, TLK2, and TEK), three are ubiquitin ligases (HECTD4, UBE3A, and UBR1), and one is a proteasome subunit (PSMD12) (Foundation SFARI, 2021).

Investigations of transcript levels in human post-mortem brain tissue from autism spectrum disorder and schizophrenia subjects further implicate PTMs. The most recent meta-analysis of RNAseq studies from PsychENCODE (Gandal et al., 2018) found that 52 protein kinases, 14 protein phosphatases, 9 proteasome subunits, and 22 ubiquitin ligases were differentially expressed in autism spectrum disorder (Gandal et al., 2018); while 123 protein kinases, 41 protein phosphatases, 7 proteasome subunits, and 62 ubiquitin ligases were differently expressed in schizophrenia (Gandal et al., 2018).

These findings are not surprising as schizophrenia and autism spectrum disorder are both widely viewed as developmental synaptopathies (Grant, 2012; Won et al., 2013; Washbourne, 2015; Guang et al., 2018) and a multitude of studies have demonstrated the essential roles of protein phosphorylation and the ubiquitin-proteasome system in synaptic plasticity, long term potentiation, and learning (Roche et al., 1994; Lee, 2006; Mabb and Ehlers, 2010; Kwon and Sabatini, 2011; Woolfrey and Dell'Acqua, 2015; Hegde, 2017). As stated above, while these genetic and transcriptomic investigations can, and have, implicated specific classes of PTMs and enzymes, they cannot capture their effects on the broader synaptic proteome. Furthermore, while altered levels of a given kinase or ubiquitin ligase can be modeled in cell culture or animal models, the

complex genetic risk factors and environmental circumstances that give rise to psychiatric disease, as well as the unique circuitry and neuronal populations of the human brain, cannot. It is important to note here that neurons and organoids derived from patient pluripotent stem cells can mimic the genetic risk profiles of psychiatric disease and provide a powerful window into pathological neurodevelopmental processes (Brennand et al., 2011; Khakipoor et al., 2020; Marton and Pasca, 2020). However, these models still lack the longevity of human adolescence and adulthood as well as interactions with systemic features (e.g., circulating hormones or the microbiome) and environmental risk factors. Thus, post-mortem brain studies are essential to investigating the molecular changes associated with psychiatric disease. In next section we will seek to answer the following questions: Can disease associated PTM differences be observed in human post-mortem brain tissue and do these PTMs have biological validity. The history of Tau gives us some hope that PTMs observed in human post-mortem brain tissue can yield insights into disease etiology (Simic et al., 2016).

A BRIEF HISTORY OF MODERN PTM STUDIES IN SCHIZOPHRENIA AND OTHER PSYCHOSIS RELATED DISORDERS

By the early 2000s dendritic spines (Glantz and Lewis, 2000) and NMDA receptors (Tsai et al., 1998; Thaker and Carpenter, 2001) had been implicated in schizophrenia pathology. As the decade progressed, genetic, transcriptomic, and early mass spectrometry studies continued to implicate postsynaptic ligands, receptors, and scaffolding proteins, such as ERBB4 (Silberberg et al., 2006), AKT (Matsubara et al., 2001; Emamian et al., 2004a; Ikeda et al., 2004; Turunen et al., 2007), NRG1 (Stefansson et al., 2002, 2003; Williams et al., 2003; Yang et al., 2003), and PSD95 (Ohnuma et al., 2000) in schizophrenia. Several groups then began utilizing traditional antibody-based approaches and eventually mass spectrometry for targeted phospho-analyses in patient tissue.

Emamian et al. (2004b) found that phosphorylation of NR1 S897 was decreased (while total NR1 levels were unaltered) in frontal cortex tissue from individuals with schizophrenia. This site was of particular interest as antipsychotic drugs were known to increase NR1 S897 phosphorylation in primary neuronal cultures (Leveque et al., 2000) and S897 is essential for antipsychotic drug-mediated gene expression (Leveque et al., 2000). A later study further demonstrated S897's importance in NMDAR synaptic incorporation, NMDAR-mediated synaptic transmission, AMPA receptor mediated synaptic transmission, and long-term potentiation (Li et al., 2009). Pinacho et al. (2015) found that S770 phosphorylation on the transcription factor SP4 was positively correlated with negative symptoms in schizophrenia subjects. Importantly, they also found that SP4 phosphorylation was inversely correlated with SP4 levels. SP4 regulates dendritic arborization (Ramos et al., 2007) and phosphorylation at SP4 S770 regulates stability of the protein (Pinacho et al., 2015). More recently, Vanderplow et al. (2021) found that phosphorylation of PI3K, AKT, and MTOR was decreased in cortical tissue from a subset of subjects with bipolar disorder. Subsequent studies in mice found that overexpression of dominant negative AKT impaired dendritic spine maintenance and performance in cognitive tasks (Vanderplow et al., 2021).

Finally, Grubisha et al. (2021) used mass spectrometry-based proteomics to investigate 18 phosphorylation sites on MAP2 in cortical tissue from schizophrenia subjects, finding differential phosphorylation at 9 while total levels of MAP2 were unaltered. Generating a transgenic mouse containing a phosphomimetic mutation at S1782 (S1782E) they found reductions in basilar dendritic length and complexity along with reduced spine density (Grubisha et al., 2021).

The studies above measured static phosphorylations, presumably preserved at death. But a few adventurous groups have pushed these studies further, attempting to capture dynamic phosphorylation activities in human post-mortem brain tissue. In two publications, Hahn and Wang combined targeted phosphorylation studies with a post-mortem tissue-stimulation paradigm to identify phosphorylation differences in schizophrenia after receptor stimulation (Hahn et al., 2006; Wang et al., 2020). In the first study they found that NRG1 stimulation of ERBB4 decreased glutamate/glycine induced phosphorylation of NMDAR2A and PLCγ, likely driven by increased association between ERBB4 and PSD95, but independent of the levels of any of the assayed proteins (Hahn et al., 2006). In the second study, they observed increased phosphorylation of mGluR5 after stimulation, which was accompanied by decreased coupling with Gq/11, indicating decreased mGluR5 activity, again independent of the levels of any of the assayed proteins. Taking a different approach, McGuire et al. (2014, 2017) utilized kinase arrays to interrogate signaling cascades in cortical tissue from schizophrenia subjects, finding significant alterations in kinome activity that further implicate cellular and ion homeostasis as well as cytoskeletal organization in schizophrenia.

A key driver underlying the incomplete correlation between mRNA and protein abundance is the fact that protein turnover is dynamic. The principal mechanism of turnover is the ubiquitin-proteasome system in which polyubiquitinated proteins are targeted to the proteasome for degradation. Additionally, the ubiquitin-proteasome system regulates synaptic protein stability and is essential for LTP and learning (Mabb and Ehlers, 2010; Hegde, 2017). Thus, while it has received less attention than phosphorylation, the ubiquitin-proteasome system is beginning to be investigated in schizophrenia. Rubio et al. (2013) first observed differences in both free and protein ubiquitination. More recently, Nucifora et al. (2019) found that increased protein ubiquitination was correlated with increased protein insolubility in cortical tissue from schizophrenia subjects. Finally, paralleling the kinome arrays used to assess kinase activity in schizophrenia, Scott and Meador-Woodruff (2020) utilized proteasome activity assays, finding altered trypsin and chymotrypsin like activity in schizophrenia tissue.

While this review has focused on ubiquitination and phosphorylation a growing body of work implicates additional PTMs such as glycosylation and myristylation in schizophrenia,

reviewed in detail in Mueller and Meador-Woodruff (2020). Briefly, alterations in N-Glycosylation on GABA (Mueller et al., 2014), NMDA (Tucholski et al., 2013b), and AMPA (Tucholski et al., 2013a) receptors have been observed in schizophrenia.

The studies reviewed above suggest several points: (1) That differences in PTMs can be observed in brain tissue from subjects with psychiatric disease; (2) that levels of multiple classes of PTMs are altered across multiple protein families; and (3) when tested in forward genetic models, individual PTMs can significantly impact disease relevant biology such as glutamatergic signaling and dendritic spine plasticity, that could not be predicted by genetics, transcriptomics, or even protein quantification. For example, MAP2 is not found at any schizophrenia risk loci and its protein levels are unaltered in schizophrenia tissue, yet it is hyperphosphorylated at multiple sites in schizophrenia and modeling just one of these sites induces a loss of dendritic spines.

The breadth of the PTM alterations observed in schizophrenia *via* mostly targeted approaches highlights the need for broad and systematic investigations of PTMs in psychiatric disease. Specifically, next generation studies should be rigorously designed to catalog post-mortem effects on individual PTM sites, be performed in well powered and well-balanced cohorts, utilize state-of-the-art mass spectrometry approaches, target selected brain areas, cortical layers, cell types, and microdomains, and take advantage of new informatic and statistical approaches to multi-omic integration to map associations between genes, multiple PTMs, and phenotypes.

EXPERIMENTAL CONSIDERATIONS FOR INVESTIGATING PTMs in POST-MORTEM BRAIN TISSUE

The impact of post-mortem interval (PMI; the time between when a subject becomes deceased and the brain tissue is fixed and/or frozen) on molecular integrity has long been appreciated and three main strategies have been employed to account and control for this confound. (1) The effect of PMI on individual PTM sites can be modeled, using either mouse (MacDonald et al., 2019b) or human (Gallego Romero et al., 2014; Jaffe et al., 2017) tissue. Several groups have used this approach to either correct for mRNA degradation (Jaffe et al., 2017) in human studies or to identify proteins that degrade non-linearly (MacDonald et al., 2019b) across PMI for removal from case-control statistical comparisons. The same approach should be employed in PTM studies in human post-mortem brain tissue, identifying which specific modifications at which sites degrade non-linearly over time. (2) PMI is often included as a co-factor in statistical analysis. (3) When possible, diagnostic groups or subject pairs should be matched as closely as possible for PMI [as well as other factors that are known to impact proteins and PTMs such as sex (Bangasser et al., 2017) and age (Carlyle et al., 2017)]. Given the dynamic nature of many PTMs, all of these approaches should be utilized, and it is especially important to identify PTMs that are rapidly degraded early in PMI and to remove them from downstream statistical analyses. In the past, generating a well-balanced and powered cohort was a significant challenge, but with the recent unification of multiple brain tissue repositories under the aegis of the NIH NeuroBioBank, researchers now have access to quality tissue from thousands of well cataloged cases and appropriate controls.

EMERGING MASS SPECTROMETRY APPROACHES FOR PTM QUANTIFICATION IN POST-MORTEM BRAIN TISSUE

Advances in mass spectrometry instrumentation and sample preparation techniques continue to increase the throughput, breadth and depth of PTM coverage, and some of these approaches have begun to see use in human post-mortem brain tissue. Next generation proteomics instruments such as the timsTOF (Bruker) and Orbitrap instruments (ThermoFisher) with increased scan speeds facilitate deep coverage of modified peptides. For example, Ping et al. (2020) utilized a tandem mass tag (TMT) based approach to quantify over 48,000 phosphopeptides (representing over 33,000 unique phosphorylation sites) in human post-mortem brain tissue. In addition to increased instrument speed and sensitivity, modern mass spectrometers now offer an array of dissociation methods (e.g., CID, HCD, and ETD) enhancing the identification, and subsequent quantification, of high energy and complex PTMs, such as phosphorylation (Jedrychowski et al., 2011; Potel et al., 2019) and glycosylation (Reiding et al., 2018; Riley et al., 2020).

Protocols to enrich phosphopeptides and glycopeptides from tryptic digests are now well developed and can be accomplished with high efficiency using commercially available kits and specialized liquid handling robots with pre-programmed proteomic applications, such as the AssayMAP BRAVO (Agilent), enabling both throughput and quantitative depth. Quantification of protein ubiquitination initially proved more challenging in standard proteomic work flows as trypsin digests off the larger ubiquitin side chain leaving only a lysine bound gly-gly which was difficult to capture. However, the recent availability of commercial antibodies and refined sample preparation now allow for deep profiling of protein ubiquitination in human samples as well; for example, over 14,000 ubiquitination sites were recently quantified in human tumor cells (Udeshi et al., 2020).

THE SPATIAL RESOLUTION LIMITS OF PTM QUANTIFICATION IN THE HUMAN BRAIN

As reviewed above, the activity, structure, and molecular pathologies associated with psychiatric illness are highly spatially localized, displaying brain area, layer, cellular, and microdomain specificity. Multiple groups have used mass spectrometry to quantify protein levels in cortical layer captures (Pabba et al., 2017; MacDonald et al., 2019a) and synaptic microdomains obtained by either biochemical fractionation (Chang-Gyu et al., 2009; MacDonald et al., 2012, 2019b; Focking et al., 2015)

or Fluorescence-activated Cell Sorting (Gylys et al., 2004; Sokolow et al., 2012) from human post-mortem brain tissue. Synaptic microdomain enrichments generated by biochemical fractionation can provide sufficient material for phosphopeptide enrichment and quantification (Trinidad et al., 2008) which has been accomplished in fresh human brain tissue (DeGiorgis et al., 2005). While it has not yet been demonstrated in human brain tissue, laser capture microdissection and Fluorescence-activated Cell Sorting both likely generate sufficient material for investigation of the phosphoproteome with the aid of isobaric labeling such as TMT and iTRAQ. Glycopeptide enrichment is sufficiently robust that it could likely be applied in the same scenarios as phosphopeptides. Conversely, ubiquitin-motif peptide enrichment still requires significant amounts of starting material, likely limiting its application to brain areas for the present. Finally, while recent advances in single cell proteomics (Levy and Slavov, 2018) such as SCoPE-MS (Budnik et al., 2018) now allow for the quantification of hundreds of proteins in single cells, deep mass spectrometry based quantification of PTMs is still in the future. Given the pace of instrument development, single cell PTM quantification is likely not too far off.

INFORMATICS

Keeping a pace with the advancements in instrumentation, the last few years has seen the release of multiple software packages for exploring PTMs in the context of known kinase-substrate relationships, kinase motifs, protein–protein interactions, and protein networks. Packages such as iGPS (Song et al., 2012) and KEA2 (Lachmann and Ma'ayan, 2009) identify known or presumptive kinase-substrate interaction from phosphoproteomics data, potentially identifying upstream kinases driving observed changes in protein phosphorylation. Other tools such as ProteoViz (Storey et al., 2020) integrate the identification of sequence motifs and kinases with gene set enrichment pathway analysis while CausalPath "identifies potentially causal dependencies between measured protein features (such as phosphorylations or global protein levels) using literature-curated biological pathways" (Babur et al., 2021). Thus, researchers in the PTM space have a rapidly expanding number of informatics resources to draw upon in exploring their datasets.

CLOSING THOUGHTS

In closing, PTMs are implicated in the etiology of neuropsychiatric diseases by unbiased genetic and transcriptomic studies, most notably autism spectrum disorder and schizophrenia. When investigated in human post-mortem brain tissue using targeted approaches, robust alterations in phosphorylation, glycosylation, and ubiquitination are observed in psychiatric disease, suggesting a much broader set of changes, with likely associations between different PTMs as well as the genome, transcriptome, and proteome. Advances in mass spectrometry instrumentation and proteomic sample preparation methods now allow for sufficiently powered studies to map these interactions, which, when combined with emerging informatics tools, will surely provide insight into the etiology of many psychiatric diseases as PTMs are the ultimate mediators of so many neuronal and circuit activities.

AUTHOR CONTRIBUTIONS

MM wrote the first draft of the mini review. MG, RS, and MM revised and reviewed the second draft of the mini review. All authors contributed to the article and approved the submitted version.

FUNDING

This work was funded by NIH grants R01MH118497, R01MH125235, and K08 MH118513.

REFERENCES

Avila, J. (2006). Tau phosphorylation and aggregation in Alzheimer's disease pathology. *FEBS Lett.* 580, 2922–2927. doi: 10.1016/j.febslet.2006.02.067

Babur, Ö, Luna, A., Korkut, A., Durupinar, F., Siper, M. C., Dogrusoz, U., et al. (2021). Causal interactions from proteomic profiles: molecular data meet pathway knowledge. *Patterns* 2:100257. doi: 10.1016/j.patter.2021.100257

Bangasser, D. A., Dong, H., Carroll, J., Plona, Z., Ding, H., Rodriguez, L., et al. (2017). Corticotropin-releasing factor overexpression gives rise to sex differences in Alzheimer's disease-related signaling. *Mol. Psychiatry* 22, 1126–1133. doi: 10.1038/mp.2016.185

Baxter, A. J., Brugha, T. S., Erskine, H. E., Scheurer, R. W., Vos, T., and Scott, J. G. (2015). The epidemiology and global burden of autism spectrum disorders. *Psychol. Med.* 45, 601–613. doi: 10.1017/s003329171400172x

Birur, B., Kraguljac, N. V., Shelton, R. C., and Lahti, A. C. (2017). Brain structure, function, and neurochemistry in schizophrenia and bipolar disorder-a systematic review of the magnetic resonance neuroimaging literature. *NPJ Schizophr.* 3:15.

Brainstorm, C., Anttila, V., Bulik-Sullivan, B., Finucane, H. K., Walters, R. K., Bras, J., et al. (2018). Analysis of shared heritability in common disorders of the brain. *Science* 360:eaa8757.

Brennand, K. J., Simone, A., Jou, J., Gelboin-Burkhart, C., Tran, N., Sangar, S., et al. (2011). Modelling schizophrenia using human induced pluripotent stem cells. *Nature* 473, 221–225.

Budnik, B., Levy, E., Harmange, G., and Slavov, N. (2018). SCoPE-MS: mass spectrometry of single mammalian cells quantifies proteome heterogeneity during cell differentiation. *Genome Biol.* 19:161.

Carlyle, B. C., Kitchen, R. R., Kanyo, J. E., Voss, E. Z., Pletikos, M., Sousa, A. M. M., et al. (2017). A multiregional proteomic survey of the postnatal human brain. *Nat. Neurosci.* 20, 1787–1795. doi: 10.1038/s41593-017-0011-2

Chang-Gyu, H., Anamika, B., Mathew, L. M., Dan-Sung, C., Joshua, K., Zhiping, N., et al. (2009). The post-synaptic density of human postmortem brain tissues: an experimental study paradigm for neuropsychiatric illnesses. *Public Libr. Sci.* 4:e5251. doi: 10.1371/journal.pone.0005251

Charlson, F. J., Ferrari, A. J., Santomauro, D. F., Diminic, S., Stockings, E., Scott, J. G., et al. (2018). Global epidemiology and burden of schizophrenia: findings from the global burden of disease study 2016. *Schizophr. Bull.* 44, 1195–1203. doi: 10.1093/schbul/sby058

Chen, C. H., Suckling, J., Lennox, B. R., Ooi, C., and Bullmore, E. T. (2011). A quantitative meta-analysis of fMRI studies in bipolar disorder. *Bipolar Disord.* 13, 1–15. doi: 10.1111/j.1399-5618.2011.00893.x

DeGiorgis, J. A., Jaffe, H., Moreira, J. E., Carlotti, C. G. Jr., Leite, J. P., Pant, H. C., et al. (2005). Phosphoproteomic analysis of synaptosomes from human cerebral cortex. *J. Proteome Res.* 4, 306–315. doi: 10.1021/pr0498436

Eggan, S. M., Lazarus, M. S., Stoyak, S. R., Volk, D. W., Glausier, J. R., Huang, Z. J., et al. (2012). Cortical glutamic acid decarboxylase 67 deficiency results in lower cannabinoid 1 receptor messenger RNA expression: implications for schizophrenia. *Biol. Psychiatry* 71, 114–119. doi: 10.1016/j.biopsych.2011.09.014

Emamian, E. S., Hall, D., Birnbaum, M. J., Karayiorgou, M., and Gogos, J. A. (2004a). Convergent evidence for impaired AKT1-GSK3beta signaling in schizophrenia. *Nat. Genet.* 36, 131–137. doi: 10.1038/ng1296

Emamian, E. S., Karayiorgou, M., and Gogos, J. A. (2004b). Decreased phosphorylation of NMDA receptor type 1 at serine 897 in brains of patients with Schizophrenia. *J. Neurosci.* 24, 1561–1564. doi: 10.1523/jneurosci.4650-03.2004

Ferrari, A. J., Stockings, E., Khoo, J. P., Erskine, H. E., Degenhardt, L., Vos, T., et al. (2016). The prevalence and burden of bipolar disorder: findings from the Global Burden of Disease Study 2013. *Bipolar Disord.* 18, 440–450. doi: 10.1111/bdi.12423

Focking, M., Lopez, L. M., English, J. A., Dicker, P., Wolff, A., Brindley, E., et al. (2015). Proteomic and genomic evidence implicates the postsynaptic density in schizophrenia. *Mol. Psychiatry* 20, 424–432. doi: 10.1038/mp.2014.63

Foundation SFARI (2021). *SFARI Human Gene Database*. Available online at: https://gene.sfari.org/database/human-gene/ (accessed May 1, 2021).

Gallego Romero, I., Pai, A. A., Tung, J., and Gilad, Y. (2014). RNA-seq: impact of RNA degradation on transcript quantification. *BMC Biol.* 12:42. doi: 10.1186/1741-7007-12-42

Gandal, M. J., Zhang, P., Hadjimichael, E., Walker, R. L., Chen, C., Liu, S., et al. (2018). Transcriptome-wide isoform-level dysregulation in ASD, schizophrenia, and bipolar disorder. *Science* 362:eaat8127. doi: 10.1126/science.aat8127

Glantz, L. A., and Lewis, D. A. (2000). Decreased dendritic spine density on prefrontal cortical pyramidal neurons in schizophrenia. *Arch. Gen. Psychiatry* 57, 65–73. doi: 10.1001/archpsyc.57.1.65

Glausier, J. R., Fish, K. N., and Lewis, D. A. (2014). Altered parvalbumin basket cell inputs in the dorsolateral prefrontal cortex of schizophrenia subjects. *Mol. Psychiatry* 19, 30–36. doi: 10.1038/mp.2013.152

Glausier, J. R., Roberts, R. C., and Lewis, D. A. (2017). Ultrastructural analysis of parvalbumin synapses in human dorsolateral prefrontal cortex. *J. Comp. Neurol.* 525, 2075–2089. doi: 10.1002/cne.24171

Grant, S. G. (2012). Synaptopathies: diseases of the synaptome. *Curr. Opin. Neurobiol.* 22, 522–529. doi: 10.1016/j.conb.2012.02.002

Grove, J., Ripke, S., Als, T. D., Mattheisen, M., Walters, R. K., Won, H., et al. (2019). Identification of common genetic risk variants for autism spectrum disorder. *Nat. Genet.* 51, 431–444.

Grubisha, M. J., Sun, X., MacDonald, M. L., Garver, M., Sun, Z., Paris, K. A., et al. (2021). MAP2 is differentially phosphorylated in schizophrenia, altering its function. *Mol. Psychiatry* 20. doi: 10.1038/s41380-021-01034-z [Epub ahead of print].

Guang, S., Pang, N., Deng, X., Yang, L., He, F., Wu, L., et al. (2018). Synaptopathology involved in autism spectrum disorder. *Front. Cell. Neurosci.* 12:470. doi: 10.3389/fncel.2018.00470

Gylys, K. H., Fein, J. A., Yang, F., and Cole, G. M. (2004). Enrichment of presynaptic and postsynaptic markers by size-based gating analysis of synaptosome preparations from rat and human cortex. *Cytometry A* 60, 90–96. doi: 10.1002/cyto.a.20031

Hahn, C.-G., Wang, H.-Y., Cho, D.-S., Talbot, K., Gur, R. E., Berrettini, W. H., et al. (2006). Altered neuregulin 1–erbB4 signaling contributes to NMDA> receptor hypofunction in schizophrenia. *Nat. Med.* 12, 824–828. doi: 10.1038/nm1418

Heckers, S., and Konradi, C. (2015). GABAergic mechanisms of hippocampal hyperactivity in schizophrenia. *Schizophr. Res.* 167, 4–11. doi: 10.1016/j.schres.2014.09.041

Hegde, A. N. (2017). Proteolysis, synaptic plasticity and memory. *Neurobiol. Learn. Mem.* 138, 98–110. doi: 10.1016/j.nlm.2016.09.003

Hernandez, L. M., Kim, M., Hoftman, G. D., Haney, J. R., de la Torre-Ubieta, L., Pasaniuc, B., et al. (2021). Transcriptomic insight into the polygenic mechanisms underlying psychiatric disorders. *Biol. Psychiatry* 89, 54–64. doi: 10.1016/j.biopsych.2020.06.005

Ikeda, M., Iwata, N., Suzuki, T., Kitajima, T., Yamanouchi, Y., Kinoshita, Y., et al. (2004). Association of AKT1 with schizophrenia confirmed in a Japanese population. *Biol. Psychiatry* 56, 698–700. doi: 10.1016/j.biopsych.2004.07.023

Jaffe, A. E., Tao, R., Norris, A. L., Kealhofer, M., Nellore, A., Shin, J. H., et al. (2017). qSVA framework for RNA quality correction in differential expression analysis. *Proc. Natl. Acad. Sci. U.S.A.* 114, 7130–7135. doi: 10.1073/pnas.1617384114

Javitt, D. C., Doneshka, P., Grochowski, S., and Ritter, W. (1995). Impaired mismatch negativity generation reflects widespread dysfunction of working memory in schizophrenia. *Arch. Gen. Psychiatry* 52, 550–558. doi: 10.1001/archpsyc.1995.03950190032005

Javitt, D. C., Shelley, A. M., and Ritter, W. (2000). Associated deficits in mismatch negativity generation and tone matching in schizophrenia. *Clin. Neurophysiol.* 111, 1733–1737. doi: 10.1016/s1388-2457(00)00377-1

Javitt, D. C., Steinschneider, M., Schroeder, C. E., and Arezzo, J. C. (1996). Role of cortical N-methyl-D-aspartate receptors in auditory sensory memory and mismatch negativity generation: implications for schizophrenia. *Proc. Natl. Acad. Sci. U.S.A.* 93, 11962–11967. doi: 10.1073/pnas.93.21.11962

Javitt, D. C., Strous, R. D., Grochowski, S., Ritter, W., and Cowan, N. (1997). Impaired precision, but normal retention, of auditory sensory ("echoic") memory information in schizophrenia. *J. Abnorm. Psychol.* 106, 315–324. doi: 10.1037/0021-843x.106.2.315

Jedrychowski, M. P., Huttlin, E. L., Haas, W., Sowa, M. E., Rad, R., and Gygi, S. P. (2011). Evaluation of HCD- and CID-type fragmentation within their respective detection platforms for murine phosphoproteomics. *Mol. Cell. Proteomics* 10:M111009910.

Khakipoor, S., Crouch, E. E., and Mayer, S. (2020). Human organoids to model the developing human neocortex in health and disease. *Brain Res.* 1742:146803. doi: 10.1016/j.brainres.2020.146803

Kolluri, N., Sun, Z., Sampson, A. R., and Lewis, D. A. (2005). Lamina-specific reductions in dendritic spine density in the prefrontal cortex of subjects with schizophrenia. *Am. J. Psychiatry* 162, 1200–1202. doi: 10.1176/appi.ajp.162.6.1200

Konopaske, G. T., Lange, N., Coyle, J. T., and Benes, F. M. (2014). Prefrontal cortical dendritic spine pathology in schizophrenia and bipolar disorder. *JAMA Psychiatry* 71, 1323–1331. doi: 10.1001/jamapsychiatry.2014.1582

Kwon, H. B., and Sabatini, B. L. (2011). Glutamate induces de novo growth of functional spines in developing cortex. *Nature* 474, 100–104. doi: 10.1038/nature09986

Lachmann, A., and Ma'ayan, A. (2009). KEA: kinase enrichment. *Bioinformatics* 25, 684–686. doi: 10.1093/bioinformatics/btp026

Lau, W. K. W., Leung, M. K., and Lau, B. W. M. (2019). Resting-state abnormalities in autism spectrum disorders: a meta-analysis. *Sci. Rep.* 9:3892.

Lee, H. K. (2006). Synaptic plasticity and phosphorylation. *Pharmacol. Ther.* 112, 810–832. doi: 10.1016/j.pharmthera.2006.06.003

Leveque, J. C., Macias, W., Rajadhyaksha, A., Carlson, R. R., Barczak, A., Kang, S., et al. (2000). Intracellular modulation of NMDA receptor function by antipsychotic drugs. *J. Neurosci.* 20, 4011–4020. doi: 10.1523/jneurosci.20-11-04011.2000

Levy, E., and Slavov, N. (2018). Single cell protein analysis for systems biology. *Essays Biochem.* 62, 595–605. doi: 10.1042/ebc20180014

Lewis, D. A., and Glausier, J. R. (2016). Alterations in prefrontal cortical circuitry and cognitive dysfunction in schizophrenia. *Nebr. Symp. Motiv.* 63, 31–75. doi: 10.1007/978-3-319-30596-7_3

Lewis, D. A., and Sweet, R. A. (2009). Schizophrenia from a neural circuitry perspective: advancing toward rational pharmacological therapies. *J. Clin. Invest.* 119, 706–716. doi: 10.1172/jci37335

Li, B., Devidze, N., Barengolts, D., Prostak, N., Sphicas, E., Apicella, A. J., et al. (2009). NMDA receptor phosphorylation at a site affected in schizophrenia controls synaptic and behavioral plasticity. *J. Neurosci.* 29, 11965–11972. doi: 10.1523/jneurosci.2109-09.2009

Liu, Q., He, H., Yang, J., Feng, X., Zhao, F., and Lyu, J. (2020). Changes in the global burden of depression from 1990 to 2017: findings from the global burden of disease study. *J. Psychiatr. Res.* 126, 134–140. doi: 10.1016/j.jpsychires.2019.08.002

Mabb, A. M., and Ehlers, M. D. (2010). Ubiquitination in postsynaptic function and plasticity. *Annu. Rev. Cell Dev. Biol.* 26, 179–210. doi: 10.1146/annurev-cellbio-100109-104129

MacDonald, M. L., Alhassan, J., Newman, J. T., Richard, M., Gu, H., Kelly, R. M., et al. (2017). Selective loss of smaller spines in schizophrenia. *Am. J. Psychiatry* 174, 586–594. doi: 10.1176/appi.ajp.2017.16070814

MacDonald, M. L., Ciccimaro, E., Prakash, A., Banerjee, A., Seeholzer, S. H., Blair, I. A., et al. (2012). Biochemical fractionation and stable isotope dilution liquid chromatography-mass spectrometry for targeted and microdomain-specific protein quantification in human postmortem brain tissue. *Mol. Cell. Proteomics* 11, 1670–1681. doi: 10.1074/mcp.m112.021766

MacDonald, M. L., Favo, D., Garver, M., Sun, Z., Arion, D., Ding, Y., et al. (2019a). Laser capture microdissection-targeted mass spectrometry: a method for multiplexed protein quantification within individual layers of the cerebral cortex. *Neuropsychopharmacology* 44, 743–748. doi: 10.1038/s41386-018-0260-0

MacDonald, M. L., Garver, M., Newman, J., Sun, Z., Kannarkat, J., Salisbury, R., et al. (2019b). Synaptic proteome alterations in the primary auditory cortex of individuals with schizophrenia. *JAMA Psychiatry* 77, 86–95. doi: 10.1001/jamapsychiatry.2019.2974

Martinez-Cerdeno, V. (2017). Dendrite and spine modifications in autism and related neurodevelopmental disorders in patients and animal models. *Dev. Neurobiol.* 77, 393–404. doi: 10.1002/dneu.22417

Martins-de-Souza, D. (2012). Proteomics tackling schizophrenia as a pathway disorder. *Schizophr. Bull.* 38, 1107–1108. doi: 10.1093/schbul/sbs094

Marton, R. M., and Pasca, S. P. (2020). Organoid and assembloid technologies for investigating cellular crosstalk in human brain development and disease. *Trends Cell Biol.* 30, 133–143. doi: 10.1016/j.tcb.2019.11.004

Matsubara, A., Wasson, J. C., Donelan, S. S., Welling, C. M., Glaser, B., and Permutt, M. A. (2001). Isolation and characterization of the human AKT1 gene, identification of 13 single nucleotide polymorphisms (SNPs), and their lack of association with Type II diabetes. *Diabetologia* 44, 910–913. doi: 10.1007/s001250100577

McGuire, J. L., Depasquale, E. A., Funk, A. J., O'Donnovan, S. M., Hasselfeld, K., Marwaha, S., et al. (2017). Abnormalities of signal transduction networks in chronic schizophrenia. *NPJ Schizophr.* 3:30.

McGuire, J. L., Hammond, J. H., Yates, S. D., Chen, D., Haroutunian, V., Meador-Woodruff, J. H., et al. (2014). Altered serine/threonine kinase activity in schizophrenia. *Brain Res.* 1568, 42–54. doi: 10.1016/j.brainres.2014.04.029

McKinney, B. C., MacDonald, M. L., Newman, J. T., Shelton, M. A., DeGiosio, R. A., Kelly, R. M., et al. (2019). Density of small dendritic spines and microtubule-associated-protein-2 immunoreactivity in the primary auditory cortex of subjects with schizophrenia. *Neuropsychopharmacology* 44, 1055–1061. doi: 10.1038/s41386-019-0350-7

Minzenberg, M. J., Laird, A. R., Thelen, S., Carter, C. S., and Glahn, D. C. (2009). Meta-analysis of 41 functional neuroimaging studies of executive function in schizophrenia. *Arch. Gen. Psychiatry* 66, 811–822. doi: 10.1001/archgenpsychiatry.2009.91

Moyer, C. E., Delevich, K. M., Fish, K. N., Asafu-Adjei, J. K., Sampson, A. R., Dorph-Petersen, K. A., et al. (2013). Intracortical excitatory and thalamocortical boutons are intact in primary auditory cortex in schizophrenia. *Schizophr. Res.* 149, 127–134. doi: 10.1016/j.schres.2013.06.024

Mueller, T. M., and Meador-Woodruff, J. H. (2020). Post-translational protein modifications in schizophrenia. *NPJ Schizophr.* 6:5.

Mueller, T. M., Haroutunian, V., and Meador-Woodruff, J. H. N. - (2014). Glycosylation of GABAA receptor subunits is altered in Schizophrenia. *Neuropsychopharmacology* 39, 528–537. doi: 10.1038/npp.2013.190

Neddens, J., Temmel, M., Flunkert, S., Kerschbaumer, B., Hoeller, C., Loeffler, T., et al. (2018). Phosphorylation of different tau sites during progression of Alzheimer's disease. *Acta Neuropathol. Commun.* 6:52.

Nucifora, L. G., MacDonald, M. L., Lee, B. J., Peters, M. E., Norris, A. L., Orsburn, B. C., et al. (2019). Increased protein insolubility in brains from a subset of patients with schizophrenia. *Am. J. Psychiatry* 176, 730–743. doi: 10.1176/appi.ajp.2019.18070864

O'Brien, P. L., Thomas, C. P., Hodgkin, D., Levit, K. R., and Mark, T. L. (2014). The diminished pipeline for medications to treat mental health and substance use disorders. *Psychiatr. Serv.* 65, 1433–1438. doi: 10.1176/appi.ps.201400044

Ohnuma, T., Kato, H., Arai, H., Faull, R. L., McKenna, P. J., and Emson, P. C. (2000). Gene expression of PSD95 in prefrontal cortex and hippocampus in schizophrenia. *Neuroreport* 11, 3133–3137. doi: 10.1097/00001756-200009280-00019

Pabba, M., Scifo, E., Kapadia, F., Nikolova, Y. S., Ma, T., Mechawar, N., et al. (2017). Resilient protein co-expression network in male orbitofrontal cortex layer 2/3 during human aging. *Neurobiol. Aging* 58, 180–190. doi: 10.1016/j.neurobiolaging.2017.06.023

Pinacho, R., Saia, G., Meana, J. J., Gill, G., and Ramos, B. (2015). Transcription factor SP4 phosphorylation is altered in the postmortem cerebellum of bipolar disorder and schizophrenia subjects. *Eur. Neuropsychopharmacol.* 25, 1650–1660. doi: 10.1016/j.euroneuro.2015.05.006

Ping, L., Kundinger, S. R., Duong, D. M., Yin, L., Gearing, M., Lah, J. J., et al. (2020). Global quantitative analysis of the human brain proteome and phosphoproteome in Alzheimer's disease. *Sci. Data* 7:315.

Potel, C. M., Lemeer, S., and Heck, A. J. R. (2019). Phosphopeptide fragmentation and site localization by mass spectrometry: an update. *Anal. Chem.* 91, 126–141. doi: 10.1021/acs.analchem.8b04746

Rabinowicz, E. F., Silipo, G., Goldman, R., and Javitt, D. C. (2000). Auditory sensory dysfunction in schizophrenia. Imprecision or distractibility? *Arch. Gen. Psychiatry* 57, 1149–1155. doi: 10.1001/archpsyc.57.12.1149

Ramos, B., Gaudilliere, B., Bonni, A., and Gill, G. (2007). Transcription factor Sp4 regulates dendritic patterning during cerebellar maturation. *Proc. Natl. Acad. Sci. U.S.A.* 104, 9882–9887. doi: 10.1073/pnas.0701946104

Reiding, K. R., Bondt, A., Franc, V., and Heck, A. J. R. (2018). The benefits of hybrid fragmentation methods for glycoproteomics. *TrAC Trends Anal. Chem.* 108, 260–268. doi: 10.1016/j.trac.2018.09.007

Riley, N. M., Malaker, S. A., Driessen, M. D., and Bertozzi, C. R. (2020). Optimal dissociation methods differ for N- and O-glycopeptides. *J. Proteome Res.* 19, 3286–3301. doi: 10.1021/acs.jproteome.0c00218

Robins, C., Wingo, A. P., Fan, W., Duong, D. M., Meigs, J., Gerasimov, E. S., et al. (2019). Genetic control of the human brain proteome. *bioRxiv* [preprint] doi: 10.1101/816652

Roche, K. W., Tingley, W. G., and Huganir, R. L. (1994). Glutamate receptor phosphorylation and synaptic plasticity. *Curr. Opin. Neurobiol.* 4, 383–388. doi: 10.1016/0959-4388(94)90100-7

Rosoklija, G., Toomayan, G., Ellis, S. P., Keilp, J., Mann, J. J., Latov, N., et al. (2000). Structural abnormalities of subicular dendrites in subjects with schizophrenia and mood disorders. *Arch. Gen. Psychiatry* 57, 349–356. doi: 10.1001/archpsyc.57.4.349

Rubio, M. D., Wood, K., Haroutunian, V., and Meador-Woodruff, J. H. (2013). Dysfunction of the ubiquitin proteasome and ubiquitin-like systems in schizophrenia. *Neuropsychopharmacology* 38, 1910–1920. doi: 10.1038/npp.2013.84

Schizophrenia Working Group of the Psychiatric Genomics Consortium (2014). Biological insights from 108 schizophrenia-associated genetic loci. *Nature* 511, 421–427. doi: 10.1038/nature13595

Scott, M. R., and Meador-Woodruff, J. H. (2020). Intracellular compartment-specific proteasome dysfunction in postmortem cortex in schizophrenia subjects. *Mol. Psychiatry* 25, 776–790. doi: 10.1038/s41380-019-0359-7

Shelton, M. A., Newman, J. T., Gu, H., Sampson, A. R., Fish, K. N., MacDonald, M. L., et al. (2015). Loss of microtubule-associated protein 2 immunoreactivity linked to dendritic spine loss in schizophrenia. *Biol. Psychiatry* 78, 374–385. doi: 10.1016/j.biopsych.2014.12.029

Silberberg, G., Darvasi, A., Pinkas-Kramarski, R., and Navon, R. (2006). The involvement of ErbB4 with schizophrenia: association and expression studies. *Am. J.Med. Genet. B Neuropsychiatr. Genet.* 141, 142–148.

Simic, G., Babic Leko, M., Wray, S., Harrington, C., Delalle, I., Jovanov-Milosevic, N., et al. (2016). Tau protein hyperphosphorylation and aggregation in Alzheimer's disease and other tauopathies, and possible neuroprotective strategies. *Biomolecules* 6:6. doi: 10.3390/biom6010006

Sokolow, S., Henkins, K. M., Williams, I. A., Vinters, H. V., Schmid, I., Cole, G. M., et al. (2012). Isolation of synaptic terminals from Alzheimer's disease cortex. *Cytometry A* 81, 248–254. doi: 10.1002/cyto.a.22009

Somerville, S. M., Lahti, A. C., Conley, R. R., and Roberts, R. C. (2011). Mitochondria in the striatum of subjects with schizophrenia: relationship to treatment response. *Synapse* 65, 215–224. doi: 10.1002/syn.20838

Song, C., Ye, M., Liu, Z., Cheng, H., Jiang, X., Han, G., et al. (2012). Systematic analysis of protein phosphorylation networks from phosphoproteomic data. *Mol. Cell. Proteomics* 11, 1070–1083. doi: 10.1074/mcp.m111.012625

Stefansson, H., Sarginson, J., Kong, A., Yates, P., Steinthorsdottir, V., Gudfinnsson, E., et al. (2003). Association of neuregulin 1 with schizophrenia confirmed in a Scottish population. *Am. J. Hum. Genet.* 72, 83–87. doi: 10.1086/345442

Stefansson, H., Sigurdsson, E., Steinthorsdottir, V., Bjornsdottir, S., Sigmundsson, T., Ghosh, S., et al. (2002). Neuregulin 1 and susceptibility to schizophrenia. *Am. J. Hum. Genet.* 71, 877–892.

Storey, A. J., Naceanceno, K. S., Lan, R. S., Washam, C. L., Orr, L. M., Mackintosh, S. G., et al. (2020). ProteoViz: a tool for the analysis and interactive visualization of phosphoproteomics data. *Mol. Omics* 16, 316–326. doi: 10.1039/c9mo00149b

Sweet, R. A., Henteleff, R. A., Zhang, W., Sampson, A. R., and Lewis, D. A. (2009). Reduced dendritic spine density in auditory cortex of subjects with schizophrenia. *Neuropsychopharmacology* 34, 374–389. doi: 10.1038/npp.2008.67

Thaker, G. K., and Carpenter, W. T. Jr. (2001). Advances in schizophrenia. *Nat. Med.* 7, 667–671.

The Schizophrenia Working Group of the Psychiatric Genomics Consortium, Ripke, S., Walters, J. T., and O'Donovan, M. C. (2020). Mapping genomic loci prioritises genes and implicates synaptic biology in schizophrenia. *medRxiv* [preprint] doi: 10.1101/2020.09.12.20192922

Trinidad, J. C., Thalhammer, A., Specht, C. G., Lynn, A. J., Baker, P. R., Schoepfer, R., et al. (2008). Quantitative analysis of synaptic phosphorylation and protein expression. *Mol. Cell. Proteomics* 7, 684–696. doi: 10.1074/mcp.m700170-mcp200

Tsai, G., Yang, P., Chung, L. C., Lange, N., and Coyle, J. T. (1998). D-serine added to antipsychotics for the treatment of schizophrenia. *Biol. Psychiatry* 44, 1081–1089. doi: 10.1016/s0006-3223(98)00279-0

Tucholski, J., Simmons, M. S., Pinner, A. L., Haroutunian, V., McCullumsmith, R. E., and Meador-Woodruff, J. H. (2013a). Abnormal N-linked glycosylation of cortical AMPA receptor subunits in schizophrenia. *Schizophr. Res.* 146, 177–183. doi: 10.1016/j.schres.2013.01.031

Tucholski, J., Simmons, M. S., Pinner, A. L., McMillan, L. D., Haroutunian, V., and Meador-Woodruff, J. H. (2013b). N-linked glycosylation of cortical N-methyl-D-aspartate and kainate receptor subunits in schizophrenia. *Neuroreport* 24, 688–691. doi: 10.1097/wnr.0b013e328363bd8a

Turunen, J. A., Peltonen, J. O., Pietilainen, O. P., Hennah, W., Loukola, A., Paunio, T., et al. (2007). The role of DTNBP1, NRG1, and AKT1 in the genetics of schizophrenia in Finland. *Schizophr. Res.* 91, 27–36. doi: 10.1016/j.schres.2006.11.028

Udeshi, N. D., Mani, D. C., Satpathy, S., Fereshetian, S., Gasser, J. A., Svinkina, T., et al. (2020). Rapid and deep-scale ubiquitylation profiling for biology and translational research. *Nat. Commun.* 11:359.

Uranova, N. A., Vikhreva, O. V., Rakhmanova, V. I., and Orlovskaya, D. D. (2018). Ultrastructural pathology of oligodendrocytes adjacent to microglia in prefrontal white matter in schizophrenia. *NPJ Schizophr.* 4:26.

Vanderplow, A. M., Eagle, A. L., Kermath, B. A., Bjornson, K. J., Robison, A. J., and Cahill, M. E. (2021). Akt-mTOR hypoactivity in bipolar disorder gives rise to cognitive impairments associated with altered neuronal structure and function. *Neuron* 109, 1479–1496.e6.

Vittala, A., Murphy, N., Maheshwari, A., and Krishnan, V. (2020). Understanding Cortical Dysfunction in Schizophrenia With TMS/EEG. *Front. Neurosci.* 14:554. doi: 10.3389/fnins.2020.00554

Wang, H. Y., MacDonald, M. L., Borgmann-Winter, K. E., Banerjee, A., Sleiman, P., Tom, A., et al. (2020). mGluR5 hypofunction is integral to glutamatergic dysregulation in schizophrenia. *Mol. Psychiatry* 25, 750–760. doi: 10.1038/s41380-018-0234-y

Washbourne, P. (2015). Synapse assembly and neurodevelopmental disorders. *Neuropsychopharmacology* 40, 4–15. doi: 10.1038/npp.2014.163

Williams, N. M., Preece, A., Spurlock, G., Norton, N., Williams, H. J., Zammit, S., et al. (2003). Support for genetic variation in neuregulin 1 and susceptibility to schizophrenia. *Mol. Psychiatry* 8, 485–487. doi: 10.1038/sj.mp.4001348

Won, H., Mah, W., and Kim, E. (2013). Autism spectrum disorder causes, mechanisms, and treatments: focus on neuronal synapses. *Front. Mol. Neurosci.* 6:19. doi: 10.3389/fnmol.2013.00019

Woolfrey, K. M., and Dell'Acqua, M. L. (2015). Coordination of protein phosphorylation and dephosphorylation in synaptic plasticity. *J. Biol. Chem.* 290, 28604–28612. doi: 10.1074/jbc.r115.657262

Yang, J. Z., Si, T. M., Ruan, Y., Ling, Y. S., Han, Y. H., Wang, X. L., et al. (2003). Association study of neuregulin 1 gene with schizophrenia. *Mol. Psychiatry* 8, 706–709.

Conflict of Interest: The authors declare that the research was conducted in the absence of any commercial or financial relationships that could be construed as a potential conflict of interest.

frontiers in Molecular Neuroscience

ORIGINAL RESEARCH
published: 24 September 2021
doi: 10.3389/fnmol.2021.745219

Treatment With Nepicastat Decreases Contextual Traumatic Memories Persistence in Post-traumatic Stress Disorder

*Raquel Martinho[1,2], Gabriela Correia[1,2], Rafaela Seixas[1,2], Ana Oliveira[1,2], Soraia Silva[1,2], Paula Serrão[2,3], Carlos Fernandes-Lopes[4], Cristina Costa[4] and Mónica Moreira-Rodrigues[1,2]**

[1]Laboratory of General Physiology, Institute of Biomedical Sciences Abel Salazar, University of Porto (ICBAS/UP), Porto, Portugal, [2]Center for Drug Discovery and Innovative Medicines, University of Porto (MedInUP), Porto, Portugal, [3]Department of Pharmacology and Therapeutics, Faculty of Medicine, University of Porto (FMUP), Porto, Portugal, [4]Department of Research, BIAL, Porto, Portugal

OPEN ACCESS

Edited by:
Nashat Abumaria,
Fudan University, China

Reviewed by:
Natasa Spasojevic,
University of Belgrade, Serbia
Bin Yin,
Fujian Normal University, China

***Correspondence:**
Mónica Moreira-Rodrigues
mirodrigues@icbas.up.pt

Specialty section:
This article was submitted to Brain Disease Mechanisms, a section of the journal Frontiers in Molecular Neuroscience

Received: 21 July 2021
Accepted: 31 August 2021
Published: 24 September 2021

Citation:
Martinho R, Correia G, Seixas R, Oliveira A, Silva S, Serrão P, Fernandes-Lopes C, Costa C and Moreira-Rodrigues M (2021) Treatment With Nepicastat Decreases Contextual Traumatic Memories Persistence in Post-traumatic Stress Disorder. Front. Mol. Neurosci. 14:745219. doi: 10.3389/fnmol.2021.745219

Post-traumatic stress disorder (PTSD) is a common anxiety mental disorder and can be manifested after exposure to a real or perceived life-threatening event. Increased noradrenaline and adrenaline in plasma and urine have been documented in PTSD. Dopamine-β-hydroxylase (DBH) catalyzes the conversion of dopamine to noradrenaline and consequently, DBH inhibition reduces catecholamines. Our aim was to evaluate if nepicastat treatment decreases PTSD signs in an animal model. Wild-type (129x1/SvJ) female mice were submitted to PTSD induction protocol. DBH-inhibitor nepicastat (30 mg/kg) or vehicle (0.2% HPMC) were administered once daily since day 0 until day 7 or 12. The percentage of freezing was calculated on days 0, 1, 2, and 7, and behavioral tests were performed. Quantification of nepicastat in plasma and DBH activity in the adrenal gland was evaluated. Catecholamines were quantified by HPLC with electrochemical detection. mRNA expression of *Npas4* and *Bdnf* in hippocampus was evaluated by qPCR. Mice in the PTSD-group and treated with nepicastat showed a decrease in freezing, and an increase in the time spent and entries in open arms in elevated plus maze test. In mice treated with nepicastat, adrenal gland DBH activity was decreased, and catecholamines were also decreased in plasma and tissues. On day 7, in mice treated with nepicastat, there was an increase of *Npas4* and *Bdnf* mRNA expression in the hippocampus. In conclusion, DBH inhibitor nepicastat has an effect consistent with a decrease in the persistence of traumatic memories and anxiety-like behavior in this PTSD mice model. The disruption of traumatic memories through interference with the formation, consolidation, retrieval, and/or expression processes may be important to decrease PTSD symptoms and signs. The increase in *Npas4* and *Bdnf* mRNA expression in the hippocampus may be important to develop a weaker traumatic contextual memory after nepicastat treatment.

Keywords: post-traumatic stress disorder, contextual traumatic memory, dopamine β-hydroxylase, noradrenaline, nepicastat

INTRODUCTION

Previous research discovered that when a stored memory is recalled, it becomes susceptible to disruption for a short period (Nader et al., 2000; Alberini, 2005). This finding suggests that it may be possible to weaken or even erase memories of traumatic experiences that have resulted in post-traumatic stress disorder (PTSD). Memories of negative emotional events tend to last a long period, frequently remaining detailed and vivid (Brown and Kulik, 1977; Kensinger et al., 2006). Memory of neutral experiences, on the other hand, tends to fade over time.

PTSD is a common anxiety disorder and may develop after exposure to exceptionally horrifying or threatening events. The persistence of memories of negative emotional events can be adaptive by influencing behavior in similar situations in the future. Nevertheless, in some cases, the persistence of negative memories can become maladaptive, as is the case of intrusive memories in PTSD, where memories of traumatic experiences continue to intrude involuntarily into consciousness, causing significant distress (American Psychiatric Association, 2013). Elucidating the mechanisms behind the recall and persistence of negative emotional memories is thus crucial for both basic cognitive science and clinical psychopathology research.

Usually, PTSD patients show symptoms of intrusion, avoidance, arousal, alterations in mood and cognition, and show deficits in the extinction of fear memory (Lissek et al., 2005; Inslicht et al., 2013). Also, these patients show an increase of stress hormones, namely catecholamines, such as noradrenaline (NA) and adrenaline (AD) in urine and plasma (Shalev et al., 1992; Sherin and Nemeroff, 2011). Besides, when exposed to trauma-related contexts they manifest greater changes in heart rate, blood pressure, and skin conductance than controls. In fact, persistent hyperactivity of the autonomic sympathetic system was detected in PTSD patients (Li et al., 2006; Sherin and Nemeroff, 2011).

Women are two to three times more likely than men to suffer from PTSD (Olff, 2017). The preponderance of PTSD in women may be due to causes not related to trauma, such as stress hormone sensitization in reaction to early adverse experiences, intrinsic neuroendocrine factors, and subjective perception of the event. In addition, there are gender disparities in rape and sexual assault rates, including greater exposure to intimate partner abuse. Women with PTSD can experience more symptoms, have a longer course of illness, and have a lower quality of life than men (Seedat et al., 2005).

To study PTSD, several animal models have been developed using different types of traumatic events (Pynoos et al., 1996; Deslauriers et al., 2018). The PTSD animal model used in this study is based on the concept that foot shock exposure will trigger the pathophysiological process and the main symptomatology of PTSD in animals, including increased contextual traumatic memory and anxiety-like behavior (Li et al., 2006; Zhang et al., 2012; Martinho et al., 2020). In this model, the administration of multiple foot shocks has been confirmed to mimic the traumatic event (Li et al., 2006; Zhang et al., 2012; Verma et al., 2016; Martinho et al., 2020). Also, contextual reminders in this animal model of PTSD seem to parallel the exposure to contextual cues present throughout an aversive stressful situation. This is expected to induce the re-experiencing of the traumatic event (Gisquet-Verrier et al., 2004), which seems to reproduce some of the features observed in PTSD patients.

We have shown in previous studies that mice deficient in AD (phenylethanolamine-*N*-methyltransferase-knockout, Pnmt-KO mice) have reduced contextual fear learning (Toth et al., 2013; Alves et al., 2016). Also, AD administered peripherally restored traumatic memories in Pnmt-KO mice (Martinho et al., 2020). In addition, catecholamines are increased in this PTSD mice model suggesting a causal role for AD in contributing to the persistence of contextual traumatic memories and anxiety-like behavior in PTSD (Martinho et al., 2020).

On the other hand, it was previously shown that dopamine-β-hydroxylase (DBH) knockout (DBH-KO) mice exhibit reduced contextual fear memory, which was restored by isoprenaline (β-adrenoceptor agonist; Murchison et al., 2004). DBH catalyzes the conversion of dopamine (DA) to NA (Rios et al., 1999) and, consequently, DBH inhibition reduces NA and AD, and increases DA (Bourdélat-Parks et al., 2005; Schroeder et al., 2010; Devoto et al., 2014; Igreja et al., 2015; Loureiro et al., 2015). Numerous DBH inhibitors have been described and reported (Ishii et al., 1975; Kruse et al., 1987; Ohlstein et al., 1987), but none had marketing approval due to poor DBH selectivity, low potency (Beliaev et al., 2009), and/or substantial adverse effects (Kruse et al., 1986). Nepicastat is a highly potent central and peripheral DBH inhibitor that, in dogs (Stanley et al., 1997) and rats (Bonifácio et al., 2015; Loureiro et al., 2015), produced a dose-dependent reduction in NA in peripheral and central tissues. Therefore, it is effective in modulating the sympathetic nervous system, which may be useful in diseases with sympathetic hyperactivity, such as PTSD.

DBH inhibition causes a gradual sympathetic slowdown by contrast to acute sympathetic inhibition triggered by β-adrenoceptor antagonists, thus reducing the negative hemodynamic impacts of the latter (Hegde and Friday, 1998). To our knowledge, there are no described studies with nepicastat treatment in PTSD mice models. The aim of the present study was to evaluate if inhibition of DBH by treatment with DBH-inhibitor nepicastat interferes with the recall and persistence of traumatic memories. This approach could be a potential new therapeutic strategy for PTSD treatment. In this study, we will induce a PTSD mice model and treat the animals daily with vehicle or nepicastat until day 12 and evaluate traumatic contextual memory and anxiety-like behavior, DBH activity in adrenal gland, catecholamines levels in plasma and tissues, and mRNA expression of hippocampal relevant genes in contextual fear memory.

MATERIAL AND METHODS

Animals

All animal care and experimental protocols were carried out in accordance with European Directive number 63/2010/EU, transposed to Portuguese legislation by Directive Law 113/2013 and 1/2019, and approved by the Organism

Responsible for Animal Welfare in Faculty of Medicine of University of Porto and National Authority for Animal Health (DGAV). Adult female mice (8–12 weeks old; 129x1/SvJ; $n = 28$) were kept under controlled environmental conditions (12 h light/dark cycle, room temperature 23 ± 1°C, humidity 50%, autoclaved drinking water, mice diet (4RF21/A); Mucedola, Milan, Italy). Animals were group-housed and experiments were performed in the light phase. The light phase started from 8 a.m. and 8 p.m. and the behavioral testing and physiological measurements were performed between 9 a.m. and 1 p.m. Between two and five mice were living in a cage and they were fed *ad libitum*. It was previously described that female rodents placed in groups synchronize their ovarian cycles (McClintock, 1978).

PTSD Mice Model

PTSD mice model was performed as previously described (Li et al., 2006; Zhang et al., 2012; Verma et al., 2016; Martinho et al., 2020). In the two experimental protocols (**Figures 1A,B**), mice were exposed to an aversive procedure consisting of two training sessions (days 0 and 1). A clear Plexiglass chamber with a metal grid floor wired to a stimulus generator was used for the training sessions. On both days, the mice had a 2-min habituation period and were then submitted to 15 electric shocks (intensity, 0.8 mA; duration, 10 s; interval between sessions, 10 s), during a total time of 5 min. After the training session, the mice were re-exposed on days 2 and 7 to the aversive context. Re-exposure consisted in introducing the mice to the same conditioned chamber without applying foot shocks for 8 min. Freezing was defined as the absence of movement except for respiration for at least 3 s (Valentinuzzi et al., 1998). In the clear Plexiglass chamber used, a timer is placed on the top of the chamber to be able to evaluate freezing time using a camera and video software. The freezing time was manually scored and monitored when freezing behavior lasts for at least 3 s. Vocalization response was defined as the audible vocalization in response to the shock. We considered audible vocalization when after footshocks were given to mice, these animals emitted a high-pitched squeak. We measured the number of times the animal vocalized during the procedure. Jump response was defined as the removal of at least three paws from the grid floor (Rocinholi et al., 1997). The mice's behavior was recorded with a digital video camera Sony HDR-CX405 (Sony Corporation, Japan). All quantifications were performed manually and blinded (**Figure 1**).

Drug Treatments

In the first and second experimental protocol, mice were administered orally (p.o.) with nepicastat (30 mg/kg; dissolved in 0.2% HPMC; $n = 15$) or vehicle (0.2% HPMC; $n = 13$) once a day from days 0–7 (**Figure 1A**) or once a day from days 0–12 (**Figure 1B**). On training sessions days, nepicastat or vehicle were administered immediately after each session. On days 2, 7, 9, and 11 nepicastat or vehicle were administered 1 h before the behavioral test. On the other days when no tests were performed, nepicastat was administered between 9 a.m. and 10 a.m. Tissue samples were collected in day 7 of the first experimental protocol approximately 1 h 30 min after drug treatments (**Figure 1A**) or in day 12 approximately 3 h after nepicastat or vehicle administration of the second protocol (**Figure 1B**). The timeline of the experimental design, behavioral protocols, treatments, and samples collection is presented in **Figure 1**. Nepicastat hydrochloride was provided by BIAL-Portela and C^a, S.A. (S. Mamede Coronado, Portugal) and was synthesized in BIAL's Chemical Research Laboratory with purities above 95%.

Behavioral Tests

Elevated Plus Maze Test

Nine days after PTSD induction the elevated plus maze test was conducted (**Figure 1**), as previously described (Pellow et al., 1985; Martinho et al., 2020). The apparatus consisted of two open arms (40 × 10 cm) alternating at right angles with two arms enclosed by 20 cm high walls. The four arms delimited a central area of 5 cm^2. The whole apparatus was placed 60 cm above the floor. The test began by placing the animal in the center with its head facing a closed arm. The time spent in open arms, open arm entries, and total arm entries during 5 min were recorded with a digital video camera Sony HDR-CX405 (Sony Corporation, Japan) and analyzed manually and blinded, and a four paws criterion was used for arm entries (Li et al., 2006; Zhang et al., 2012).

Open Field Test

Eleven days after PTSD induction the open field test was conducted (**Figure 1**), as previously described (Pynoos et al., 1996; Mitra et al., 2016; Martinho et al., 2020). The open field wooden chamber (50 × 50 × 30 cm) had black lines on the floor delineating twelve peripheral squares (12.5 × 12.5 cm) and a central square (25 × 25 cm). Each animal was placed in the corner of the arena and the number of squares crossed, entries in the center, and feces were recorded for 10 min with a digital video camera Sony HDR-CX405 (Sony Corporation, Japan) and analyzed manually and blinded. The total distance traveled was recorded and analyzed using ToxTrac ver 2.84[1] (Rodriguez et al., 2017, 2018; Henry et al., 2019).

Quantification of Nepicastat in Plasma Samples

Mice were anesthetized (ketamine, 100 mg/kg and xylazine, 10 mg/kg; i.p.) and blood was collected from the left ventricle to heparinized tubes approximately 1h30 min after the last administration of nepicastat (30 mg/kg) and after contextual behavior evaluation on day 7 (**Figure 1A**). After collection, blood samples were centrifuged at 1,500× *g*, for 10 min, at 4°C. The resulting plasma was stored at −80°C. Plasma nepicastat concentration was quantified by liquid chromatography coupled to tandem mass spectrometry (LC-MS/MS; 6460, Triple Quad LC-MS Agilent Technologies, USA) by BIAL-Portela and C^a, S.A. (S. Mamede Coronado, Portugal), as previously described (Loureiro et al., 2013; Pires et al., 2015). The limit of quantification was 50 ng/ml.

[1] https://sourceforge.net/projects/toxtrac/

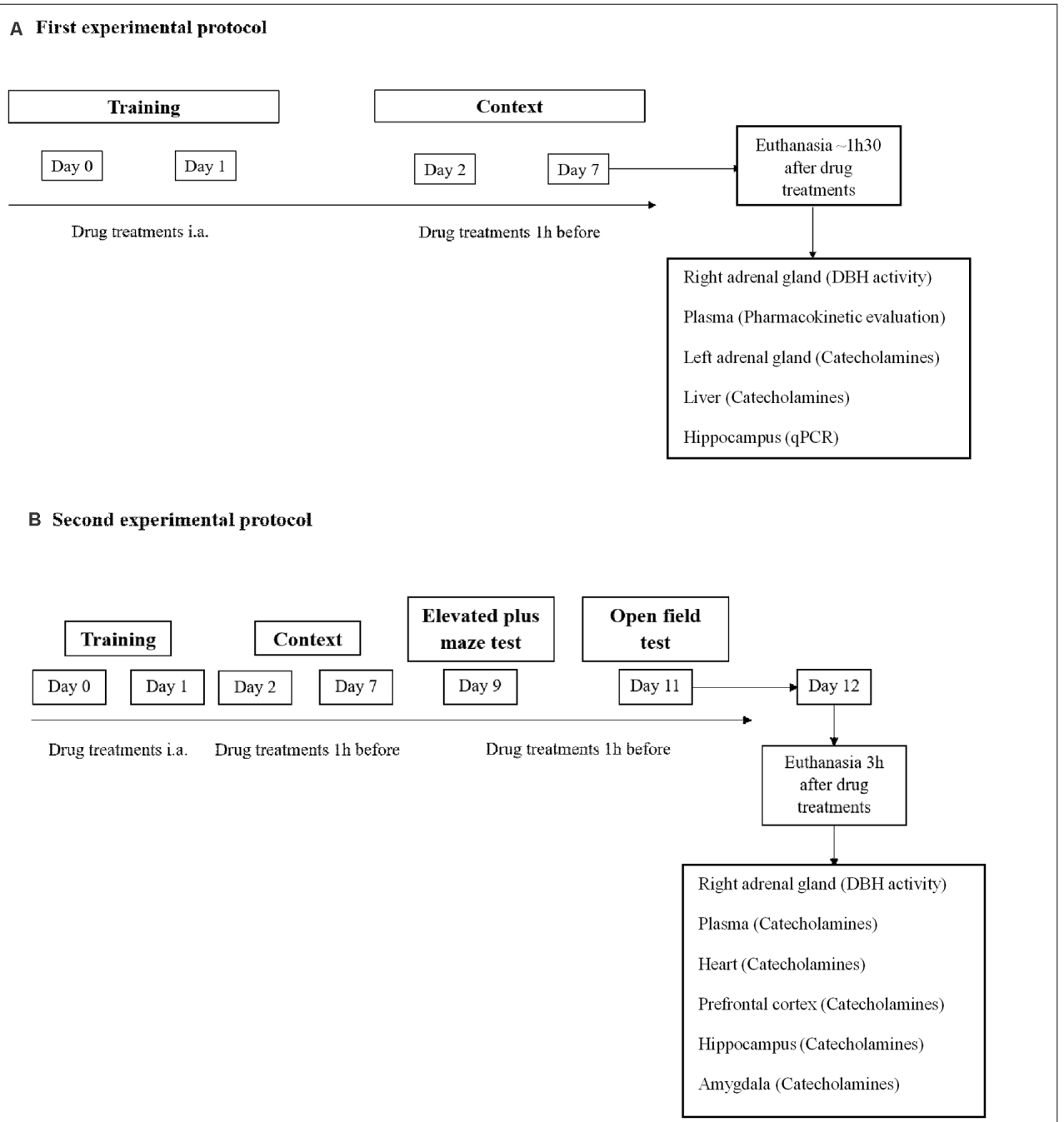

FIGURE 1 | Schematic representation of the experimental design: treatments, behavioral protocols, and samples collection. **(A)** First experimental protocol and **(B)** second experimental protocol. i.a., immediately after.

Dopamine-β-Hydroxylase (DBH) Activity Determination

Right adrenal gland (AG) samples were collected approximately 1 h 30 min (day 7) and 3 h (day 12) after the last administration of nepicastat (30 mg/kg) or vehicle (0.2% HPMC; **Figure 1**), submerged in Tris-HCl (50 mM; pH 7.4) and kept at −80 °C. DBH activity was measured by BIAL-Portela and C^{a}, S.A., as previously described (Loureiro et al., 2014).

Quantification of Catecholamines

Seven and 12 days after PTSD induction mice were anesthetized (ketamine, 100 mg/kg and xylazine, 10 mg/kg; i.p.), the left adrenal gland was collected on day 7 and submerged in perchloric acid (PCA) 0.2 M overnight, at 4°C, and frozen at −80°C. Also, the liver was collected on day 7 (**Figure 1A**), and the heart, prefrontal cortex, amygdala, and hippocampus were collected on day 12 (**Figure 1B**) submerged in perchloric acid (PCA) 0.2 M

overnight, at 4 °C, and frozen at −80 °C. The brain dissection was as follows. The cerebellum and the pons were separated from the brain by a coronal incision in the transverse fissure. An incision was made between the olfactory bulb and the frontal cortex, and between the frontal cortex and the beginning of the corpus callosum. Then the hippocampus was gently separated from the cortex and collected (Chiu et al., 2007). Finally, the amygdala was identified ventrally to the temporal lobe and separated from the cortex.

Twelve days after PTSD induction, blood was collected by left ventricle puncture to a heparinized tube and the samples were centrifuged and frozen at −80°C. The catecholamines present in plasma, liver, heart, prefrontal cortex, hippocampus, and amygdala were concentrated by alumina method, as previously described (Moreira-Rodrigues et al., 2014). Briefly, 50 mg of alumina and 20 μl (100 ng/ml), or 50 μl of 3,4-Dihydroxybenzylamine (DHBA, 500 ng/ml), respectively, were added to plasma or tissue samples (liver, heart, and hippocampus). After adjustment to pH of 8.3–8.6, with Tris-EDTA (1.5 M, pH = 8.6), the samples were shaken using an autonomic shaker (Analogue Orbital Shaker 3005, GFL) for 15 min at room temperature and maximum frequency. Subsequently, alumina was rested and after two successive washes with bi-distilled water at 4°C, 500 μl of bi-distilled water at 4°C were added. The alumina was then centrifuged at 1,250× *g*, for 2 min at 4°C, in a tube with a filter. The filter with the alumina and 200 μl of PCA (0.2 M) was added to a new tube and centrifuged at 1,250× *g*, for 2 min at 4°C. For catecholamines quantification in the adrenal gland, the PCA of each sample was transferred to tubes with filters and centrifuged at 1,250× *g*, for 2 min at 4°C. Fifty microliter of the left adrenal gland, plasma, liver, heart, and hippocampus samples were injected and separated by reverse-phase high-performance liquid chromatography (HPLC) and quantified by electrochemical detection. The results of catecholamines were expressed in nmol/AG for the adrenal gland, pmol/ml for plasma, and pmol/mg for liver, heart, amygdala, and hippocampus, after normalization for DHBA.

RNA Isolation and Relative Quantification of mRNA Expression

Real-time PCR (qPCR) was performed in hippocampus samples collected on day 7 of PTSD induction (**Figure 1**), as previously described (Moreira-Rodrigues et al., 2007; Mendes et al., 2018; Oliveira et al., 2018; Martinho et al., 2020). Total RNA isolation was carried out with the illustra^{TM} Isolate II RNA Mini Kit (Bioline, London, UK). The concentration and purity of the isolated RNA were measured using the NanoDrop 2000 spectrophotometer (Thermo Scientific, Waltham, MA, USA). Reverse transcription was performed in a T100^{TM} Thermal Cycler (Bio-Rad, Hercules, CA, USA) using a Reverse Transcription kit (NZY First-Strand cDNA Synthesis Kit NZYTech-Genes and Enzymes, Lisbon, Portugal). qPCR reactions were carried out in StepOne^{TM} real-time PCR System (Applied BioSystems, Waltham, MA, USA). Gene-specific primers (10 μM), Maxima SYBR Green qPCR Master Mix (Thermo Scientific, Waltham, MA, USA), RNase-free H_2O (Bioline, London, UK) were mixed and cDNA was added (1:20). Instead of cDNA, RNase-free H_2O (Bioline, London, UK) was added as a negative control. Gene-specific primers are in **Table 1**. Results of mRNA quantification are expressed in an arbitrary unit (AU) after normalization for Glyceraldehyde 3-phosphate dehydrogenase (GAPDH).

TABLE 1 | Primers used in gene expression analysis.

Gene	Primer (5'→ 3')
Npas4	F: AGCATTCCAGGCTCATCTGAA
	R: GGCGAAGTAAGTCTTGGTAGGATT
Bdnf	F: GGACATATCCATGACCAGAAAGAAA
	R: GCAACAAACCACAACATTATCGAG
Gapdh	F: CCATCACCATCTTCCAGGAG
	R: GCATGGACTGTGGTCATGAG

Npas4, neuronal PAS domain protein 4; Bdnf, brain-derived neurotrophic factor; Gapdh, Glyceraldehyde 3-phosphate dehydrogenase; F, forward primer; R, reverse primer.

Other Drugs

Hydroxypropyl methylcellulose, (-)-adrenaline, L-(-)-noradrenaline, dopamine hydrochloride, 2, 3-dihydroxybenzoic acid, and perchloric acid were purchased from Sigma-Aldrich (St. Louis, USA). Ketamine (Imalgene 1000, Merial, Lisboa, Portugal) and xylazine (Rompum 2%, Bayer, Lisboa, Portugal) were purchased from Agrofauna (Gaia, Portugal).

Statistics

We used an online Sample Size Calculator[2] to determine the minimum number of subjects that needed to be enrolled in the experiments of this study. All results were presented as means ± standard error of the means (SEM). GraphPad Prism 6 (GraphPad Software Inc., La Jolla, CA, USA) was used for all statistical analyses. Freezing behavior results were analyzed by Two-Way Analysis of Variance (ANOVA) repeated measures followed by Sidak's *post hoc* test using treatment as "between-subjects factor" and time as "within-subjects factor" (repeated measure). Results regarding jump, vocalization, elevated plus maze test, open field test, DBH activity, catecholamines concentration, and qPCR were analyzed by Student's *t*-test. Cohen's *d* effect sizes were calculated for Student's *t*-tests and partial eta squared (η_p^2) effect sizes were calculated for ANOVAs. We also evaluated the presence of outliers using GraphPad Prism 6. For all analyses, significance level was set at 0.05.

RESULTS

Nepicastat Treatment Decreases Contextual Fear Memory in PTSD Mice Model

The effects of nepicastat treatment in freezing behavior of PTSD animals were assessed and are shown in **Figure 2**. During training days 0 and 1, no differences were observed in jump ($t_{(26)}$= 1.05, p = 0.3041; Cohen's d = 0.41; **Figure 2A**; $t_{(26)}$ = 1.79, p = 0.085; Cohen's d = 0.68; **Figure 2B**), vocalization ($t_{(26)}$= 0.021, p = 0.9835; Cohen's d = 0.0076; **Figure 2A**; $t_{(26)}$ = 0.64,

[2]https://clincalc.com/Stats/SampleSize.aspx

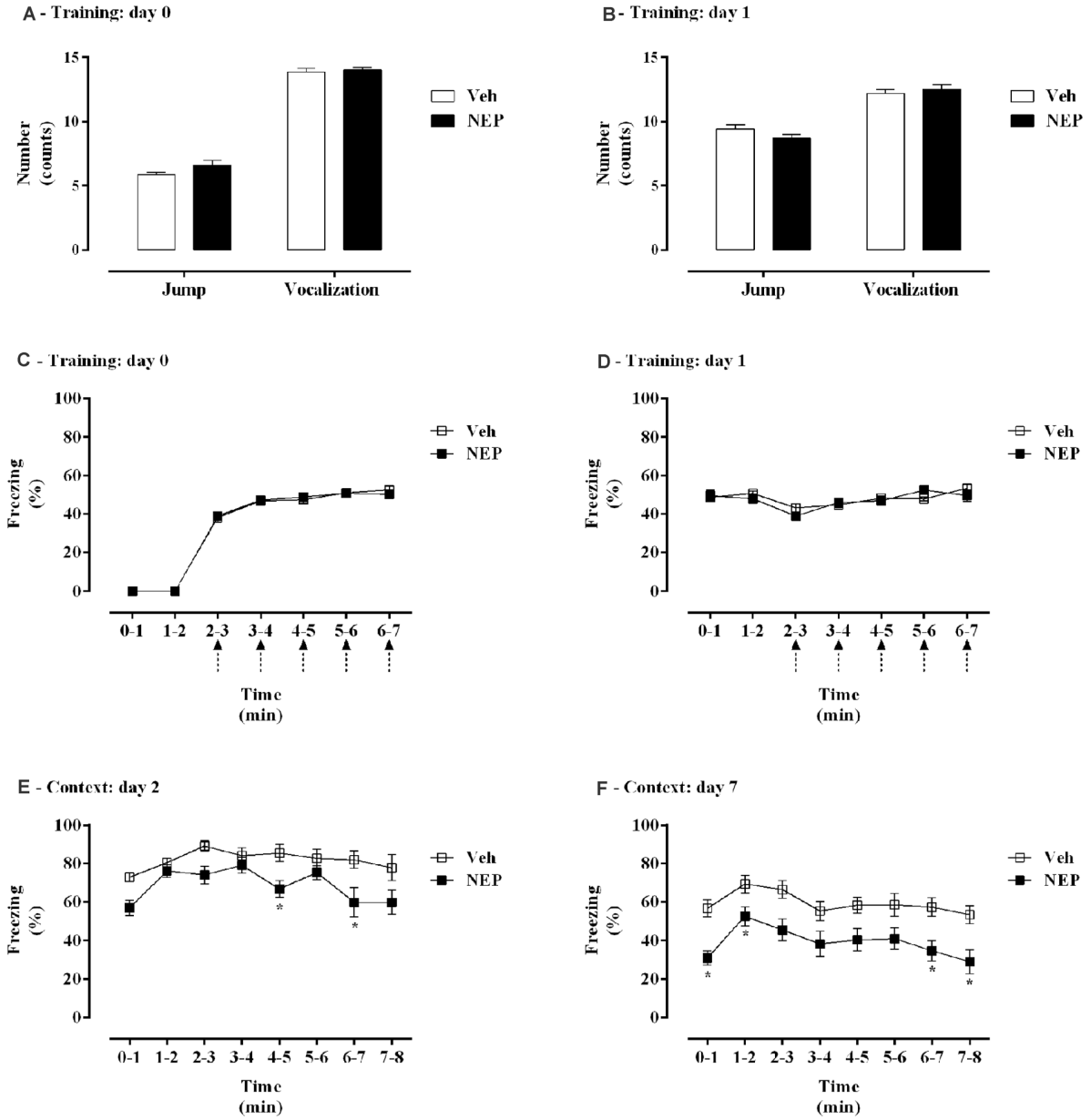

FIGURE 2 | (A,B) Shock responsivity and **(C–F)** freezing behavior during induction of post-traumatic stress disorder (PTSD) on **(A,C)** day 0, **(B,D)** day 1, **(E)** day 2, and **(F)** day 7. Values are means ± SEM of 13–15 mice per group from both experimental protocols. Veh, mice in the PTSD-group and treated with vehicle; NEP, mice in the PTSD-group and treated with nepicastat; ↑ = 3 footshocks delivered with a duration of 10 s and a 10 s interval; *, significantly different from correspondent values in mice in the PTSD-group and treated with vehicle ($p < 0.05$).

$p = 0.5261$; Cohen's $d = 0.25$; **Figure 2B**), or freezing responses (treatment: $F_{(1,26)} = 0.0001832$, $p = 0.9893$, $\eta_p^2 = 0.000007$, **Figure 2C**; treatment: $F_{(1,26)} = 0.2999$, $p = 0.5886$, $\eta_p^2 = 0.01$, **Figure 2D**) between groups. Moreover, on days 2 and 7 mice in the PTSD-group and treated with nepicastat showed a significant decrease in freezing behavior compared to mice treated with vehicle (**Figures 2E,F**). A significant effect of time ($F_{(7,182)} = 5.14$, $p < 0.0001$, $\eta_p^2 = 0.16$; **Figure 2E**; $F_{(7,238)} = 5.31$, $p < 0.0001$, $\eta_p^2 = 0.13$; **Figure 2F**) and treatment ($F_{(1,26)} = 10.49$, $p = 0.0033$, $\eta_p^2 = 0.29$; **Figure 2E**; $F_{(1,34)} = 15.93$, $p = 0.0003$, $\eta_p^2 = 0.32$; **Figure 2F**) was observed.

Nepicastat Treatment Decreases Anxiety-Like Behavior in PTSD

Nine days after PTSD induction the elevated plus maze test was performed to assess the effects of nepicastat treatment on anxiety-like behavior. In this test, the time spent in open arms ($t_{(22)} = 2.68$, $p = 0.0141$, Cohen's $d = 1.06$; **Figure 3A**), open arm

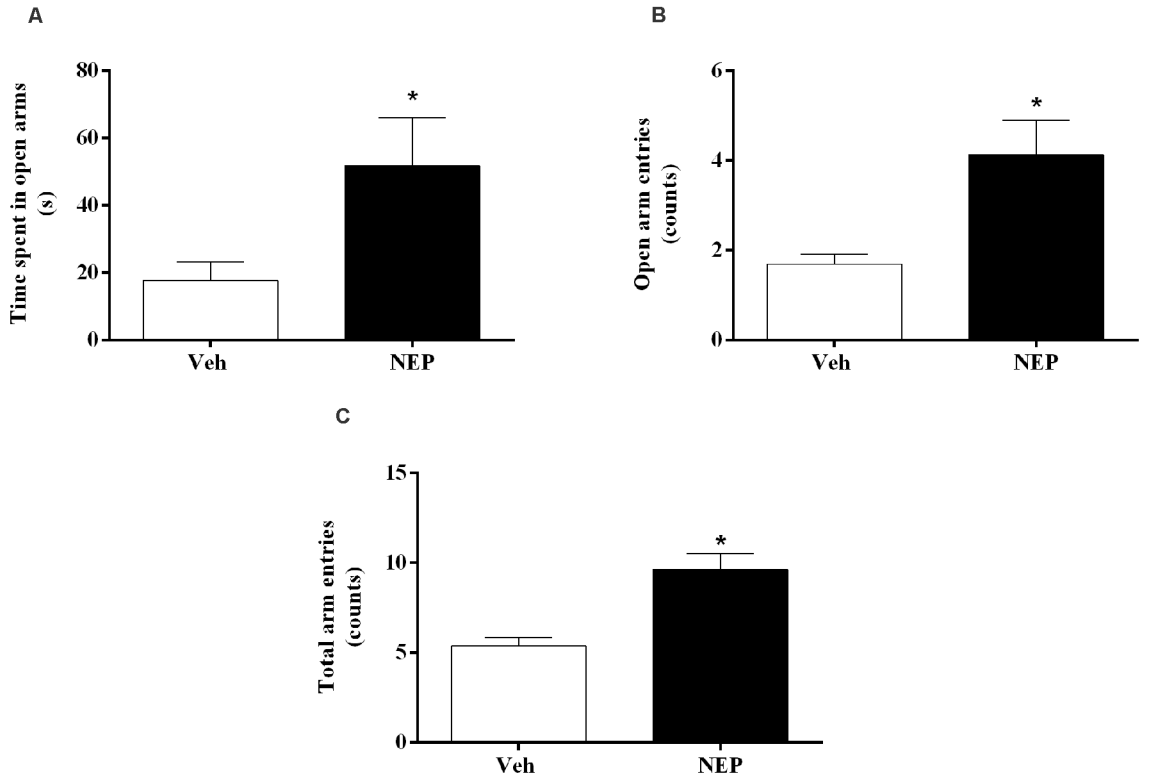

FIGURE 3 | (A) Time spent in open arms, **(B)** open arm entries, and **(C)** total arm entries of the elevated plus maze test, on day 9 after post-traumatic stress disorder (PTSD) induction. Values are means ± SEM of eight mice per group. Veh, mice in the PTSD-group and treated with vehicle; NEP, mice in the PTSD-group and treated with nepicastat; *, significantly different from correspondent values in mice in the PTSD-group and treated with vehicle ($p < 0.05$).

entries ($t_{(22)} = 3.97$, $p = 0.0007$, Cohen's $d = 1.48$; **Figure 3B**), and the total number of arm entries ($t_{(22)} = 4.61$, $p = 0.0001$, Cohen's $d = 1.90$; **Figure 3C**) were significantly increased in mice in the PTSD-group and treated with nepicastat when compared to mice treated with vehicle.

Nepicastat Treatment Did Not Affect Spontaneous Locomotor Activity

Eleven days after PTSD induction the open field test was performed to assess the effects of nepicastat treatment on locomotor activity. There were no significant differences in the total distance traveled ($t_{(14)} = 0.97$, $p = 0.3467$, Cohen's $d = 0.49$; **Figure 4A**), the number of squares crossed ($t_{(14)} = 1.33$, $p = 0.2038$, Cohen's $d = 0.67$; **Figure 4B**), entries in the center ($t_{(14)} = 0.40$, $p = 0.6987$, Cohen's $d = 0.20$; **Figure 4C**), and feces ($t_{(14)} = 0.13$, $p = 0.2216$, Cohen's $d = 0.64$; **Figure 4D**) between groups of animals. Detailed point of estimates of **Figure 4** are in **Supplementary Table 1**.

Accurate Concentration of Nepicastat in Plasma Samples

To assess the effective exposure of nepicastat in administered animals, the levels of the compound were quantified in plasma. Seven days after PTSD induction and daily treatment with nepicastat, the mean concentration of nepicastat in plasma 1 h after last oral administration was 10,046 ± 767 ng/ml. Plasma nepicastat levels in mice treated with vehicle were 0.0000 ng/ml.

Nepicastat Decreases Dopamine-β-Hydroxylase (DBH) Activity in the Adrenal Gland

To evaluate the inhibitory profile on DBH by nepicastat, DBH activity in the adrenal gland was measured. After daily treatment with nepicastat, DBH activity in the adrenal gland was significantly decreased seven ($t_{(10)} = 4.42$, $p = 0.0013$, Cohen's $d = 2.58$; **Figure 5A**) and 12 days ($t_{(14)} = 2.57$, $p = 0.0223$, Cohen's $d = 1.28$; **Figure 5B**) after PTSD induction compared to mice treated with vehicle.

Nepicastat Decreases NA and AD in PTSD

To assess the effects of nepicastat treatment in catecholamines, catecholamine levels were quantified in plasma and tissues. Seven days after PTSD induction, NA ($t_{(10)} = 3.42$, $p = 0.0065$, Cohen's $d = 2.03$; **Figure 6A**) and AD ($t_{(10)} = 5.46$, $p = 0.0003$, Cohen's $d = 3.13$; **Figure 6B**) in the adrenal gland were decreased whereas DA ($t_{(10)} = 6.99$, $p < 0.0001$, Cohen's $d = 4.48$; **Figure 6C**) was increased in mice in the PTSD-group and treated with nepicastat compared to mice treated with vehicle.

Moreover, NA decreased in the prefrontal cortex ($t_{(10)} = 11.79$, $p < 0.0001$, Cohen's $d = 7.39$, **Figure 7A**),

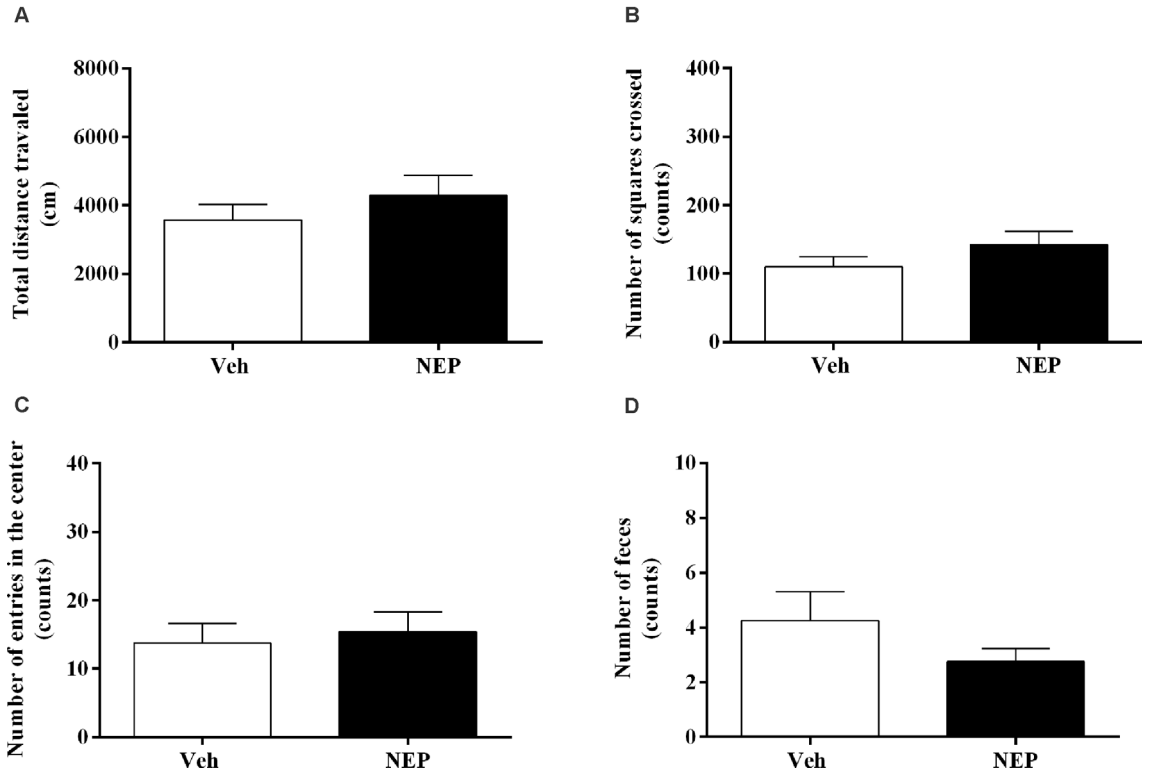

FIGURE 4 | **(A)** Total distance traveled and number of **(B)** squares crossed, **(C)** entries in the center, and **(D)** feces of the open field test, on day 11 after post-traumatic stress disorder (PTSD) induction. Values are means ± SEM of eight mice per group. Veh, mice in the PTSD-group and treated with vehicle; NEP, mice in the PTSD-group and treated with nepicastat.

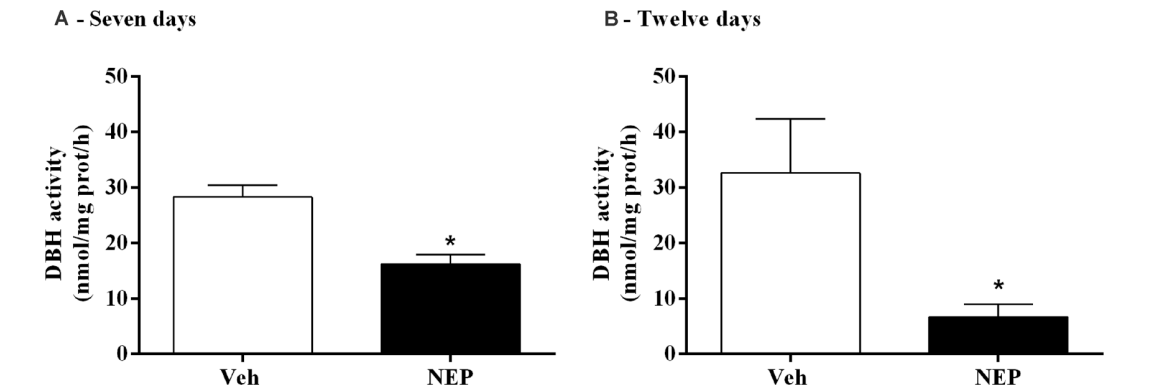

FIGURE 5 | DBH activity in the adrenal gland after treatment with nepicastat **(A)** 7 and **(B)** 12 days after post-traumatic stress disorder (PTSD) induction. Values are means ± SEM of 5–8 mice per group. Veh, mice in the PTSD-group and treated with vehicle; NEP, mice in the PTSD-group and treated with nepicastat; *, significantly different from correspondent values in mice in the PTSD-group and treated with vehicle ($p < 0.05$).

liver ($t_{(10)} = 2.55$, $p = 0.0288$, Cohen's $d = 1.35$; **Figure 7B**), heart ($t_{(14)} = 7.64$, $p < 0.0001$, Cohen's $d = 3.82$; **Figure 7C**), and plasma ($t_{(14)} = 3.69$, $p = 0.0024$, Cohen's $d = 1.84$; **Figure 7D**) of mice in the PTSD-group and treated with nepicastat compared to mice treated with vehicle. No significant differences were observed in NA in the hippocampus ($t_{(14)} = 0.98$, $p = 0.3479$, Cohen's $d = 0.49$; **Figure 7E**) and in the amygdala ($t_{(14)} = 1.765$, $p = 0.1010$, Cohen's $d = 0.90$; **Figure 7F**) between groups of animals.

Nepicastat Decreases *Npas4* and *Bdnf* Gene Expression in the Hippocampus

Hippocampus mRNA expression of neuronal PAS domain protein (*Npas4*, $t_{(10)} = 3.77$, $p = 0.0044$; Cohen's $d = 2.63$;

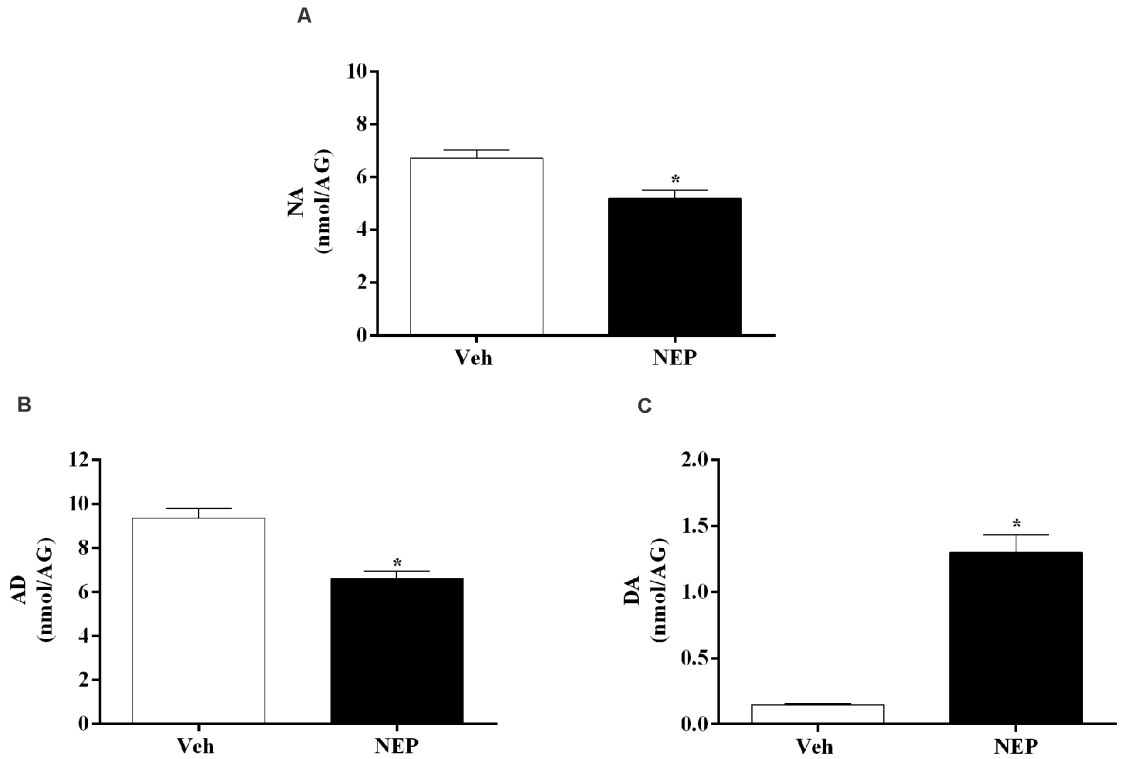

FIGURE 6 | Concentration of **(A)** noradrenaline (NA), **(B)** adrenaline (AD), and **(C)** dopamine (DA) in the adrenal gland (AG) expressed as nmol/AG on day 7 after post-traumatic stress disorder (PTSD) induction. Values are means ± SEM of 5–7 mice per group. Veh, mice in the PTSD-group and treated with vehicle; NEP, mice in the PTSD-group and treated with nepicastat; *, significantly different from correspondent values in mice in the PTSD-group and treated with vehicle ($p < 0.05$).

Figure 8A) and brain-derived neurotrophic factor (*Bdnf*, $t_{(10)} = 2.33$, $p = 0.0450$; Cohen's $d = 1.61$; **Figure 8B**) were significantly increased in mice in the PTSD-group and treated with nepicastat when compared to mice treated with vehicle.

DISCUSSION

After exposure to a traumatic event, PTSD is more likely to develop in females than in males since estrogen promotes catecholamine production (Breslau et al., 1999; McDermott et al., 2015). In fact, sex may be critical concerning the pathogenesis of anxiety disorders and its treatments (Milad et al., 2006). Thus, considering the existence of sex dimorphism in brain morphology and neurotransmission (de Vries and Södersten, 2009; de Lima Xavier et al., 2019), it would be interesting to pay more attention to PTSD treatments in women, and therefore this study is with female mice.

A validated mice model of PTSD was used in this study (Li et al., 2006; Zhang et al., 2012; Verma et al., 2016; Martinho et al., 2020). The absence of differences in vocalization, jump, and freezing responses in both days 0 and 1 (first and second training days of PTSD mice model, respectively) suggests that pain perception of the foot shocks was not different between groups. Contextual reminders in this PTSD animal model may induce the re-experiencing of the traumatic event, which may be analogous to what is experienced by PTSD patients (Gisquet-Verrier et al., 2004). A measure of conditioned associative fear memory is the freezing response upon re-exposure to the contextual reminders, reflecting the response to trauma-related cues as a PTSD symptom (Siegmund and Wotjak, 2007).

We have previously shown that AD may contribute to the persistence of contextual traumatic memories in this PTSD mice model (Martinho et al., 2020). Following a stressful event, an increase in catecholamines in the bloodstream can result in the activation of the β-adrenoceptors of liver cells and the subsequent breakdown of glycogen stores, increasing blood glucose levels (Sutherland et al., 1968; Gray et al., 1980; Dufour et al., 2009). The released glucose crosses the blood-brain barrier and may improve hippocampal-dependent contextual learning (Gold, 2014). In a stressful environment, this increase in glucose may lead to the synthesis of neuromodulators, which will activate signalling pathways that can influence the process of learning and memory consolidation (Durkin et al., 1992; Gold, 2014). Therefore, in the central nervous system, glucose may be a mediator of catecholamines by providing additional energy for specific memory mechanisms, such as contextual fear learning, and in long-term memory formation be a critical component of fear memory modulation (Durkin et al., 1992; Pych et al., 2005; Alves et al., 2016; Oliveira et al., 2018).

DBH catalyzes the conversion of DA to NA and, consequently, DBH inhibition reduces NA and AD, and

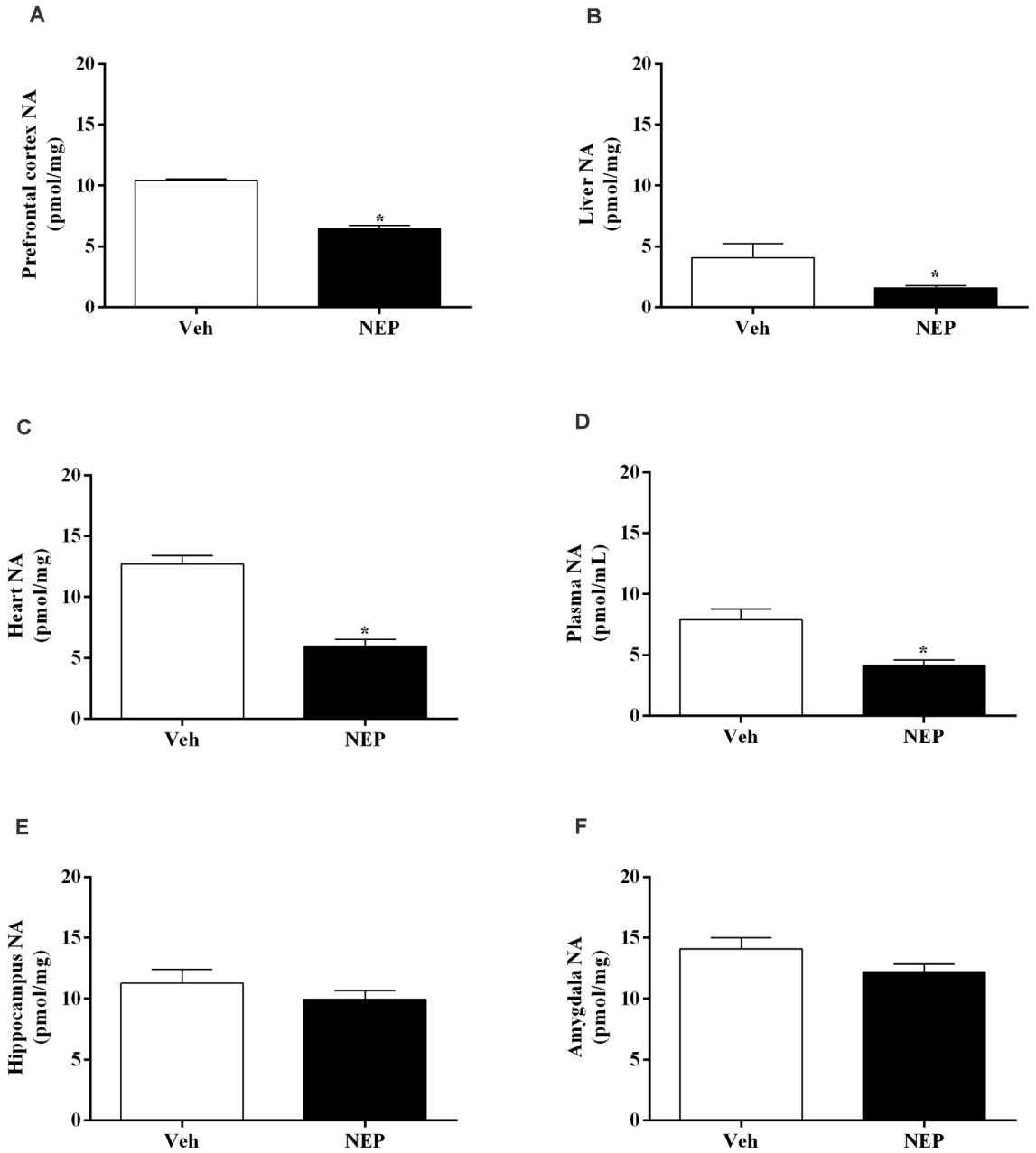

FIGURE 7 | Noradrenaline (NA) concentration in the **(A)** prefrontal cortex, **(B)** liver, **(C)** heart, **(D)** plasma, **(E)** hippocampus, and **(F)** amygdala in mice induced with post-traumatic stress disorder (PTSD). Values are means ± SEM of eight mice per group. Veh, mice in the PTSD-group and treated with vehicle; NEP, mice in the PTSD-group and treated with nepicastat; *, significantly different from correspondent values in mice in the PTSD-group and treated with vehicle ($p < 0.05$).

increases DA (Bourdélat-Parks et al., 2005; Schroeder et al., 2010; Devoto et al., 2014; Igreja et al., 2015; Loureiro et al., 2015). Nepicastat is a highly potent reversible DBH inhibitor. It has the potential to cause a gradual sympathetic slowdown (Stanley et al., 1997; Bonifácio et al., 2015; Loureiro et al., 2015), which may be useful in diseases with sympathetic hyperactivity, such as PTSD. This is the first study to report the effect of nepicastat in modulating the sympathetic nervous system in a PTSD mice model. Since nepicastat exhibits high oral absorption and distribution (Loureiro et al., 2015) it was orally administered. In our study, nepicastat plasma concentration was in agreement with previous reports (Bonifácio et al., 2015; Loureiro et al., 2015), and is consistent with an unbound plasma drug concentration that is pharmacologically active (Braggio et al., 2010). The dosage of 30 mg/kg used leads to maximal adrenal gland DBH enzyme inhibition between 1 and 8 h post-administration (Bonifácio et al., 2015; Loureiro et al., 2015; Catelas et al., 2020). This high inhibition of DBH activity

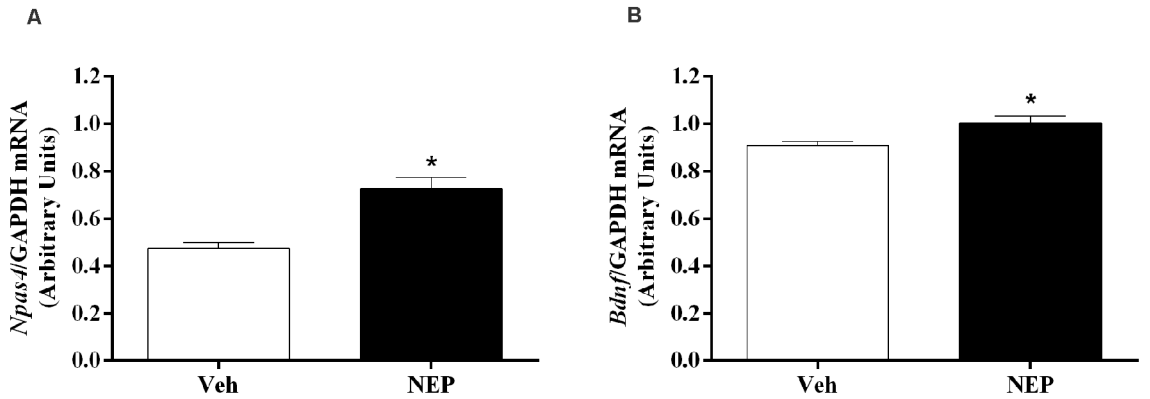

FIGURE 8 | Hippocampus mRNA expression of **(A)** *Npas4* and **(B)** *Bdnf* on day 7 of post-traumatic stress disorder (PTSD) induction. Values are means ± SEM of 5–7 mice per group. Results of mRNA are expressed as arbitrary units (AUs) after normalization for Glyceraldehyde 3-phosphate dehydrogenase (GAPDH). Veh, mice in the PTSD-group and treated with vehicle; NEP, mice in the PTSD-group and treated with nepicastat; *, significantly different from correspondent values in mice in the PTSD-group and treated with vehicle ($p < 0.05$).

allows to effectively elicit pharmacological effects, namely a gradual decrease in catecholamine levels in the following 24 h (Bonifácio et al., 2015; Loureiro et al., 2015), and therefore nepicastat was administered once daily. This dosage was already used in several studies, namely in hypertension (Stanley et al., 1997; Sabbah et al., 2000; Manvich et al., 2013; Bonifácio et al., 2015; Devoto et al., 2015; Loureiro et al., 2015; Catelas et al., 2020). Since we performed nepicastat treatment daily, in the first protocol from days 0–7 and in the second protocol from days 0–12, this administration was chronic. We cannot rule out the possibility that the acute administration of nepicastat 1 h before the behavioral tests would be sufficient to trigger the observed effects since acute administration was not evaluated. However, since catecholamine levels in the adrenal gland only decrease 4 h after acute administration (Catelas et al., 2020) it is unlikely that the acute administration could trigger the observed effects. Our study is in agreement with previous reports (Bonifácio et al., 2015; Loureiro et al., 2015; Catelas et al., 2020) and shows that nepicastat successfully inhibited adrenal gland DBH activity in this PTSD mice model, which was translated into the observed decrease in catecholamine levels. In fact, nepicastat treatment reduced AD and NA in the adrenal gland, and NA in the liver, plasma, and heart in PTSD-group mice.

In the present work, the observed traumatic contextual memory, anxiety-like behavior, and catecholamines in vehicle-treated PTSD mice were similar to our previous publication in which we compared PTSD and control mice (Martinho et al., 2020). In addition, a significant decrease in freezing behavior was observed in mice treated with nepicastat compared to mice treated with vehicle on both days of re-exposure to contextual reminders (days 2 and 7 of PTSD mice model). Thus, in this way, nepicastat treatment by decreasing catecholamines may have blunted the increase of glucose which is known to result from stressful events (Sutherland et al., 1968), and therefore decrease the recall and persistence of contextual traumatic memories in this PTSD mice model. We administered nepicastat immediately after traumatic fear learning to decrease the catecholamines surge elicited by the trauma, which may influence the traumatic memory formation and consolidation processes, and also 1 h before contextual tests to maintain a decreased catecholamines content on these days, which may influence the traumatic memory retrieval and expression processes. Therefore, nepicastat may weaken the formation, consolidation, retrieval, and/or expression processes of traumatic contextual memory. We cannot exclude that auditory cue-induced traumatic memory has a role in nepicastat treatment in PTSD since this cue-induced traumatic memory was not evaluated.

The elevated plus maze is a test based on the natural tendency of animals to avoid elevated and open places, as well as on their natural exploratory behavior in novel environments (Zhang et al., 2012). This test is a method for assessing anxiety-like responses in rodents (Pellow et al., 1985). Our results showed an increase in the time spent and the number of entries in the open arms and total arm entries in mice in the PTSD-group and treated with nepicastat compared to mice treated with vehicle. Thus, this suggests that nepicastat treatment decreases the anxiety-like behavior in mice in the PTSD-group. Since traumatic contextual memory has been described to contribute to the persistence of PTSD symptoms and signs, weakening traumatic memory with nepicastat may, therefore, play a role in decreasing PTSD symptoms and signs.

Previous studies showed that foot shocks related to situational reminders did not affect the locomotor activity of mice in an open field test performed 3–6 weeks (Pynoos et al., 1996) or 10 days (Martinho et al., 2020) after the PTSD mice model induction. In agreement, our results showed no differences between groups in the total distance traveled, number of squares crossed, and entries in the center of the open field test. Also, total arm entries in the elevated plus maze may not be an optimal measure of locomotor activity (Walf and Frye, 2007). In fact, the observed increase in total arm entries induced by nepicastat treatment was not associated with a similar effect on locomotor activity, as revealed in the open field test. Therefore, we suggest that the

behavioral changes observed with nepicastat treatment are not due to differences in locomotor activity.

Nepicastat reduced NA levels in the prefrontal cortex. However, there were no changes in catecholamine levels in hippocampus and amygdala in mice induced with PTSD. Thus, nepicastat possibly showed preferential distribution to the prefrontal cortex than to hippocampus and amygdala. Taken all together, these results are in agreement with a previous study that described central and peripheral catecholamine modulation by nepicastat in spontaneously hypertensive rats and dogs (Stanley et al., 1997). The prefrontal cortex seems to be important in memory retrieval and consolidation. NA release in the prefrontal cortex operates in an inverted-U shape (Arnsten, 2007; Arnsten et al., 2015). If moderate levels of NA are released, there is preferential activation of α_2-adrenoceptors which enhance prefrontal cortex function (Li and Mei, 1994). However, when higher levels of NA are released occurs the activation of the α_1-adrenoceptors (Arnsten, 2000) that impairs prefrontal cortex function which is associated with symptomatic PTSD (Shin et al., 2006). Since we found a decrease of NA in the prefrontal cortex after nepicastat treatment compared to vehicle-treated PTSD mice, the DBH inhibitor nepicastat may reduce NA levels in prefrontal cortex contributing to prefrontal cortex noradrenergic hyporesponsiveness and decrease PTSD traumatic contextual memories and anxiety-like behavior.

The hippocampus is involved in contextual fear conditioning (Rudy et al., 2004). Contextual stimuli are processed in the hippocampus and the hippocampal afferents to the amygdala synapse primarily on basal nuclei. Indeed, selective neurotoxic bilateral damage to the basal nuclei disrupted contextual, but not auditory fear conditioning (Onishi and Xavier, 2010). Since the hippocampus is involved in contextual fear conditioning (Rudy et al., 2004) and catecholamines in this brain area were seen to be unaffected by nepicastat treatment, we decided to explore possible molecular mechanisms in the hippocampus underlying the observed decrease in contextual traumatic memory.

The weakening of the formation, consolidation, retrieval, and/or expression processes of traumatic contextual memory by nepicastat lead to an increase in *Npas4* mRNA expression in the hippocampus on day 7 of PTSD induction. *Npas4* is a neuronal immediate early gene and a transcription factor highly expressed in the adult hippocampus (Lin et al., 2008; Ploski et al., 2011). In previous studies, it has been suggested that higher hippocampal *Npas4* mRNA expression was related to higher activation of the hippocampus (Drouet et al., 2018), and this was shown to be consistent with a decrease in fear memory (Deschaux et al., 2015). In the hippocampal CA3 region, *Npas4* may regulate a gene induction program essential for contextual fear memory (Ramamoorthi et al., 2011). Also, it has been shown that *Npas4* controls a transcriptional program that includes *Bdnf* gene (Lin et al., 2008). *Bdnf* mRNA expression also increases in the hippocampus on day 7 of PTSD mice model after treatment with nepicastat. BDNF is a neurotrophin implicated in neuronal survival (Barde et al., 1982; Lewin and Barde, 1996) and in neuronal maturation (Lindsay et al., 1994), which may be important in weakening traumatic memory after nepicastat treatment.

The effectiveness of drugs to treat PTSD is being challenged (Ipser and Stein, 2012) and there are evidence-based suggestions that psychotherapy decreases rather than remits PTSD symptoms (Steenkamp and Litz, 2013). In a previous study, safety analyses showed that nepicastat was well-tolerated in healthy adults and no differences in adverse events were observed (De La Garza et al., 2015). Our study showed that nepicastat treatment might be effective in reducing PTSD symptoms in a PTSD mice model with increased catecholamine levels (AD and NA; Martinho et al., 2020), and thus could be an efficient treatment at least in humans with PTSD that have increased catecholamine plasma levels.

In conclusion, DBH inhibitor nepicastat has an effect consistent with a decrease in the persistence of traumatic memories and anxiety-like behavior in this PTSD mice model. The disruption of traumatic memories through interference with the formation, consolidation, retrieval, and/or expression processes may be important to decrease PTSD symptoms and signs. The increase in *Npas4* and *Bdnf* mRNA expression in the hippocampus may be important to develop a weaker traumatic contextual memory after nepicastat treatment.

DATA AVAILABILITY STATEMENT

The original contributions presented in the study are included in the article/**Supplementary Materials**, further inquiries can be directed to the corresponding author.

ETHICS STATEMENT

The animal study was reviewed and approved by Organism Responsible for Animal Welfare in Faculty of Medicine of University of Porto and National Authority for Animal Health.

AUTHOR CONTRIBUTIONS

MM-R and RM conceived the study. RM performed most of the experiments and respective statistical analysis (sections "PTSD Mice Model", "Drug Treatments", "Behavioral Tests", and "Quantification of Catecholamines"). GC (section "RNA Isolation" and "Relative Quantification of mRNA Expression"), RS (sections "PTSD Mice Model" and "Open Field Test"), AO (sections "PTSD Mice Model" and "Quantification of Catecholamines"), SS (section "PTSD Mice Model"), and PS (section "Quantification of Catecholamines") performed some experiments and respective statistical analysis. CF-L and CC [sections "Quantification of Nepicastat in Plasma Samples" and "Dopamine-β-Hydroxylase (DBH) Activity Determination"] performed some experiments. RM and MM-R reviewed the statistical analysis, interpreted results, and wrote the manuscript. All authors contributed to the article and approved the submitted version.

FUNDING

This work was supported by BIAL-Portela and C[a], S.A. and by Foundation for Science and Technology (FCT,

project UIDB/04308/2020). RM and AO were in receipt of Ph.D. studentships from FCT (SFRH/BD/133860/2017 and SFRH/BD/138984/2018, respectively). The funder, BIAL-Portela and C[a], S.A., had the following involvement with the study: the provision of Nepicastat hydrochloride, pharmacokinetic evaluation of nepicastat in plasma, DBH activity evaluation in the adrenal gland, and a final revision of the written manuscript. The funder was not involved in the study design, samples collection, data analysis (freezing, jump, vocalization, elevated plus maze test, open field test, catecholamines quantification, and qPCR results), interpretation of data, the writing of this article or the decision to submit it in this Journal for publication.

ACKNOWLEDGMENTS

We thank Sónia Soares and António Carlos Ferreira for their technical support, and to Vânia Batalha and Nuno Pires for the revision of the manuscript.

SUPPLEMENTARY MATERIALS

The Supplementary Material for this article can be found online at: https://www.frontiersin.org/articles/10.3389/fnmol.2021.745219/full#supplementary-material.

REFERENCES

Alberini, C. M. (2005). Mechanisms of memory stabilization: are consolidation and reconsolidation similar or distinct processes? *Trends Neurosci.* 28, 51–56. doi: 10.1016/j.tins.2004.11.001

Alves, E., Lukoyanov, N., Serrao, P., Moura, D., and Moreira-Rodrigues, M. (2016). Epinephrine increases contextual learning through activation of peripheral β2-adrenoceptors. *Psychopharmacology* 233, 2099–2108. doi: 10.1007/s00213-016-4254-5

American Psychiatric Association. (2013). *Diagnostic and Statistical Manual of Mental Disorders, Fifth Edition: (DSM-5).* Washington, DC: American Psychiatric Association.

Arnsten, A. F. (2000). Through the looking glass: differential noradenergic modulation of prefrontal cortical function. *Neural Plast.* 7, 133–146. doi: 10.1155/NP.2000.133

Arnsten, A. F. T. (2007). Catecholamine and second messenger influences on prefrontal cortical networks of "representational knowledge": a rational bridge between genetics and the symptoms of mental illness. *Cereb. Cortex* 17, i6–i15. doi: 10.1093/cercor/bhm033

Arnsten, A. F. T., Raskind, M. A., Taylor, F. B., and Connor, D. F. (2015). The effects of stress exposure on prefrontal cortex: translating basic research into successful treatments for post-traumatic stress disorder. *Neurobiol. Stress* 1, 89–99. doi: 10.1016/j.ynstr.2014.10.002

Barde, Y. A., Edgar, D., and Thoenen, H. (1982). Purification of a new neurotrophic factor from mammalian brain. *EMBO J.* 1, 549–553. doi: 10.1002/j.1460-2075.1982.tb01207.x

Beliaev, A., Ferreira, H., Learmonth, D., and Soares-da-Silva, P. (2009). Dopamine β-monooxygenase: mechanism, substrates and inhibitors. *Curr. Enzym. Inhib.* 5, 27–43. doi: 10.2174/157340809787314265

Bonifácio, M. J., Sousa, F., Neves, M., Palma, N., Igreja, B., Pires, N. M., et al. (2015). Characterization of the interaction of the novel antihypertensive etamicastat with human dopamine-β-hydroxylase: comparison with nepicastat. *Eur. J. Pharmacol.* 751, 50–58. doi: 10.1016/j.ejphar.2015.01.034

Bourdélat-Parks, B. N., Anderson, G. M., Donaldson, Z. R., Weiss, J. M., Bonsall, R. W., Emery, M. S., et al. (2005). Effects of dopamine β-hydroxylase genotype and disulfiram inhibition on catecholamine homeostasis in mice. *Psychopharmacology* 183, 72–80. doi: 10.1007/s00213-005-0139-8

Braggio, S., Montanari, D., Rossi, T., and Ratti, E. (2010). Drug efficiency: a new concept to guide lead optimization programs towards the selection of better clinical candidates. *Expert Opin. Drug Discov.* 5, 609–618. doi: 10.1517/17460441.2010.490553

Breslau, N., Peterson, E. L., Kessler, R. C., and Schultz, L. R. (1999). Short screening scale for DSM-IV posttraumatic stress disorder. *Am. J. Psychiatry* 156, 908–911. doi: 10.1176/ajp.156.6.908

Brown, R., and Kulik, J. (1977). Flashbulb memories. *Cognition* 5, 73–99. doi: 10.1016/0010-0277(77)90018-X

Catelas, D. N., Serrao, M. P., and Soares-Da-Silva, P. (2020). Effects of nepicastat upon dopamine-β-hydroxylase activity and dopamine and norepinephrine levels in the rat left ventricle, kidney, and adrenal gland. *Clin. Exp. Hypertens.* 42, 118–125. doi: 10.1080/10641963.2019.1583245

Chiu, K., Lau, W. M., Lau, H. T., So, K.-F., and Chang, R. C.-C. (2007). Micro-dissection of rat brain for RNA or protein extraction from specific brain region. *J. Vis. Exp.* 7:269. doi: 10.3791/269

De La Garza, R., Bubar, M. J., Carbone, C. L., Moeller, F. G., Newton, T. F., Anastasio, N. C., et al. (2015). Evaluation of the dopamine β-hydroxylase (DβH) inhibitor nepicastat in participants who meet criteria for cocaine use disorder. *Prog. Neuropsychopharmacol. Biol. Psychiatry* 59, 40–48. doi: 10.1016/j.pnpbp.2015.01.009

de Lima Xavier, L., Hanekamp, S., and Simonyan, K. (2019). Sexual dimorphism within brain regions controlling speech production. *Front. Neurosci.* 13:795. doi: 10.3389/fnins.2019.00795

de Vries, G. J., and Södersten, P. (2009). Sex differences in the brain: the relation between structure and function. *Horm. Behav.* 55, 589–596. doi: 10.1016/j.yhbeh.2009.03.012

Deschaux, O., Koumar, O.-C., Canini, F., Moreau, J.-L., and Garcia, R. (2015). High-frequency stimulation of the hippocampus blocks fear learning sensitization and return of extinguished fear. *Neuroscience* 286, 423–429. doi: 10.1016/j.neuroscience.2014.12.001

Deslauriers, J., Toth, M., Der-Avakian, A., and Risbrough, V. B. (2018). Current status of animal models of posttraumatic stress disorder: behavioral and biological phenotypes and future challenges in improving translation. *Biol. Psychiatry* 83, 895–907. doi: 10.1016/j.biopsych.2017.11.019

Devoto, P., Flore, G., Saba, P., Bini, V., and Gessa, G. L. (2014). The dopamine β-hydroxylase inhibitor nepicastat increases dopamine release and potentiates psychostimulant-induced dopamine release in the prefrontal cortex. *Addict. Biol.* 19, 612–622. doi: 10.1111/adb.12026

Devoto, P., Flore, G., Saba, P., Frau, R., and Gessa, G. L. (2015). Selective inhibition of dopamine-β-hydroxylase enhances dopamine release from noradrenergic terminals in the medial prefrontal cortex. *Brain Behav.* 5:e00393. doi: 10.1002/brb3.393

Drouet, J.-B., Peinnequin, A., Faure, P., Denis, J., Fidier, N., Maury, R., et al. (2018). Stress-induced hippocampus Npas4 mRNA expression relates to specific psychophysiological patterns of stress response. *Brain Res.* 1679, 75–83. doi: 10.1016/j.brainres.2017.11.024

Dufour, S., Lebon, V., Shulman, G. I., and Petersen, K. F. (2009). Regulation of net hepatic glycogenolysis and gluconeogenesis by epinephrine in humans. *Am. J. Physiol. Endocrinol. Metab.* 297, E231–E235. doi: 10.1152/ajpendo.00222.2009

Durkin, T. P., Messier, C., de Boer, P., and Westerink, B. H. (1992). Raised glucose levels enhance scopolamine-induced acetylcholine overflow from the hippocampus: an *in vivo* microdialysis study in the rat. *Behav. Brain Res.* 49, 181–188. doi: 10.1016/s0166-4328(05)80163-9

Gisquet-Verrier, P., Botreau, F., Venero, C., and Sandi, C. (2004). Exposure to retrieval cues improves retention performance and induces changes in ACTH and corticosterone release. *Psychoneuroendocrinology* 29, 529–556. doi: 10.1016/s0306-4530(03)00085-4

Gold, P. E. (2014). Regulation of memory—from the adrenal medulla to liver to astrocytes to neurons. *Brain Res. Bull.* 105, 25–35. doi: 10.1016/j.brainresbull.2013.12.012

Gray, D. E., Lickley, H. L. A., and Vranic, M. (1980). Physiologic effects of epinephrine on glucose turnover and plasma free fatty acid concentrations

mediated independently of glucagon. *Diabetes* 29, 600–609. doi: 10.2337/diab.29.8.600

Hegde, S. S., and Friday, K. F. (1998). Dopamine-β-hydroxylase inhibition: a novel sympatho-modulatory approach for the treatment of congestive heart failure. *Curr. Pharm. Des.* 4, 469–479.

Henry, J., Rodriguez, A., and Wlodkowic, D. (2019). Impact of digital video analytics on accuracy of chemobehavioral phenotyping in aquatic toxicology. *PeerJ* 7:e7367. doi: 10.7717/peerj.7367

Igreja, B., Pires, N. M., Bonifacio, M. J., Loureiro, A. I., Fernandes-Lopes, C., Wright, L. C., et al. (2015). Blood pressure-decreasing effect of etamicastat alone and in combination with antihypertensive drugs in the spontaneously hypertensive rat. *Hypertens Res.* 38, 30–38. doi: 10.1038/hr.2014.143

Inslicht, S. S., Metzler, T. J., Garcia, N. M., Pineles, S. L., Milad, M. R., Orr, S. P., et al. (2013). Sex differences in fear conditioning in posttraumatic stress disorder. *J. Psychiatr. Res.* 47, 64–71. doi: 10.1016/j.jpsychires.2012.08.027

Ipser, J. C., and Stein, D. J. (2012). Evidence-based pharmacotherapy of post-traumatic stress disorder (PTSD). *Int. J. Neuropsychopharmacol.* 15, 825–840. doi: 10.1017/S1461145711001209

Ishii, Y., Natsugoe, K., and Umezawa, H. (1975). Pharmacological action of FD-008, a new dopamine-β-hydroxylase inhibitor. *Arzneimittelforschung* 25, 213–215.

Kensinger, E. A., Garoff-Eaton, R. J., and Schacter, D. L. (2006). Memory for specific visual details can be enhanced by negative arousing content. *J. Mem. Lang.* 54, 99–112. doi: 10.1016/j.jml.2005.05.005

Kruse, L. I., Kaiser, C., DeWolf, W. E. J., Frazee, J. S., Erickson, R. W., Ezekiel, M., et al. (1986). Substituted 1-benzylimidazole-2-thiols as potent and orally active inhibitors of dopamine β-hydroxylase. *J. Med. Chem.* 29, 887–889. doi: 10.1021/jm00156a002

Kruse, L. I., Kaiser, C., DeWolf, W. E. J., Frazee, J. S., Ross, S. T., Wawro, J., et al. (1987). Multisubstrate inhibitors of dopamine β-hydroxylase. 2. Structure-activity relationships at the phenethylamine binding site. *J. Med. Chem.* 30, 486–494. doi: 10.1021/jm00386a008

Lewin, G. R., and Barde, Y.-A. (1996). Physiology of the neurotrophins. *Annu. Rev. Neurosci.* 19, 289–317. doi: 10.1146/annurev.ne.19.030196.001445

Li, B.-M., and Mei, Z.-T. (1994). Delayed-response deficit induced by local injection of the α2-adrenergic antagonist yohimbine into the dorsolateral prefrontal cortex in young adult monkeys. *Behav. Neural Biol.* 62, 134–139. doi: 10.1016/s0163-1047(05)80034-2

Li, S., Murakami, Y., Wang, M., Maeda, K., and Matsumoto, K. (2006). The effects of chronic valproate and diazepam in a mouse model of posttraumatic stress disorder. *Pharmacol. Biochem. Behav.* 85, 324–331. doi: 10.1016/j.pbb.2006.08.015

Lin, Y., Bloodgood, B. L., Hauser, J. L., Lapan, A. D., Koon, A. C., Kim, T.-K., et al. (2008). Activity-dependent regulation of inhibitory synapse development by Npas4. *Nature* 455, 1198–1204. doi: 10.1038/nature07319

Lindsay, R. M., Wiegand, S. J., Altar, C. A., and DiStefano, P. S. (1994). Neurotrophic factors: from molecule to man. *Trends Neurosci.* 17, 182–190. doi: 10.1016/0166-2236(94)90099-x

Lissek, S., Powers, A. S., McClure, E. B., Phelps, E. A., Woldehawariat, G., Grillon, C., et al. (2005). Classical fear conditioning in the anxiety disorders: a meta-analysis. *Behav. Res. Ther.* 43, 1391–1424. doi: 10.1016/j.brat.2004.10.007

Loureiro, A. I., Bonifacio, M. J., Fernandes-Lopes, C., Igreja, B., Wright, L. C., and Soares-da-Silva, P. (2014). Etamicastat, a new dopamine-ss-hydroxylase inhibitor, pharmacodynamics and metabolism in rat. *Eur. J. Pharmacol.* 740, 285–294. doi: 10.1016/j.ejphar.2014.07.027

Loureiro, A. I., Bonifácio, M. J., Fernandes-Lopes, C., Pires, N., Igreja, B., Wright, L. C., et al. (2015). Role of P-glycoprotein and permeability upon the brain distribution and pharmacodynamics of etamicastat: a comparison with nepicastat. *Xenobiotica* 45, 828–839. doi: 10.3109/00498254.2015.1018985

Loureiro, A. I., Fernandes-Lopes, C., Bonifacio, M. J., Wright, L. C., and Soares-da-Silva, P. (2013). N-acetylation of etamicastat, a reversible dopamine-β-hydroxylase inhibitor. *Drug Metab. Dispos.* 41, 2081–2086. doi: 10.1124/dmd.113.053736

Manvich, D. F., DePoy, L. M., and Weinshenker, D. (2013). Dopamine β-hydroxylase inhibitors enhance the discriminative stimulus effects of cocaine in rats. *J. Pharmacol. Exp. Ther.* 347, 564–573. doi: 10.1124/jpet.113.207746

Martinho, R., Oliveira, A., Correia, G., Marques, M., Seixas, R., Serrão, P., et al. (2020). Epinephrine may contribute to the persistence of traumatic memories in a post-traumatic stress disorder animal model. *Front. Mol. Neurosci.* 13:588802. doi: 10.3389/fnmol.2020.588802

McClintock, M. K. (1978). Estrous synchrony and its mediation by airborne chemical communication (Rattus norvegicus). *Horm. Behav.* 10, 264–275. doi: 10.1016/0018-506x(78)90071-5

McDermott, C. M., Liu, D., Ade, C., and Schrader, L. A. (2015). Estradiol replacement enhances fear memory formation, impairs extinction and reduces COMT expression levels in the hippocampus of ovariectomized female mice. *Neurobiol. Learn. Mem.* 118, 167–177. doi: 10.1016/j.nlm.2014.12.009

Mendes, P., Martinho, R., Leite, S., Maia-Moço, L., Leite-Moreira, A. F., Lourenço, A. P., et al. (2018). Chronic exercise induces pathological left ventricular hypertrophy in adrenaline-deficient mice. *Int. J. Cardiol.* 253, 113–119. doi: 10.1016/j.ijcard.2017.10.014

Milad, M. R., Goldstein, J. M., Orr, S. P., Wedig, M. M., Klibanski, A., Pitman, R. K., et al. (2006). Fear conditioning and extinction: influence of sex and menstrual cycle in healthy humans. *Behav. Neurosci.* 120, 1196–1203. doi: 10.1037/0735-7044.120.5.1196

Mitra, S., Sameer Kumar, G. S., Tiwari, V., Lakshmi, B. J., Thakur, S. S., and Kumar, S. (2016). Implication of genetic deletion of Wdr13 in mice: mild anxiety, better performance in spatial memory task, with upregulation of multiple synaptic proteins. *Front. Mol. Neurosci.* 9:73. doi: 10.3389/fnmol.2016.00073

Moreira-Rodrigues, M., Graça, A. L., Ferreira, M., Afonso, J., Serrão, P., Morato, M., et al. (2014). Attenuated aortic vasodilation and sympathetic prejunctional facilitation in epinephrine-deficient mice: selective impairment of β2-adrenoceptor responses. *J. Pharmacol. Exp. Ther.* 351, 243–249. doi: 10.1124/jpet.114.217281

Moreira-Rodrigues, M., Roncon-Albuquerque, R. Jr., Henriques-Coelho, T., Lourenco, A. P., Sampaio-Maia, B., Santos, J., et al. (2007). Cardiac remodeling and dysfunction in nephrotic syndrome. *Kidney Int.* 71, 1240–1248. doi: 10.1038/sj.ki.5002204

Murchison, C. F., Zhang, X.-Y., Zhang, W.-P., Ouyang, M., Lee, A., and Thomas, S. A. (2004). A distinct role for norepinephrine in memory retrieval. *Cell* 117, 131–143. doi: 10.1016/s0092-8674(04)00259-4

Nader, K., Schafe, G. E., and LeDoux, J. E. (2000). The labile nature of consolidation theory. *Nat. Rev. Neurosci.* 1, 216–219. doi: 10.1038/35044580

Ohlstein, E. H., Kruse, L. I., Ezekiel, M., Sherman, S. S., Erickson, R., DeWolf, W. E. J., et al. (1987). Cardiovascular effects of a new potent dopamine β-hydroxylase inhibitor in spontaneously hypertensive rats. *J. Pharmacol. Exp. Ther.* 241, 554–559.

Olff, M. (2017). Sex and gender differences in post-traumatic stress disorder: an update. *Eur. J. Psychotraumatol.* 8:1351204. doi: 10.1080/20008198.2017.1351204

Oliveira, A., Martinho, R., Serrão, P., and Moreira-Rodrigues, M. (2018). Epinephrine released during traumatic events may strengthen contextual fear memory through increased hippocampus mRNA expression of Nr4a transcription factors. *Front. Mol. Neurosci.* 11:334. doi: 10.3389/fnmol.2018.00334

Onishi, B. K. A., and Xavier, G. F. (2010). Contextual, but not auditory, fear conditioning is disrupted by neurotoxic selective lesion of the basal nucleus of amygdala in rats. *Neurobiol. Learn. Mem.* 93, 165–174. doi: 10.1016/j.nlm.2009.09.007

Pellow, S., Chopin, P., File, S. E., and Briley, M. (1985). Validation of open:closed arm entries in an elevated plus-maze as a measure of anxiety in the rat. *J. Neurosci. Methods* 14, 149–167. doi: 10.1016/0165-0270(85)90031-7

Pires, N. M., Loureiro, A. I., Igreja, B., Lacroix, P., and Soares-da-Silva, P. (2015). Cardiovascular safety pharmacology profile of etamicastat, a novel peripheral selective dopamine-β-hydroxylase inhibitor. *Eur. J. Pharmacol.* 750, 98–107. doi: 10.1016/j.ejphar.2015.01.035

Ploski, J. E., Monsey, M. S., Nguyen, T., DiLeone, R. J., and Schafe, G. E. (2011). The neuronal PAS domain protein 4 (Npas4) is required for new and reactivated fear memories. *PLoS One* 6:e23760. doi: 10.1371/journal.pone.0023760

Pych, J. C., Chang, Q., Colon-Rivera, C., Haag, R., and Gold, P. E. (2005). Acetylcholine release in the hippocampus and striatum during place and response training. *Learn. Mem.* 12, 564–572. doi: 10.1101/lm.33105

Pynoos, R. S., Ritzmann, R. F., Steinberg, A. M., Goenjian, A., and Prisecaru, I. (1996). A behavioral animal model of posttraumatic stress disorder featuring repeated exposure to situational reminders. *Biol. Psychiatry* 39, 129–134. doi: 10.1016/0006-3223(95)00088-7

Ramamoorthi, K., Fropf, R., Belfort, G. M., Fitzmaurice, H. L., McKinney, R. M., Neve, R. L., et al. (2011). Npas4 regulates a transcriptional program in CA3 required for contextual memory formation. *Science* 334, 1669–1675. doi: 10.1126/science.1208049

Rios, M., Habecker, B., Sasaoka, T., Eisenhofer, G., Tian, H., Landis, S., et al. (1999). Catecholamine synthesis is mediated by tyrosinase in the absence of tyrosine hydroxylase. *J. Neurosci.* 19, 3519–3526. doi: 10.1523/JNEUROSCI.19-09-03519.1999

Rocinholi, L. F., Almeida, S. S., and De-Oliveira, L. M. (1997). Response threshold to aversive stimuli in stimulated early protein-malnourished rats. *Braz. J. Med. Biol. Res.* 30, 407–413. doi: 10.1590/s0100-879x1997000300016

Rodriguez, A., Zhang, H., Klaminder, J., Brodin, T., and Andersson, M. (2017). ToxId: an efficient algorithm to solve occlusions when tracking multiple animals. *Sci. Rep.* 7:14774. doi: 10.1038/s41598-017-15104-2

Rodriguez, A., Zhang, H., Klaminder, J., Brodin, T., Andersson, P. L., and Andersson, M. (2018). ToxTrac: a fast and robust software for tracking organisms. *Methods Ecol. Evol.* 9, 460–464. doi: 10.1111/2041-210x.12874

Rudy, J. W., Huff, N. C., and Matus-Amat, P. (2004). Understanding contextual fear conditioning: insights from a two-process model. *Neurosci. Biobehav. Rev.* 28, 675–685. doi: 10.1016/j.neubiorev.2004.09.004

Sabbah, H. N., Stanley, W. C., Sharov, V. G., Mishima, T., Tanimura, M., Benedict, C. R., et al. (2000). Effects of dopamine β-hydroxylase inhibition with nepicastat on the progression of left ventricular dysfunction and remodeling in dogs with chronic heart failure. *Circulation* 102, 1990–1995. doi: 10.1161/01.cir.102.16.1990

Schroeder, J. P., Cooper, D. A., Schank, J. R., Lyle, M. A., Gaval-Cruz, M., Ogbonmwan, Y. E., et al. (2010). Disulfiram attenuates drug-primed reinstatement of cocaine seeking *via* inhibition of dopamine β-hydroxylase. *Neuropsychopharmacology* 35, 2440–2449. doi: 10.1038/npp.2010.127

Seedat, S., Stein, D. J., and Carey, P. D. (2005). Post-traumatic stress disorder in women: epidemiological and treatment issues. *CNS Drugs* 19, 411–427. doi: 10.2165/00023210-200519050-00004

Shalev, A. Y., Orr, S. P., Peri, T., Schreiber, S., and Pitman, R. K. (1992). Physiologic responses to loud tones in Israeli patients with posttraumatic stress disorder. *Arch. Gen. Psychiatry* 49, 870–875. doi: 10.1001/archpsyc.1992.01820110034005

Sherin, J. E., and Nemeroff, C. B. (2011). Post-traumatic stress disorder: the neurobiological impact of psychological trauma. *Dialogues Clin. Neurosci.* 13, 263–278. doi: 10.31887/DCNS.2011.13.2/jsherin

Shin, L. M., Rauch, S. L., and Pitman, R. K. (2006). Amygdala, medial prefrontal cortex, and hippocampal function in PTSD. *Ann. N Y Acad. Sci.* 1071, 67–79. doi: 10.1196/annals.1364.007

Siegmund, A., and Wotjak, C. T. (2007). A mouse model of posttraumatic stress disorder that distinguishes between conditioned and sensitised fear. *J. Psychiatr. Res.* 41, 848–860. doi: 10.1016/j.jpsychires.2006.07.017

Stanley, W. C., Li, B., Bonhaus, D. W., Johnson, L. G., Lee, K., Porter, S., et al. (1997). Catecholamine modulatory effects of nepicastat (RS-25560–197), a novel, potent and selective inhibitor of dopamine-β-hydroxylase. *Br. J. Pharmacol.* 121, 1803–1809. doi: 10.1038/sj.bjp.0701315

Steenkamp, M. M., and Litz, B. T. (2013). Psychotherapy for military-related posttraumatic stress disorder: review of the evidence. *Clin. Psychol. Rev.* 33, 45–53. doi: 10.1016/j.cpr.2012.10.002

Sutherland, E. W., Robison, G. A., and Butcher, R. W. (1968). Some aspects of the biological role of adenosine 3', 5'-monophosphate (cyclic AMP). *Circulation* 37, 279–306. doi: 10.1161/01.cir.37.2.279

Toth, M., Ziegler, M., Sun, P., Gresack, J., and Risbrough, V. (2013). Impaired conditioned fear response and startle reactivity in epinephrine deficient mice. *Behav. Pharmacol.* 24:1. doi: 10.1097/FBP.0b013e32835cf408

Valentinuzzi, V. S., Kolker, D. E., Vitaterna, M. H., Shimomura, K., Whiteley, A., Low-Zeddies, S., et al. (1998). Automated measurement of mouse freezing behavior and its use for quantitative trait locus analysis of contextual fear conditioning in (BALB/cJ × C57BL/6J)F(2) mice. *Learn. Mem.* 5, 391–403.

Verma, M., Bali, A., Singh, N., and Jaggi, A. S. (2016). Investigating the role of nisoldipine in foot-shock-induced post-traumatic stress disorder in mice. *Fundam. Clin. Pharmacol.* 30, 128–136. doi: 10.1111/fcp.12174

Walf, A. A., and Frye, C. A. (2007). The use of the elevated plus maze as an assay of anxiety-related behavior in rodents. *Nat. Protoc.* 2, 322–328. doi: 10.1038/nprot.2007.44

Zhang, L.-M., Yao, J.-Z., Li, Y., Li, K., Chen, H.-X., Zhang, Y.-Z., et al. (2012). Anxiolytic effects of flavonoids in animal models of posttraumatic stress disorder. *Evid. Based Complement. Alternat. Med.* 2012:623753. doi: 10.1155/2012/623753

Conflict of Interest: CF-L and CC are employed by BIAL—Portela & C[a], S.A. (S. Mamede Coronado, Portugal).

The remaining authors declare that the research was conducted in the absence of any commercial or financial relationships that could be construed as a potential conflict of interest.

Publisher's Note: All claims expressed in this article are solely those of the authors and do not necessarily represent those of their affiliated organizations, or those of the publisher, the editors and the reviewers. Any product that may be evaluated in this article, or claim that may be made by its manufacturer, is not guaranteed or endorsed by the publisher.

frontiers | Frontiers in Molecular Neuroscience

ORIGINAL RESEARCH
published: 12 May 2022
doi: 10.3389/fnmol.2022.845970

Differences in Cortical Thickness in Schizophrenia Patients With and Without Auditory Verbal Hallucinations

Honghong Ren[1,2†], Qianjin Wang[1,2†], Chunwang Li[3], Zongchang Li[1,2], Jinguang Li[1,2], Lulin Dai[1,2], Min Dong[4], Jun Zhou[1,2], Jingqi He[1,2], Yanhui Liao[5], Ying He[1,2], Xiaogang Chen[1,2] and Jinsong Tang[5*]*

[1] Department of Psychiatry, and National Clinical Research Center for Mental Disorders, The Second Xiangya Hospital of Central South University, Changsha, China, [2] Hunan Key Laboratory of Psychiatry and Mental Health, Changsha, China, [3] Department of Radiology, Hunan Children's Hospital, Changsha, China, [4] Guangdong Mental Health Center, Guangdong Provincial People's Hospital, Guangdong Academy of Medical Sciences, Guangzhou, China, [5] Department of Psychiatry, School of Medicine, Sir Run-Run Shaw Hospital, Zhejiang University, Hangzhou, China

Auditory verbal hallucinations (AVHs) are one of the most common and severe symptoms of schizophrenia (SCZ), but the neuroanatomical mechanisms underlying AVHs remain unclear. This study aimed to investigate whether persistent AVHs (pAVH) are associated with cortical thinning of certain brain regions in patients with SCZ. With the use of the 3T magnetic resonance imaging (MRI) technology, we acquired and analyzed data from 79 SCZ patients with pAVH (pAVH group), 60 SCZ patients without AVHs (non-AVH group), and 83 healthy controls (HC group). The severity of pAVH was assessed by the P3 hallucination items in the Positive and Negative Syndrome Scale (PANSS) and the Auditory Hallucinations Rating Scale (AHRS). Cortical thickness analysis was used to compare the region of interest (ROI) cortical thickness between the groups. The relationship between the severity of pAVH and cortical thickness was also explored. Compared with the non-AVH and HC groups, the pAVH group exhibited significantly reduced cortical thickness in the bilateral lateral orbitofrontal region ($p < 0.0007$, after Bonferroni correction); no significant difference was found between the non-AVH group and the HC group. The cortical thickness of the left lateral orbitofrontal cortex (P3: $r = -0.44$, $p < 0.001$; AHRS: $r = -0.45$, $p < 0.001$) and the right lateral orbitofrontal cortex (P3: $r = -0.36$, $p = 0.002$; AHRS: $r = -0.33$, $p = 0.004$) were negatively correlated with the severity of pAVH (after Bonferroni correction, $p < 0.0125$). Therefore, abnormal thickness of the bilateral lateral orbitofrontal cortices might be associated with pAVHs in SCZ patients.

Keywords: schizophrenia, auditory verbal hallucinations, orbitofrontal, cortical thickness, magnetic resonance imaging

OPEN ACCESS

Edited by:
Mónica Isa Moreira-Rodrigues, Universidade do Porto, Portugal

Reviewed by:
Jiajia Zhu, First Affiliated Hospital of Anhui Medical University, China
Qinghua Luo, First Affiliated Hospital of Chongqing Medical University, China
Maria Augusta Vieira Coelho, University of Porto, Portugal

***Correspondence:**
Xiaogang Chen
chenxiaogang@csu.edu.cn
orcid.org/0000-0002-3706-1697
Jinsong Tang
tangjinsong@zju.edu.cn
orcid.org/0000-0003-3796-1377

† These authors have contributed equally to this work

Specialty section:
This article was submitted to Brain Disease Mechanisms, a section of the journal Frontiers in Molecular Neuroscience

Received: *30 December 2021*
Accepted: *11 April 2022*
Published: *12 May 2022*

Citation:
Ren H, Wang Q, Li C, Li Z, Li J, Dai L, Dong M, Zhou J, He J, Liao Y, He Y, Chen X and Tang J (2022) Differences in Cortical Thickness in Schizophrenia Patients With and Without Auditory Verbal Hallucinations. Front. Mol. Neurosci. 15:845970. doi: 10.3389/fnmol.2022.845970

INTRODUCTION

Schizophrenia (SCZ) is a chronic debilitating psychiatric disorder characterized by positive symptoms, negative symptoms, and cognitive dysfunction (Khan et al., 2018). Auditory verbal hallucinations (AVHs), as a hallmark positive symptom, are an important diagnostic criterion for SCZ (Chen et al., 2015). Persistent AVHs (pAVH) are AVHs that persist for more than one year despite treatment with two different antipsychotics (González et al., 2006). Affecting approximately 60–80% of patients with SCZ (Sartorius et al., 1986), AVHs have brought a huge and continuous burden to the patients and are usually associated with social and occupational dysfunction as well as poor prognosis (Shergill et al., 1998; Goghari et al., 2013). Although antipsychotics can quickly reduce the frequency and severity of AVHs for most patients (Sommer et al., 2012), there are still 25–30% of SCZ cases being chronically resistant to conventional antipsychotics Liu et al. (2015).

Neuroimaging evidence has shown that AVHs are usually associated with abnormal structure and neuro-metabolism of frontal areas (Steinmann et al., 2014; Psomiades et al., 2018a). The frontal lobe, which is connected to the temporal lobe through the arcuate fasciculus, is a part of a key pathway in the language network (Glasser and Rilling, 2008) and plays a well-established functional role in auditory perception and language processing (Giraud et al., 2004). Previous studies have shown that patients with AVHs have lower gray matter volume (Kubera et al., 2014) and lower functional connectivity (Scheinost et al., 2019) in the frontal regions compared to patients without AVHs and healthy controls (HC). Furthermore, a series of studies using voxel-based morphometry (VBM) to investigate SCZ patients with AVHs showed structural changes in the extra-sensory regions other than the auditory cortex; specifically, SCZ patients with AVHs were found to have reduced gray matter volumes in the left insular cortex and the adjacent temporal pole (Shapleske et al., 2002), thalamus and cerebellum (Neckelmann et al., 2006), left transverse gyrus (Heschl gyrus, HG) (Modinos et al., 2013), left superior limbic gyrus, and dorsolateral prefrontal cortex (DLPFC) (Gaser et al., 2004).

Although both the surface area and thickness have been studied frequently, cortical thickness has so far received the most attention in developmental studies, with evidence suggesting that cortical thickness is less affected by individual differences in the surface area than the gray matter volume (Foland-Ross et al., 2016; Walhovd et al., 2017). Meanwhile, changes in cortical thickness were found to be more sensitive to disease status than changes in volume or surface area (Zuo et al., 2018). Cortical thickness specifically reflects the cellular structure of cortical neurons, neuropil, and neuroglia, including density and arrangement; regarding neuropathology, it affects the synaptogenesis, synaptic pruning, and myelination in the human brain (Selemon and Goldman-Rakic, 1999; Vidal-Pineiro et al., 2020).

Previous studies have found widespread declines in cortical thickness in patients with SCZ (Rodriguez-Perez et al., 2021), suggesting that cortical thinning might be a potential factor for the development of SCZ symptoms, including AVHs. However, only a small number of studies directly compared the cortical thickness between SCZ patients with and without AVHs, and they yielded inconsistent results. For instance, Cui et al. (2018) found reduced cortical thickness in the left middle temporal gyrus (MTG) in 115 patients with AVHs, as compared with 93 patients without AVH and 216 HCs. Mørch-Johnsen et al. (2017) found that the cortical thickness of the left HG was significantly reduced in 145 patients with AVHs, compared with 49 patients without AVHs and 279 HCs. However, Chen et al. (2015) reported that the cortex was significantly thinner in 18 first-episode SCZ patients with persistent AVHs regarding the right HG, compared with 31 first-episode SCZ patients who had never experienced AVHs and 50 HCs. However, the above studies only found significant results in the auditory regions of interest (ROI), and there have been few reports on areas other than the auditory areas. Some further previous studies using vertex-wise analysis found that AVHs were associated not only with cortical thinning in the language regions in the dominant hemisphere but also with increased cortical thickness in regions related to self-monitoring (van Swam et al., 2012; Cui et al., 2018). For instance, van Swam et al. (2012) found that patients with AVHs had increased cortical thickness in the cingulate cortex and parahippocampal gyrus, which play an important role in self-monitoring, compared with patients without AVHs. More specifically, self-monitoring showed that AVHs were produced by improper monitoring of internal speech production, leading to erroneous attributions to internal speech and external perception (Simons et al., 2017; Psomiades et al., 2018b). Oertel-Knöchel et al. (2013) investigated the vertex-wise cortical thickness among 31 patients with chronic SCZ, 29 first-degree relatives of SCZ patients, and 37 HCs, and found that the cortical thickness of SCZ patients was significantly lower than that of the HCs, most notably in the frontal and temporal lobes, the superior parietal lobe, and several limbic regions, with intermediate levels of cortical thickness in relatives. In view of the limited and inconsistent evidence available, the extent and nature of the impact of cortical thinning on AVHs remain to be explored.

In recent years, clinical practitioners and researchers have paid little attention to the study of pAVH in SCZ. The purpose of the present study was to investigate the relationship between cortical thickness and pAVH in SCZ patients. We explored the relationship between cortical thickness and severity of pAVH based on ROI analysis. Based on the results of previous studies, we hypothesized that the cortex thickness of the language-related brain regions might be thinner in SCZ patients with pAVH, compared to patients without AVHs and HCs. We also hypothesized that the cortex thickness in these areas might be associated with the severity of pAVH.

MATERIALS AND METHODS

Participants

A total of 140 SCZ patients were recruited from the Psychiatric Clinic at the Second Xiangya Hospital of Central South University in China. Meanwhile, 85 HCs were recruited via advertisements from local communities. All the patients were diagnosed with SCZ according to the Diagnostic and Statistical Manual of Mental Disorders, Fifth Edition (DSM-5) by two trained senior psychiatrists using Mini-International Neuropsychiatric Interviews (Sheehan et al., 1998). The patients were included if they were: (1) Han Chinese aged between 16 and 45 years; (2) right-handed; (3) normal in hearing and intelligence; (4) with no history of substance abuse; and (5) with no history of major medical or neurological diseases or trauma. The patients were divided into two subgroups based on whether they had auditory hallucination. Through the assessment using the P3 subscale of the Positive and Negative Syndrome Scale (PANSS) (Benetti et al., 2015), 80 patients with a score > 3 (i.e., presence of pAVH) were assigned to the pAVH group, and 60 patients with a score of = 1 (i.e., absence of AVHs) were assigned to the non-AVH group (Andreasen et al., 2005). In the present study, SCZ patients with pAVH all met the diagnostic criteria for treatment-resistant SCZ, and the severity of their symptoms was significantly greater than that of the non-AVH group. Also, we required that SCZ patients with non-AVH never experienced AVHs throughout the course of their illness. The severity of pAVH was assessed using the Auditory Hallucinations Rating Scale (AHRS) for the pAVH group (Chen et al., 2015). None of the HCs met the diagnostic criteria for any DSM-5 mental disorder or had a history of early mental disorder or family history of mental illnesses. This study was approved by the Ethics Committee of the Second Xiangya Hospital, Central South University (No. S006, 2018), and was conducted in accordance with the Declaration of Helsinki. After being duly informed of the study details, including benefits and potential risks, all the participants provided written informed consent.

To minimize the effects of neuroleptic medications on brain structure, this study preferentially recruited patients who received second-generation antipsychotics (SGAs) and matched the medication dose between the two patient groups. Current and previous antipsychotic regimens (type, dose, and duration of use) were recorded. In the patient groups, 18 patients (12.9%) were treated with first-generation antipsychotics (FGAs) in combination with SGAs; The remaining 121 patients (87.1%) were treated with SGAs in combination with SGAs. Type of medicine: FGAs include Haloperidol, Sulpiride. SGAs include Aripiprazole, Clozapine, Olanzapine, Quetiapine, Risperidone, Paliperidone, Ziprasidone, and Amisulpride.

Magnetic Resonance Imaging Data Acquisition

Magnetic resonance imaging (MRI) data of all participants were obtained within 24 h after enrollment. All the MRI data were acquired using a 3.0T MRI scanner (Siemens, Munich, Germany) with a 16-channel headcoil at the Magnetic Imaging Center of Hunan Children's Hospital, Changsha, China. None of the patients used antipsychotic medications on the day of the MRI scan, and their medications were not adjusted prior to the scan. During the scanning, foam pads and earplugs were used to restrain head movement and attenuate noise. Anatomical T1-weighted MRI data were acquired using a 3D magnetization-prepared rapid acquisition gradient echo (3D MPRAGE) sequence with the following parameters: repetition time (TR) = 2,530 ms, echo time (TE) = 2.33 ms, flip angle = 7°, field of view = 256 × 256 mm, slice thickness = 1 mm, slice gap = 0 mm, and number of slices = 192. All data sets were visually inspected for distortion and motion artifacts. There were no major scanner upgrades or instrument replacements during the study period.

Measurement of Cortical Thickness

All the MRI images were processed using the FreeSurfer software package (version 7.1.0),[1] which has been described and validated in previous studies (Dale et al., 1999; Fischl et al., 1999). Image preprocessing included the following steps: motion correction, brain extraction, Talairach transformation, intensity correction, brain tissue segmentation, automatic topology correction, and surface deformation (Chen et al., 2015). The measurement of cortical thickness was obtained by reconstructing the boundary of gray matter and white matter and the surface of the cortex, and then calculating the distance between the surfaces at each point across the cortical mantle (Dale et al., 1999). The generated cortical surfaces were then carefully reviewed and manually corrected for technical accuracy. The thickness of each vertex on the cortical surface was mapped into a common spherical system, and the maps were smoothed using a Gaussian kernel with a full width at half maximum (FWHM) of 10 mm. The results were inspected and checked for quality according to the ENIGMA protocol.[2] The cortex was parcellated into 68 regions according to the Desikan-Killiany atlas.

Statistical Analysis

All statistical analyses were performed using SPSS 26.0 (SPSS Inc., Chicago, IL, United States). Prior to all the analyses, we tested the normality of each variable using the Kolmogorov-Smirnov test. Demographic and clinical data were compared between groups using Chi-squared test, one-way analysis of variance (ANOVA), or Mann-Whitney *U*-test, when appropriate. Univariate covariance analysis (ANCOVA) was used to compare the cortical thickness of brain regions between the three groups, with age, gender, education, and estimated total intracranial volume (eTIV) being covariates. *Post hoc* tests were then performed when significant differences were found in the above comparisons, using Bonferroni correction for ANCOVA ($p < 0.05/68 = 0.0007$) and multiple comparisons ($p < 0.05/14 = 0.0036$). Partial correlation analysis was used to investigate the relationship between the severity of AVHs and the cortical thickness of brain regions in the pAVH group, with age, gender, education, and eTIV being covariates (with Bonferroni

[1] http://surfer.nmr.mgh.harvard.edu

[2] www.enigma.ini.usc.edu

correction, $p < 0.05/2 \times 2 = 0.0125$). The threshold of statistical significance was set at $p = 0.05$ (two-tailed).

RESULTS

Demographic and Clinical Characteristics

Data for 1 pAVH patient and 2 HCs were excluded due to loss to follow-up and contraindications to MRI, respectively. The final analysis included 79 pAVH patients, 60 non-AVH patients, and 83 HCs. The demographic and clinical characteristics are summarized in **Table 1**. There were no significant differences in age, gender, smoking status, and drinking status between the three groups. The education level of both the pAVH and non-AVH groups were significantly lower than that of the HC group, and the education level of the pAVH group was significantly lower than that of the non-AVH group (*post hoc* results for pAVH vs. non-AVH, $p = 0.03$; pAVH vs. HC, $p < 0.001$; non-AVH vs. HC, $p = 0.01$). The score of P3 hallucination item of PANSS for the pAVH group was significantly higher than that for the non-AVH group ($p < 0.001$). The pAVH and non-AVH groups did not differ in age at onset, illness duration, CPZ equivalent dosage, as well as PANSS-P, PANSS-N, PANSS-G, and PANSS-T scores ($p > 0.05$).

Differences in Cortical Thickness Between Groups

Inter-group ANCOVA with Bonferroni correction showed that the cortical thickness of the bilateral lateral orbitofrontal cortices was significantly lower in the pAVH group compared with the non-AVH and HC groups, while no differences were observed between the non-AVH and HC groups (see **Table 2** and **Figure 1**). Although the level of education was different in the covariance analysis of the three groups, it did not affect the thickness of the bilateral lateral orbitofrontal cortices. Covariance analysis with education level as a covariate showed no difference in cortical thickness of bilateral lateral orbitofrontal cortices between the three groups (left lateral orbitofrontal cortex: $F = 0.07$, $p = 0.79$; right lateral orbitofrontal cortex: $F = 1.59$, $p = 0.21$). However, there were no differences

TABLE 1 | Demographic and clinical characteristics of patients and healthy controls.

Characteristics	HC (n = 83)	Patients (n = 139)		Significance			
		pAVH (n = 79)	non-AVH (n = 60)	HC vs. pAVH vs. non-AVH	HC vs. non-AVH	HC vs. pAVH	pAVH vs. non-AVH
					p-value		
Gender (M/F), n	38/45	39/40	36/24	$\chi^2 = 2.93$ (0.23)	0.09	0.65	0.21
Age (y), (M ± SD)	26.80 ± 5.91	25.58 ± 5.51	26.95 ± 5.90	$F = 1.26$ (0.29)	1.00	0.55	0.50
Education (y), (M ± SD)	14.43 ± 2.65	11.68 ± 3.16	13.00 ± 2.82	$F = 18.37$ (<0.001)**	0.01*	<0.001**	0.03*
Smoker/non-smoker, n	12/71	12/67	14/46	$\chi^2 = 2.26$ (0.32)	0.17	0.90	0.22
Drinker/non-drinker, n	2/81	0/79	1/59	$\chi^2 = 1.82$ (0.40)	0.76	0.17	0.25
Age at onset (y), (M ± SD)	–	19.78 ± 4.11	21.17 ± 5.05	–	–	–	$U = 1{,}983$ (0.10)
Illness duration (y), (M ± SD)	–	7.16 ± 4.59	5.83 ± 3.81	–	–	–	$U = 1{,}975$ (0.09)
PANSS-P (M ± SD)	–	13.65 ± 2.83	13.00 ± 3.66	–	–	–	$U = 2{,}069$ (0.24)
PANSS-N (M ± SD)	–	15.08 ± 5.66	14.10 ± 7.31	–	–	–	$U = 1{,}940$ (0.09)
PANSS-G (M ± SD)	–	26.85 ± 6.56	27.02 ± 8.65	–	–	–	$U = 2{,}168$ (0.46)
P3 hallucination item of PANSS (M ± SD)	–	5.11 ± 0.87	1.00 ± 0.00	–	–	–	$U = 0.00$ (<0.001)**
PANSS-T (M ± SD)	–	54.87 ± 12.51	54.12 ± 16.65	–	–	–	$U = 1{,}974$ (0.09)
AHRS (M ± SD)	–	26.10 ± 4.46	–	–	–	–	–
CPZ equivalent (mg/d), (M ± SD)	–	654.04 ± 280.65	588.63 ± 332.58	–	–	–	$U = 1{,}952$ (0.08)

*M, mean; SD, standard deviation; n, number; M/F, male/female; pAVH, persistent auditory verbal hallucinations; non-AVH, without auditory verbal hallucinations; HC, health control; PANSS, Positive and Negative Symptoms Scale; PANSS-T, PANSS total score; PANSS-P, PANSS positive score; PANSS-N, PANSS negative score; PANSS-G, PANSS general psychopathology score; AHRS: the Auditory Hallucinations Rating Scale; CPZ, chlorpromazine; -, not applicable; *p < 0.05; **p < 0.01.*

TABLE 2 | Brain regions with significant inter-group differences in cortical thickness.

Variable	Cortical thickness (mm) M ± SD			ANCOVA	Pairwise comparisons *P*-value		
	pAVH	non-AVH	HC		pAVH vs. non-AVH	pAVH vs. HC	non-AVH vs. HC
Left caudal middle frontal cortex	2.35 ± 0.14	2.39 ± 0.15	2.44 ± 0.13	F = 10.54, (<0.0007)	0.02	0.47	0.57
Left lateral orbitofrontal cortex	2.57 ± 0.13	2.63 ± 0.14	2.69 ± 0.11	F = 21.92, (<0.0007)	0.001*	<0.001*	0.01
Left pars opercularis cortex	2.32 ± 0.14	2.36 ± 0.16	2.42 ± 0.12	F = 11.74, (<0.0007)	0.26	<0.001*	0.01
Left pars orbitalis cortex	2.44 ± 0.17	2.42 ± 0.18	2.54 ± 0.17	F = 8.43, (0.0003)	1.00	0.001*	0.002
Left pars triangularis cortex	2.19 ± 0.14	2.21 ± 0.18	2.28 ± 0.15	F = 8,38, (0.0003)	0.36	<0.001*	0.05
Left rostral middle frontal cortex	2.14 ± 0.12	2.17 ± 0.11	2.22 ± 0.12	F = 10.57, (<0.0007)	0.20	<0.001*	0.03
Left superior frontal cortex	2.58 ± 0.14	2.60 ± 0.16	2.66 ± 0.14	F = 9.54, (0.0001)	0.32	<0.001*	0.03
Right caudal middle frontal cortex	2.38 ± 0.13	2.38 ± 0.16	2.45 ± 0.14	F = 8.29, (0.0003)	1.00	0.001*	0.003
Right lateral orbitofrontal cortex	2.57 ± 0.13	2.64 ± 0.14	2.68 ± 0.13	F = 19.63, (<0.0007)	<0.001*	<0.001*	0.11
Right medial orbitofrontal cortex	2.35 ± 0.14	2.40 ± 0.15	2.46 ± 0.13	F = 15.57, (<0.0007)	0.02	<0.001*	0.03
Right pars orbitalis cortex	2.48 ± 0.18	2.54 ± 0.16	2.62 ± 0.16	F = 20.09, (<0.0007)	0.007	<0.001*	0.007
Right pars triangularis cortex	2.22 ± 0.14	2.24 ± 0.15	2.33 ± 0.14	F = 14.78, (<0.0007)	0.19	<0.001*	0.003
Right rostral middle frontal cortex	2.12 ± 0.12	2.16 ± 0.13	2.19 ± 0.12	F = 9.42, (0.0001)	0.03	<0.001*	0.34
Right superior frontal cortex	2.53 ± 0.14	2.56 ± 0.16	2.64 ± 0.16	F = 12.28, (<0.0007)	0.15	<0.001*	0.02

*M, mean; SD, standard deviation; mm, millimeter; ANCOVA, univariate covariance analysis; pAVH, persistent auditory verbal hallucinations; non-AVH, without auditory verbal hallucinations; HC, health control; Bonferroni correction was used for ANCOVA ($p < 0.05/68 = 0.0007$) and multiple comparisons ($p < 0.05/14 = 0.0036$). *$p < 0.0036$.*

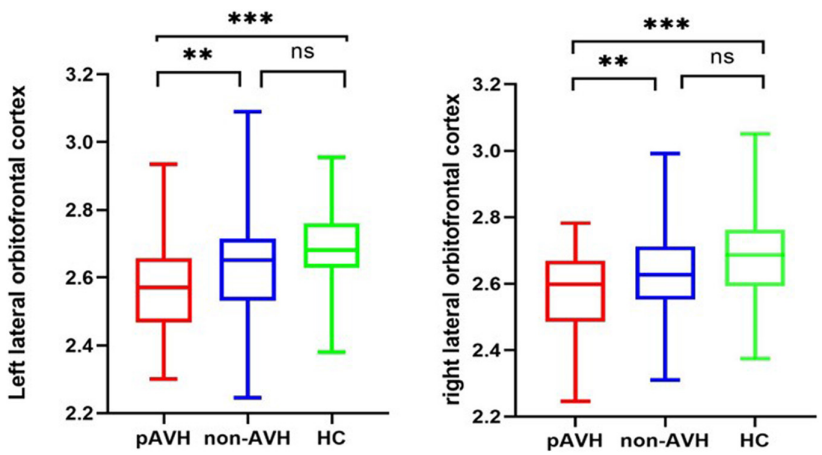

FIGURE 1 | Cortical thickness of brain regions with significant differences between the three groups (with Bonferroni correction). **$p < 0.01$, ***$p < 0.001$; ns: not significant ($p > 0.05$); Bonferroni correction was used for ANCOVA ($p < 0.0007$) and multiple comparisons ($p < 0.0036$).

in cortical thickness in other brain regions ($p > 0.05$) or differences without Bonferroni correction (all $p > 0.0007$) (see **Supplementary Table 1**).

Correlation Analysis Results

Correlation analysis was performed between the brain regions with different cortical thicknesses identified by ANCOVA and the severity of pAVH to explore the potential relationship between the differences in cortical thickness and the severity of pAVH. The cortical thickness of the bilateral lateral orbitofrontal cortices was negatively correlated with the severity of pAVH (i.e., AHRS or P3 scores) (with Bonferroni correction, $p < 0.0125$; see **Table 3** and **Figure 2**).

DISCUSSION

In the present study, we investigated the characteristics of cortical thickness in the ROI of SCZ patients with and without AVHs and its relationship with the severity of pAVH by using surface-based analysis. Our findings indicated that the brain regions with decreased cortical thickness in SCZ patients with pAVH were mainly in the frontal lobe, especially in bilateral lateral orbitofrontal cortices. We also found that the cortical thickness of the bilateral lateral orbitofrontal cortices in the pAVH group was negatively correlated with the severity of pAVH. In other words, thinner cortical thickness in these brain regions indicated higher severity of pAVH. The above findings are also consistent with our hypotheses.

TABLE 3 | Correlation between the cortical thickness of brain regions and the severity of pAVH.

	P3		AHRS	
Variable	***r***	***p***	***r***	***p***
Left lateral orbitofrontal cortex	−0.44	<0.001	−0.45	<0.001
Right lateral orbitofrontal cortex	−0.36	0.002	−0.33	0.004

P3, the P3 hallucination item in the Positive and Negative Syndrome Scale (PANSS); AHRS, the Auditory Hallucinations Rating Scale; Bonferroni correction ($p < 0.05/2\times 2 = 0.0125$).

We found that the cortical thickness of bilateral lateral orbitofrontal cortices decreased in the pAVH group compared with the non-AVH and HC groups. These areas belong to the orbital frontal cortex (OFC), which is involved in language, cognition, and emotional processing (Rubin et al., 2017; Gul and Yousaf, 2019). Previous studies have demonstrated that dysfunction of the OFC was associated with AVHs that are similar to those found in patients with SCZ. For example, a study using structural MRI (sMRI) found that the gray matter volume and cortical thickness of the OFC were lower in patients with SCZ and were negatively correlated with the score of the subscale for positive symptoms (including hallucinations) (Takayanagi et al., 2020). Previous studies using positron emission tomography (PET) and functional MRI (fMRI) also found abnormal activation of the OFC in SCZ patients with AVHs (Silbersweig et al., 1995; Ait Bentaleb et al., 2006). At present, the main theory of the neurocognitive model of AVHs is the neurocognitive action self-monitoring system (Frith et al., 2000), which holds that individuals erroneously perceive events that actually occur within as they are originated from outside. Patients with SCZ, especially those with AVHs, may have self-monitoring dysfunction (Waters et al., 2012), whereby they are unable to recognize events occurring within their minds and perceive them as events that have actually happened externally. Therefore, the OFC may play a key role in the self-monitoring system, which mediates the occurrence and development of AVHs.

Previous studies have also reported structural abnormalities in other brain regions, such as the temporal (Sun et al., 2009; Chen et al., 2015) and insular cortices (O'Daly et al., 2007); however, we did not find any alterations in the cortical thickness

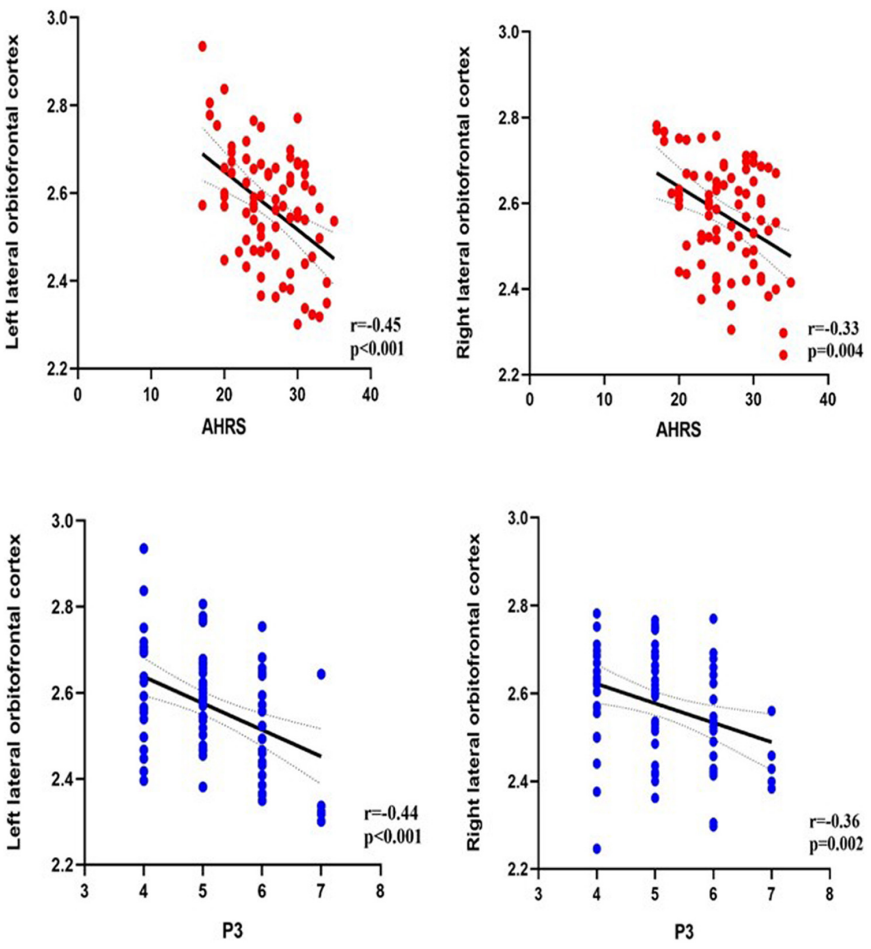

FIGURE 2 | The relationship between the severity of pAVH (measured by P3 and AHRS) and cortical thickness of brain regions. P3, the P3 hallucination item in the Positive and Negative Syndrome Scale (PANSS); AHRS, the Auditory Hallucinations Rating Scale; Bonferroni correction ($p < 0.0125$).

of these regions. Similarly, there was no difference in cortical thickness between the non-AVH group and the HC group in this study, while some studies found varying degrees of difference between the two groups (Köse et al., 2018). The inconsistent results might be attributed to methodological differences and heterogeneity in samples of SCZ. Most previous studies used voxel-based morphological (VBM) analysis, which focuses on structural changes in gray matter volume or density rather than cortical thickness. To the best of our knowledge, the samples of SCZ patients with AVHs were relatively small previous studies assessing cortical thickness (van Swam et al., 2012; Chen et al., 2015). Furthermore, SCZ patients present with a variety of clinical symptoms and different durations of illness. Evidence has demonstrated that patients with SCZ have cortical thinning over time throughout the course of the disease (van Haren et al., 2011), suggesting that the chronicity of the disease might be an important contributor to cortical thinning. In addition, the results of the present study are also indirectly supported by the results of previous studies on white matter volume, especially the studies involving arcuate fasciculus. The arcuate fasciculus, as it is known, is a bundle of nerve fibers connecting the frontal and temporal lobes within each cerebral hemisphere by passing dorsally beneath the parietal lobe, and is widely considered as a critical tract for language processing (Glasser and Rilling, 2008; Ivanova et al., 2021). For example, Salisbury et al. (2021) found that in the first psychotic episode, AVHs were more robustly associated with the microstructural deficits of the arcuate fasciculus and interhemispheric auditory fibers in the left hemisphere. Furthermore, a meta-analysis of studies involving diffusion tensor imaging of the arcuate fasciculus in patients with AVHs showed that the anisotropy score of the left arcuate fasciculus of the hallucinators was lower (Geoffroy et al., 2014). In this context, it was suggested that dysfunctional neuronal interconnections in white matter fibers between these regions are associated with the misperception of internal speech (Catani and ffytche, 2005). A disease-related cortical disorganization in the speech dominant hemisphere might affect white-matter connectivity in adjacent brain regions (van Swam et al., 2012).

There are some limitations to our study that need to be addressed. Firstly, the study is cross-sectional and follow-up visits are needed to further explore the development of symptoms and the prognosis, as well as the relationship between symptoms and cerebral cortical thickness. Secondly, all the patients were taking antipsychotics during the study period; although the results showed no difference in antipsychotic dosages between the two groups in the most recent year, the effect of drugs on cortical thickness could not be ruled out. In future works, the relationship between cortical thickness alterations and AVHs in first-episode treatment-naive patients with SCZ needs to be further explored. Finally, using illness duration as a covariance, covariance analysis found no difference in bilateral lateral orbitofrontal cortex thickness between the two patient groups. The possible reason is that the subjects in this study were all patients with chronic schizophrenia, and this study was cross-sectional, so it may not be able to highlight the influence of the illness duration on the disease. In future studies, follow-up or comparative studies involving first-episode patients, acute patients and chronic patients are needed to remedy this limitation.

CONCLUSION

In summary, the present study showed that SCZ patients with pAVH exhibited decreased cortical thickness in the bilateral lateral orbitofrontal cortices, which were negatively correlated with the severity of pAVH. These findings suggest that anatomical defects in the frontal cortex, especially the bilateral lateral orbitofrontal cortices, may be associated with the pathogenesis of pAVH in patients with SCZ.

DATA AVAILABILITY STATEMENT

The datasets generated for this study are available on request to the corresponding author.

ETHICS STATEMENT

The studies involving human participants were reviewed and approved by the Ethics Committee of the Second Xiangya Hospital, Central South University (No. S006, 2018). The patients/participants provided their written informed consent to participate in this study.

AUTHOR CONTRIBUTIONS

JT and XC designed and supervised the study. HR, JL, JH, LD, MD, and JZ collected the data. CL processed the scanning. HR, QW, JT, ZL, YL, and YH analyzed the data and interpreted the results. HR and QW first drafted the manuscript. JT, XC, ZL, and YL critically revised for important intellectual content. All authors revised and approved the final manuscript to be published.

FUNDING

This research was supported by the National Natural Science Foundation of China (Nos. 82171495 and 81871057 to JT and No. 81871056 to XC).

ACKNOWLEDGMENTS

We would like to express our sincere thanks to all participants in this work.

SUPPLEMENTARY MATERIAL

The Supplementary Material for this article can be found online at: https://www.frontiersin.org/articles/10.3389/fnmol.2022.845970/full#supplementary-material

REFERENCES

Ait Bentaleb, L., Stip, E., Mendrek, A., Mensour, B., and Beauregard, M. (2006). [Effects of listening to previously hallucinated words by schizophrenia patients in remission: a functional magnetic resonance imaging study of six cases]. *Encephale* 32(1 Pt 1), 27–40. doi: 10.1016/s0013-7006(06)76134-6

Andreasen, N. C., Carpenter, W. T. Jr., Kane, J. M., Lasser, R. A., Marder, S. R., and Weinberger, D. R. (2005). Remission in schizophrenia: proposed criteria and rationale for consensus. *Am. J. Psychiatr.* 162, 441–449. doi: 10.1176/appi.ajp.162.3.441

Benetti, S., Pettersson-Yeo, W., Allen, P., Catani, M., Williams, S., Barsaglini, A., et al. (2015). Auditory verbal hallucinations and brain dysconnectivity in the perisylvian language network: a multimodal investigation. *Schizophr. Bull.* 41, 192–200.

Catani, M., and ffytche, D. H. (2005). The rises and falls of disconnection syndromes. *Brain* 128, 2224–2239. doi: 10.1093/brain/awh622

Chen, X., Liang, S., Pu, W., Song, Y., Mwansisya, T. E., Yang, Q., et al. (2015). Reduced cortical thickness in right Heschl's gyrus associated with auditory verbal hallucinations severity in first-episode schizophrenia. *BMC Psychiatr.* 15:152. doi: 10.1186/s12888-015-0546-2

Cui, Y., Liu, B., Song, M., Lipnicki, D. M., Li, J., Xie, S., et al. (2018). Auditory verbal hallucinations are related to cortical thinning in the left middle temporal gyrus of patients with schizophrenia. *Psychol. Med.* 48, 115–122. doi: 10.1017/s0033291717001520

Dale, A. M., Fischl, B., and Sereno, M. I. (1999). Cortical surface-based analysis. I. Segmentation and surface reconstruction. *Neuroimage* 9, 179–194. doi: 10.1006/nimg.1998.0395

Fischl, B., Sereno, M. I., and Dale, A. M. (1999). Cortical surface-based analysis. II: inflation, flattening, and a surface-based coordinate system. *Neuroimage* 9, 195–207. doi: 10.1006/nimg.1998.0396

Foland-Ross, L. C., Behzadian, N., LeMoult, J., and Gotlib, I. H. (2016). Concordant Patterns of Brain Structure in Mothers with Recurrent Depression and Their Never-Depressed Daughters. *Dev. Neurosci.* 38, 115–123. doi: 10.1159/000444448

Frith, C. D., Blakemore, S., and Wolpert, D. M. (2000). Explaining the symptoms of schizophrenia: abnormalities in the awareness of action. *Brain Res. Brain Res. Rev.* 31, 357–363. doi: 10.1016/s0165-0173(99)00052-1

Gaser, C., Nenadic, I., Volz, H. P., Büchel, C., and Sauer, H. (2004). Neuroanatomy of "hearing voices": a frontotemporal brain structural abnormality associated with auditory hallucinations in schizophrenia. *Cereb. Cortex* 14, 91–96. doi: 10.1093/cercor/bhg107

Geoffroy, P. A., Houenou, J., Duhamel, A., Amad, A., De Weijer, A. D., Curčić-Blake, B., et al. (2014). The Arcuate Fasciculus in auditory-verbal hallucinations: a meta-analysis of diffusion-tensor-imaging studies. *Schizophr. Res.* 159, 234–237. doi: 10.1016/j.schres.2014.07.014

Giraud, A. L., Kell, C., Thierfelder, C., Sterzer, P., Russ, M. O., Preibisch, C., et al. (2004). Contributions of sensory input, auditory search and verbal comprehension to cortical activity during speech processing. *Cereb. Cortex* 14, 247–255. doi: 10.1093/cercor/bhg124

Glasser, M. F., and Rilling, J. K. (2008). DTI tractography of the human brain's language pathways. *Cereb. Cortex* 18, 2471–2482. doi: 10.1093/cercor/bhn011

Goghari, V. M., Harrow, M., Grossman, L. S., and Rosen, C. (2013). A 20-year multi-follow-up of hallucinations in schizophrenia, other psychotic, and mood disorders. *Psychol. Med.* 43, 1151–1160. doi: 10.1017/S0033291712002206

González, J., Aguilar, E., Berenguer, V., Leal, C., and Sanjuan, J. (2006). Persistent auditory hallucinations. *Psychopathology* 39, 120–125.

Gul, A., and Yousaf, J. (2019). Effect of levodopa on frontal-subcortical and posterior cortical functioning in patients with Parkinson's disease. *Sin. Med. J.* 60, 414–417. doi: 10.11622/smedj.2018116

Ivanova, M. V., Zhong, A., Turken, A., Baldo, J. V., and Dronkers, N. F. (2021). Functional Contributions of the Arcuate Fasciculus to Language Processing. *Front. Hum. Neurosci.* 15:672665. doi: 10.3389/fnhum.2021.672665

Khan, M. S., Boileau, I., Kolla, N., and Mizrahi, R. (2018). A systematic review of the role of the nociceptin receptor system in stress, cognition, and reward: relevance to schizophrenia. *Transl. Psychiatr.* 8:38. doi: 10.1038/s41398-017-0080-8

Köse, G., Jessen, K., Ebdrup, B. H., and Nielsen, M. (2018). Associations between cortical thickness and auditory verbal hallucinations in patients with schizophrenia: a systematic review. *Psychiatr. Res. Neuroimaging* 282, 31–39. doi: 10.1016/j.pscychresns.2018.10.005

Kubera, K. M., Sambataro, F., Vasic, N., Wolf, N. D., Frasch, K., Hirjak, D., et al. (2014). Source-based morphometry of gray matter volume in patients with schizophrenia who have persistent auditory verbal hallucinations. *Prog. Neuro-Psychopharmacol. Biol. Psychiatr.* 50, 102–109.

Liu, W., Yu, H., Jiang, B., Pan, B., Yu, S., Li, H., et al. (2015). The predictive value of baseline NAA/Cr for treatment response of first-episode schizophrenia: a 1H MRS study. *Neurosci. Lett.* 600, 199–205.

Modinos, G., Costafreda, S. G., van Tol, M. J., McGuire, P. K., Aleman, A., and Allen, P. (2013). Neuroanatomy of auditory verbal hallucinations in schizophrenia: a quantitative meta-analysis of voxel-based morphometry studies. *Cortex* 49, 1046–1055. doi: 10.1016/j.cortex.2012.01.009

Mørch-Johnsen, L., Nesvåg, R., Jørgensen, K. N., Lange, E. H., Hartberg, C. B., Haukvik, U. K., et al. (2017). Auditory Cortex Characteristics in Schizophrenia: associations With Auditory Hallucinations. *Schizophr. Bull.* 43, 75–83. doi: 10.1093/schbul/sbw130

Neckelmann, G., Specht, K., Lund, A., Ersland, L., Smievoll, A. I., Neckelmann, D., et al. (2006). Mr morphometry analysis of grey matter volume reduction in schizophrenia: association with hallucinations. *Int. J. Neurosci.* 116, 9–23. doi: 10.1080/00207450690962244

O'Daly, O. G., Frangou, S., Chitnis, X., and Shergill, S. S. (2007). Brain structural changes in schizophrenia patients with persistent hallucinations. *Psychiatr. Res.* 156, 15–21. doi: 10.1016/j.pscychresns.2007.03.001

Oertel-Knöchel, V., Knöchel, C., Rotarska-Jagiela, A., Reinke, B., Prvulovic, D., Haenschel, C., et al. (2013). Association between psychotic symptoms and cortical thickness reduction across the schizophrenia spectrum. *Cereb. Cortex* 23, 61–70. doi: 10.1093/cercor/bhr380

Psomiades, M., Mondino, M., Fonteneau, C., Bation, R., Haesebaert, F., Suaud-Chagny, M.-F., et al. (2018a). N-Acetyl-Aspartate in the dorsolateral prefrontal cortex in men with schizophrenia and auditory verbal hallucinations: a 1.5 T Magnetic Resonance Spectroscopy Study. *Sci. Rep.* 8, 1–7.

Psomiades, M., Mondino, M., Fonteneau, C., Bation, R., Haesebaert, F., Suaud-Chagny, M. F., et al. (2018b). N-Acetyl-Aspartate in the dorsolateral prefrontal cortex in men with schizophrenia and auditory verbal hallucinations: a 1.5 T Magnetic Resonance Spectroscopy Study. *Sci. Rep.* 8:4133. doi: 10.1038/s41598-018-22597-y

Rodriguez-Perez, N., Ayesa-Arriola, R., Ortiz-García de la Foz, V., Setien-Suero, E., Tordesillas-Gutierrez, D., and Crespo-Facorro, B. (2021). Long term cortical thickness changes after a first episode of non- affective psychosis: the 10 year follow-up of the PAFIP cohort. *Prog Neuropsychopharmacol. Biol. Psychiatr.* 108:110180. doi: 10.1016/j.pnpbp.2020.110180

Rubin, L. H., Yao, L., Keedy, S. K., Reilly, J. L., Bishop, J. R., Carter, C. S., et al. (2017). Sex differences in associations of arginine vasopressin and oxytocin with resting-state functional brain connectivity. *J. Neurosci. Res.* 95, 576–586. doi: 10.1002/jnr.23820

Salisbury, D. F., Wang, Y., Yeh, F. C., and Coffman, B. A. (2021). White Matter Microstructural Abnormalities in the Broca's-Wernicke's-Putamen "Hoffman Hallucination Circuit" and Auditory Transcallosal Fibers in First-Episode Psychosis With Auditory Hallucinations. *Schizophr Bull* 47, 149–159. doi: 10.1093/schbul/sbaa105

Sartorius, N., Jablensky, A., Korten, A., Ernberg, G., Anker, M., Cooper, J. E., et al. (1986). Early manifestations and first-contact incidence of schizophrenia in different cultures. A preliminary report on the initial evaluation phase of the WHO Collaborative Study on determinants of outcome of severe mental disorders. *Psychol. Med.* 16, 909–928. doi: 10.1017/s0033291700011910

Scheinost, D., Tokoglu, F., Hampson, M., Hoffman, R., and Constable, R. T. (2019). Data-driven analysis of functional connectivity reveals a potential auditory verbal hallucination network. *Schizophr. Bull.* 45, 415–424.

Selemon, L. D., and Goldman-Rakic, P. S. (1999). The reduced neuropil hypothesis: a circuit based model of schizophrenia. *Biol. Psychiatr.* 45, 17–25. doi: 10.1016/s0006-3223(98)00281-9

Shapleske, J., Rossell, S. L., Chitnis, X. A., Suckling, J., Simmons, A., Bullmore, E. T., et al. (2002). A computational morphometric MRI study of schizophrenia: effects of hallucinations. *Cereb. Cortex* 12, 1331–1341. doi: 10.1093/cercor/12.12.1331

Sheehan, D. V., Lecrubier, Y., Sheehan, K. H., Amorim, P., Janavs, J., Weiller, E., et al. (1998). The Mini-International Neuropsychiatric Interview (M.I.N.I.): the

development and validation of a structured diagnostic psychiatric interview for DSM-IV and ICD-10. *J. Clin. Psychiatr.* 59, 22–33;quiz34–57.

Shergill, S. S., Murray, R. M., and McGuire, P. K. (1998). Auditory hallucinations: a review of psychological treatments. *Schizophr. Res.* 32, 137–150. doi: 10.1016/s0920-9964(98)00052-8

Silbersweig, D. A., Stern, E., Frith, C., Cahill, C., Holmes, A., Grootoonk, S., et al. (1995). A functional neuroanatomy of hallucinations in schizophrenia. *Nature* 378, 176–179. doi: 10.1038/378176a0

Simons, J. S., Garrison, J. R., and Johnson, M. K. (2017). Brain Mechanisms of Reality Monitoring. *Trends Cogn. Sci.* 21, 462–473. doi: 10.1016/j.tics.2017.03.012

Sommer, I. E., Slotema, C. W., Daskalakis, Z. J., Derks, E. M., Blom, J. D., and van der Gaag, M. (2012). The treatment of hallucinations in schizophrenia spectrum disorders. *Schizophr. Bull.* 38, 704–714. doi: 10.1093/schbul/sbs034

Steinmann, S., Leicht, G., and Mulert, C. (2014). Interhemispheric auditory connectivity: structure and function related to auditory verbal hallucinations. *Front. Hum. Neurosci.* 8:55. doi: 10.3389/fnhum.2014.00055

Sun, J., Maller, J. J., Guo, L., and Fitzgerald, P. B. (2009). Superior temporal gyrus volume change in schizophrenia: a review on region of interest volumetric studies. *Brain Res. Rev.* 61, 14–32. doi: 10.1016/j.brainresrev.2009.03.004

Takayanagi, Y., Sasabayashi, D., Takahashi, T., Furuichi, A., Kido, M., Nishikawa, Y., et al. (2020). Reduced Cortical Thickness in Schizophrenia and Schizotypal Disorder. *Schizophr. Bull.* 46, 387–394. doi: 10.1093/schbul/sbz051

van Haren, N. E., Schnack, H. G., Cahn, W., van den Heuvel, M. P., Lepage, C., Collins, L., et al. (2011). Changes in cortical thickness during the course of illness in schizophrenia. *Arch. Gen. Psychiatr.* 68, 871–880. doi: 10.1001/archgenpsychiatry.2011.88

van Swam, C., Federspiel, A., Hubl, D., Wiest, R., Boesch, C., Vermathen, P., et al. (2012). Possible dysregulation of cortical plasticity in auditory verbal hallucinations-A cortical thickness study in schizophrenia. *J. Psychiatr. Res.* 46, 1015–1023. doi: 10.1016/j.jpsychires.2012.03.016

Vidal-Pineiro, D., Parker, N., Shin, J., French, L., Grydeland, H., Jackowski, A. P., et al. (2020). Cellular correlates of cortical thinning throughout the lifespan. *Sci. Rep.* 10:21803. doi: 10.1038/s41598-020-78471-3

Walhovd, K. B., Fjell, A. M., Giedd, J., Dale, A. M., and Brown, T. T. (2017). Through Thick and Thin: a Need to Reconcile Contradictory Results on Trajectories in Human Cortical Development. *Cereb. Cortex* 27, 1472–1481. doi: 10.1093/cercor/bhv301

Waters, F., Woodward, T., Allen, P., Aleman, A., and Sommer, I. (2012). Self-recognition deficits in schizophrenia patients with auditory hallucinations: a meta-analysis of the literature. *Schizophr. Bull.* 38, 741–750. doi: 10.1093/schbul/sbq144

Zuo, Z., Ran, S., Wang, Y., Li, C., Han, Q., Tang, Q., et al. (2018). Altered Structural Covariance Among the Dorsolateral Prefrontal Cortex and Amygdala in Treatment-Naïve Patients With Major Depressive Disorder. *Front. Psychiatr.* 9:323. doi: 10.3389/fpsyt.2018.00323

Conflict of Interest: The authors declare that the research was conducted in the absence of any commercial or financial relationships that could be construed as a potential conflict of interest.

Publisher's Note: All claims expressed in this article are solely those of the authors and do not necessarily represent those of their affiliated organizations, or those of the publisher, the editors and the reviewers. Any product that may be evaluated in this article, or claim that may be made by its manufacturer, is not guaranteed or endorsed by the publisher.

frontiers | Frontiers in Molecular Neuroscience

ORIGINAL RESEARCH
published: 07 July 2022
doi: 10.3389/fnmol.2022.882396

Identification of a Novel Functional Non-synonymous Single Nucleotide Polymorphism in Frizzled Class Receptor 6 Gene for Involvement in Depressive Symptoms

Haijun Han[1], Mengxiang Xu[1], Li Wen[1], Jiali Chen[1], Qiang Liu[1], Ju Wang[2], Ming D. Li[1,3] and Zhongli Yang[1]**

[1] State Key Laboratory for Diagnosis and Treatment of Infectious Diseases, National Clinical Research Center for Infectious Diseases, Collaborative Innovation Center for Diagnosis and Treatment of Infectious Diseases, The First Affiliated Hospital, Zhejiang University School of Medicine, Hangzhou, China, [2] Department of Medical Engineering, Tianjin Medical University, Tianjin, China, [3] Research Center for Air Pollution and Health, Zhejiang University, Hangzhou, China

OPEN ACCESS

Edited by:
Melanie Grubisha,
University of Pittsburgh, United States

Reviewed by:
Fabio Marti,
Institut National de la Santé et de la Recherche Médicale (INSERM), France
Byung-Hoon Jeong,
Jeonbuk National University, South Korea

***Correspondence:**
Ming D. Li
ml2km@zju.edu.cn
Zhongli Yang
zy3p@zju.edu.cn

Specialty section:
This article was submitted to Brain Disease Mechanisms, a section of the journal Frontiers in Molecular Neuroscience

Received: 23 February 2022
Accepted: 16 June 2022
Published: 07 July 2022

Citation:
Han H, Xu M, Wen L, Chen J, Liu Q, Wang J, Li MD and Yang Z (2022) Identification of a Novel Functional Non-synonymous Single Nucleotide Polymorphism in Frizzled Class Receptor 6 Gene for Involvement in Depressive Symptoms. Front. Mol. Neurosci. 15:882396. doi: 10.3389/fnmol.2022.882396

Although numerous susceptibility loci for depression have been identified in recent years, their biological function and molecular mechanism remain largely unknown. By using an exome-wide association study for depressive symptoms assessed by the Center for Epidemiological Studies Depression (CES-D) score, we discovered a novel missense single nucleotide polymorphism (SNP), rs61753730 (Q152E), located in the fourth exon of the frizzled class receptor 6 gene (*FZD6*), which is a potential causal variant and is significantly associated with the CES-D score. Computer-based *in silico* analysis revealed that the protein configuration and stability, as well as the secondary structure of FZD6 differed greatly between the wild-type (WT) and Q152E mutant. We further found that rs61753730 significantly affected the luciferase activity and expression of *FZD6* in an allele-specific way. Finally, we generated *Fzd6*-knockin (*Fzd6*-KI) mice with rs61753730 mutation using the CRISPR/Cas9 genome editing system and found that these mice presented greater immobility in the forced swimming test, less preference for sucrose in the sucrose preference test, as well as decreased center entries, center time, and distance traveled in the open filed test compared with WT mice after exposed to chronic social defeat stress. These results indicate the involvement of rs61753730 in depression. Taken together, our findings demonstrate that SNP rs61753730 is a novel functional variant and plays an important role in depressive symptoms.

Keywords: depression, genetic association, rs61753730, *Fzd6*, CRISPR/Cas9

INTRODUCTION

Major depressive disorder (MDD) has a high prevalence among psychiatric diseases (Charlson et al., 2019). It is not only a potentially fatal disease, with approximately 2% of affected patients committing suicide (Bostwick and Pankratz, 2000), but also one of the leading causes of lost productivity worldwide (Ustun et al., 2004; Ebmeier et al., 2006). It has been projected by the World Health Organization that MDD will become the cause

of the greatest disease burden worldwide by 2030 (Malhi and Mann, 2018).

Major depressive disorder is moderately heritable with an estimated heritability of 37% (Sullivan et al., 2000; Kendler et al., 2006). Although a great number of susceptibility loci have been identified (Bosker et al., 2011; Wray et al., 2012, 2018; Consortium, 2015; Hyde et al., 2016; Direk et al., 2017; Power et al., 2017; Howard et al., 2019), most of them are synonymous variants and failed to be replicated in multiple independent studies. Even for a few of those identified non-synonymous variants, the biological functions and molecular mechanisms underlying their involvement in the pathogenesis of MDD are rarely studied (Kendall et al., 2021). Given the presence of high heterogeneity in depression, low chances of finding non-synonymous variants associated with MDD, and technical difficulties of characterizing those identified non-synonymous variants, the genetic and functional study of non-synonymous variants for MDD is challenging, as for other complex diseases (Ormel et al., 2019; Cai et al., 2020).

The Wnt/β-catenin pathway has been widely accepted to participate in the pathophysiology of mood disorders, including depression (Duman and Voleti, 2012; Sani et al., 2012). The frizzled (FZD) proteins are seven transmembrane-spanning receptors for Wnt ligands involved in this pathway (Huang and Klein, 2004). There is an increasing number of human and animal studies reporting that FZD family is related to depression and other psychiatric disorders. For example, Jang and colleagues reported that three SNPs in *FZD3* were significantly associated with early antidepressant responses in a clinical cohort (Jang et al., 2013). Calabro et al. (2020) found that SNP rs352428 located in *FZD3* was associated with depression and that G allele carriers showed a higher risk of previous depressive episode. *FZD3* was also reported to be highly associated with the risk of schizophrenia (Yang et al., 2003; Zhang et al., 2004). Liu et al. (2020) found that SNP rs10252923 in *FZD1* was significantly associated with schizophrenia. Voleti et al. (2012) reported *Fzd6* knockdown in rat brain resulted in depressive and anxiety behaviors. However, the genetic and mechanistical studies on FZD6 in depression are rare.

In the present study, we aimed not only to identify genetic variants associated significantly with depression but also to demonstrate their involvement at the molecular level. Specifically, we wanted to demonstrate, using various molecular techniques and behavioral tests in both *in vivo* and *in vitro* models, that non-synonymous variant rs61753730, located in the fourth exon of the *FZD6*, is a functional one and plays an important role in depression.

MATERIALS AND METHODS

Subjects and Genotyping

The subjects used in this study were recruited during 2005–2011 primarily from the Mid-South states in the United States as part of the Mid-South Tobacco Case-Control (MSTCC) study. For a detailed description of these samples, please refer to our previously reported studies (Yang et al., 2015; Yang and Li, 2016). All materials related to subject recruitment were approved by the local ethics committees, and all subjects provided written informed consent.

Depressive symptoms were measured with a 20-item version of the Center for Epidemiological Studies Depression (CES-D) scale (Radloff, 1977), and the score of each subject from the baseline examination was used (Harlow et al., 1991; Kuchibhatla et al., 2012). Questionnaires assessing various other characteristics of interest were also administered, and individuals exhibiting other substance abuse (except smoking) or other psychiatric disorders (except depression) were excluded. As previously reported (Yang et al., 2015; Yang and Li, 2016; Jiang et al., 2019; Xu et al., 2020), genomic DNA was isolated from the peripheral blood of each patient, and genotyping was performed using the Illumina Infinium HumanExome BeadChip v 1.0 (Illumina Inc., San Diego, CA, United States). This exome chip includes more than 240,000 functional exonic variants that have been detected in several sequencing data sets, and it was designed to concentrate on rare variants.[1] A total of 4,817 unrelated participants with both genotypic and phenotypic data was enrolled in this study. More detailed descriptions of these participants are shown in **Supplementary Table 1**.

Exome-Wide Association Analysis

We excluded SNPs from further analysis if they: (1) were located on sex chromosomes or the mitochondrial genome; (2) had a call rate of <0.95; (3) deviated from the Hardy-Weinberg equilibrium at a p-value of $<1 \times 10^{-6}$; or (4) had a minor allele frequency (MAF) of <0.01. After these quality control steps, 38,943 SNPs and 4,817 individuals remained for the analyses reported in this paper.

Single-marker association analysis was carried out with a linear regression model adjusted for age, sex, ethnicity, smoking status, and the first three MDS using PLINK (Purcell et al., 2007). Association analysis results were considered significant after Bonferroni correction for the 38,943 SNPs (i.e., $p < 0.05/38{,}943 = 1.28 \times 10^{-6}$). Considering that only 11 SNPs were included on the Illumina Infinium HumanExome BeadChip for *FZD6*, we carried out SNP imputation with IMPUTE2 (Howie et al., 2012) after phasing in SHAPEIT2 (Delaneau et al., 2013) using the 1000 Genome Phase 3 data (Build 38) as a reference, which extended the number of SNPs in *FZD6* from 11 to 132 after excluding those with low imputation quality (info < 0.3). Then, we conducted gene-based association analysis to examine the presence of association between *FZD6* and the CES-D score using SNP-set Kernel Association Test (SKAT) software (Ionita-Laza et al., 2013). The EWAS dataset used in the current study has been submitted to public database and it is available from NCBI GEO (Accession: GSE148375).[2]

In silico Analysis of Protein Variant Effect

SWISS-MODEL[3] was used to generate a three-dimensional (3D) structure for wild-type (WT) FZD6 protein (Arnold et al., 2006).

[1]https://genome.sph.umich.edu/wiki/Exome_Chip_Design

[2]https://www.ncbi.nlm.nih.gov/geo/

[3]http://swissmodel.expasy.org/interactive

A template of human Smoothened in complex with cholesterol (SMTL ID 5I7d.1), which was searched through a BlastP algorithm against the PDB database, showed 27.18% identity and was used for homology modeling of FZD6. The mutant models also were constructed and analyzed in relation to the WT by PyMOL.[4]

Changes in protein stability resulting from a single point mutation were predicted by I-Mutant 3.0[5] based on the Support Vector Machine (SVM) algorithm. It predicted the $\Delta\Delta G$ value as a regression estimator and sign of the stability change, and classified mutations into three categories: neutral (-0.5 – 0.5), decrease (< -0.5), and increase (>0.5) (Schymkowitz et al., 2005). We also used Mutation Cutoff Scanning Matrix (mCSM; Pires et al., 2014b), which applies the concept of graph-based structural signatures to predict the effect of a single point mutation on protein stability. DUET, an integrated computational web server, applies mCSM to predict missense mutation effects on protein stability (Pires et al., 2014a). The $\Delta\Delta G$ value < 0 means a decrease in the stability; otherwise, an increase in the stability. NetSurfP 2.0[6] is a sequence-based tool to predict protein structures, including secondary structure, structural disorder, and backbone dihedral angles for each residue of the input sequences (Klausen et al., 2019).

Cell Culture

Human embryonic kidney 293T (HEK293T) cells were purchased from the American Type Culture Collection (Manassas, VA, United States). Cells were cultured in Dulbecco's Modified Eagle Medium (Hyclone, Logan, UT, United States) supplemented with 10% fetal bovine serum (Gibco, Grand Island, NY, United States) and 1% penicillin/streptomycin (Gibco) in a humidified atmosphere of 5% CO_2 at 37°C.

Luciferase and mRNA Decay Assays

The *FZD6* DNA fragment containing the C allele of rs61753730 was synthesized and cloned into the pGL3-promoter (Promega, Madison, WI, United States). The G allele was introduced into the rs61753730-C allele construct using a QuikChange Lightning Multi Site-Directed Mutagenesis Kit (Agilent, Santa Clara, CA, United States), and its sequence was verified by Sanger sequencing. When HEK293T cells reached 80–90% confluence, transfection was conducted with a pGL3-promoter construct and pRL-TK vector (Promega) by Lipofectamine 2000.

For the luciferase assay, cells were lysed 48 h after transfection and assayed with the Dual-Luciferase Report Assay System (Promega). For the mRNA decay assay, actinomycin D (5 μg/ml) was added 24 h after transfection, and total RNA was extracted at 0, 1, or 3 h. The quantitative real-time PCR (qRT-PCR) was then conducted to determine the relative expression of the luciferase reporter gene.

[4]http://pymol.org/

[5]http://gpcr2.biocomp.unibo.it/cgi/predictors/I-Mutant3.0/I-Mutant3.0.cgi

[6]https://services.healthtech.dtu.dk/service.php?NetSurfP-2.0

RNA Extraction and Quantitative Real-Time PCR

Total RNA was isolated from the cells after treatment and homogenized by an ultrasonic disruptor in TRIzol reagent (Life Technologies, Grand Island, NY, United States) according to the manufacturer's instructions. The purity and quantity of total RNA were measured at the optical densities of 260 and 280 nm with NanoDrop 2000 (Thermo Scientific, Waltham, MA, United States). First-strand cDNAs were synthesized from 1 μg of total RNA using an iScript cDNA Synthesis Kit (Bio-Rad, Hercules, CA, United States). The qRT-PCR amplification was conducted in a volume of 10 μl containing 5 μl of 2 × Power SYBR Green PCR Master Mix (Applied Biosystems), mixed with equal amounts of sense and antisense primers (2.5 μl; final concentration 250 nM each), and 2.5 μl of diluted cDNA in a 384-well plate using 7900 HT Fast Real Time PCR system (Applied Biosystems) as described previously (Yang et al., 2016; Han et al., 2019; Chen et al., 2020; Fan et al., 2021). The PCR conditions were as follows: 50°C for 2 min, 95°C for 10 min, followed by 40 cycles of 95°C for 15 s and 60°C for 1 min. The primers for the reporter gene are forward: 5′-TGCACATATCGAGGTGGACATC-3′ and reverse: 5′-TGCCAACCGAACGGACAT-3′; both were synthesized at Sango Biotech (Shanghai) Co., Ltd. The expression of the gene of interest was normalized to the housekeeping gene glyceraldehyde 3-phosphate dehydrogenase (*GAPDH*) and then analyzed using a comparative C_t method (Winer et al., 1999).

Animals

All animals were purchased from GemPharmatech Co., Ltd., (Nanjing, China) and maintained in the Animal Core Facility at Zhejiang University. Mice were kept under the standard housing conditions on a 12-h light/dark cycle. Food and water were freely available. Mice were deeply anesthetized before sacrifice. All experimental procedures used in the study were approved by the Animal Use and Care Committee of the First Affiliated Hospital of Zhejiang University.

Generation of *Fzd6*-Knockin Mice Using CRISPR/Cas9 Editing System

The *Fzd6*-knockin (*Fzd6*-KI) mice based on C57BL/6J were generated *via* the optimized CRISPR/Cas9 system at GemPharmatech Co., Ltd., with almost no off-target effects detected (Shen et al., 2014). Briefly, Cas9 mRNA, sgRNA, and donor compounds were co-microinjected into fertilized C57BL/6J mouse zygotes. The sgRNA directed to Cas9 endonuclease cleavage near the mutation site and created a double-strand break. Such a break was repaired and resulted in a Q152E point mutation, which was then inserted into exon 4 by homologous recombination and we obtained the *Fzd6*-KI mice.

DNA was isolated from the tail of each pup, and PCR was conducted for genotyping. The PCR products were electrophorized to screen if it is wild-type or mutant mouse. Then, Sanger sequencing was used to validate the gene sequence, especially at the mutant site. The

sequence of sgRNA was 5′-CACCAAAATCCAATGTCTCT-3′, and the donor sequence was 5′-CCTGTAAC TTCTCATCCACACACAGAGCTTTCTGGGCCACAGAAGA AATCAGATGAAGTCCCACGCGACATTGGATTTTGGTGT CCAAAGCACCTTAGGACTTCCGGGGACCAAGGCTAT-3′. The primers for genotyping were forward 1: 5′- TCT GTGAATGCAGCAAAGTCATGG-3′, reverse 1: 5′- ATCCA ATGTCGCGTGGGACTTC-3′; forward 2: 5′-TCTGTGAATGC AGCAAAGTCATGG-3′, reverse 2: 5′-GTCTCTCTGGGTATC TGAATCGTC-3′. The primers for sequencing was 5′-GTC TCTCTGGGTATCTGAATCGTC-3′. After genotyping, through crossbreeding of the heterozygote mice, we obtained *Fzd6*-KI homozygous and WT mice, which were used for the following studies. For the identification of some representative animals with different genotypes, please see the attached **Supplementary Material**.

Behavioral Tests

The adult (2–3-month old) male and female homozygous *Fzd6*-KI and WT mice were subjected to behavioral tests (n = 7–9 mice/genotype). All mice were habituated to the testing room for 1 h prior to each test. After completion of all relevant behavioral tests, all mice were sacrificed.

Chronic Social Defeat Stress Model for Depression

The chronic social defeat stress (CSDS) model of depression was carried out as described previously (Golden et al., 2011; Harris et al., 2018; Shen et al., 2019). Briefly, prior to each experiment, more than the number of 50 retired male breeder CD1 mice (known as aggressor mice) were screened for three consecutive days to determine the aggressive characteristics of each animal, which was done by placing the screener C57BL/6J mouse directly into the home cage of the CD1 mice for 3 min with the presence of an aggressor. The following two criteria were used to select the CD1 aggressor mice: (1) mouse must attack in at least two consecutive sessions during three 3-min screening sessions; and (2) the latency to initial aggression must be less than 60 s. Then, each experimental mouse (male *Fzd6*-KI mouse) was introduced into the home cage of a CD1 aggressor for 5 min. At the end of 5 min of social defeat, the experimental mice were moved to the other side separated from the aggressors with a perforated Plexiglas divider where animals were maintained for 24 h. After 24 h of sensory but not physical contact, the above procedure was repeated daily for 10 consecutive days. The non-defeated control animals were also pair-housed with an identical home cage setup. The two mice on each side were never allowed physical or sensory contact with CD1 mice or their home mates. Each experimental mouse was faced with a different aggressor every day. The social interaction test was conducted 24 h later after 10 days of social defeat.

Social Interaction Test

Social avoidance behavior was evaluated by the social interaction (SI) test in an open-field apparatus (44 cm × 44 cm × 44 cm) consisting of two consecutive phases each for 2.5 min. During the first phase (target absent), experimental animals were placed individually in the apparatus containing an empty wire-mesh enclosure (10 cm × 6.5 cm × 25 cm) with the target CD1 aggressor absent, and their movements were monitored with Any-maze video tracking software. In the second phase (target present), a novel aggressive CD1 mouse was placed in the wire-mesh enclosure with the same metrics measured. Between the two phases, the experimental animals were returned to their home cages for an approximately 30 s interval. The time spent in the interaction zone (a 14 cm × 26 cm rectangular area projecting 8 cm around the wire-mesh enclosure) and in the corner zones (a 9 cm × 9 cm area projecting from both corner joints opposing the wire-mesh enclosure) were counted.

Open Field Test

The experimental animals were placed individually in the center of the open field test (OFT) apparatus (44 cm × 44 cm × 44 cm) with a dim light for 10 min. A video camera was arranged directly above the apparatus to monitor the movement of each animal. Locomotor activity was measured as the total distance traveled. Anxiety-like behavior was defined by the distance traveled, time spent in the central zone (15 cm × 15 cm), and center entries during the 10 min period. The apparatus was cleaned with 75% ethanol after each experiment. Data were collected by Any-maze software (Any-maze, Stoelting, Wood Dale, IL, United States).

Forced Swim Test

The forced swim test (FST) was conducted as previously described (Yang et al., 2018). Each experimental animal was placed individually in a cylinder (12 cm diameter; 25 cm height) filled with water (23–25°C) and allowed to swim for 6 min. The depth of water in the cylinder (∼16 cm) was set to prevent animals from touching the bottom with their tails or hind limbs. The behaviors were recorded with a camera from the side. The total duration of immobility (no movement except keeping the head above water) in the last 4 min was counted.

Sucrose Preference Test

The sucrose preference test (SPT) was conducted according to published protocols (Monteggia et al., 2007; Chaudhury et al., 2013; Shen et al., 2019) with minor changes. Animals were single housed and habituated with two bottles of water for two consecutive days. After habituation, the mice were allowed free access to a two-bottle choice of 2% sucrose solution or tap water. The positions of the two bottles were switched (left to right and right to left) every 6 h to avoid side preference. The total duration of the test was 48 h. The bottles were weighed at the start and end of each testing period. Sucrose preference was calculated as sucrose consumption/(water consumption + sucrose consumption) × 100% during the test phase.

Statistical Analyses

All experimental data were analyzed with GraphPad Prism 8.0 (San Diego, CA, United States). All data are presented as means ± standard error of the mean (SEM). We used a two-tailed unpaired t-test for two-group comparisons and one-way ANOVA followed by Bonferroni multiple testing for more

than two-group comparisons. Two-way ANOVA was applied to compare data from the behavioral tests after CSDS with two factors (Genotype × Stress). A p-value of <0.05 was considered statistically significant.

RESULTS

Characteristics of Samples in This Study

The characteristics of the study population are presented in **Supplementary Table 1**. A total of 4,817 subjects with an average age of 42.8 years (± 13.5; SD) were included. Of them, 3,279 (68.1%) were self-reported African Americans, and 45.2% were males. In line with the population-based design of the study, the mean depressive symptom scores were 6.3 (± 9.5; SD) for the 20-item version of the CES-D.

Single-Marker Based Association Analysis

Table 1 lists the association results of the top 11 SNPs with $p < 1 \times 10^{-5}$, among which two loci showed significant association with the CES-D score after Bonferroni correction: rs61753730 (Chr. 8: 104336788; MAF = 0.012; $p = 8.46 \times 10^{-9}$) in *FZD6*; and rs35024632 (Chr. 7: 38433726; MAF = 0.025; $p = 3.08 \times 10^{-8}$) in the amphiphysin (*AMPH*) gene. **Figure 1A** shows the Manhattan plot of the association results by chromosome location, and two SNPs, located in chromosomes 7 and 8, showed signal above the commonly defined genome-wide significance threshold ($p < 5 \times 10^{-8}$) (Sullivan et al., 2009). Of these two SNPs, both are missense variants resulting in amino acid changes in their encoded proteins (rs61753730 from glutamine to glutamate; rs35024632 from lysine to threonine). **Figure 1B** depicts the quantile-quantile plot of observed vs. expected $-\log_{10}$ (p- value) for all 38,943 SNPs. The distribution of p- values was similar to what would be expected by chance, with a genomic control λ value of 1.000, indicating no detectable inflation of test statistics (Devlin and Roeder, 1999).

To characterize the most significantly associated SNP rs61753730 in *FZD6*, we performed gene-based association analysis for 11 genotyped and 121 imputed SNPs (info > 0.3) located in the gene as well as in a 2-kb region both upstream and downstream, which showed a significant association of *FZD6*

TABLE 1 | A list of top 11 single nucleotide polymorphisms (SNPs) with $p < 1 \times 10^{-5}$ resulted from genome-wide association analysis.

db SNP ID	Chr.	Position	Gene	Alleles	MAF	Function	Amino acid change	*P*-value
rs61753730	8	104336788	*FZD6*	[C/G]	0.01214	Missense	Gln120Glu/Gln152Glu	**8.46E−09**
rs35024632	7	38433726	*AMPH*	[T/G]	0.02545	Missense	Lys454Thr/Lys496Thr	**3.08E−08**
rs117406702	7	100346094	*ZAN*	[A/G]	0.01443	Splice	NA	5.46E−07
rs62620991	1	46669276	*LURAP1*	[A/C]	0.01121	Missense	Met60Leu	1.41E−06
rs74424604	3	36931397	*TRANK1*	[T/C]	0.016	Missense	Arg233His	1.42E−06
rs6710212	2	152490458	*NEB*	[A/G]	0.0518	Missense	Cys3042Arg	1.56E−06
rs72658825	7	21934511	*DNAH11*	[A/G]	0.01766	Missense	Ala4322Thr	1.95E−06
rs61740788	4	4440183	*STX18*	[T/G]	0.0503	Missense	Glu184Ala	1.97E−06
rs61731432	16	3254418	*OR1F1*	[G/C]	0.02181	Missense	Pro58Ala	3.44E−06
rs61738623	6	109468136	*CEP57L1*	[A/G]	0.01195	Synonymous	Lys112Lys	8.21E−06
rs114567837	19	55870379	*FAM71E2*	[A/C]	0.02928	Missense	Glu619Asp	8.40E−06

All SNP shown in the table are ranked based on the order of p-value. Three significantly associated SNPs after Bonferroni correction ($p < 1.28 \times 10^{-6}$) are given in bold. Chr., chromosome; MAF, minor allele frequencies; NA, not applicable.

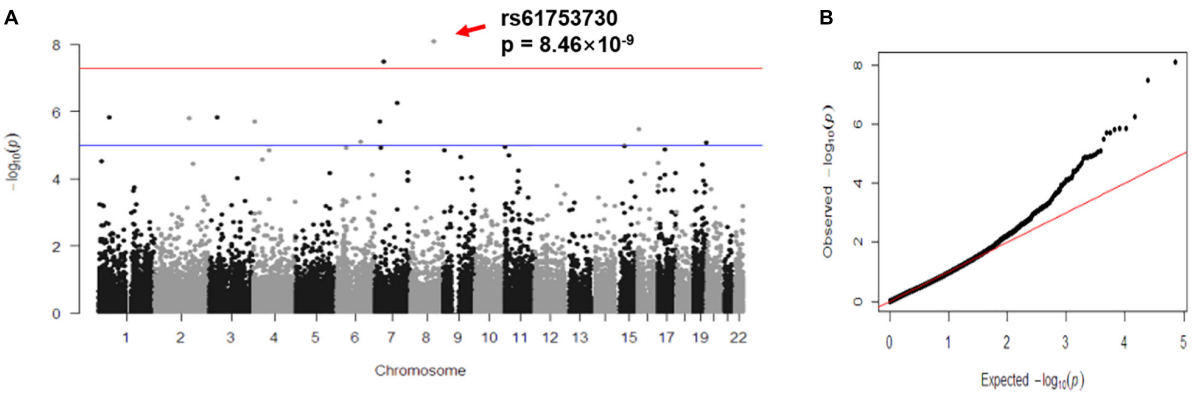

FIGURE 1 | Genetic findings of rs61753730 in *FZD6* associated with depressive symptoms. **(A)** Manhattan plot of all results from exome-wide association study (EWAS) for CES-D score according to chromosome location. **(B)** Quantile–quantile plot of observed vs. expected $-\log_{10}$ (p-value) of SNPs from EWAS. λ, genomic inflation factor, estimated at close to 1. Red arrow indicates the location of rs61753730.

with the CES-D score ($p = 0.0078$). Of these SNPs, 102 were rare and 30 were common variants.

Allele-Specific Effect of rs61753730 on Frizzled Class Receptor 6 Gene

To further investigate the biological role of rs61753730 on FZD6 in depression, we carried out *in silico* analysis and found that the different alleles of rs61753730 lead to an altered protein configuration (**Figure 2A**). Although no obvious difference was observed in the physiochemical characteristics of the protein and disulfide bonds, several distinctions were discovered in the secondary structure and transmembrane helices (**Supplementary Table 2**). On the basis of the prediction by NetSurfP-2.0, the secondary structure was quite different at position 152 of FZD6 (**Figure 2B**), which was a coil in the WT (Gln, Q) but a helix in the mutant FZD6 (Glu, E). We further predicted the stability of the protein after mutation by I-Mutant 3.0 and found that the $\Delta\Delta G$ value was −0.18 kcal/mol, which means the mutation decreased the stability of the FZD6 protein because of the amino acid change from Gln (rs61753730-C) to Glu (rs61753730-G) at position 152. These findings were further supported by another structure-based prediction tool mCSM with an online server DUET ($\Delta\Delta G = -0.039$ kcal/mol). Together, these *in silico* results indicated that the different allele of rs61753730 changed the structure of FZD6.

In determining the allele-specific function of rs61753730 on *FZD6* experimentally, HEK293T cells transfected with the rs61753730-G allele construct showed a 20% decrease in luciferase activity ($p = 0.014$) compared with the cells transfected with the rs61753730-C allele (**Figure 2C**). Further, when the cells were treated with actinomycin D, the mRNA quantity of the luciferase reporter gene was significantly reduced in both C and G allele-transfected cells, whereas the construct carrying the rs61753730-C allele decayed significantly more slowly than that containing the G allele, with a p-value of 0.0349 and 0.0267 after 1 and 3 h, respectively, of actinomycin D treatment (**Figure 2D**).

By analyzing the expression quantitative trait loci (eQTL) dataset from GTEx Portal, we found that rs61753730 showed eQTL regulation with allele-specific significance on *FZD6* mRNA expression, especially in the cerebellum ($p = 1.3 \times 10^{-5}$), a brain region implicated in depression (Depping et al., 2018). These results demonstrated that the missense mutation rs61753730 contributed to the effect of FZD6 on depression.

Generation of *Fzd6*-Knockin Mice

As shown in **Supplementary Figures 1A,B**, the glutamine residue at position 152 (rs61753730-C) was highly conserved from human to mouse and rat, suggesting it has functional importance, and the mouse model could be used to investigate the biological role of rs61753730 in depressive symptoms. **Supplementary Figure 1C** shows the strategy used to generate the rs61753730 mutant *Fzd6*-KI mice with the CRISPR/Cas9 system. Since rs61753730 is located in the fourth exon of FZD6, the CRISPR/Cas9 system targeted to it to obtain the *Fzd6*-KI mice carrying G allele. The sequence was validated by Sanger sequencing with the C allele in WT mice and the G allele in *Fzd6*-KI mice (**Supplementary Figure 1D**).

Construction of Chronic Social Defeat Stress Depression Model in *Fzd6*-Knockin Mice

To characterize the role of rs61753730 in depression in the mouse model, the 10-day CSDS-induced depression model, a well-validated and widely used model (Golden et al., 2011), was employed (**Figures 3A,B**). After the 10-day CSDS, the social interaction test was performed (**Figures 3C–E**). When there was no target, the two-way ANOVA showed no significant interaction for Stress × Genotype ($F_{(1,13)} = 0.04783$, $p = 0.8303$), and both the Genotype factor ($F_{(1,13)} = 0.3138$, $p = 0.5849$) and Stress factor ($F_{(1,13)} = 2.643$, $p = 0.1280$) also showed no significant difference, respectively, which means the baseline is similar for the four groups. When the target present, although the results showed no significant interactions for Stress × Genotype ($F_{(1,13)} = 2.212$, $p = 0.1608$) and the Genotype factor ($F_{(1,13)} = 2.212$, $p = 0.1608$), the stress factor showed a close to significant difference ($F_{(1,13)} = 4.353$, $p = 0.0572$). As shown in **Figure 3E**, in the presence of target mice, the WT mice who subjected to CSDS spent less time in the interaction zone than the WT mice without CSDS ($p < 0.05$), and the *Fzd6*-KI mice spent less time in the interaction zone compared with the WT mice ($p < 0.05$). No significant difference was observed between *Fzd6*-KI mice whether subjected to CSDS or not ($p > 0.05$). It suggests that the *Fzd6*-KI mice is not susceptible to stress, however, this type of mice still can present the similar depressive-like symptoms similar with WT-CSDS mice. Thus, more depressive-like and anxiety-like behaviors need to be conducted to verify this phenomenon.

Alterations of rs61753730 Mutation on Depressive-Like and Anxiety-Like Behaviors After Chronic Social Defeat Stress in *Fzd6*-Knockin Mice

To identify the depressive-like behaviors in *Fzd6*-KI mice, we carried out FST and SPT experiments and used the measurement of immobility duration and sucrose preference ratio to evaluate anhedonia. In the FST, two-way ANOVA showed significance for Stress factor ($F_{(1,13)} = 9.415$, $p = 0.0090$), but not for Genotype factor ($F_{(1,13)} = 1.631$, $p = 0.2239$) and for their interactions ($F_{(1,13)} = 3.312$, $p = 0.0919$). Compared with the WT control mice, the immobility duration increased significantly ($p < 0.05$; **Figure 4A**) after the WT mice were subjected to CSDS. The *Fzd6*-KI mice exposed to CSDS also showed significantly greater immobility compared with the WT control mice ($p < 0.05$), whereas no significant difference was observed between the *Fzd6*-KI mice with and without CSDS exposure. In the SPT, two-way ANOVA showed that significant difference for Genotype factor ($F_{(1,12)} = 7.452$, $p = 0.0183$), but not for the Stress factor ($F_{(1,12)} = 3.088$, $p = 0.1044$) and their interactions ($F_{(1,12)} = 0.08952$, $p = 0.7699$). Although no significant difference in the sucrose preference ratio was detected between the WT mice exposed and not exposed to CSDS (**Figure 4B**), the results

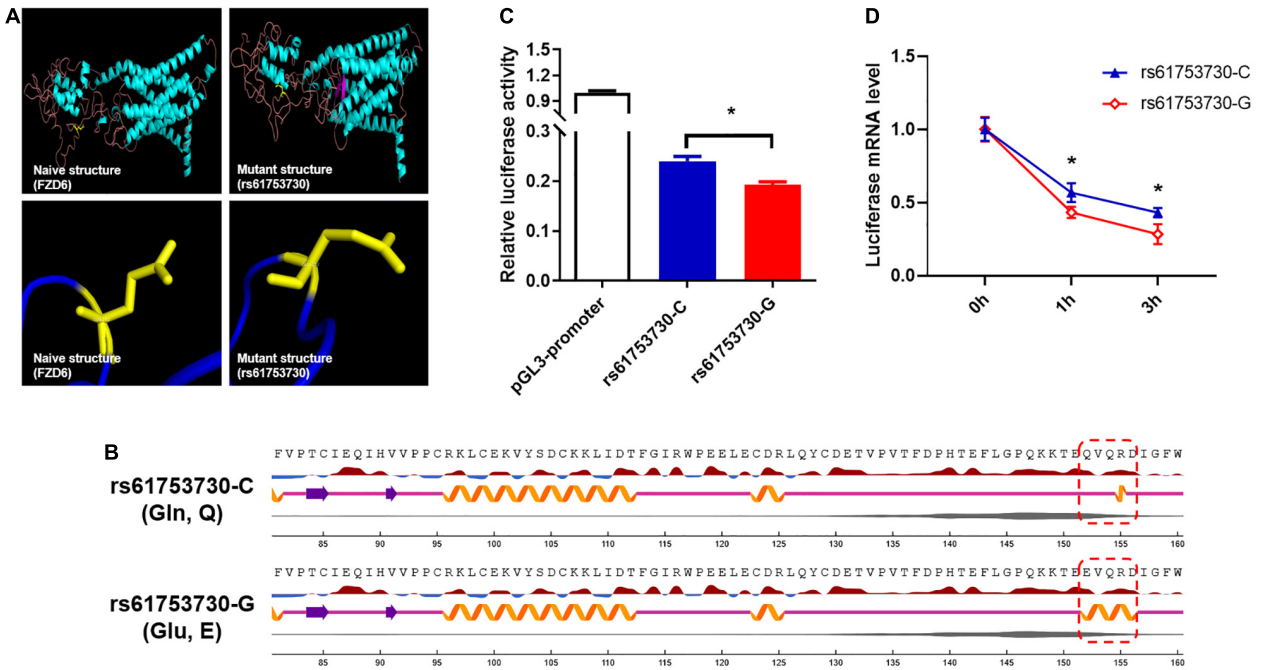

FIGURE 2 | Allele-specific effects of rs61753730 on *FZD6*. **(A)** Effect of rs61753730 mutation on predicted structure of FZD6 protein generated by PyMOL. Upper panel: Naive 3D structure of FZD6 and mutant structure of rs61753730 (Q152E). Bottom panel: Naive structure of FZD6 shows glutamine at position 152, and predicted mutant structure of rs61753730 shows glutamic acid at corresponding position. **(B)** Effect of rs61753730 mutation on secondary structure of FZD6 at position 152 predicted by NetSurfP-2.0. Box with dashed line in red indicates different structure of WT (C) and mutant SNP (G). **(C)** Effect of rs61753730 on luciferase activity. HEK293T cells were transfected with rs61753730 C- and G-allele constructs of pGL3-promoter vector. Luciferase activity was measured 48 h later. Data are reported as relative firefly luciferase activity normalized to *Renilla* luciferase activity and represented as mean ± SEM (n = 3). *$p < 0.05$. **(D)** Effect of rs61753730 on mRNA stability of luciferase reporter gene. HEK293T cells were transfected with rs61753730 C- and G-allele constructs of pGL3-promoter vector for 24 h prior to adding actinomycin D (5 μg/ml). The mRNA of luciferase expression was measured at different times (0, 1, and 3 h) and normalized to *GAPDH*. Data are presented as mean ± SEM (n = 3). *$p < 0.05$.

showed the same trend; and *Fzd6*-KI mice exposed to CSDS displayed significantly less sucrose preference than the WT control mice ($p < 0.05$).

As anxiety-like behaviors correlated highly with depression, we measured these behaviors in *Fzd6*-KI mice with the OFT, which was measured by the number of times the mice entered or spent time in the central area. Two-way ANOVA showed significant differences for Stress × Genotype interactions for total distance traveled ($F_{(1,13)} = 8.376$, $p = 0.0125$) and center entries ($F_{(1,13)} = 6.317$, $p = 0.0259$), but not for time spent in the center zone ($F_{(1,13)} = 3.289$, $p = 0.0929$). As shown in **Figure 4C**, the locomotor activities with total distance traveled (**Figure 4D**), center entries (**Figure 4E**), and time spent in the center zone (**Figure 4F**) were all greatly decreased after the WT mice were subjected to CSDS ($p < 0.01$), and the *Fzd6*-KI mice with or without CSDS exposure showed a comparable reduction. In *Fzd6*-KI mice exposed to CSDS, it also presented a significant decrease in locomotor activities compared with the WT control mice ($p < 0.05$), but there was no significant difference in *Fzd6*-KI mice with or without CSDS exposure. Taken together, these behavioral results strongly indicated that the *Fzd6*-KI mice presented depressive symptoms like those in WT mice subjected to CSDS, suggesting an important role of rs61753730 in depression.

DISCUSSION

In this study, we found two SNPs ($P_{rs61753730} = 8.46 \times 10^{-9}$; $P_{rs35024632} = 3.08 \times 10^{-8}$) to be significantly associated with the CES-D score at a genome-wide significance level. We further revealed rs61753730 to be a functional SNP modulating the structure and function of FZD6 in an allele-specific manner. Finally, we generated the single point mutation *Fzd6*-KI mouse model, which expressed depressive-like behaviors. All these findings strongly demonstrated the functional roles of rs61753730 in depression.

In recent years, numerous studies have been conducted to identify susceptible SNPs for depression, and most identified variants found so far appear to be non-coding (Wray et al., 2018; Howard et al., 2019). For example, Wray et al. (2018) found 44 significant loci associated with depression, and all of them were non-coding. In another study, Howard et al. (2019) identified 102 variants associated with depression, of which only one SNP was coding, this one located in the exon region of the DENN domain containing 1B (*DENND1B*). As we all know, those SNPs that alter the amino acid coding (i.e., a non-synonymous SNP) are likely to play more important roles in a disease or phenotype of interest because the missense SNP can change the protein structure and thus alter the function of the protein (Ormel et al., 2019). Luckily,

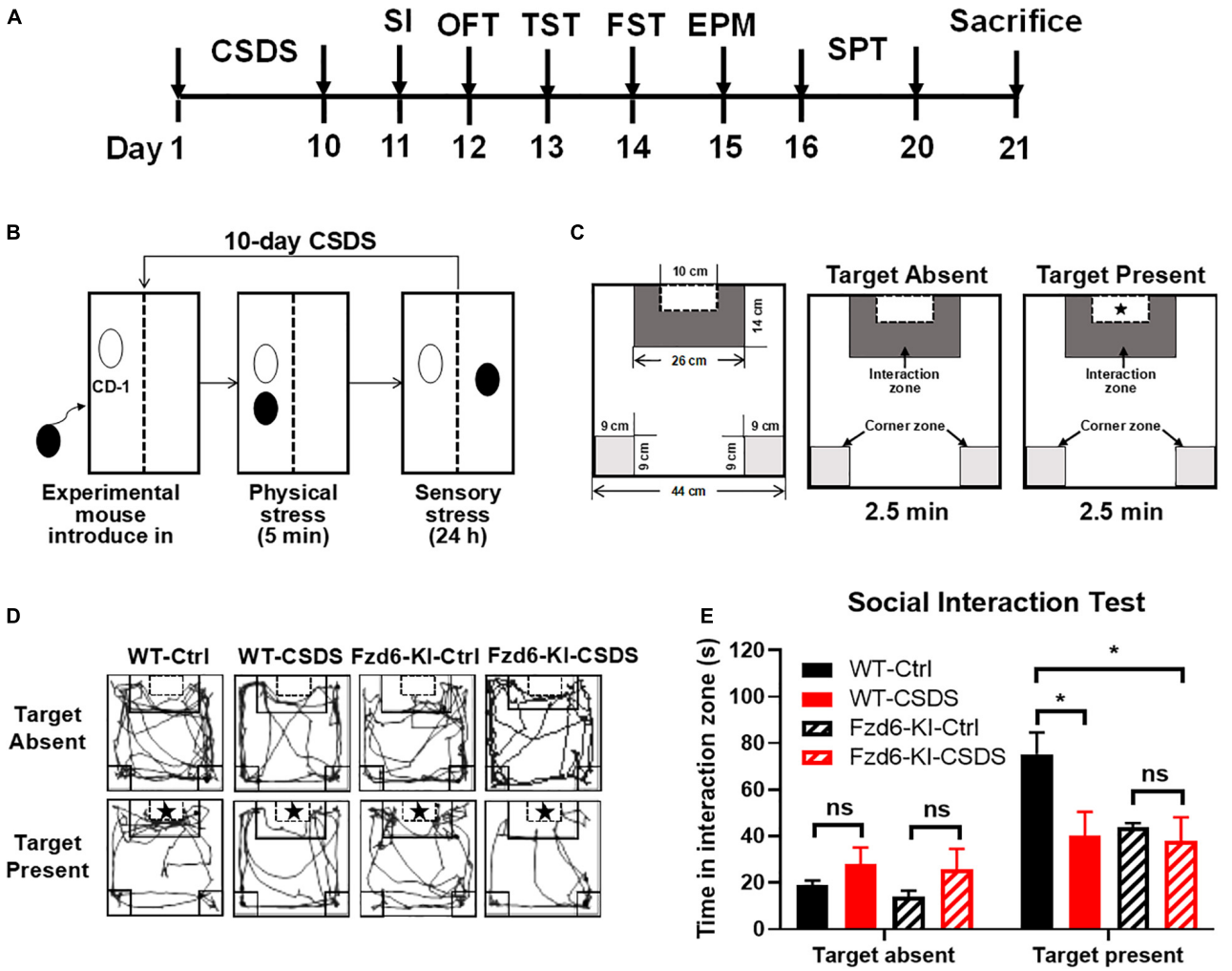

FIGURE 3 | Construction of 10-day CSDS depressive model in *Fzd6*-knockin (*Fzd6*-KI) mice. **(A)** Schematic diagram of experimental design. **(B)** Schematic of 10-day CSDS model. **(C)** Schematic of open field arena and zones for social interaction (SI) test in absence or presence of target CD-1 mice. Pentagram marks target mice. **(D)** Representative tracking plot of SI test in absence (top line) and presence (bottom line) of target. **(E)** Time spent in interaction zone in absence and presence of target in both wild-type and *Fzd6*-KI mice after CSDS. $^*p < 0.05$, ns, not significant.

our current study discovered a missense SNP rs61753730 in *FZD6* that is significantly associated with depression, in which the person who carries rs61753730-G (the risk allele) may have an increased risk for depression.

The FZD proteins are Wnt ligands in Wnt/β-catenin pathway (Huang and Klein, 2004). A number of studies have reported that the member in FZD family is involved in depression or antidepressant. Jang et al. (2013) identified FZD3 as a molecular target for antidepressant treatments in both animal model and human studies. Recently, Li et al. (2021) found that FZD7 represents a novel GPCR regulator in depression, which is dysregulated in chronic unpredictable mild stress (CUMS) mouse model. This gene was also identified as tentative biomarkers for antidepressant drug resistance through *in vitro* study (Breitfeld et al., 2017). Okamoto et al. (2010) indicated that antidepressants can upregulate *Fzd9* expression in the hippocampus of rat. Furthermore, FZD6 is not only implicated in the process of human cancer (Corda and Sala, 2017), neural tube defects (De Marco et al., 2012; Shi et al., 2014), and brain morphogenesis defect (Stuebner et al., 2010), but also in depression. A previously reported animal study demonstrated that *Fzd6* knockdown in the hippocampus of rats induces depressive-like and anxiety-like behaviors (Voleti et al., 2012). Knocking down of Wnt2/Wnt3, the ligand of FZD6, also results in depressive-like behaviors; in contrast, overexpression of Wnt2/Wnt3 reverses depressive-like behaviors (Zhou et al., 2016). These studies highlight the essential role of FZD6 in depression.

The change in an amino acid to create the missense SNP may cause unstable structure and dysfunction of the gene where it occurs. To define the biological role of SNP rs61753730 in the regulation of FZD6 in depression, we carried out a series of investigations at different levels. The computer-based *in silico* technique is an effective way to predict the potential function of an SNP of interest prior to initiating experiments

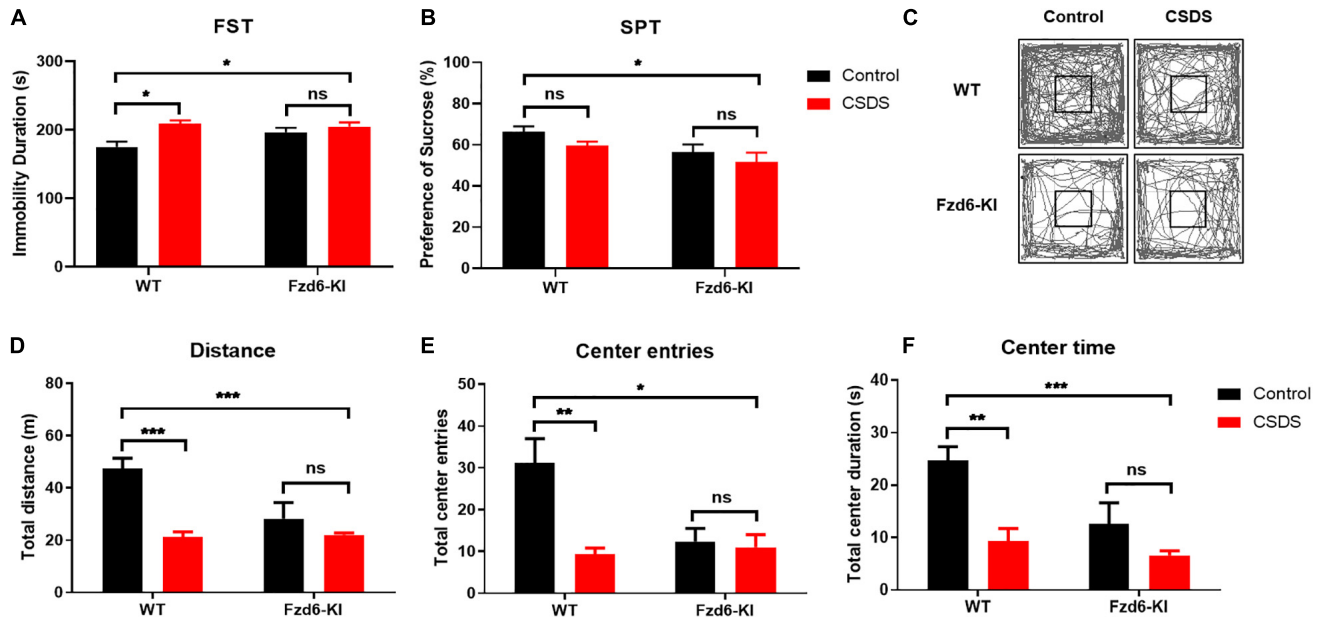

FIGURE 4 | Changes of depressive- and anxiety-like behaviors in *Fzd6*-KI mice after CSDS. **(A,B)** Depressive-like behaviors. Graphs show immobility time, scored in seconds, in panel **(A)** forced swimming test (FST) and percentage of sucrose consumption over total fluid consumption in panel **(B)** sucrose preference test (SPT). **(C–F)** Anxiety-like behaviors. **(C)** Representative tracking plot of open field test (OFT). Graphs present **(D)** total distance traveled, **(E)** center entries, and **(F)** time spent in center area. Animals were tested in 3–5 mice/group. Data were analyzed using two-way ANOVA, and all data are presented as mean ± SEM. $^{*}p < 0.05$, $^{**}p < 0.01$, $^{***}p < 0.001$, ns, not significant.

in a "wet" laboratory (Rajasekaran et al., 2007; Khalid and Almaghrabi, 2020). Through predictions by various software programs, we found the protein configuration and stability of FZD6 to be altered by the change of glutamine to glutamic acid at position 152. Although most of the risk variants that regulate gene expression are located in non-coding regions, the missense mutations also exerted regulatory functions as reflected in luciferase activity (Shimajiri et al., 2001; Kato et al., 2003; van Steensel et al., 2009; Hemming et al., 2020). Our functional studies demonstrated that the rs61753730-G allele significantly decreased the activity and mRNA stability of the luciferase reporter gene. The eQTL analysis can be used to link the risk SNP to the expression of a specific gene or nearby genes (Fu et al., 2012). Through the GTEx Portal database, we found rs61753730 to be an eQTL regulating *FZD6* mRNA expression in an allele-specific manner. All these results imply that rs61753730 is a functional SNP modulating FZD6.

Animals with depression usually exhibited anhedonia, anxiety, or despair-like behaviors (Yan et al., 2010; Wang et al., 2017; Hao et al., 2019). The behavioral paradigms such as TST or FST can be used to assess despairing behavior. The anxiety-like behavior can be determined by OFT or EPM, and the anhedonia can be detected by SPT (Yan et al., 2010; Wang et al., 2017; Hao et al., 2019). In this study, to better determine the functional role of rs61753730 in depression, we generated an *Fzd6*-KI mouse model with rs61753730 mutation by applying the cutting-edge CRISPR/Cas9 technique, which can target even a single nucleotide (Heidenreich and Zhang, 2016; Pickar-Oliver and Gersbach, 2019; Wu et al., 2019, 2020). By performing various animal behavior tests, we found the *Fzd6*-KI mice presented a significant increase in immobility in FST, reduced sucrose preference, and decreased locomotor activities in OFT after exposure to 10-day CSDS, suggesting these animals presented anhedonia, anxiety, or despair. Consistent with our behavioral results, a previous study has shown that partial *Fzd6* knockdown in the brain of rats induced anhedonic responses and anxiety, such as decreased sucrose preference, suppressed feeding, and altered performance in the EPM (Voleti et al., 2012). In a most recent paper, Morel et al. (2022) utilized the same paradigm CSDS to induce anxiety- and depressive-like phenotypes, and the results showed that the ventral tegmental area (VTA) to basolateral amygdala (BLA) dopamine projection is an important circuit mechanism for anxiety-like behaviors and anxiety-depressive comorbid conditions, but not for depressive-like behaviors in mice. Thus, the behavioral alterations observed in the present study further demonstrated the functional role of rs61753730 in depression, which may attribute to a VTA→BLA dopamine neural circuit.

In summary, we carried out an exome-wide association study of the CES-D score with 4,817 samples and identified two significant SNPs at the genome-wide level. The strongest signal was rs61753730, a missense variant predicted to alter protein configuration and decrease the structural stability of FZD6 in an allele-specific manner. Through animal behavioral tests in chronic stress, we further showed that rs61753730 in *FZD6* is highly related to depressive symptoms. Taken together, our current results systematically elucidated that rs61753730 is a functional SNP playing significant roles in depression.

DATA AVAILABILITY STATEMENT

The raw data supporting the conclusions of this article will be made available by the authors, without undue reservation.

ETHICS STATEMENT

The studies involving human participants were reviewed and approved by the Institutional Review Boards of the University of Virginia and University of Mississippi Medical Center. The patients/participants provided their written informed consent to participate in this study. The animal study was reviewed and approved by Animal Use and Care Committee of The First Affiliated Hospital of Zhejiang University.

AUTHOR CONTRIBUTIONS

HH, MX, LW, and JC carried out the molecular experiments. LW, QL, and JW performed the bioinformatic analyses. HH, LW, MDL, and ZY wrote and edited the manuscript. MDL and ZY conceptualized and supervised the project. All authors contributed to the article and approved the submitted version.

FUNDING

This study was supported in part by the China Precision Medicine Initiative (2016YFC0906300), the China National Postdoctoral Program for Innovative Talent (BX20190295), the China Postdoctoral Science Foundation (2020M681891), the Research Center for Air Pollution and Health of Zhejiang University, and the State Key Laboratory for Diagnosis and Treatment of Infectious Diseases of The First Affiliated Hospital of Zhejiang University.

ACKNOWLEDGMENTS

We thank Thomas J. Payne of the University of Mississippi Medical Center for his leading role in recruiting subjects for this study and David L. Bronson for excellent editing of this manuscript. We also are grateful for the technical support by the Core Facilities, Zhejiang University School of Medicine.

SUPPLEMENTARY MATERIAL

The Supplementary Material for this article can be found online at: https://www.frontiersin.org/articles/10.3389/fnmol.2022.882396/full#supplementary-material

Supplementary Figure 1 | Generation of *Fzd6-KI* mice by CRISPR/Cas9 system. **(A,B)** Conservation analysis of rs61753730 (Q152E). **(A)** The UCSC Genome Browser Alignments depict nucleotide alignment of human *FZD6* gene and homologs from other species. Position of rs61753730 variant is indicated by dashed red line. **(B)** Glutamine (Q) is conserved at same point in human, mouse, rat, and other animals. **(C)** Schematic of strategy for construction of *Fzd6* point-mutation mice *via* the CRISPR/Cas9 system. The rs61753730 is located in fourth exon of *Fzd6*. Red asterisk indicates mutation site. **(D)** Sequencing chromatogram to identify WT (with C allele) and *Fzd6*-KI (with G allele) mice from tail genome DNA. Dashed red line marks location of rs61753730 in two types of mice.

REFERENCES

Arnold, K., Bordoli, L., Kopp, J., and Schwede, T. (2006). The SWISS-MODEL workspace: a web-based environment for protein structure homology modelling. *Bioinformatics* 22, 195–201. doi: 10.1093/bioinformatics/bti770

Bosker, F. J., Hartman, C. A., Nolte, I. M., Prins, B. P., Terpstra, P., Posthuma, D., et al. (2011). Poor replication of candidate genes for major depressive disorder using genome-wide association data. *Mol. Psychiatr.* 16, 516–532. doi: 10.1038/mp.2010.38

Bostwick, J. M., and Pankratz, V. S. (2000). Affective disorders and suicide risk: a reexamination. *Am. J. Psychiatr.* 157, 1925–1932. doi: 10.1176/appi.ajp.157.12.1925

Breitfeld, J., Scholl, C., Steffens, M., Laje, G., and Stingl, J. C. (2017). Gene expression and proliferation biomarkers for antidepressant treatment resistance. *Transl. Psychiatr.* 7:e1061. doi: 10.1038/tp.2017.16

Cai, N., Choi, K. W., and Fried, E. I. (2020). Reviewing the genetics of heterogeneity in depression: operationalizations, manifestations and etiologies. *Hum. Mol. Genet.* 29, R10–R18. doi: 10.1093/hmg/ddaa115

Calabro, M., Porcelli, S., Crisafulli, C., Albani, D., Kasper, S., Zohar, J., et al. (2020). Genetic variants associated with psychotic symptoms across psychiatric disorders. *Neurosci. Lett.* 720, 134754. doi: 10.1016/j.neulet.2020.134754

Charlson, F., van Ommeren, M., Flaxman, A., Cornett, J., Whiteford, H., and Saxena, S. (2019). New WHO prevalence estimates of mental disorders in conflict settings: a systematic review and meta-analysis. *Lancet* 394, 240–248. doi: 10.1016/S0140-6736(19)30934-1

Chaudhury, D., Walsh, J. J., Friedman, A. K., Juarez, B., Ku, S. M., Koo, J. W., et al. (2013). Rapid regulation of depression-related behaviours by control of midbrain dopamine neurons. *Nature* 493, 532–536. doi: 10.1038/nature11713

Chen, J., Liu, Q., Fan, R., Han, H., Yang, Z., Cui, W., et al. (2020). Demonstration of critical role of GRIN3A in nicotine dependence through both genetic association and molecular functional studies. *Addict. Biol.* 25:e12718. doi: 10.1111/adb.12718

Consortium, C. (2015). Sparse whole-genome sequencing identifies two loci for major depressive disorder. *Nature* 523, 588–591. doi: 10.1038/nature14659

Corda, G., and Sala, A. (2017). Non-canonical WNT/PCP signalling in cancer: Fzd6 takes centre stage. *Oncogenesis* 6:e364. doi: 10.1038/oncsis.2017.69

De Marco, P., Merello, E., Rossi, A., Piatelli, G., Cama, A., Kibar, Z., et al. (2012). FZD6 is a novel gene for human neural tube defects. *Hum. Mutat.* 33, 384–390. doi: 10.1002/humu.21643

Delaneau, O., Zagury, J. F., and Marchini, J. (2013). Improved whole-chromosome phasing for disease and population genetic studies. *Nat. Methods* 10, 5–6. doi: 10.1038/nmeth.2307

Depping, M. S., Schmitgen, M. M., Kubera, K. M., and Wolf, R. C. (2018). Cerebellar Contributions to Major Depression. *Front. Psychiatr.* 9:634. doi: 10.3389/fpsyt.2018.00634

Devlin, B., and Roeder, K. (1999). Genomic control for association studies. *Biometrics* 55, 997–1004. doi: 10.1111/j.0006-341x.1999.00997.x

Direk, N., Williams, S., Smith, J. A., Ripke, S., Air, T., Amare, A. T., et al. (2017). An Analysis of Two Genome-wide Association Meta-analyses Identifies a New Locus for Broad Depression Phenotype. *Biol. Psychiatr.* 82, 322–329. doi: 10.1016/j.biopsych.2016.11.013

Duman, R. S., and Voleti, B. (2012). Signaling pathways underlying the pathophysiology and treatment of depression: novel mechanisms for rapid-acting agents. *Trends Neurosci.* 35, 47–56. doi: 10.1016/j.tins.2011.11.004

Ebmeier, K. P., Donaghey, C., and Steele, J. D. (2006). Recent developments and current controversies in depression. *Lancet* 367, 153–167. doi: 10.1016/S0140-6736(06)67964-6

Fan, R., Cui, W., Chen, J., Ma, Y., Yang, Z., Payne, T. J., et al. (2021). Gene-based association analysis reveals involvement of LAMA5 and cell adhesion pathways in nicotine dependence in African- and European-American samples. *Addict. Biol.* 26:e12898. doi: 10.1111/adb.12898

Fu, J., Wolfs, M. G., Deelen, P., Westra, H. J., Fehrmann, R. S., Te Meerman, G. J., et al. (2012). Unraveling the regulatory mechanisms underlying tissue-dependent genetic variation of gene expression. *PLoS Genet.* 8:e1002431. doi: 10.1371/journal.pgen.1002431

Golden, S. A., Covington, H. E. III, Berton, O., and Russo, S. J. (2011). A standardized protocol for repeated social defeat stress in mice. *Nat. Protoc.* 6, 1183–1191. doi: 10.1038/nprot.2011.361

Han, H., Huang, W., Du, W., Shen, Q., Yang, Z., Li, M. D., et al. (2019). Involvement of Interferon Regulatory Factor 7 in Nicotine's Suppression of Antiviral Immune Responses. *J. Neuroimmun. Pharmacol.* 14, 551–564. doi: 10.1007/s11481-019-09845-2

Hao, Y., Ge, H., Sun, M., and Gao, Y. (2019). Selecting an Appropriate Animal Model of Depression. *Int. J. Mol. Sci.* 20:4827. doi: 10.3390/ijms20194827

Harlow, S. D., Goldberg, E. L., and Comstock, G. W. (1991). A longitudinal study of risk factors for depressive symptomatology in elderly widowed and married women. *Am. J. Epidemiol.* 134, 526–538. doi: 10.1093/oxfordjournals.aje.a116125

Harris, A. Z., Atsak, P., Bretton, Z. H., Holt, E. S., Alam, R., Morton, M. P., et al. (2018). A Novel Method for Chronic Social Defeat Stress in Female Mice. *Neuropsychopharmacology* 43, 1276–1283. doi: 10.1038/npp.2017.259

Heidenreich, M., and Zhang, F. (2016). Applications of CRISPR-Cas systems in neuroscience. *Nat. Rev. Neurosci.* 17, 36–44. doi: 10.1038/nrn.2015.2

Hemming, I. A., Blake, S., Agostino, M., and Heng, J. I. (2020). General population ZBTB18 missense variants influence DNA binding and transcriptional regulation. *Hum. Mutat.* 41, 1629–1644. doi: 10.1002/humu.24069

Howard, D. M., Adams, M. J., Clarke, T. K., Hafferty, J. D., Gibson, J., Shirali, M., et al. (2019). Genome-wide meta-analysis of depression identifies 102 independent variants and highlights the importance of the prefrontal brain regions. *Nat. Neurosci.* 22, 343–352. doi: 10.1038/s41593-018-0326-7

Howie, B., Fuchsberger, C., Stephens, M., Marchini, J., and Abecasis, G. R. (2012). Fast and accurate genotype imputation in genome-wide association studies through pre-phasing. *Nat. Genet.* 44, 955–959. doi: 10.1038/ng.2354

Huang, H. C., and Klein, P. S. (2004). The Frizzled family: receptors for multiple signal transduction pathways. *Genom. Biol.* 5:234. doi: 10.1186/gb-2004-5-7-234

Hyde, C. L., Nagle, M. W., Tian, C., Chen, X., Paciga, S. A., Wendland, J. R., et al. (2016). Identification of 15 genetic loci associated with risk of major depression in individuals of European descent. *Nat. Genet.* 48, 1031–1036. doi: 10.1038/ng.3623

Ionita-Laza, I., Lee, S., Makarov, V., Buxbaum, J. D., and Lin, X. (2013). Sequence kernel association tests for the combined effect of rare and common variants. *Am. J. Hum. Genet.* 92, 841–853. doi: 10.1016/j.ajhg.2013.04.015

Jang, M. H., Kitabatake, Y., Kang, E., Jun, H., Pletnikov, M. V., Christian, K. M., et al. (2013). Secreted frizzled-related protein 3 (sFRP3) regulates antidepressant responses in mice and humans. *Mol. Psychiatr.* 18, 957–958. doi: 10.1038/mp.2012.158

Jiang, K., Yang, Z., Cui, W., Su, K., Ma, J. Z., Payne, T. J., et al. (2019). An Exome-Wide Association Study Identifies New Susceptibility Loci for Age of Smoking Initiation in African- and European-American Populations. *Nicotine Tob. Res.* 21, 707–713. doi: 10.1093/ntr/ntx262

Kato, S., Han, S. Y., Liu, W., Otsuka, K., Shibata, H., Kanamaru, R., et al. (2003). Understanding the function-structure and function-mutation relationships of p53 tumor suppressor protein by high-resolution missense mutation analysis. *Proc. Natl. Acad. Sci. U S A* 100, 8424–8429. doi: 10.1073/pnas.1431692100

Kendall, K. M., Van Assche, E., Andlauer, T. F. M., Choi, K. W., Luykx, J. J., Schulte, E. C., et al. (2021). The genetic basis of major depression. *Psychol. Med.* 51, 2217–2230. doi: 10.1017/S0033291721000441

Kendler, K. S., Gatz, M., Gardner, C. O., and Pedersen, N. L. (2006). A Swedish national twin study of lifetime major depression. *Am. J. Psychiatr.* 163, 109–114. doi: 10.1176/appi.ajp.163.1.109

Khalid, Z., and Almaghrabi, O. (2020). Mutational analysis on predicting the impact of high-risk SNPs in human secretary phospholipase A2 receptor (PLA2R1). *Sci. Rep.* 10:11750. doi: 10.1038/s41598-020-68696-7

Klausen, M. S., Jespersen, M. C., Nielsen, H., Jensen, K. K., Jurtz, V. I., Sonderby, C. K., et al. (2019). NetSurfP-2.0: improved prediction of protein structural features by integrated deep learning. *Proteins* 87, 520–527. doi: 10.1002/prot.25674

Kuchibhatla, M. N., Fillenbaum, G. G., Hybels, C. F., and Blazer, D. G. (2012). Trajectory classes of depressive symptoms in a community sample of older adults. *Acta Psychiatr. Scand.* 125, 492–501. doi: 10.1111/j.1600-0447.2011.01801.x

Li, S., Luo, H., Lou, R., Tian, C., Miao, C., Xia, L., et al. (2021). Multiregional profiling of the brain transmembrane proteome uncovers novel regulators of depression. *Sci. Adv.* 7:eabf0634. doi: 10.1126/sciadv.abf0634

Liu, X., Low, S. K., Atkins, J. R., Wu, J. Q., Reay, W. R., Cairns, H. M., et al. (2020). Wnt receptor gene FZD1 was associated with schizophrenia in genome-wide SNP analysis of the Australian Schizophrenia Research Bank cohort. *Aust. N. Z. J. Psychiatr.* 54, 902–908. doi: 10.1177/0004867419885443

Malhi, G. S., and Mann, J. J. (2018). Depression. *Lancet* 392, 2299–2312. doi: 10.1016/S0140-6736(18)31948-2

Monteggia, L. M., Luikart, B., Barrot, M., Theobold, D., Malkovska, I., Nef, S., et al. (2007). Brain-derived neurotrophic factor conditional knockouts show gender differences in depression-related behaviors. *Biol. Psychiatr.* 61, 187–197. doi: 10.1016/j.biopsych.2006.03.021

Morel, C., Montgomery, S. E., Li, L., Durand-de Cuttoli, R., Teichman, E. M., Juarez, B., et al. (2022). Midbrain projection to the basolateral amygdala encodes anxiety-like but not depression-like behaviors. *Nat. Commun.* 13:1532. doi: 10.1038/s41467-022-29155-1

Okamoto, H., Voleti, B., Banasr, M., Sarhan, M., Duric, V., Girgenti, M. J., et al. (2010). Wnt2 expression and signaling is increased by different classes of antidepressant treatments. *Biol. Psychiatr.* 68, 521–527. doi: 10.1016/j.biopsych.2010.04.023

Ormel, J., Hartman, C. A., and Snieder, H. (2019). The genetics of depression: successful genome-wide association studies introduce new challenges. *Transl. Psychiatr.* 9:114. doi: 10.1038/s41398-019-0450-5

Pickar-Oliver, A., and Gersbach, C. A. (2019). The next generation of CRISPR-Cas technologies and applications. *Nat. Rev. Mol. Cell Biol.* 20, 490–507. doi: 10.1038/s41580-019-0131-5

Pires, D. E., Ascher, D. B., and Blundell, T. L. (2014a). DUET: a server for predicting effects of mutations on protein stability using an integrated computational approach. *Nucleic Acids Res.* 42, W314–W319. doi: 10.1093/nar/gku411

Pires, D. E., Ascher, D. B., and Blundell, T. L. (2014b). mCSM: predicting the effects of mutations in proteins using graph-based signatures. *Bioinformatics* 30, 335–342. doi: 10.1093/bioinformatics/btt691

Power, R. A., Tansey, K. E., Buttenschon, H. N., Cohen-Woods, S., Bigdeli, T., Hall, L. S., et al. (2017). Genome-wide Association for Major Depression Through Age at Onset Stratification: major Depressive Disorder Working Group of the Psychiatric Genomics Consortium. *Biol. Psychiatr.* 81, 325–335. doi: 10.1016/j.biopsych.2016.05.010

Purcell, S., Neale, B., Todd-Brown, K., Thomas, L., Ferreira, M. A., Bender, D., et al. (2007). PLINK: a tool set for whole-genome association and population-based linkage analyses. *Am. J. Hum. Genet.* 81, 559–575. doi: 10.1086/519795

Radloff, L. S. (1977). The CES-D Scale:A Self-Report Depression Scale for Research in the General Population. *Appl. Psychol. Measurement* 1, 385–401. doi: 10.1177/014662167700100306

Rajasekaran, R., Sudandiradoss, C., Doss, C. G., and Sethumadhavan, R. (2007). Identification and in silico analysis of functional SNPs of the BRCA1 gene. *Genomics* 90, 447–452. doi: 10.1016/j.ygeno.2007.07.004

Sani, G., Napoletano, F., Forte, A. M., Kotzalidis, G. D., Panaccione, I., Porfiri, G. M., et al. (2012). The wnt pathway in mood disorders. *Curr. Neuropharmacol.* 10, 239–253. doi: 10.2174/157015912803217279

Schymkowitz, J., Borg, J., Stricher, F., Nys, R., Rousseau, F., and Serrano, L. (2005). The FoldX web server: an online force field. *Nucleic Acids Res.* 33, W382–W388. doi: 10.1093/nar/gki387

Shen, B., Zhang, W., Zhang, J., Zhou, J., Wang, J., Chen, L., et al. (2014). Efficient genome modification by CRISPR-Cas9 nickase with minimal off-target effects. *Nat. Methods* 11, 399–402. doi: 10.1038/nmeth.2857

Shen, C. J., Zheng, D., Li, K. X., Yang, J. M., Pan, H. Q., Yu, X. D., et al. (2019). Cannabinoid CB1 receptors in the amygdalar cholecystokinin glutamatergic afferents to nucleus accumbens modulate depressive-like behavior. *Nat. Med.* 25, 337–349. doi: 10.1038/s41591-018-0299-9

Shi, O. Y., Yang, H. Y., Shen, Y. M., Sun, W., Cai, C. Y., and Cai, C. Q. (2014). Polymorphisms in FZD3 and FZD6 genes and risk of neural tube defects in a northern Han Chinese population. *Neurol. Sci.* 35, 1701–1706. doi: 10.1007/s10072-014-1815-4

Shimajiri, Y., Sanke, T., Furuta, H., Hanabusa, T., Nakagawa, T., Fujitani, Y., et al. (2001). A missense mutation of Pax4 gene (R121W) is associated with type 2 diabetes in Japanese. *Diabetes* 50, 2864–2869. doi: 10.2337/diabetes.50.12.2864

Stuebner, S., Faus-Kessler, T., Fischer, T., Wurst, W., and Prakash, N. (2010). Fzd3 and Fzd6 deficiency results in a severe midbrain morphogenesis defect. *Dev. Dyn.* 239, 246–260. doi: 10.1002/dvdy.22127

Sullivan, P. F., de Geus, E. J., Willemsen, G., James, M. R., Smit, J. H., Zandbelt, T., et al. (2009). Genome-wide association for major depressive disorder: a possible role for the presynaptic protein piccolo. *Mol. Psychiatr.* 14, 359–375. doi: 10.1038/mp.2008.125

Sullivan, P. F., Neale, M. C., and Kendler, K. S. (2000). Genetic epidemiology of major depression: review and meta-analysis. *Am. J. Psychiatr.* 157, 1552–1562. doi: 10.1176/appi.ajp.157.10.1552

Ustun, T. B., Ayuso-Mateos, J. L., Chatterji, S., Mathers, C., and Murray, C. J. (2004). Global burden of depressive disorders in the year 2000. *Br. J. Psychiatr.* 184, 386–392. doi: 10.1192/bjp.184.5.386

van Steensel, M. A., Damstra, R. J., Heitink, M. V., Bladergroen, R. S., Veraart, J., Steijlen, P. M., et al. (2009). Novel missense mutations in the FOXC2 gene alter transcriptional activity. *Hum. Mutat.* 30, E1002–E1009. doi: 10.1002/humu.21127

Voleti, B., Tanis, K. Q., Newton, S. S., and Duman, R. S. (2012). Analysis of target genes regulated by chronic electroconvulsive therapy reveals role for Fzd6 in depression. *Biol. Psychiatr.* 71, 51–58. doi: 10.1016/j.biopsych.2011.08.004

Wang, Q., Timberlake, M. A. II, Prall, K., and Dwivedi, Y. (2017). The recent progress in animal models of depression. *Prog. Neuropsychopharmacol. Biol. Psychiatr.* 77, 99–109. doi: 10.1016/j.pnpbp.2017.04.008

Winer, J., Jung, C. K., Shackel, I., and Williams, P. M. (1999). Development and validation of real-time quantitative reverse transcriptase-polymerase chain reaction for monitoring gene expression in cardiac myocytes in vitro. *Anal. Biochem.* 270, 41–49. doi: 10.1006/abio.1999.4085

Wray, N. R., Pergadia, M. L., Blackwood, D. H., Penninx, B. W., Gordon, S. D., Nyholt, D. R., et al. (2012). Genome-wide association study of major depressive disorder: new results, meta-analysis, and lessons learned. *Mol. Psychiatr.* 17, 36–48. doi: 10.1038/mp.2010.109

Wray, N. R., Ripke, S., Mattheisen, M., Trzaskowski, M., Byrne, E. M., Abdellaoui, A., et al. (2018). Genome-wide association analyses identify 44 risk variants and refine the genetic architecture of major depression. *Nat. Genet.* 50, 668–681. doi: 10.1038/s41588-018-0090-3

Wu, J., Tang, B., and Tang, Y. (2020). Allele-specific genome targeting in the development of precision medicine. *Theranostics* 10, 3118–3137. doi: 10.7150/thno.43298

Wu, W., Yang, Y., and Lei, H. (2019). Progress in the application of CRISPR: from gene to base editing. *Med. Res. Rev.* 39, 665–683. doi: 10.1002/med.21537

Xu, Y., Cao, L., Zhao, X., Yao, Y., Liu, Q., Zhang, B., et al. (2020). Prediction of Smoking Behavior From Single Nucleotide Polymorphisms With Machine Learning Approaches. *Front. Psychiatr.* 11:416. doi: 10.3389/fpsyt.2020.00416

Yan, H. C., Cao, X., Das, M., Zhu, X. H., and Gao, T. M. (2010). Behavioral animal models of depression. *Neurosci. Bull.* 26, 327–337. doi: 10.1007/s12264-010-0323-7

Yang, J., and Li, M. D. (2016). Converging findings from linkage and association analyses on susceptibility genes for smoking and other addictions. *Mol. Psychiatr.* 21, 992–1008. doi: 10.1038/mp.2016.67

Yang, J., Si, T., Ling, Y., Ruan, Y., Han, Y., Wang, X., et al. (2003). Association study of the human FZD3 locus with schizophrenia. *Biol. Psychiatr.* 54, 1298–1301. doi: 10.1016/s0006-3223(03)00291-9

Yang, J., Wang, S., Yang, Z., Hodgkinson, C. A., Iarikova, P., Ma, J. Z., et al. (2015). The contribution of rare and common variants in 30 genes to risk nicotine dependence. *Mol. Psychiatr.* 20, 1467–1478. doi: 10.1038/mp.2014.156

Yang, Y., Cui, Y., Sang, K., Dong, Y., Ni, Z., Ma, S., et al. (2018). Ketamine blocks bursting in the lateral habenula to rapidly relieve depression. *Nature* 554, 317–322. doi: 10.1038/nature25509

Yang, Z., Nesil, T., Connaghan, K. P., Li, M. D., and Chang, S. L. (2016). Modulation Effect of HIV-1 Viral Proteins and Nicotine on Expression of the Immune-Related Genes in Brain of the HIV-1 Transgenic Rats. *J. Neuroimmun, Pharmacol.* 11, 562–571. doi: 10.1007/s11481-016-9679-4

Zhang, Y., Yu, X., Yuan, Y., Ling, Y., Ruan, Y., Si, T., et al. (2004). Positive association of the human frizzled 3 (FZD3) gene haplotype with schizophrenia in Chinese Han population. *Am. J. Med. Genet. B Neuropsychiatr. Genet.* 129B, 16–19. doi: 10.1002/ajmg.b.30076

Zhou, W. J., Xu, N., Kong, L., Sun, S. C., Xu, X. F., Jia, M. Z., et al. (2016). The antidepressant roles of Wnt2 and Wnt3 in stress-induced depression-like behaviors. *Transl. Psychiatr.* 6:e892. doi: 10.1038/tp.2016.122

Conflict of Interest: The authors declare that the research was conducted in the absence of any commercial or financial relationships that could be construed as a potential conflict of interest.

Publisher's Note: All claims expressed in this article are solely those of the authors and do not necessarily represent those of their affiliated organizations, or those of the publisher, the editors and the reviewers. Any product that may be evaluated in this article, or claim that may be made by its manufacturer, is not guaranteed or endorsed by the publisher.

frontiers | Frontiers in Molecular Neuroscience

TYPE Original Research
PUBLISHED 01 September 2022
DOI 10.3389/fnmol.2022.970031

OPEN ACCESS

EDITED BY
Melanie Grubisha,
University of Pittsburgh, United States

REVIEWED BY
Peter K. Giese,
King's College London,
United Kingdom
Kohji Fukunaga,
Tohoku University, Japan
Kim Dore,
University of California, San Diego,
United States

*CORRESPONDENCE
Hajime Fujii
hajime@m.u-tokyo.ac.jp
Haruhiko Bito
hbito@m.u-tokyo.ac.jp

†These authors have contributed equally to this work and share first authorship

SPECIALTY SECTION
This article was submitted to Brain Disease Mechanisms, a section of the journal Frontiers in Molecular Neuroscience

RECEIVED 15 June 2022
ACCEPTED 25 July 2022
PUBLISHED 01 September 2022

CITATION
Fujii H, Kidokoro H, Kondo Y, Kawaguchi M, Horigane S, Natsume J, Takemoto-Kimura S and Bito H (2022) Förster resonance energy transfer-based kinase mutation phenotyping reveals an aberrant facilitation of Ca^{2+}/calmodulin-dependent CaMKIIα activity in *de novo* mutations related to intellectual disability. *Front. Mol. Neurosci.* 15:970031. doi: 10.3389/fnmol.2022.970031

Förster resonance energy transfer-based kinase mutation phenotyping reveals an aberrant facilitation of Ca^{2+}/calmodulin-dependent CaMKIIα activity in *de novo* mutations related to intellectual disability

Hajime Fujii[1*†], Hiroyuki Kidokoro[2†], Yayoi Kondo[1], Masahiro Kawaguchi[2], Shin-ichiro Horigane[3,4], Jun Natsume[2,5], Sayaka Takemoto-Kimura[3,4] and Haruhiko Bito[1*]

[1]Department of Neurochemistry, Graduate School of Medicine, The University of Tokyo, Tokyo, Japan, [2]Department of Pediatrics, Nagoya University Graduate School of Medicine, Nagoya, Japan, [3]Department of Neuroscience I, Research Institute of Environmental Medicine (RIEM), Nagoya University, Nagoya, Japan, [4]Department of Molecular/Cellular Neuroscience, Nagoya University Graduate School of Medicine, Nagoya, Japan, [5]Department of Developmental Disability Medicine, Nagoya University Graduate School of Medicine, Nagoya, Japan

CaMKIIα plays a fundamental role in learning and memory and is a key determinant of synaptic plasticity. Its kinase activity is regulated by the binding of Ca^{2+}/CaM and by autophosphorylation that operates in an activity-dependent manner. Though many mutations in CAMK2A were linked to a variety of neurological disorders, the multiplicity of its functional substrates renders the systematic molecular phenotyping challenging. In this study, we report a new case of CAMK2A P212L, a recurrent mutation, in a patient with an intellectual disability. To quantify the effect of this mutation, we developed a FRET-based kinase phenotyping strategy and measured aberrance in Ca^{2+}/CaM-dependent activation dynamics *in vitro* and in synaptically connected neurons. CaMKIIα P212L revealed a significantly facilitated Ca^{2+}/CaM-dependent activation *in vitro*. Consistently, this mutant showed faster activation and more delayed inactivation in neurons. More prolonged kinase activation was also accompanied by a leftward shift in the CaMKIIα input frequency tuning curve. In keeping with this, molecular phenotyping of other reported CAMK2A *de novo* mutations linked to intellectual disability revealed aberrant facilitation of Ca^{2+}/CaM-dependent activation of CaMKIIα in most cases. Finally, the pharmacological reversal of CAMK2A P212L phenotype in neurons was demonstrated using an FDA-approved NMDA receptor antagonist memantine, providing a basis for targeted therapeutics in CAMK2A-linked intellectual disability. Taken together,

FRET-based kinase mutation phenotyping sheds light on the biological impact of CAMK2A mutations and provides a selective, sensitive, quantitative, and scalable strategy for gaining novel insights into the molecular etiology of intellectual disability.

KEYWORDS

CaMKII, intellectual disability, neurodevelopmental disorders, imaging, FRET, *de novo* mutation

Introduction

Intellectual disabilities (ID) are prevalent in approximately 1% of the world population, and genetic as well as environmental factors play critical roles in ID pathogenesis (Vissers et al., 2016). Recently, *de novo* mutations in a key synaptic enzyme CAMK2A (Ca^{2+}/calmodulin (CaM)- dependent protein kinase II alpha, CaMKIIα) have been shown to be associated with ID (Küry et al., 2017; Akita et al., 2018). CaMKIIα, which regulates synaptic plasticity, learning, and memory, is a protein kinase that is activated by Ca^{2+} transients caused by synaptic inputs or neuronal firing and modulates neuronal circuit properties *via* phosphorylation of key synaptic substrates leading to the up-regulation of AMPA-type glutamate receptor functions (Lisman et al., 1997, 2012; Woolfrey and Dell'Acqua, 2015; Takemoto-Kimura et al., 2017; Bayer and Schulman, 2019). Autoinhibitory domains self-inhibit their kinase activity under the baseline conditions, but are unblocked when Ca^{2+}/CaM-binding is triggered, thus transforming neuronal activity into spatiotemporal domains of biochemical signaling (Bayer and Schulman, 2019). Upon autophosphorylation at threonine 286, an autonomous activity is achieved in which the kinase remains active even after the cessation of a Ca^{2+} rise (Hudmon and Schulman, 2002). Previously, it was determined that high-frequency neuronal stimuli facilitate this autonomy state in neurons (De Koninck and Schulman, 1998; Fujii et al., 2013). Frequency-tuning of CaMKIIα integrates synaptic inputs during rapid learning and is thought to underlie the multifaceted roles of CaMKIIα in learning and memory (Bayer and Schulman, 2019; Fujii and Bito, 2022).

Relatively small disturbances in CaMKIIα expression cause significant brain dysfunction. Consistently, previous biochemical studies examining threonine 286 autophosphorylation in various ID-related *de novo* CAMK2A mutations suggested that some mutants were indeed upregulated, while others were downregulated (Küry et al., 2017; Akita et al., 2018). However, whether these mutations affected the key molecular phenotype, namely Ca^{2+}/CaM-dependent activation and frequency-tuning, of CaMKIIα have not been tested.

With a view to achieving a mechanistic understanding of ID and to begin to identify novel disease-modifying therapeutic strategies, in this study, we developed a quantitative molecular phenotyping pipeline of ID-related *de novo* CAMK2A mutations. First, we identified an ID patient with a *de novo* CAMK2A Pro212Leu (P212L) mutation. In keeping with three previously identified cases, our patient with P212L mutation had a mild clinical phenotype, showing moderate ID and autistic features, but no dysmorphic features and no seizure events. Previous *in vitro* studies, however, have failed to identify any dysregulation of CaMKIIα molecular phenotype as the heterologous expression of P212L mutant protein showed no change in protein expression or threonine 286 autophosphorylation levels (Küry et al., 2017).

To overcome this lack in molecular resolution, we built an analysis pipeline to quantitate the Ca^{2+}/CaM-dependent activation of CaMKIIα and uncover possible alteration in its frequency-tuning in neurons. We developed a Förster resonance energy transfer (FRET)-based optical molecular phenotyping system, in which we combined an optical CaMKIIα FRET sensor hK2α with multiple wavelength optical interrogation devices to analyze Ca^{2+}/CaM-dependent activation in CaMKIIα mutants related to ID.

Materials and methods

The studies involving human participants were reviewed and approved by the Ethics Committee of the Nagoya University Graduate School of Medicine. Written informed consent to participate in this study was provided by the participants' parents. All recombinant DNA and animal experiments in this study were performed in accordance with the regulations and guidelines for the care and use of experimental animals at the University of Tokyo and approved by the institutional review committees of the University of Tokyo Graduate School of Medicine.

Whole-exome sequencing

Genomic DNA was extracted from peripheral blood mononuclear cells using the QIAamp DNA Blood Mini Kit (Qiagen, Hilden, Germany). Trio-WES (patient, father, and

mother) for the patient was performed using the Sure Select Human All Exon V6 kit for capture (Agilent Technologies, Santa Clara, CA, USA) and a HiSeq2500 system (Illumina, Inc., San Diego, CA, USA) for sequencing 101-bp paired-end reads. Obtained reads were aligned to the hg19 reference genome using the Burrows–Wheeler aligner (BWA, http://bio-bwa.sourceforge.net/) with default parameters and a –mem option. Polymerase chain reaction duplicates were removed using Picard tools (http://broadinstitute.github.io/picard/). Sequence variations were detected and annotated using VarScan2 (Koboldt et al., 2012) and ANNOVA R (Wang et al., 2010), respectively. For germline variations, we removed common single-nucleotide polymorphisms (SNPs) (defined as those with >1% allele frequency) using ExAC (http://exac.broadinstitute.org/), gnomAD (https://gnomad.broadinstitute.org/), 1,000 genomes (http://www.1000genomes.org/), ESP6500 (http://evs.gs.washington.edu/EVS/), and an in-house database. A conclusive assessment of molecular variants was performed according to guidelines issued by the American College of Medical Genetics and Genomics (ACMG) (Richards et al., 2015).

Sanger sequencing of *de novo* mutation

After genome extraction, the fragment from *CAMK2A* (NG_047040.1), including the mutation site, was amplified using PrimeSTAR GXL DNA polymerase (Takara) with primers, 5'-GGTTTGCAGGGACTCCTG-3' (forward) and 5'-CTGGTCAGTCTTCATGCTC-3' (reverse). Sanger sequencing was performed using the PCR fragments with the same forward primer.

Plasmid construction

The human *CAMK2A* clone (NM_171825.2) was purchased from GenScript. To construct humanized CaMKIIα FRET probe hK2α, a fragment containing kinase, regulatory and variable linker domain of CaMKIIα, mVenus, and a fragment containing variable domain to association domain of CaMKIIα were amplified by PCR using 5′-GGACTCAGATCTCGAGCCAGGATGGCCACCATCACCTGC-3′ and 5′-CTTCACACCATCGCTCTT-3′, 5′-AGCGATGGTGTGAAGGGTGGCGTGAGCAAGGGCGAGGAG-3′ and 5′-GCTCTCTGAGGATTCGCCACCCTTGTACAGCTCGTCCAT-3′, and 5′-GAATCCTCAGAGAGCACC-3′ and 5′-TAGATCCGGTGGATCCTCAGTGGGGCAGGACGGAGGG-3′, respectively. The three fragments were assembled between XhoI and BamHI sites of pmCerulean-C1 to give pN1-hK2α. The hK2α containing *de novo* mutations was generated by quick change cite-directed mutagenesis methods. Forward and reverse primers used for each mutants were F98S: 5′-GGTGGGGAACTGTCTGAAGATATCGTG-3′ and 5′-CACGATATCTTCAGACAGTTCCCCACC-3′; E109D: 5′-GAGTATTACAGTGACGCGGATGCCAGT-3′ and 5′-ACTGGCATCCGCGTCACTGTAATACTC−3′; A112V: 5′-AGTGAGGCGGATGTCAGTCACTGTATC-3′ and 5′-GATACAGTGACTGACATCCGCCTCACT-3′; E183V: 5′-TATCTCTCCCCAGTAGTGCTGCGGAAG-3′ and 5′-CTTCCGCAGCACTACTGGGGAGAGATA-3′; P212L: 5′-GTTGGGTACCCCCTGTTCTGGGATGAG-3′ and 5′-CTCATCCCAGAACAGGGGGTACCCAAC-3′; P212Q: 5′-GTTGGGTACCCCCAGTTCTGGGATGAG-3′ and 5′-CTCATCCCAGAACTGGGGGTACCCAAC−3′; P235L: 5′-GATTTCCCATCGCTGGAATGGGACACT-3′ and 5′-AGTGTCCCATTCCAGCGATGGGAAATC-3′; H282R: 5′-GCATCCTGCATGCGCAGACAGGAGACC-3′ and 5′-GGTCTCCTGTCTGCGCATGCAGGATGC−3′; T286P: 5′-CACAGACAGGAGCCCGTGGACTGCCTG−3′; and 5′-CAGGCAGTCCACGGGCTCCTGTCTGTG−3′. Sequences of PCR-amplified region were confirmed by Sanger sequencing service (FASMAC, Japan). For the expression of cultured neurons, hK2α was subcloned under the CaMKII promoter to obtain pCaMKII-hK2α.

In vitro fluorescent plate reader

For FRET measurement in cell lysate, HEK293T cells (CRL11268, ATCC) were cultured in Dulbecco's Modified Eagle's Medium (D5796, Sigma-Aldrich) supplemented with fetal bovine serum and penicillin–streptomycin in 6-well-plates (IWAKI) and transfected with probe plasmids using XtremeGENE 9 (6365809001, Merck). Two to three days after transfection, cell lysates were collected with buffer containing 40 mM HEPES-Na, pH 8.0, 0.1 mM EGTA, 5 mM magnesium acetate, 0.01% Tween 20, sonicated using a sonicator (MICROSON ULTRASONIC CELL DISRUPTOR, XL2000-600, Misonix), and then centrifuged (TOMY, MX-300) to collect the supernatant. The protein concentration of the supernatant was determined by the Pierce BCA Protein Assay Kit (23227, Thermo Fisher Scientific) according to the manufacturer's protocol using the dilution series of pierce bovine serum albumin standard ampules, 2 mg/mL as the standard. The absorbance at 570 nm was quantified in a plate reader (IWAKI EZS-ABS Microplate Reader). To quantify the relative concentration of the probes in each sample, YFP fluorescence was measured by excitation at 510 nm and emission at 560 nm using a fluorescent plate reader (Infinite 200 PRO, Tecan).

In vitro FRET measurements were performed in 96-well-plates (PerkinElmer) and the probes were excited by 435 nm and measured by 485 nm for the CFP channel and were excited by 435 nm and measured by 535 nm for the YFP(FRET) channel, respectively. Lysate prepared from cells transfected with an empty vector was used for background subtraction. Total protein concentrations were adjusted to 70 or 80 μg/ml using the empty vector lysate, and the relative fluorescent intensities

of each mutant sample were adjusted to give similar conditions between the mutants. As expression levels of E183V and P212Q were lower compared to other mutants, E183V, P212Q, and WT were compared in separate low expression groups, and other mutants (F98S, E109D, A112V, P212L, P235L, H282R, T286P) and WT were compared in the high expression group in Figure 5. For comparison of WT, P212L, and P212Q, the probe concentrations were adjusted to that of P212Q. Measurements were started at the volume of 99 μl including the final 0.03 to 3 μM of bovine calmodulin (Millipore or FUJIFILM Wako Chemicals) or a vehicle was added, and binding reactions were initiated by the addition of 2 μl of 0.15 mM $CaCl_2$ (Nacalai Tesque, final 0.3 mM, 0.2 mM of free Ca^{2+} in the presence of 0.1 mM EGTA) and stopped by the addition of 2 μl of 0.25 mM EGTA (Nacalai Tesque). For Ca^{2+}/CaM vs. response plots, the mean FRET ratio of the last three points before the addition of EGTA was plotted against added CaM concentration.

Multiplex imaging of living neuron

Dissociated hippocampal neurons were prepared from the CA1/CA3 regions of the hippocampus of P0 Sprague–Dawley rat pups (Japan SLC) as described previously. At 9 days *in vitro*, neurons were co-transfected with plasmids encoding hK2α and R-CaMP2 under CaMKII promoter using Lipofectamine 2000 (Thermo Fisher Scientific). After 4–6 days, the neurons were subjected to live cell imaging in Mg^{2+}-free Tyrode's solution (129 mM NaCl, 5 mM KCl, 30 mM glucose, 25 mM HEPES-NaOH, pH 7.4, 2 mM $CaCl_2$; osmolality was adjusted to that of the conditioned culture medium using sucrose) supplemented with 0.5 mM MNI-glutamate (Tocris Bioscience) and 1 μM TTX (Tocris Bioscience) to prevent contamination from spontaneous and recurrent activity. For the measurement of memantine dose-response curves, 1, 10, and 100 μM memantine hydrochloride (Tokyo Chemical Industry) or vehicle (water) was added to the imaging solution. Neurons were maintained at around 37°C in a stage incubator (Tokai Hit) during all imaging sessions.

Neuronal cell bodies and dendritic spines were imaged using an inverted microscope (IX81, Olympus) equipped with an EM-CCD camera (C9100-13, Hamamatsu Photonics). UV photolysis of MNI-glutamate was performed with a 100x objective (UPlanSApo 100, NA 1.40, Olympus) and a 355-nm UV pulse laser (Polaris II, New Wave Research) that was controlled with a UV photolysis system (Hamamatsu Photonics) operated on an AQUACOSMOS software platform (Hamamatsu Photonics). Uncaging pulse rates were varied from 2.5 to 20 Hz with the use of a Master-8 pulse stimulator (A.M.P.I.). Excitation filters were FF01-438/24 (Semrock) for hK2α excitation and ET555/20× (Chroma) for R-CaMP2 excitation, and each of the probes was sequentially excited with the use of filter exchanger OSP-EXA (Olympus) equipped with a mercury lamp (Olympus, USH-103OL). The emission filter was FF01-483/32 (Semrock) for the CFP channel and a combination of long-pass BA510IF (Olympus) and multiband band-pass fluorescence filter (FF01-433/517/613; Semrock) for YFP and R-CaMP2 channels. Camera exposure time was 10 ms for both hK2α and R-CaMP2, and the data acquisition rate was about 25 Hz for neuronal soma imaging. For dendritic spine measurements, the exposure time was 100 ms and the acquisition rate was about 4 Hz. For comparison of baseline CFP/YFP ratio in the neuronal soma, neurons expressing hK2α probes were live-imaged in normal Tyrode's solution (129 mM NaCl, 5 mM KCl, 30 mM glucose, 25 mM HEPES-NaOH, pH 7.4, 2 mM $CaCl_2$, 1 mM $MgCl_2$; osmolality was adjusted to that of the conditioned culture medium using sucrose) supplemented with 1 μM TTX (Tocris Bioscience) using 10x objective (UPlanApo 10x, NA 0.40, Olympus), FF01-438/24 (Semrock) for excitation, FF01-483/32 (Semrock) for CFP emission, and FF01-542/27 (Semrock) for YFP emission. Data acquisition and ROI analysis were performed blindly in genotypes of hK2α, except for memantine pharmacology experiments where about half of the data are acquired in open-label and the remaining half of the data were collected in blind in genotypes, drugs, and concentrations. Since the results from open- and blind-label experiments were similar, data from the open and blind labels were pooled and analyzed together in memantine pharmacology in Figure 8. For kinetics comparison in Figure 3, a neuron expressing WT hK2α that showed little R-CaMP2 signal was excluded from the analysis, and CFP fluorescence intensities during the baseline period measured under the same acquisition conditions were not significantly different between WT and P212L (8,163 ± 857 for WT, $n = 19$, 6913 ± 566 for P212L, $n = 19$, $p = 0.23$, unpaired t-test), suggesting the expression levels of the measured cells were similar. For comparison of 9 mutants and WT in Figure 7, a total of 16 neurons was measured in response to 5 and 20 Hz stimulations for each mutant in a blind manner, and R-CaMP2 responses were manually checked before the opening of the labels, and those cells that showed little R-CaMP2 responses at 20 Hz (one WT, one E183V, and two H282R cells), unstable baseline (one E183V cell), or experimental human error (one T286P cell) were excluded from the analysis. Quantitative analysis of images was performed using AQUACOSMOS (Hamamatsu photonics). ROI was made in the cell body, and the cell-free area of the acquired images and the CFP, YFP, and RFP fluorescence intensities were measured at each time point. After background subtraction, the data at the time of uncaging light was contaminated, which was detected by thresholding, removed, and interpolated by linear interpolation of the previous and following frames. The rolling average was performed on the average of 5 consecutive time points.

The FRET signal was calculated by taking the CFP/YFP ratio as R and the increment ΔR (=$R-R_0$) from the pre-stimulus mean R_0 was normalized by R_0, giving a normalized FRET ratio $\Delta R/R_0$. The R-CaMP2 signal was normalized by the pre-stimulus mean fluorescence F_0, and the difference ΔF

from F_0 was divided by F_0, giving a normalized fluorescence change $\Delta F/F_0$. To compare kinetics, the maximum value of $\Delta R/R_0$ or $\Delta F/F_0$ during a period of about 20 s after stimulus onset was detected and defined as peak $\Delta R/R_0$ and peak $\Delta F/F_0$, respectively. To compare the activation kinetics, half rise time, which is the time to reach half the magnitude of peak amplitude, was calculated. Specifically, half rise time point was defined as the time from the stimulus onset to the midpoint between the first time point when the response trace exceeded half of the peak amplitude and the last time point when the response trace was under half of the peak amplitude, during the time period from stimulus onset until the peak amplitude was reached. Next, to compare the inactivation kinetics, half decay time, which is the time from peak to decay to half the peak amplitude, was calculated. Specifically, half decay time was defined as the time from the peak to the midpoint between the first time point when the response trace decayed to half of the peak amplitude and the last time point that the response trace was above half of the peak amplitude. $\Delta F/F_0$ images of hK2α and fluorescent images of R-CaMP2 in neurons were generated using Fiji. For neuronal soma, 10 average images were generated by excluding image frames containing artifacts due to uncaging, and ratiometric images were generated. The ratiometric images were normalized by dividing by the pre-stimulus R_0 images. For localization analysis in dendritic spines, mean YFP fluorescence intensities of hK2α and mean R-CaMP2 fluorescence intensities during baseline periods before application of stimulations were used as proxies for the amount of hK2α and volume, respectively. Spine enrichment index was defined as (hK2α in spine / R-CaMP2 in spine) / (hK2α in adjacent shaft / R-CaMP2 in adjacent shaft). For hK2α and R-CaMP2 response measurements, those spines that showed a large decrease in FRET probe fluorescence (detected if CFP fluorescence was <85% of baseline or YFP fluorescence was less than 85% and CFP fluorescence was less than 90% of baseline after stimulation) or dim baseline fluorescence of R-CaMP2 (detected if baseline R-CaMP2 fluorescence intensities were less than twice of their standard deviations during the baseline period) were excluded from the analysis (WT had 17 decreased and 5 dim R-CaMP2 spines, P212L had 13 decreased and 2 dim R-CaMP2 spines excluded. Remaining 41 and 51 spines from 18 and 19 neurons were analyzed for WT and P212L, respectively). Peak amplitude was defined as the maximum of hK2α and R-CaMP2 during 5 frames from the end of stimulation. To create hK2α response images for 10 s before, immediately after, and 20 s after stimulation, CFP and YFP images were Gaussian-filtered [sigma (radius) = 1 in ImageJ], and CFP/YFP ratio images were created. It was then divided by the pre-stimulus average ratio image and thresholded with a cellular mask to create $\Delta R/R_0$ images. A total of 3 frames of $\Delta R/R_0$ images were averaged and displayed. Similarly, for R-CaMP2 images, 3 frames of $\Delta F/F_0$ images were averaged and displayed. Statistical analysis was performed using Excel (Microsoft), BellCurve for Excel (Social Survey Research Information Co., Ltd.), and EZR (Kanda, 2013) (Saitama Medical Center, Jichi Medical University, Saitama, Japan), a graphical user interface for R.

Results

Identification of *de novo* P212L mutation in CAMK2A from a patient with ID and ASD

An 18-month-old Japanese girl presented to our clinic because she was unable to walk independently. She was the first child born to healthy non-consanguineous parents. She was born at the gestational age of 40 weeks with a birth weight of 3,550 g (+1.42 SD) and a birth head circumference of 34.0 cm (+0.35 SD). The family history is unremarkable. She was able to sit after age 7 months, creep after 10 months of age, and was able to stand with support at 15 months of age. She was able to speak some meaningful words.

Initial physiological and neurological examinations at 18 months of age revealed no abnormalities except for mild hypotonia. No distinctive facial features were observed. Screening blood tests, including metabolic and karyotyping, were normal.

At age 2 years, she was able to walk independently, but her speech development was delayed. Her total score on the Modified Checklist for Autism in Toddlers (M-CHAT) was 3, indicating that she was at risk for autism spectrum disorder (ASD). Brain MRI at age 2 years was normal. At age 3 years, she was able to run and speak three-word sentences. At age 4 years, inattention behavior and difficulty in controlling affection were present. At age 5 years, her parents noted difficulty with reading and writing, including the inability to read numbers, and she was asking the same questions. She was diagnosed with moderate ID as well as ASD, attention-deficit/hyperactivity disorder (ADHD), and developmental coordination disorder, according to the Tanaka-Binet test (Tanaka, 1987) and clinical interview of the Diagnostic Interview for Social and Communication Disorders (DISCO) (Wing et al., 2002).

After obtaining written informed consent for genetic testing and publication of identifying information/images in an online open-access publication, trio-based whole exome sequencing identified a *de novo* heterozygous missense variant (NM_015981: c.635C>T; p.Pro212Leu) in *CAMK2A*, which was subsequently confirmed by Sanger sequencing (Figure 1A). This variant is not listed in public SNP databases, including ExAC (http://exac.broadinstitute.org/) and the Human Genetic Variation Database (http://www.hgvd.genome.med.kyoto-u.ac.jp/). The same variant is reported to be a pathogenic variant, which leads to an ID (Küry et al., 2017).

At age 5 years, a follow-up brain MRI showed no structural or volumetric abnormalities, including

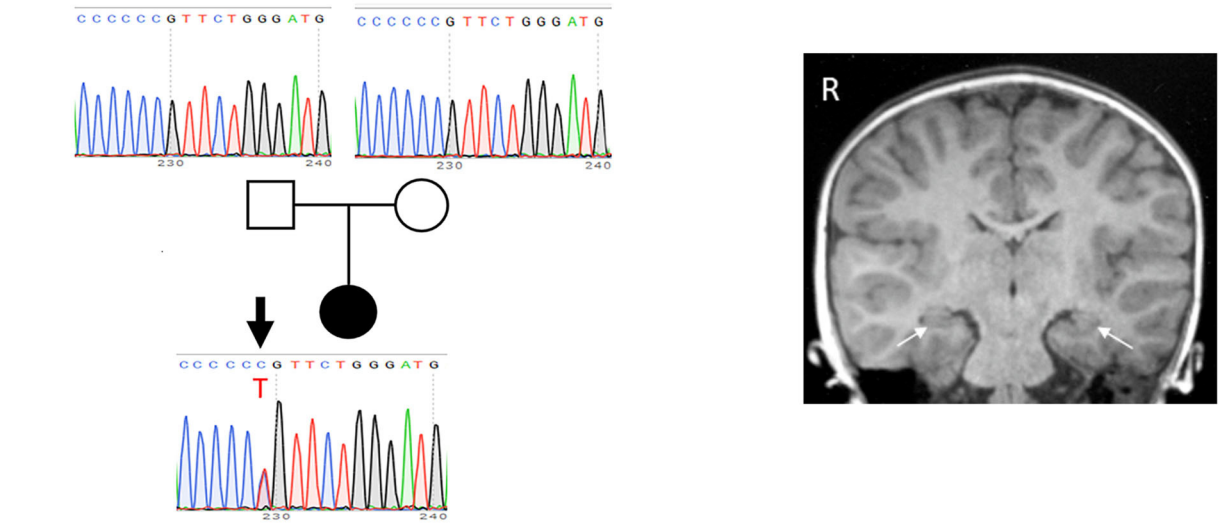

FIGURE 1
Identification of *de novo* P212L mutation in CAMK2A from a patient with ID and ASD. **(A)** The pedigree and electropherogram of the proband. Whole exome sequencing reveals a *de novo* heterozygous c.635C>T variant, which is confirmed by Sanger sequencing. **(B)** A coronal T1-weighted MR image at age 5 years shows no structural and volumetric abnormality, including hippocampi (arrows).

in the amygdalae and hippocampi (Figure 1B). Electroencephalography was normal. She had no other comorbidities such as epilepsy, infectious diseases, and visual and hearing impairments.

Development of FRET-based optical molecular phenotyping system for mutational analysis of CAMK2A

P212L mutation in a patient is the fourth report after three cases that have been reported (Küry et al., 2017), and thus it has been considered to be a recurrent *de novo* mutation in neurodevelopmental disorders. In addition, in the paralogous isoform CAMK2B, P213L mutation, which is in the same position as P212L in CAMK2A, has been found in a patient with neurodevelopmental disorders (Akita et al., 2018; Mutoh et al., 2022). These lines of clinical data strongly suggest the possibility that CAMK2A P212L mutation could alter the biochemical properties of CaMKIIα that underlie neurodevelopmental disorders. However, previous attempts had failed to reveal how P212L mutation affects biochemical properties of CaMKIIα, since protein expression levels and autophosphorylation level of threonine286 of P212L mutant under baseline conditions in heterologous cells or the migration of neuronal cells expressed with P212L mutant during cortical development were similar to those of WT (Küry et al., 2017). Although Ca^{2+}/CaM-dependent activation is one of the most fundamental properties of CaMKIIα (Hudmon and Schulman, 2002; Lisman et al., 2012; Bayer and Schulman, 2019), previous studies had not examined how P212L mutation affects Ca^{2+}/CaM-dependent activation, partly because of the lack of a sensitive, selective, quantitative, and scalable method to measure CaMKIIα activation. To meet these requirements, we took advantage of the humanized version of K2α, a FRET (Förster Resonance Energy Transfer)-based probe to monitor CaMKIIα activation that we developed previously (Fujii et al., 2013). Previously, CaMKIIα sensors that had one of the two fluorescent proteins attached to the C-terminus were developed (Takao et al., 2005; Lee et al., 2009), but to circumvent the potential folding problem (Shibata et al., 2015), K2α incorporated it in the middle of the flexible variable linker region exposed to the external surface of the holoenzyme (Fujii et al., 2013; Myers et al., 2017). Its FRET changes reported Ca^{2+}/CaM-dependent activation as well as the autophosphorylation to threonine 286 (Figure 2A) (Fujii et al., 2013), which is another hallmark of CaMKIIα activation. Furthermore, its optical readout was shown to be quantitatively correlated with a conventional biochemical readout of CaMKIIα activation, and it was able to perform quantitative pharmacological analysis using the FRET signal, providing a rationale for the quantification (Fujii et al., 2013). Therefore, we analyzed the effect of mutation by introducing a mutation into the hK2α probe and comparing its signal change upon activation with WT hK2α. We took two schemes for the mutational analysis, (1) plate reader FRET assay, in which quantitative Ca^{2+}/CaM-dependent activation

curve of hK2α was obtained using *in vitro* high-throughput fluorescent plate reader and (2) multiplexed imaging of live neuron co-expressed with hK2α and red colorfast and linear Ca^{2+} indicator R-CaMP2 (Inoue et al., 2015) in response to various patterns of local glutamate uncaging stimulations (Figure 2B).

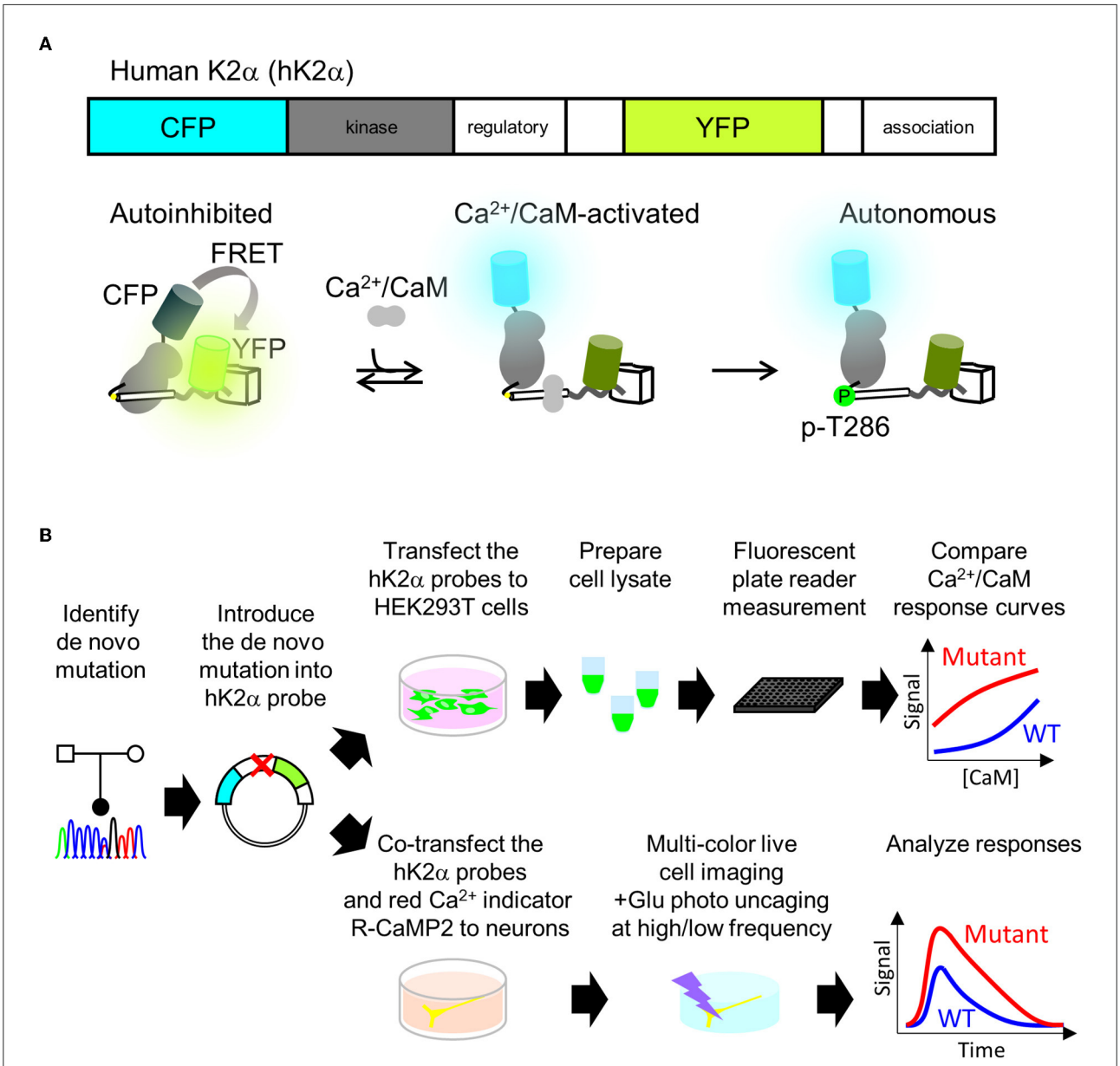

FIGURE 2
Plate reader FRET assay and multi-probe live neuron imaging analysis pipelines for analyzing *de novo* mutations in CAMK2A. **(A)** human CaMKIIα activation FRET probe hK2α. Schematics of primary structure (top) and expected conformational changes (bottom) of human CaMKIIα activation probe hK2α. Under baseline conditions, the kinase domain (gray) is autoinhibited by calmodulin-binding domain and autoinhibitory domain (white cylinder), and this conformation enhances FRET from CFP to YFP (bottom left, "autoinhibited"). Also, Ca^{2+}/CaM binding relieves the autoinhibition, and thus the FRET from CFP to YFP is decreased (bottom middle, "Ca^{2+}/CaM-activated). Subsequent autophosphorylation of threonine 286 keeps the activated conformation even after Ca^{2+}/CaM dissociates from the kinase (bottom right, "autonomous"). Only one kinase subunit in the holoenzyme is illustrated for clarity. To show that activation of CaMKIIα is indicated by increase of the ratio, in this paper, CFP/YFP ratio R or $\Delta R/R_0$, normalized change from the baseline is presented. **(B)** Mutational analysis of CAMK2A gene for kinase activation profiles using plate reader FRET assay and multi-probe live neuron imaging. Identified mutations are introduced into hK2α FRET probe plasmid. For plate reader FRET assay, WT and mutant plasmids are transfected to HEK293T cells, lysates containing the probes are prepared and subjected to plate reader fluorescence measurements under various CaM concentrations to quantitatively compare the effect of the *de novo* mutations on Ca^{2+}/CaM-dependent activation of CaMKIIα (top right). For a multi-probe live neuron imaging scheme, hK2α probes are co-transfected with red-color Ca^{2+} indicator R-CaMP2 into hippocampal dissociated cultured neurons. The transfected neurons are then subjected to multi-color live cell imaging under fluorescent microscopy to analyze responses against local glutamate uncaging delivered by various temporal patterns.

P212L mutation aberrantly facilitated Ca^{2+}/CaM-dependent CaMKIIα activation and rendered the intracellular CaMKIIα activation larger, faster and more sustained

For plate reader FRET assay, cell lysates prepared from HEK293T cells expressing hK2α were mixed with CaM, and after measurement at baseline, Ca^{2+} was added to induce Ca^{2+}/CaM-dependent activation. Both WT and P212L showed an increase in the CFP/YFP ratio (FRET ratio) upon the addition of Ca^{2+} (Figure 3A). Subsequent addition of EGTA lowered the increased FRET ratio (Figure 3A), confirming that FRET change represents Ca^{2+}/CaM-dependent activation as in the previous study (Fujii et al., 2013). By changing the concentration of added CaM, CaM dose-response curves were obtained for WT and P212L (Figures 2A,B). P212L clearly showed enhanced Ca^{2+}/CaM-dependent activation compared to WT under all the CaM concentrations examined (0, 0.03, 0.1, 0.3, 1, 3 μM). Furthermore, P212L clearly showed activation under 0.03 μM CaM, whereas WT activation occurred at 0.1 μM or higher CaM concentrations, indicating facilitated Ca^{2+}/CaM-dependent activation in P212L (Figures 3A,B).

In neurons, CaMKIIα is activated by intracellular Ca^{2+} rises through NMDAR triggered by glutamate release, and it plays important roles in synaptic plasticity, learning, and neural development (Lisman et al., 2012), and the precise regulation of CaMKIIα activity is required for normal brain functions (Fujii and Bito, 2022). As hK2α P212L was activated at low concentrations of Ca^{2+}/CaM, glutamate-input-dependent CaMKIIα activation in neurons may be enhanced by P212L mutation. To investigate this possibility, hK2α probes were transfected into hippocampal dissociated cultured neurons along with red Ca^{2+} indicator R-CaMP2 to check for Ca^{2+} rise induced by stimulation (Inoue et al., 2015). The cell bodies were stimulated by local glutamate uncaging in Mg^{2+}-free solutions in the presence of TTX, which has been used to efficiently trigger NMDAR-mediated Ca^{2+} influx and CaMKII activation (Matsuzaki et al., 2004; Lee et al., 2009; Fujii et al., 2013), as we previously demonstrated that frequency-dependency of CaMKIIα was observed in soma as well as in dendritic spines (Fujii et al., 2013). High-frequency stimulation (50 uncaging stimuli at 20 Hz), which efficiently triggers CaMKIIα activation, resulted in a fast increase in the R-CaMP2 signal, followed by a slower increase in the hK2α FRET signal (Figure 3C). The hK2α signal persisted even after the R-CaMP2 signal returned to the baseline (Figures 3C,D,H), suggesting that CaMKIIα keeps activated conformation by autonomous state and CaM trapping, consistent with the previous studies (Meyer et al., 1992; Hudmon and Schulman, 2002; Lisman et al., 2012; Fujii et al., 2013; Bayer and Schulman, 2019). Strikingly, P212L showed about ∼60% larger peak amplitude of hK2α compared to WT ($\Delta R/R_0$ of hK2α: 0.28 ± 0.039 for WT, 0.44 ± 0.038 for P212L, $p < 0.01$, unpaired *t*-test) (Figure 3E). Furthermore, hK2α activation was faster and more sustained in P212L compared to WT (Figure 3D). To quantitatively compare the kinetics, from the traces of each neuron, we calculated half-rise time, time from the start of stimulation to rise to half of the maximum amplitude, and the half-decay time, time from the peak to decay down to half of the maximum amplitude. These kinetics analyses demonstrated that P212L was activated about ∼30% faster (half rise time: 1.9 ± 0.09 s for WT and 1.5 ± 0.09 s for P212L, $p<0.01$, unpaired *t*-test) and sustained the activation about ∼50% longer time (half decay time: 7.4 ± 0.64 s for WT and 11.0 ± 1.02 s for P212L, $p < 0.01$, unpaired *t*-test) (Figures 3F,G). There were no significant differences in peak amplitude, half rise time, and half decay time of R-CaMP2 signals ($\Delta F/F_0$ of R-CaMP2: 2.0 ± 0.11 for WT, 1.9 ± 0.09 for P212L, $p = 0.77$, unpaired *t*-test; half rise time: 0.81 ± 0.08 s for WT and 0.68 ± 0.05 s for P212L, $p = 0.13$, unpaired *t*-test; half decay time: 3.0 ± 0.4 s for WT and 3.4 ± 0.4 s for P212L, $p = 0.48$, unpaired *t*-test) (Figures 3H–K). CFP/YFP baseline ratio were not significantly different between WT and P212L (0.55 ± 0.012 for WT, 0.56 ± 0.012 for P212L, $p = 0.696$, unpaired *t*-test), suggesting comparable baseline activation levels. Thus, our multi-probe imaging and quantitative analysis revealed that P212L mutation resulted in greater, faster, and more sustained CaMKIIα activation in the neurons.

Since biochemical reactions in the dendritic spine can be different from that of neuronal soma, considering the distribution of the molecules and small volumes (Kennedy et al., 2005), we compared hK2α probe localization and response in the dendritic spine. To examine localization, we compared the relative enrichment of the hK2α probe in the dendritic spine to the adjacent shaft using baseline fluorescence intensity R-CaMP2 before photo-stimulation as a proxy for volume marker (Figure 3L). hK2α showed enrichment in the dendritic spine relative to the dendritic shaft, consistent with the previous reports (Otmakhov et al., 2004; Zhang et al., 2008), but there was no significant difference between WT and P212L (1.36 ± 0.032 for WT, 1.32 ± 0.031 for P212L, $p = 0.323$, unpaired *t*-test) (Figure 3M). Next, hK2α and R-CaMP2 responses were measured against high-frequency uncaging stimuli (100 UV-uncaging stimuli delivered at 20 Hz) (Fujii et al., 2013). Consistent with the measurements in the neuronal soma, we observed that P212L showed larger responses in the stimulated dendritic spines ($\Delta R/R_0$ of hK2α: 0.12 ± 0.032 for WT, 0.28 ± 0.026 for P212L, $p < 0.001$, Kolmogorov-Smirnov test, $p < 0.001$, unpaired *t*-test) (Figures 3O,P), while R-CaMP2 showed no significant difference ($\Delta F/F_0$ of R-CaMP2: 0.62 ± 0.05 for WT, 0.66 ± 0.046 for P212L, $p = 0.95$, Kolmogorov-Smirnov test, $p = 0.52$, unpaired *t*-test) (Figures 3Q,R). Together, our results clearly demonstrated that a P212L mutation caused a facilitated CaMK2α activity, both in the soma and in the dendritic spines.

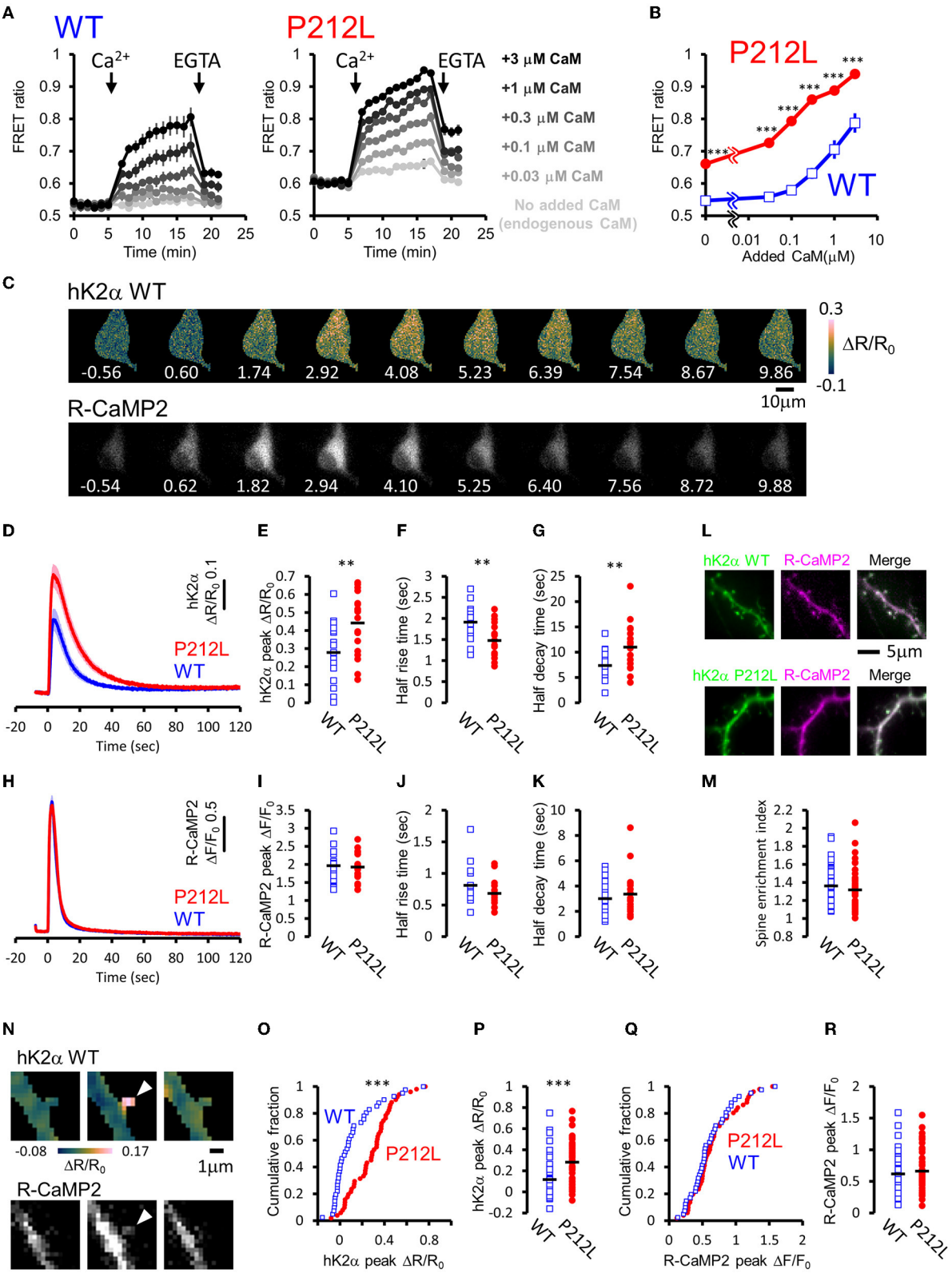

FIGURE 3
P212L mutation facilitated Ca^{2+}/CaM-dependent activation of CaMKIIα, accelerates activation and decelerates inactivation processes. **(A)** Plate reader FRET measurement of WT (left) and P212L (right) mutant of hK2α under various concentrations of added CaM. Ca^{2+} and EGTA are added
(Continued)

FIGURE 3 (Continued)
as indicated by arrows. Concentrations of added CaM are coded by the darkness of the traces, as indicated at the right. Mean ± s.e.m are shown ($n = 4$ for WT, $n = 4$ for P212L). **(B)** CaM concentration to FRET response plots for **(A)**. The mean of the last three points just before the addition of EGTA are plotted against CaM concentrations. Mean ± s.e.m are shown ($n = 4$ for each). *** $p < 0.001$ for WT vs P212L, at each CaM concentration, Tukey *post-hoc* analysis followed by ANOVA. **(C)** Representative images for multi-probe live neuron imaging. FRET ratio images of WT hK2α (top) and fluorescence images of R-CaMP2 (bottom) in response to local glutamate uncaging (50 photo-uncaging stimulations at 20 Hz) are shown. The time from the initiation of the stimulus sequence is indicated in seconds below in each image. **(D)** hK2α response traces of WT (blue) and P212L (red) against glutamate uncaging (50 stimulations at 20 Hz). Mean ± s.e.m are shown ($n = 19$ neurons for WT, $n = 19$ for P212L). **(E–G)** Comparison of hK2α response peak $\Delta R/R_0$ **(E)**, activation half rise time **(F)**, deactivation half decay time **(G)** between WT (blue open square) and P212L (red filled circle). Each plot represents data from each individual neurons, and black bar represents the mean. ** $p < 0.01$, unpaired *t*-test, $n = 19$ for WT $n = 19$ for P212L. **(H)** R-CaMP2 response traces in neurons co-transfected with hK2α WT (blue) and hK2α P212L (red) against glutamate uncaging (50 stimulations at 20 Hz). Mean ± s.e.m are shown by line and shaded areas, respectively ($n = 19$ neurons for WT, $n = 19$ for P212L). **(I–K)** Comparison of R-CaMP2 response peak amplitude **(I)**, activation half rise time **(J)**, deactivation half decay time **(K)** between neurons co-transfected with hK2α WT (blue open square) and hK2α P212L (red filled circle). Each plot represents data from each individual neuron, and the black bar represents the mean. n.s., not significant, unpaired *t*-test ($n = 19$ neurons for WT, $n = 19$ for P212L). **(L,M)** Comparison of spine enrichment of hK2α. **(L)** Representative images of hK2α (left, green), baseline R-CaMP2 (middle, magenta), and their merged images for WT (top) and P212L (bottom). **(M)** Comparison of spine enrichment ($p = 0.323$, unpaired *t*-test, $n = 41$ spines, 18 neurons for WT, $n = 51$ spines, 19 neurons for P212L). **(N–R)** Comparison of responses in dendritic spines. **(N)** Representative images for hK2α (top) and R-CaMP2 (bottom) responses ~10 seconds before the stimulation (left), immediately after the stimulation (middle), and ~20 seconds after the stimulation (right). **(O,P)** Cumulative distribution **(O)** and quantitative comparison **(P)** of hK2α responses between WT and P212L ($p < 0.001$, Kolmogorov-Smirnov test, $p < 0.001$, unpaired *t*-test, $n = 41$ spines from 18 neurons for WT, $n = 51$ spines from 19 neurons for P212L). **(Q,R)** Cumulative distribution **(Q)** and quantitative comparison **(R)** of R-CaMP2 responses between WT and P212L ($p = 0.95$, Kolmogorov-Smirnov test, $p = 0.52$, unpaired *t*-test, $n = 41$ spines from 18 neurons for WT, $n = 51$ spines from 19 neurons for P212L).

Input frequency decoding properties of CaMKIIα are tuned to lower frequencies in P212L mutant

Does the introduction of P212L only affect response amplitude and rise the decay kinetics of CaMKIIα activation? Or is it possible that there is some effect on the information processing properties of neural inputs? It has been biochemically demonstrated that CaMKIIα is activated depending on the frequency of Ca^{2+} pulses (De Koninck and Schulman, 1998) and accordingly, on the frequency of glutamate uncaging stimulation (Fujii et al., 2013). Such stimulus frequency-dependent activation of CaMKIIα may play an important role in the regulation of the induction of input frequency-dependent plasticity as well as learning and memory (Bach et al., 1995; Mayford et al., 1995; Rotenberg et al., 1996; Chang et al., 2017; Bayer and Schulman, 2019; Fujii and Bito, 2022). Since CaMKIIα activity sums up if the next input comes before the CaMKIIα activation returns to the baseline (Hanson et al., 1994; Chang et al., 2017; Bayer and Schulman, 2019), slower deactivation kinetics in P212L could possibly alter input frequency tuning of CaMKIIα. To investigate this possibility, glutamate uncaging stimulation was repeated 30 times at various frequencies (2.5, 5, 10, and 20 Hz), and multiplexed imaging of hK2α and R-CaMP2 was performed (Figures 4A–D). Consistent with the previous studies (Fujii et al., 2013), WT showed little response up to 5 Hz, but the response increased at 10 and 20 Hz, and a frequency-dependent activation response was observed (Figures 4A,B). In contrast, P212L showed lowered frequency tuning (Figures 4A,B). Although little response was observed at 2.5 Hz, 5 Hz stimulus triggered a more pronounced response compared to WT (Figures 4A,B). hK2α P212L reached nearly plateau level activation at 10 Hz (Figures 4A,B) (hK2α amplitude for WT and P212L: 2.5 Hz: 0.0061 ± 0.00082, 0.024 ± 0.016, $p = 0.63$; 5 Hz: 0.017 ± 0.0055, 0.16 ± 0.037, $p < 0.001$; 10 Hz 0.11 ± 0.025, 0.32 ± 0.036, $p < 0.001$; 20 Hz: 0.20 ± 0.029, 0.35 ± 0.028, $p < 0.001$; repeated measures ANOVA and Turkey's test, $n = 16$ for both WT and P212L). For R-CaMP2, significant dependency on the input frequency was observed in R-CaMP2 amplitude, but there was no difference between genotypes (repeated measures ANOVA, $p < 0.001$ for frequency, $p = 0.1411$ for genotype, $p = 0.1419$ for interaction). These results demonstrate that P212L mutation shifted the input tuning curve to a lower frequency and disrupted the information processing properties of the neurons.

Aberrantly facilitated Ca^{2+}/CaM-dependent activation is a prevalent molecular phenotype among CAMK2A mutants related to ID

Is the facilitated Ca^{2+}/CaM-dependent activation a molecular phenotype of CaMKIIα solely observed in P212L? Or is it a phenotype that is also prevalent in other CAMK2A mutations found in ID? To answer this question, we took advantage of the high-throughput capability of our analytical pipeline and investigated a series of CAMK2A de novo mutations (F98S, E109D, A112V, E183V, P212L, P212Q, P235L, H282R, and T286P) identified from patients with ID (Küry et al., 2017; Akita et al., 2018).

In this analysis, to adjust for total protein concentration and probe concentration between the mutants being compared, 2 mutants (E183V and P212Q) that were particularly low in expression levels were compared to WT in one group, and 7

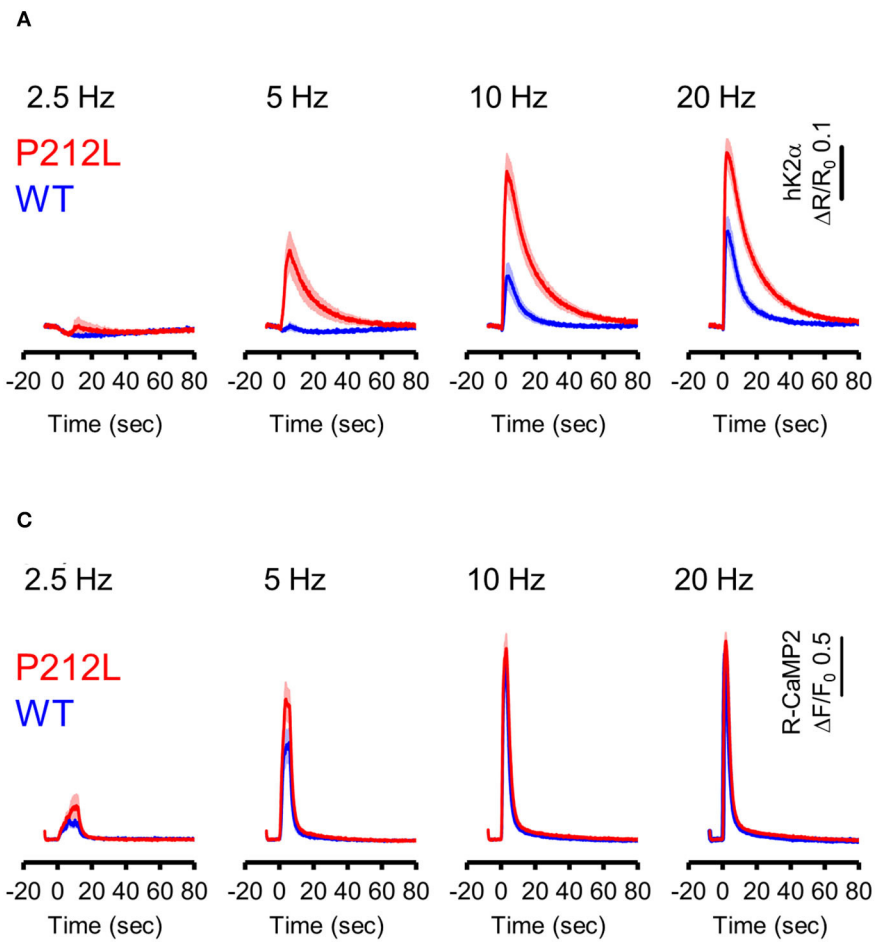

FIGURE 4
P212L mutation shifted frequency-dependent CaMKIIα activation curve toward lower stimulation frequencies. **(A)** hK2α WT (blue) or P212L (red) response traces in response to glutamate uncaging (30 stimulations at 2.5, 5, 10, 20 Hz). Mean ± s.e.m are shown, $n = 16$ for WT, $n = 16$ for P212L. **(B)** Comparison of hK2α response peak amplitude between WT (blue open square) and P212L (red filled circle). Each shaded line represents data from each individual neuron. $^{**}p < 0.01$, $^{***}p < 0.001$, WT vs. P212L, repeated measures ANOVA followed by Tukey's test, $n = 16$ for WT, $n = 16$ for P212L. **(C)** R-CaMP2 responses to 30 stimulations delivered at 2.5, 5, 10, 20 Hz in neurons co-expressed with K2α WT (blue) or P212L (red). Mean ± s.e.m are shown ($n = 16$ for WT, $n = 16$ for P212L). **(D)** Comparison of R-CaMP2 response peak amplitude between WT (blue open square) and P212L (red filled circle). Each shaded line represents data from each individual neuron. $n = 16$ for WT, $n = 16$ for P212L.

mutants (F98S, E109D, A112V, P212L, P235L, H282R, T286P) were analyzed in another group, although the WT response was almost identical between these conditions.

The results revealed three qualitatively different types. First, 6 mutants (F98S, E109D, P212L, P212Q, H282R, and T286P) showed a CaM dose-response curve similar to that of P212L and were more activated than WT, especially at low Ca^{2+}/CaM concentrations (Figures 5A–C,F,G,I,J). Next, 2 mutants (A112V, P235L) showed Ca^{2+}/CaM dose-response curves similar to WT (Figures 5A,D,H). The remaining one mutant (E183V) showed an elevated CFP/YFP ratio even in the basal state, and the modulation by Ca^{2+}/CaM concentration was small (Figure 5E). These data demonstrate that facilitated CaM-dependent activation was not P212L-specific but observed in 6 of the 9 CAMK2A *de novo* mutations related to ID.

Among the mutations analyzed, P212Q is a missense mutation that is altered at the same amino acid position as P212L. Although a small sample size precludes precise comparison, on comparing the current case with the reported case, the pathological phenotype of the patient with P212L reported here was milder compared to that of P212Q reported previously in terms of ID and the absence of seizures (Akita et al., 2018). Furthermore, autophosphorylation of threonine 286 was upregulated in P212Q, while P212L showed no significant difference (Küry et al., 2017; Akita et al., 2018). So, it can be predicted that facilitated Ca^{2+}/CaM-dependent activation is more profound in P212Q compared to P212L. To elucidate if

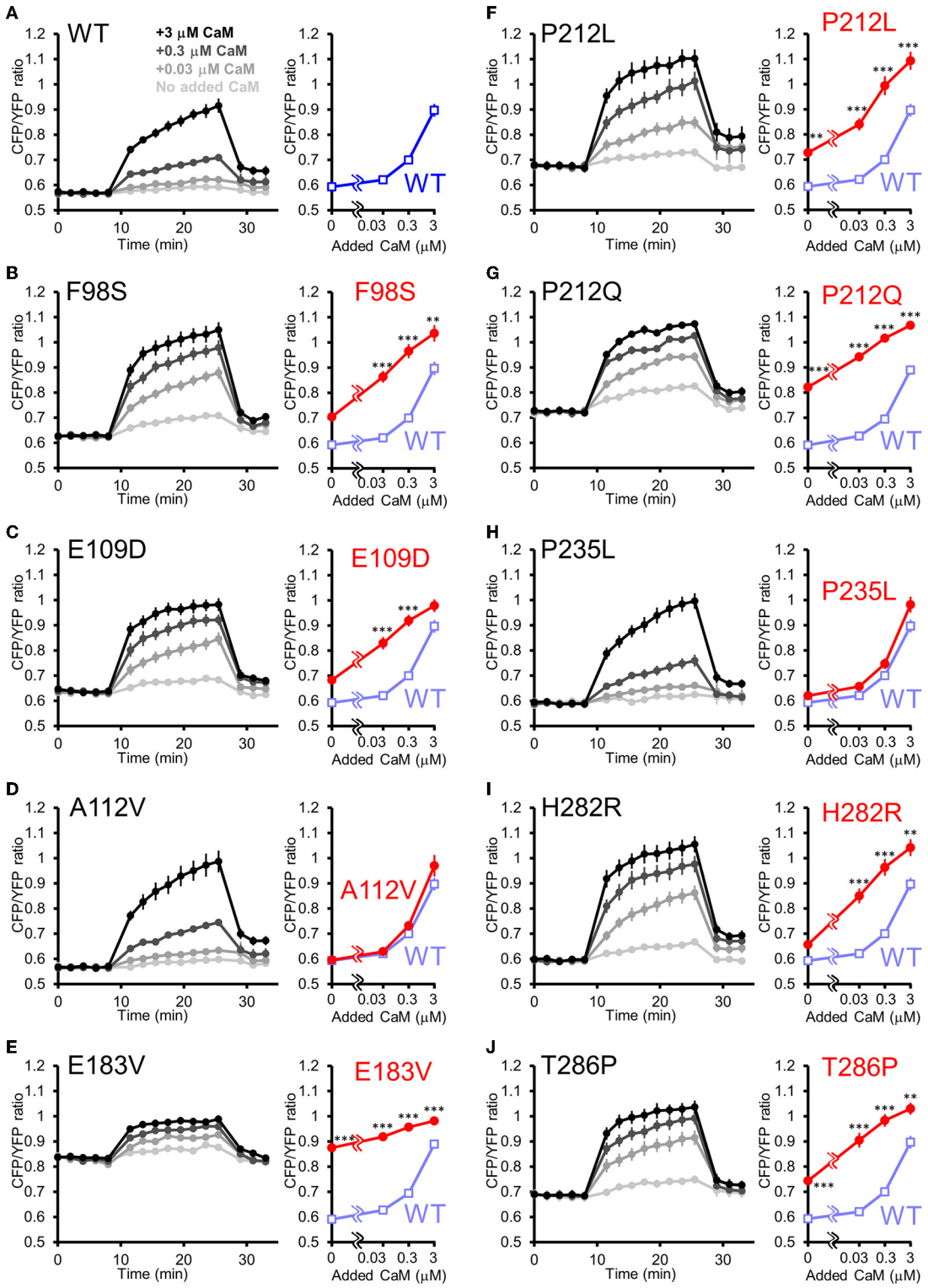

FIGURE 5
FRET plate reader analysis of effects of *de novo* mutations identified from ID on Ca^{2+}/CaM-dependent activation of CaMKIIα. **(A–J)** Plate reader FRET assay (left) and CaM dose response curves (right) for hK2α WT and *de novo* mutants stimulated by 0, 0.03, 0.3, 3 μM added CaM. To ease comparison, dose-response curves of WT (shaded blue open square) are overlayed that of each mutant [red filled circle, **(B–J)**]. Mean ± s.e.m. are indicated, two-way ANOVA followed by *post-hoc* Turkey's test $^{**}p < 0.01$, $^{***}p < 0.001$. $n = 9$ for WT, F98S, E109D, A112V, P212L, P235L, H282R and T286P and $n = 14$ for WT, E183V and P212Q.

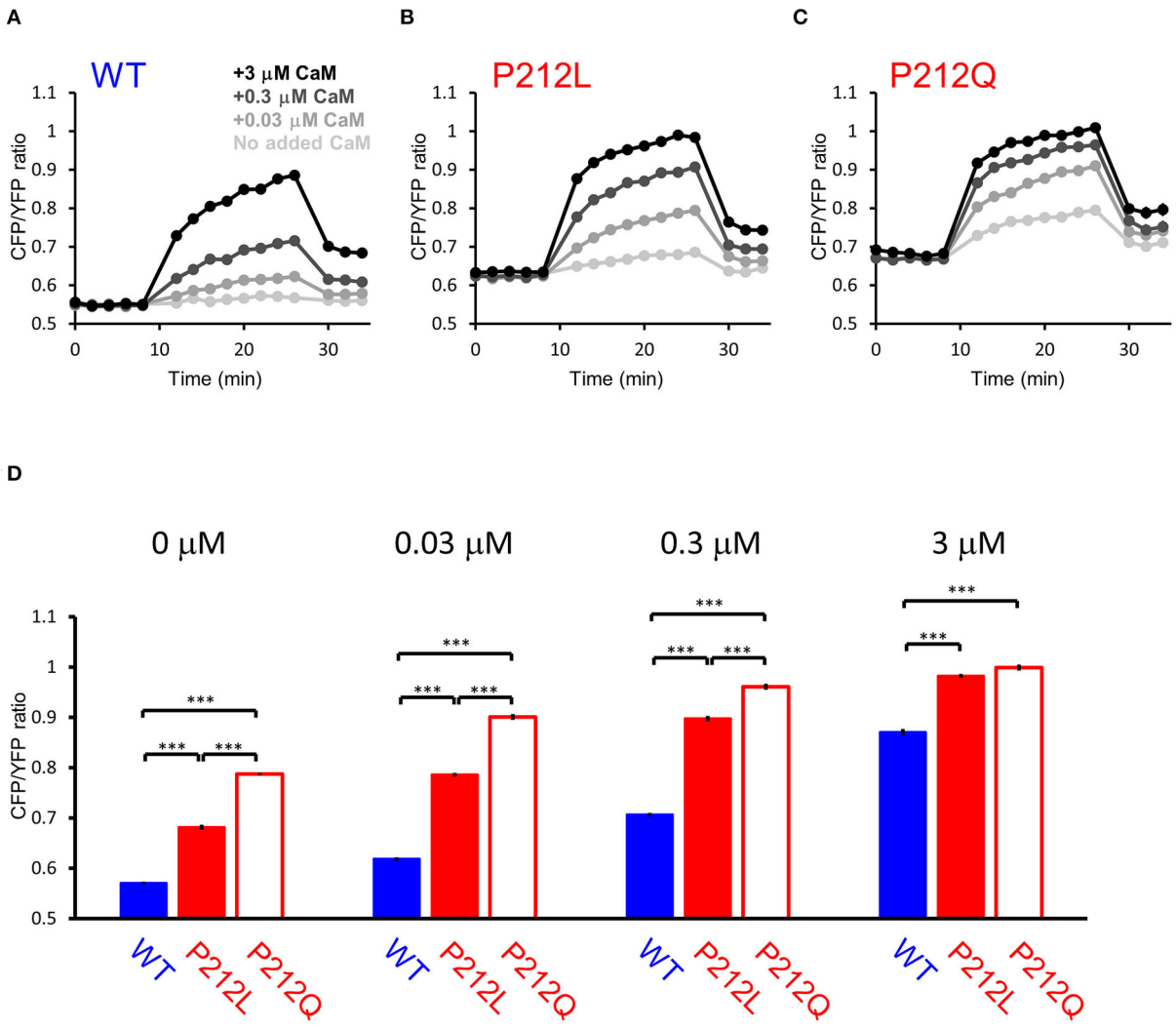

FIGURE 6
FRET plate reader analysis revealed quantitative differences in Ca^{2+}/CaM-dependent activation between WT, P212L and P212Q. Plate reader FRET assay for WT **(A)**, P212L **(B)**, P212Q **(C)**, and their CaM dose responses **(D)** under 0, 0.03, 0.3, 3 μM added CaM. Mean ± s.e.m., two-way ANOVA followed by Turkey's test. ***$p < 0.001$. $n = 18$ for each plot, except for P212L under 3 μM CaM ($n = 17$), in which one measurement showed no response, which was considered to be a procedural error of Ca^{2+} addition and excluded.

there is a quantitative difference between P212L and P212Q, we directly compared P212L, P212Q, and WT by FRET plate reader assay. The results showed that P212Q was more readily activated than P212L at low concentrations of CaM (Figure 6).

Next, to elucidate the activation profiles of the *de novo* mutants of CaMKIIα in living neurons, we performed multiplex imaging for a series of hK2α mutants and measured their responses to 30 glutamate uncaging stimulations delivered at 5 or 20 Hz (Figures 7A–J, Supplementary Figures 1, 2).

Under these conditions, R-CaMP2 peak amplitudes for E109D, H282R, and T286P were significantly lower than WT for both 5- and 20-Hz stimuli (Supplementary Figures 1, 2). A112V and P235L showed a slight but significant decrease in R-CaMP2 response against 20-Hz stimuli compared with WT (Supplementary Figure 2D). To best correct for the different Ca^{2+} levels between mutants, we took advantage of the fact that R-CaMP2 responds relatively linearly under a wide range of Ca^{2+} concentration (Inoue et al., 2015) and plotted hK2α peak amplitude against R-CaMP2 peak amplitude (Figures 7K,L). By considering a line connecting the WT plot and the origin (baseline conditions), the responses of mutants plotted above this line are considered to be enhanced, while the responses of mutants plotted below it are considered to be attenuated (Figures 7K,L, blue dash lines). Consistent with the results from FRET plate reader assays, F98S, E109D, P212L, P212Q, H282R, and T286P were plotted above these lines, P235L was almost overlayed with these lines, and E183V was plotted below these lines. A112V was unexpectedly plotted under the line, and

10.3389/fnmol.2022.970031

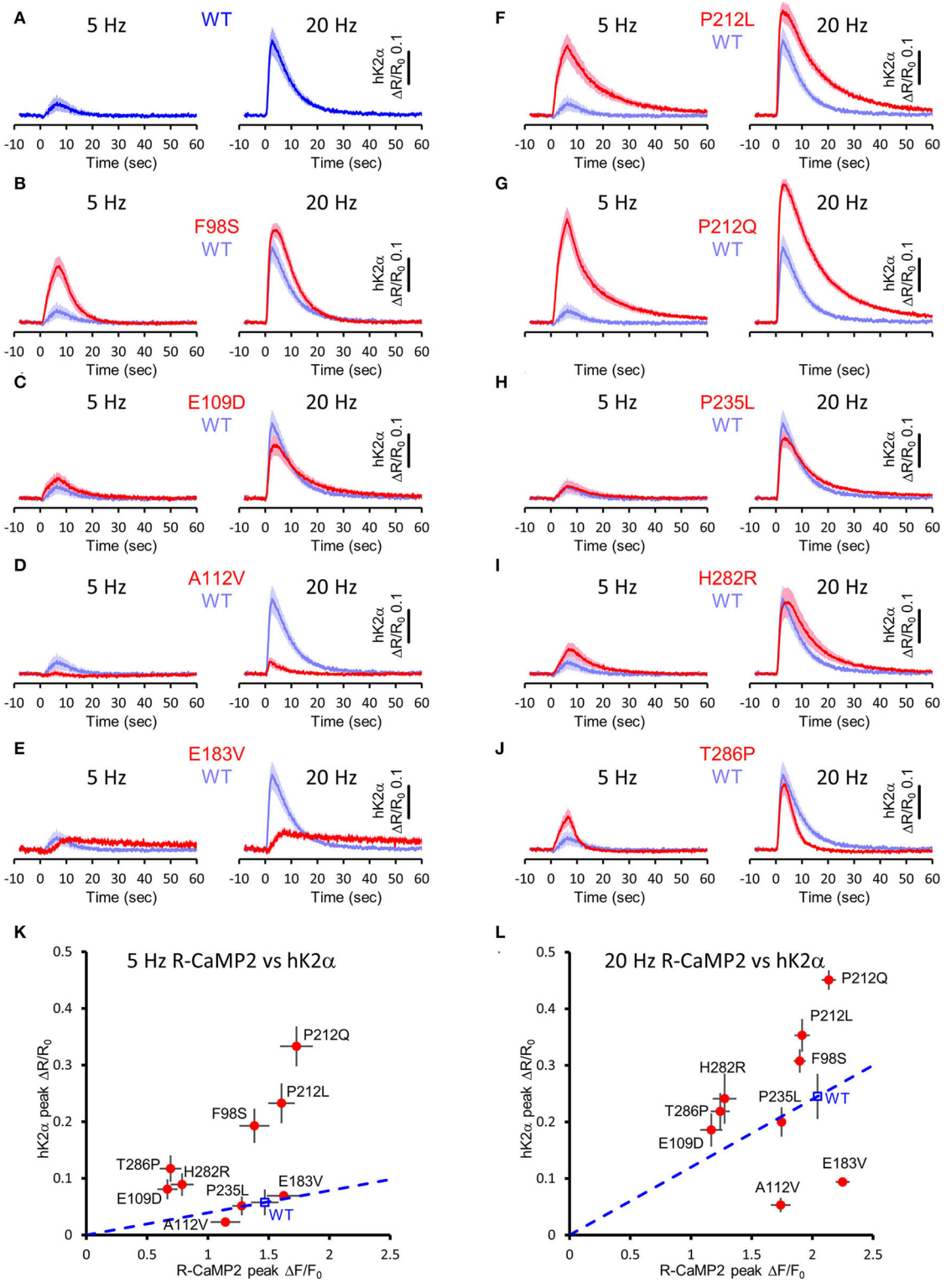

FIGURE 7
Activation profiles of CAMK2A *de novo* mutations associated with ID in living neurons. **(A–J)** hK2α activation traces in response to 30 photo-stimulations delivered at 5 Hz (left) or 20 Hz (right) To aid comparison, WT response traces (shaded blue traces) are overlayed in each mutant traces [red traces, **(B–J)**]. Mean ± s.e.m. are shown. $n = 14$ for E183V and H282R, $n = 15$ for WT, E109D, and T286P, $n = 16$ for F98S, A112V, P212L, P212Q, and P235L. **(K,L)** R-CaMP2 peak amplitude vs. hK2α peak amplitude plots. Mean ± s.e.m. are shown.

the response was significantly lower that of WT under 20 Hz stimulation, suggesting that processes other than Ca^{2+}/CaM-dependent activation could be impaired in neuronal conditions. Taken together, aberrantly facilitated Ca^{2+}/CaM-dependent CaMKIIα activation was observed in two-thirds of ID-related *de novo* CAMK2A mutations reported so far, and is considered to be the prevalent molecular phenotype in ID.

Attenuation of NMDAR signaling normalized aberrant activation of P212L

Our data suggest that pharmaceutical intervention on CaMKIIα activation is a reasonable candidate for ID caused by aberrantly facilitated Ca^{2+}/CaM-dependent CaMKIIα activation. Since there is no approved CaMKII inhibitor for clinical use (Pellicena and Schulman, 2014; Nassal et al., 2020), we attempted to target upstream NMDAR-mediated Ca^{2+} influx using memantine, an NMDAR agonist clinically used for Alzheimer's disease (Parsons et al., 2007) and well-tolerated in children (Findling et al., 2007; Bouhadoun et al., 2021). Since memantine can potentially have pharmacological effects on targets other than NMDAR (Parsons et al., 2007; Moriguchi et al., 2018), we investigated whether memantine can potentially have an inhibitory effect on P212L in cultured neuron conditions. Multiplex imaging of R-CaMP2 and hK2α was performed in response to 30 photostimulations at 20 Hz in the presence of 0, 1, 10, and 100 μM of memantine. R-CaMP2 peak amplitude was decreased in a memantine concentration-dependent manner, with the signal being reduced to about half at 10 μM and most of the responses being lost at 100 μM (0 μM: 2.1 ± 0.056, $n = 22$; 1 μM: 1.9 ± 0.064, $p = 0.56$, $n = 27$; 10 μM 1.3 ± 0.17, $p < 0.001$, $n = 23$; 100 μM: 0.26 ± 0.068, $n = 22$, $p < 0.001$, compared to 0 μM, one-way ANOVA followed by Dunnett's test) (Figure 8B), suggesting inhibition of NMDAR. Accordingly, the responses of hK2α P212L were also attenuated at 10 and 100 μM memantine (0 μM: 0.32 ± 0.030, $n = 22$; 1 μM: 0.25 ± 0.032, $p = 0.24$, $n = 27$; 10 μM 0.13 ± 0.033, $p < 0.001$, $n = 23$; 100 μM: 0.020 ± 0.0054, $p < 0.001$, $n = 22$, compared to 0 μM, one-way ANOVA followed by Dunnett's test, compared with 0 μM) (Figure 8A). Similarly, WT hK2α showed a memantine concentration-dependent suppression of R-CaMP2 and hK2α responses (Figures 8C,D). These findings suggest that memantine may be a candidate agent for an interventional approach to suppress the accelerated Ca^{2+}/CaM-dependent activation of P212L.

Discussion

In this study, we identified the P212L *de novo* mutation in a patient with ID. Previous studies have examined the effect of P212L mutation on protein expression, threonine 286 phosphorylation, and cortical neuronal cell migration during development, but the effects of this mutation on the CaMKIIα at the molecular and cellular levels were not clarified. In this study, to examine Ca^{2+}/CaM-dependent activation, which is fundamental to CaMKIIα function but had never been examined in P212L, we utilized our hK2α probe to develop a FRET-based optical molecular phenotyping system. Conventionally, Ca^{2+}/CaM-dependent CaMKII activation has been performed by kinase assays measuring the incorporation of radiolabeled phosphate into substrates (De Koninck and Schulman, 1998). However, quantifying Ca^{2+}/CaM-dependent activation using substrate-based readout can be complicated by different Ca^{2+}/CaM-dependency between substrates (Coultrap et al., 2014) and kinase regulation mediated by Ca^{2+}/CaM-dependent autophosphorylation of threonine 286, threonine 305, and threonine 306 (Cook et al., 2021), making it critical for direct readout of kinase activation state *per se*. Since hK2α probe reports activated conformation of the kinase (Fujii et al., 2013), it has the advantage of specifically detecting the activation state of the kinase without the need for the substrates, allowing for a more direct comparison of the mutations found in the kinase gene (Fujii and Bito, 2022). Thus, our FRET-based optical molecular phenotyping system provides a selective, sensitive, quantitative, and a scalable platform for the mutational analysis of the human CaMK2A gene. The platform will be applicable to other mutations in CAMK2A and CAMK2 isoforms related to various diseases (Iossifov et al., 2014; Küry et al., 2017; Akita et al., 2018; Chia et al., 2018; Brown et al., 2021; Proietti Onori and van Woerden, 2021; Mutoh et al., 2022) to reveal unappreciated molecular phenotypes in the future.

The present study clearly revealed that P212L mutation aberrantly facilitated Ca^{2+}/CaM-dependent activation. P212L is located in the kinase domain at a hydrophobic core formed with the regulatory domain, and *in silico* analysis predicted that P212L substitution destabilized the hydrophobic core and impaired the interaction between the kinase and the regulatory domains (Akita et al., 2018). Adding our findings, it could be suggested that Ca^{2+}/CaM can be more readily accessible or the regulatory domain can be more ready to release the kinase domain, which likely leads to a faster activation and a slower deactivation process in P212L.

High throughput FRET-based optical molecular phenotyping system revealed that aberrantly facilitated Ca^{2+}/CaM-dependent activation was observed not only in P212L-specific molecular phenotype, but rather it was more widespread among CAMK2A *de novo* mutations associated with ID. So far, mutations associated with ID have been found in the kinase and the regulatory domains of CaMKIIα (Küry et al., 2017; Akita et al., 2018), while mutations found in schizophrenia patients were distributed in the kinase domain and the association domain (Brown et al., 2021). Since the kinase domain and the regulatory domain are involved in Ca^{2+}/CaM-dependent activation, and the association domain is involved in dodecameric to tetradecameric holoenzyme formation, which is crucial for the regulation of autophosphorylation

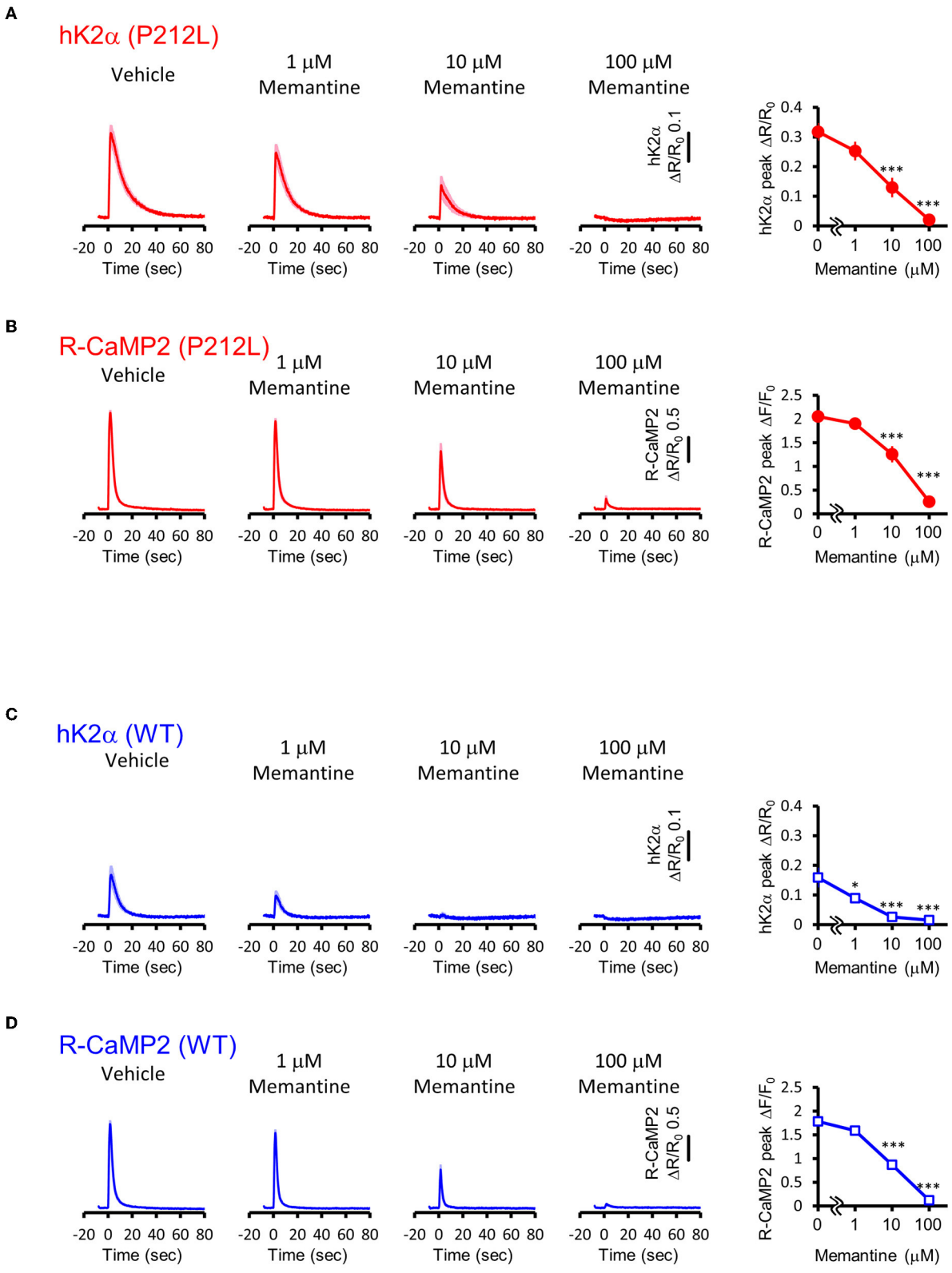

FIGURE 8
Memantine suppressed augmented activation of P212L. **(A)** Activation traces (left) and dose-response curve (right) of hK2α P212L in response to 30 photo-stimulations delivered at 20 Hz under 0, 1, 10, 100 μM memantine. $n = 22$ for 0 μM, 27 for 1 μM, 23 for 10 μM and 22 for 100 μM.
(Continued)

FIGURE 8 (Continued)
$^{***}p < 0.001$, one-way ANOVA followed by Dunnett's test. **(B)** Activation traces (left) and dose-response curve (right) of R-CaMP2 in neurons co-expressed with hK2α P212L in response to 30 photo-stimulations delivered at 20 Hz under 0, 1, 10, 100 μM Memantine. $n = 22$ for 0 μM, 27 for 1 μM, 23 for 10 μM and 22 for 100 μM. $^{***}p < 0.001$, one-way ANOVA followed by Dunnett's test. **(C)** Activation traces (left) and dose-response curve (right) of hK2α WT in response to 30 photo-stimulations delivered at 20 Hz under 0, 1, 10, 100 μM memantine. $n = 22$ for 0 μM, 22 for 1 μM, 23 for 10 μM and 23 for 100 μM. $^{*}p < 0.05$, $^{***}p < 0.001$, one-way ANOVA followed by Dunnett's test. **(D)** Activation traces (left) and dose-response curve (right) of R-CaMP2 in neurons co-expressed with hK2α WT in response to 30 photo-stimulations delivered at 20 Hz under 0, 1, 10, 100 μM Memantine. $n = 22$ for 0 μM, 22 for 1 μM, 23 for 10 μM and 23 for 100 μM. $^{***}p < 0.001$, one-way ANOVA followed by Dunnett's test.

of threonine 286 through inter-subunit reaction, it raises the possibility that distinct molecular phenotypes of CaMKIIα can be underlying different disease phenotypes, and our data supports this hypothesis.

The mechanism of how the abnormal facilitation of Ca^{2+}/CaM-dependent activation of P212L leads to the ID phenotype is currently unknown. However, in various animal models having CaMKIIα mutants with altered Ca^{2+}/CaM-dependent activation, activation kinetics and frequency tuning of CaMKIIα have been shown to correlate with abnormalities in the regulation synaptic plasticity as well as learning and memory.

In CaMKIIα T286A knock-in mice, the frequency dependence of CaMKIIα activation and synaptic plasticity was tuned toward high-frequency input (Chang et al., 2017). The T286A knock-in mice had learning deficiency and required more repetition to form memory (Giese et al., 1998; Irvine et al., 2005). Transgenic mice constitutively expressing phosphor-mimicking mutant T286D had an altered frequency-tuning curve for synaptic plasticity that favored the induction of long-term depression at 5–10 Hz stimulation (Mayford et al., 1995). The mice showed impaired spatial memory (Bach et al., 1995) and abnormal properties of hippocampal place cells firing (Rotenberg et al., 1996), suggesting that abnormal plasticity tuning may induce altered network-level properties in the brain. Furthermore, in inducible T286D transgenic mice, in which transgene expression levels could be altered by changing Dox administration during development, high T286D expression suppressed hippocampal LTP, while low T286D expression promoted LTP (Mayford et al., 1996; Bejar et al., 2002). There were correlations between T286D expression and fear conditioning or water maize performance, consistent with our hypothesis that abnormal activation of CaMKIIα drives the behavioral phenotypes. In mutants in which the inhibitory phosphorylation sites of CaMKIIα, threonine 305, and threonine 306 were mutated with alanine, the dissociation of Ca^{2+}/CaM was slower (Chang et al., 2019). In T305V/T306A mutant mice, although protein expression levels, abundant in the PSD, or threonine 286 autophosphorylation levels were comparable to the control, frequency tuning of long-term potentiation was tuned to lower frequency and flexibility in learning and the specificity of memory was reduced (Elgersma et al., 2002).

Based on these previous results and our results that P212L showed aberrantly enhanced Ca^{2+}/CaM-dependent activation and frequency-response of CaMKIIα, we speculate that P212L mutation would lead to altered frequency tuning of synaptic plasticity tuning and induce deficiencies in learning and memory. However, facilitated Ca^{2+}/CaM-dependent activation also possibly affects the level of Ca^{2+}/CaM-stimulated phosphorylation of threonine 286, the level of inhibitory phosphorylation of threonine 305 and threonine 306, and binding to NMDAR. So, it is important to investigate these properties as well as to generate a knock-in mouse model of P212L in future studies.

Some of the mutants analyzed could have molecular phenotypes other than facilitated Ca^{2+}/CaM-dependent activation. A112V mutant showed Ca^{2+}/CaM-dependent activation similar to WT in a plate reader FRET assay but showed a significantly smaller response in living neurons. This suggests the possibility that molecular processes other than Ca^{2+}/CaM-dependent activation could be disrupted in A112V, which remains to be elucidated. In E183V, although Ca^{2+}/CaM-dependent modulation was significantly smaller compared to WT, consistent with the decreased catalytic activity of E183V (Stephenson et al., 2017), the baseline FRET ratio was unexpectedly elevated. A previous study had shown that CaMKIIα introduced with E183V mutation had enhanced ubiquitination and reduced stability (Stephenson et al., 2017). Therefore, it may be possible that accelerated degradation may break down the donor and acceptor of FRET probe, or may prohibit sufficient maturation of fluorescent proteins (Liu et al., 2018), increasing the baseline FRET ratio. P235L showed no significant changes in our optical molecular phenotyping system, although multiple comparison made phenotypic detection difficult. It is necessary to clarify the molecular phenotype of these mutations by combinatorially examining other molecular properties of CaMKIIα in future studies.

Our results suggest that WT is slightly more sensitive to memantine than P212L; however the underlying mechanism is currently not well-understood. Under conditions partially inhibited by memantine (1-10 μM), the influx of Ca^{2+} is partially reduced rather than completely blocked (Figure 8) and forms a lower concentration of Ca^{2+}/CaM. Under these conditions, P212L, which can be activated at lower Ca^{2+}/CaM concentrations (Figure 3), is likely to be activated more than

WT. Furthermore, as the binding of activated CaMKIIα to GluN2B further enhances the interaction with Ca^{2+}/CaM and results in an autonomous state (Strack and Colbran, 1998; Bayer et al., 2001), these molecular processes may possibly amplify CaMKIIα activation and lead to the differences in memantine sensitivity.

WT and P212L kinase subunits are considered to form hetero dodecamers in patients having heterozygous WT and P212L CAMK2A alleles, making it difficult to selectively inhibit P212L over WT pharmacologically. Since the dose-response curve of WT/P212L for memantine would be intermediate between the WT and the P212L, 1–10 μM of memantine could potentially reduce the aberrant activation of CaMKIIα in the WT/P212L to the same degree as in the WT under vehicle conditions. In future studies, the effectiveness of this approach needs to be assessed in knock-in model mice.

Data availability statement

The whole-exome sequencing datasets presented in this study can be found in online repositories. The name of the repository and accession number can be found at: DNA Data Bank of Japan (DDBJ) Japanese Genotype-phenotype Archive (JGA), https://www.ddbj.nig.ac.jp/jga/index-e.html, JGAS000522. Other datasets that support the findings are available from the corresponding authors, HF and HB, upon reasonable request.

Ethics statement

The studies involving human participants were reviewed and approved by the Ethics Committee of the Nagoya University Graduate School of Medicine. Written informed consent to participate in this study was provided by the participants' legal guardian/next of kin. The animal study was reviewed and approved by the institutional review committees of the University of Tokyo Graduate School of Medicine.

Author contributions

HF, HK, ST-K, and HB conceived the study. HF performed plasmid construction, multiplex imaging, plate reader assays, statistical analysis, and wrote the manuscript. HK collected clinical data, assisted in data interpretation and manuscript preparation, and reviewed the manuscript. YK performed plasmid construction and plate reader assays. MK collected clinical data, assisted in data interpretation, and reviewed the manuscript. SH performed Sanger sequence. JN coordinated and supervised data collection and critically reviewed the manuscript for important intellectual content. All authors contributed to the article and approved the submitted version.

Funding

This work was supported in part by grants from Grant-in-Aid for Brain Mapping by Integrated Neurotechnologies for Disease Studies (Brain/MINDS) (JP19dm0207079 to HB), Brain Information Dynamics (BID) (JP17H06312 to HB), JSPSKAKENHI (JP17K13270 to HF, JP22H00432, and JP22H05160 to HB, and JP21H05091 to ST-K), Takeda Science Foundation (to HF and HB), Nakatani Foundation (to HB), Astellas Foundation for Research on Metabolic Disorders (to HF), Hitachi Global Foundation (to HB), and the Toray Science Foundation (ST-K).

Acknowledgments

We thank the following researchers for kindly sharing their reagents: A. Miyawaki and T. Nagai (Venus). We also thank the members of the HB laboratory for their support and discussion. We also thank the Tokai regional branch of the Initiative on Rare and Undiagnosed Diseases (TOKAI-IRUD). More importantly, we are grateful to the patient and their families for participating in this study.

Conflict of interest

The authors declare that the research was conducted in the absence of any commercial or financial relationships that could be construed as a potential conflict of interest.

Publisher's note

Supplementary material

The Supplementary Material for this article can be found online at: https://www.frontiersin.org/articles/10.3389/fnmol.2022.970031/full#supplementary-material

SUPPLEMENTARY FIGURE 1
R-CaMP2 Responses in Living Neurons co-Expressing hK2α Mutants Associated With ID. **(A–J)** R-CaMP2 activation kinetics in response to 30 photo-stimulations delivered at 5 Hz (left) and 20 Hz (right) To aid comparison, response curve of R-CaMP2 co-expressed with hK2α WT are overlayed (shaded blue traces) in each mutant data [red traces, **(B–J)**]. Mean ± s.e.m. are shown. $n = 14$ for E183V and H282R, $n = 15$ for WT, E109D, and T286P, $n = 16$ for F98S, A112V, P212L, P212Q, and P235L.

SUPPLEMENTARY FIGURE 2
Comparison of hK2α and R-CaMP2 responses. **(A–D)** Peak amplitude of hK2α and R-CaMP2 responses in response to photo-stimulations delivered at 5 Hz **(A,B)** or 20 Hz **(C,D)**. Each dot plots represent data from each neuron and black bar represents mean. $^{*}p < 0.05$, $^{**}p < 0.01$, $^{***}p < 0.001$, one-way ANOVA followed by Dunnett's test compared with WT. $n = 14$ for E183V and H282R, $n = 15$ for WT, E109D, and T286P, $n = 16$ for F98S, A112V, P212L, P212Q, and P235L.

References

Akita, T., Aoto, K., Kato, M., Shiina, M., Mutoh, H., Nakashima, M., et al. (2018). *De novo* variants in CAMK2A and CAMK2B cause neurodevelopmental disorders. *Ann. Clin. Transl. Neurol.* 5, 280–296. doi: 10.1002/acn3.528

Bach, M. E., Hawkins, R. D., Osman, M., Kandel, E. R., and Mayford, M. (1995). Impairment of spatial but not contextual memory in CaMKII mutant mice with a selective loss of hippocampal LTP in the range of the theta frequency. *Cell* 81, 905–915. doi: 10.1016/0092-8674(95)90010-1

Bayer, K. U., De Koninck, P., Leonard, A. S., Hell, J. W., and Schulman, H. (2001). Interaction with the NMDA receptor locks CaMKII in an active conformation. *Nature* 411, 801–805. doi: 10.1038/35081080

Bayer, K. U., and Schulman, H. (2019). CaM kinase: still inspiring at 40. *Neuron* 103, 380–394. doi: 10.1016/j.neuron.2019.05.033

Bejar, R., Yasuda, R., Krugers, H., Hood, K., and Mayford, M. (2002). Transgenic calmodulin-dependent protein kinase II activation: dose-dependent effects on synaptic plasticity, learning, and memory. *J. Neurosci.* 22, 5719–5726. doi: 10.1523/JNEUROSCI.22-13-05719.2002

Bouhadoun, S., Poulin, C., Berrahmoune, S., and Myers, K. A. (2021). A retrospective analysis of memantine use in a pediatric neurology clinic. *Brain Dev.* 43, 997–1003. doi: 10.1016/j.braindev.2021.05.012

Brown, C. N., Cook, S. G., Allen, H. F., Crosby, K. C., Singh, T., Coultrap, S. J., et al. (2021). Characterization of six CaMKIIα variants found in patients with schizophrenia. *iScience*. 24, 103184. doi: 10.1016/j.isci.2021.103184

Chang, J. Y., Nakahata, Y., Hayano, Y., and Yasuda, R. (2019). Mechanisms of Ca2+/calmodulin-dependent kinase II activation in single dendritic spines. *Nat. Commun.* 10, 2784. doi: 10.1038/s41467-019-10694-z

Chang, J. Y., Parra-Bueno, P., Laviv, T., Szatmari, E. M., Lee, S. R., and Yasuda, R. (2017). CaMKII autophosphorylation is necessary for optimal integration of Ca2+ signals during LTP induction, but not maintenance. *Neuron*. 94, 800–808.e4. doi: 10.1016/j.neuron.2017.04.041

Chia, P. H., Zhong, F. L., Niwa, S., Bonnard, C., Utami, K. H., Zeng, R., et al. (2018). A homozygous loss-of-function CAMK2A mutation causes growth delay, frequent seizures and severe intellectual disability. *Elife* 7, e32451. doi: 10.7554/eLife.32451

Cook, S. G., Buonarati, O. R., Coultrap, S. J., and Bayer, K. U. (2021). CaMKII holoenzyme mechanisms that govern the LTP versus LTD decision. *Sci Adv.* 7, eabe2300. doi: 10.1126/sciadv.abe2300

Coultrap, S. J., Freund, R. K., O'Leary, H., Sanderson, J. L., Roche, K. W., Dell'Acqua, M. L., et al. (2014). Autonomous CaMKII mediates both LTP and LTD using a mechanism for differential substrate site selection. *Cell Rep.* 6, 431–437. doi: 10.1016/j.celrep.2014.01.005

De Koninck, P., and Schulman, H. (1998). Sensitivity of CaM kinase II to the frequency of Ca2+ oscillations. *Science* 279, 227–230. doi: 10.1126/science.279.5348.227

Elgersma, Y., Fedorov, N. B., Ikonen, S., Choi, E. S., Elgersma, M., Carvalho, O. M., et al. (2002). Inhibitory autophosphorylation of CaMKII controls PSD association, plasticity, and learning. *Neuron* 36, 493–505. doi: 10.1016/S0896-6273(02)01007-3

Findling, R. L., McNamara, N. K., Stansbrey, R. J., Maxhimer, R., Periclou, A., Mann, A., et al. (2007). A pilot evaluation of the safety, tolerability, pharmacokinetics, and effectiveness of memantine in pediatric patients with attention-deficit/hyperactivity disorder combined type. *J. Child Adolesc. Psychopharmacol.* 17, 19–33. doi: 10.1089/cap.2006.0044

Fujii, H., and Bito, H. (2022). Deciphering Ca2+-controlled biochemical computation governing neural circuit dynamics via multiplex imaging. *Neurosci Res.* 179, 79–90. doi: 10.1016/j.neures.2022.04.004

Fujii, H., Inoue, M., Okuno, H., Sano, Y., Takemoto-Kimura, S., Kitamura, K., et al. (2013). Nonlinear decoding and asymmetric representation of neuronal input information by CaMKIIα and calcineurin. *Cell Rep.* 3, 978–987. doi: 10.1016/j.celrep.2013.03.033

Giese, K. P., Fedorov, N. B., Filipkowski, R. K., and Silva, A. J. (1998). Autophosphorylation at Thr286 of the alpha calcium-calmodulin kinase II in LTP and learning. *Science* 279, 870–873. doi: 10.1126/science.279.5352.870

Hanson, P. I., Meyer, T., Stryer, L., and Schulman, H. (1994). Dual role of calmodulin in autophosphorylation of multifunctional CaM kinase may underlie decoding of calcium signals. *Neuron* 12, 943–956. doi: 10.1016/0896-6273(94)90306-9

Hudmon, A., and Schulman, H. (2002). Neuronal CA2+/calmodulin-dependent protein kinase II: the role of structure and autoregulation in cellular function. *Annu. Rev. Biochem.* 71, 473–510. doi: 10.1146/annurev.biochem.71.110601.135410

Inoue, M., Takeuchi, A., Horigane, S., Ohkura, M., Gengyo-Ando, K., Fujii, H., et al. (2015). Rational design of a high-affinity, fast, red calcium indicator R-CaMP2. *Nat. Methods*. 12, 64–70. doi: 10.1038/nmeth.3185

Iossifov, I., O'Roak, B. J., Sanders, S. J., Ronemus, M., Krumm, N., Levy, D., et al. (2014). The contribution of de novo coding mutations to autism spectrum disorder. *Nature* 515, 216–221. doi: 10.1038/nature13908

Irvine, E. E., Vernon, J., and Giese, K. P. (2005). AlphaCaMKII autophosphorylation contributes to rapid learning but is not necessary for memory. *Nat. Neurosci.* 8, 411–412. doi: 10.1038/nn1431

Kanda, Y. (2013). Investigation of the freely available easy-to-use software 'EZR' for medical statistics. *Bone Marrow Transplant.* 48, 452–458. doi: 10.1038/bmt.2012.244

Kennedy, M. B., Beale, H. C., Carlisle, H. J., and Washburn, L. R. (2005). Integration of biochemical signalling in spines. *Nat. Rev. Neurosci.* 6, 423–434. doi: 10.1038/nrn1685

Koboldt, D. C., Zhang, Q., Larson, D. E., Shen, D., McLellan, M. D., Lin, L., et al. (2012). VarScan 2: somatic mutation and copy number alteration discovery in cancer by exome sequencing. *Genome Res.* 22, 568–576. doi: 10.1101/gr.129684.111

Küry, S., van Woerden, G. M., Besnard, T., Proietti Onori, M., Latypova, X., Towne, M. C., et al. (2017). *De novo* mutations in protein kinase genes CAMK2A and CAMK2B cause intellectual disability. *Am. J. Hum. Genet.* 101, 768–788. doi: 10.1016/j.ajhg.2017.10.003

Lee, S. J., Escobedo-Lozoya, Y., Szatmari, E. M., and Yasuda, R. (2009). Activation of CaMKII in single dendritic spines during long-term potentiation. *Nature* 458, 299–304. doi: 10.1038/nature07842

Lisman, J., Malenka, R. C., Nicoll, R. A., and Malinow, R. (1997). Learning mechanisms: the case for CaMKII. *Science* 276, 2001–2002. doi: 10.1126/science.276.5321.2001

Lisman, J., Yasuda, R., and Raghavachari, S. (2012). Mechanisms of CaMKII action in long-term potentiation. *Nat. Rev. Neurosci.* 13, 169–182. doi: 10.1038/nrn3192

Liu, B., Mavrova, S. N., van den Berg, J., Kristensen, S. K., Mantovanelli, L., Veenhoff, L. M., et al. (2018). Influence of fluorescent protein maturation on FRET measurements in living cells. *ACS Sens.* 3, 1735–1742. doi: 10.1021/acssensors.8b00473

Matsuzaki, M., Honkura, N., Ellis-Davies, G. C., and Kasai, H. (2004). Structural basis of long-term potentiation in single dendritic spines. *Nature* 429, 761–766. doi: 10.1038/nature02617

Mayford, M., Bach, M. E., Huang, Y. Y., Wang, L., Hawkins, R. D., and Kandel, E. R. (1996). Control of memory formation through regulated expression of a CaMKII transgene. *Science* 274, 1678–1683. doi: 10.1126/science.274.5293.1678

Mayford, M., Wang, J., Kandel, E. R., and O'Dell, T. J. (1995). CaMKII regulates the frequency-response function of hippocampal synapses for the production of both LTD and LTP. *Cell* 81, 891–904. doi: 10.1016/0092-8674(95)90009-8

Meyer, T., Hanson, P. I., Stryer, L., and Schulman, H. (1992). Calmodulin trapping by calcium-calmodulin-dependent protein kinase. *Science* 256, 1199–1202. doi: 10.1126/science.256.5060.1199

Moriguchi, S., Ishizuka, T., Yabuki, Y., Shioda, N., Sasaki, Y., Tagashira, H., et al. (2018). Blockade of the KATP channel Kir6.2 by memantine represents a novel mechanism relevant to Alzheimer's disease therapy. *Mol. Psychiatry*. 23, 211–221. doi: 10.1038/mp.2016.187

Mutoh, H., Aoto, K., Miyazaki, T., Fukuda, A., and Saitsu, H. (2022). Elucidation of pathological mechanism caused by human disease mutation in CaMKIIβ. *J. Neurosci. Res.* 100, 880–896. doi: 10.1002/jnr.25013

Myers, J. B., Zaegel, V., Coultrap, S. J., Miller, A. P., Bayer, K. U., and Reichow, S. L. (2017). The CaMKII holoenzyme structure in activation-competent conformations. *Nat. Commun.* 8, 15742. doi: 10.1038/ncomms15742

Nassal, D., Gratz, D., and Hund, T. J. (2020). Challenges and opportunities for therapeutic targeting of calmodulin kinase II in heart. *Front. Pharmacol.* 11, 35. doi: 10.3389/fphar.2020.00035

Otmakhov, N., Tao-Cheng, J. H., Carpenter, S., Asrican, B., Dosemeci, A., Reese, T. S., et al. (2004). Persistent accumulation of calcium/calmodulin-dependent protein kinase II in dendritic spines after induction of NMDA receptor-dependent chemical long-term potentiation. *J. Neurosci.* 24, 9324–9331. doi: 10.1523/JNEUROSCI.2350-04.2004

Parsons, C. G., Stöffler, A., and Danysz, W. (2007). Memantine: a NMDA receptor antagonist that improves memory by restoration of homeostasis in the glutamatergic system–too little activation is bad, too much is even worse. *Neuropharmacology* 53, 699–723. doi: 10.1016/j.neuropharm.2007.07.013

Pellicena, P., and Schulman, H. (2014). CaMKII inhibitors: from research tools to therapeutic agents. *Front. Pharmacol.* 5, 21. doi: 10.3389/fphar.2014.00021

Proietti Onori, M., and van Woerden, G. M. (2021). Role of calcium/calmodulin-dependent kinase 2 in neurodevelopmental disorders. *Brain Res. Bull.* 171, 209–220. doi: 10.1016/j.brainresbull.2021.03.014

Richards, S., Aziz, N., Bale, S., Bick, D., Das, S., Gastier-Foster, J., et al. (2015). Standards and guidelines for the interpretation of sequence variants: a joint consensus recommendation of the American college of medical genetics and genomics and the association for molecular pathology. *Genet. Med.* 17, 405–424. doi: 10.1038/gim.2015.30

Rotenberg, A., Mayford, M., Hawkins, R. D., Kandel, E. R., and Muller, R. U. (1996). Mice expressing activated CaMKII lack low frequency LTP and do not form stable place cells in the CA1 region of the hippocampus. *Cell.* 87, 1351–1361. doi: 10.1016/S0092-8674(00)81829-2

Shibata, A. C., Maebashi, H. K., Nakahata, Y., Nabekura, J., and Murakoshi, H. (2015). Development of a molecularly evolved, highly sensitive CaMKII FRET sensor with improved expression pattern. *PLoS ONE.* 10, e0121109. doi: 10.1371/journal.pone.0121109

Stephenson, J. R., Wang, X., Perfitt, T. L., Parrish, W. P., Shonesy, B. C., Marks, C. R., et al. (2017). A novel human CAMK2A mutation disrupts dendritic morphology and synaptic transmission, and causes ASD-related behaviors. *J. Neurosci.* 37, 2216–2233. doi: 10.1523/JNEUROSCI.2068-16.2017

Strack, S., and Colbran, R. J. (1998). Autophosphorylation-dependent targeting of calcium/ calmodulin-dependent protein kinase II by the NR2B subunit of the N-methyl- D-aspartate receptor. *J. Biol. Chem.* 273, 20689–20692. doi: 10.1074/jbc.273.33.20689

Takao, K., Okamoto, K., Nakagawa, T., Neve, R. L., Nagai, T., Miyawaki, A., et al. (2005). Visualization of synaptic Ca2+ /calmodulin-dependent protein kinase II activity in living neurons. *J. Neurosci.* 25, 3107–3112. doi: 10.1523/JNEUROSCI.0085-05.2005

Takemoto-Kimura, S., Suzuki, K., Horigane, S. I., Kamijo, S., Inoue, M., Sakamoto, M., et al. (2017). Calmodulin kinases: essential regulators in health and disease. *J. Neurochem.* 141, 808–818. doi: 10.1111/jnc.14020

Tanaka, H. (1987). *Tanaka-Binet Scale of Intelligence*. Tokyo: Taken Shuppan.

Vissers, L. E., Gilissen, C., and Veltman, J. A. (2016). Genetic studies in intellectual disability and related disorders. *Nat. Rev. Genet.* 17, 9–18. doi: 10.1038/nrg3999

Wang, K., Li, M., and Hakonarson, H. (2010). ANNOVAR: functional annotation of genetic variants from high-throughput sequencing data. *Nucleic Acids Res.* 38, e164. doi: 10.1093/nar/gkq603

Wing, L., Leekam, S. R., Libby, S. J., Gould, J., and Larcombe, M. (2002). The diagnostic interview for social and communication disorders: background, inter-rater reliability and clinical use. *J. Child Psychol. Psychiatry.* 43, 307–325. doi: 10.1111/1469-7610.00023

Woolfrey, K. M., and Dell'Acqua, M. L. (2015). Coordination of protein phosphorylation and dephosphorylation in synaptic plasticity. *J. Biol. Chem.* 290, 28604–28612. doi: 10.1074/jbc.R115.657262

Zhang, Y. P., Holbro, N., and Oertner, T. G. (2008). Optical induction of plasticity at single synapses reveals input-specific accumulation of alphaCaMKII. *Proc. Natl. Acad. Sci. USA*. 105, 12039–12044. doi: 10.1073/pnas.0802940105

frontiers | Frontiers in Molecular Neuroscience

TYPE Original Research
PUBLISHED 13 September 2022
DOI 10.3389/fnmol.2022.927357

OPEN ACCESS

EDITED BY
Melanie Grubisha,
University of Pittsburgh, United States

REVIEWED BY
Francisco Javier del Castillo,
Ramón y Cajal University Hospital, Spain
Christoph Wiegreffe,
University of Ulm, Germany

*CORRESPONDENCE
Ying Yang
yying1930@163.com

SPECIALTY SECTION
This article was submitted to Brain Disease Mechanisms, a section of the journal Frontiers in Molecular Neuroscience

RECEIVED 24 April 2022
ACCEPTED 22 August 2022
PUBLISHED 13 September 2022

CITATION
Che F, Tie X, Lei H, Zhang X, Duan M, Zhang L and Yang Y (2022) Identification of two novel variants of the *BCL11B* gene in two Chinese pedigrees associated with neurodevelopmental disorders. *Front. Mol. Neurosci.* 15:927357. doi: 10.3389/fnmol.2022.927357

Identification of two novel variants of the *BCL11B* gene in two Chinese pedigrees associated with neurodevelopmental disorders

Fengyu Che[1], Xiaoling Tie[2], Hong Lei[1], Xi Zhang[1], Mingyue Duan[1], Liyu Zhang[1] and Ying Yang[1]*

[1]Shaanxi Institute for Pediatric Diseases, Xi'an Children's Hospital, Xi'an, China, [2]Department of Rehabilitation, Xi'an Children's Hospital, Xi'an, China

Objective: According to a recent report, the mutation of transcription factor gene *BCL11B* is associated with the development of neurodevelopmental disorders and immune deficiency. By analyzing both clinical features and genetic variations, this study aims to reveal the genetic etiology of four patients with neurodevelopmental disorders from two unrelated Chinese pedigrees.

Methods: From the 4 cases, the clinical data were collected. The potential pathogenic gene variations were analyzed by means of based-trio whole exome sequencing (Trio-WES) and then validated through Sanger sequencing in their respective pedigrees. Furthermore, both the *in vitro* minigene assay and the NMD assay were performed to evaluate the impact of splicing and frameshift variants.

Results: The 4 patients displayed mild-to-severe intellectual developmental disorder, which was accompanied by speech delay, dysmorphic facies, and serious caries. In addition, the extended phenotype of developmental regression was observed in the proband from Family 1, which has been unreported previously. Molecular analysis was conducted to identify two novel heterozygous variants in the *BCL11B* gene: a maternal splicing variant c.427 + 1G > A in Family 1 and a *de novo* frameshift variant c.2461_2462insGAGCCACACCGGCG (p.Glu821Glyfs*28) in Family 2. As revealed by the *in vitro* minigene assay, the c.427 + 1G > A variant activated a new cryptic splice site. As confirmed by an overexpression assay, there was no significant difference in the level of mRNA and protein expression between the mutate-BCL11B (p.Glu821Glyfs*28) and the wild type. It confirms that p.Glu821Glyfs*28 variant could be an NMD escaping variant.

Conclusion: The extended phenotype of *BCL11B*-related disorders is reported in this study to reveal the clinical and genetic heterogeneity of the disease. The study starts by identifying a splicing variant and a novel frameshift variant of the *BCL11B* gene, thus confirming its aberrant translation. The findings of

this study expand the mutation spectrum of the genetic *BCL11B* gene, which not only improves the understanding of the associated neurodevelopmental disorders from a clinical perspective but also provides guidance on diagnosis and genetic counseling for patients.

KEYWORDS

***BCL11B* gene, neurodevelopmental disorders (NDD), intellectual disorder, minigene, immunodeficiency**

Introduction

Neurodevelopmental disorders, including intellectual disability and language disorder, have become a major public health concern that places a heavy burden on both families and the whole society (Maia et al., 2021). In recent years, the rapid development of genome sequencing technology has provided an effective solution to diagnosing neurodevelopmental disorders, which is conducive to the prevention of birth defects. *BCL11B*-related disorder has been a recently reported hereditary disease caused by the *BCL11B* gene *de novo* variant. Up to now, there have been plenty of reports on the role of the *BCL11B* gene in the nervous and immune systems (Arlotta et al., 2005; Li L. et al., 2010; Li P. et al., 2010; Kominami, 2012; Yu et al., 2015; Simon et al., 2016, 2020; Fang et al., 2018; Daher et al., 2020), i.e., early studies demonstrate that Bcl11b plays a critical role in the development of corticospinal motor neurons axonal projections to the spinal cord *in vivo* by loss-of-function experiments in null mutant mice for Bcl11b (Arlotta et al., 2005); on the other hand, Bcl11b was expressed in all T cell compartments and was indispensable for T lineage development and commitment in mice (Li L. et al., 2010; Li P. et al., 2010). Those patients carrying the pathogenic variations of the *BCL11B* gene tend to have immune deficiency or intellectual developmental disorder, the major clinical manifestions are speech delay, dysmorphic facies, and T-Cell abnormalities. Meanwhile, it is accompanied by various phenotypes, such as autistic symptoms, attention deficit-hyperactivity disorder, anxiety, dental anomalies, and other behavioral abnormalities (Punwani et al., 2016; Lessel et al., 2018). So far, there have been merely19 cases reported worldwide (Punwani et al., 2016; Lessel et al., 2018; Qiao et al., 2019; Prasad et al., 2020; Yan et al., 2020; Yang et al., 2020).

Located at chromosome 14q32.1, the human *BCL11B* gene encodes a C2H2-type zinc finger protein. The isoform 1 (NM_138576.2) of *BCL11B* consists of 894 amino acids and 4 exons (Lennon et al., 2016). All of these six zinc finger domains are located in the last exon (exon 4), in which the ZnF2 and ZnF3 domains are responsible for DNA binding. Besides, the N-terminal CCHC zinc finger motif plays a vital role in the formation of the BCL11B dimer (Kominami, 2012; Grabarczyk et al., 2018). Currently, there are 17 variants of the *BCL11B* gene identified in 19 patients through different studies. The major types of *BCL11B* genetic variation include frameshift, non-sense, missense, and complex chromosome rearrangement. However, there is still no report on splicing variation.

In this study, 4 patients with neurodevelopmental disorders and extended phenotypes were reported. Notably, a novel splicing variant and a *de novo* frameshift variant were detected through whole exome sequencing from the two studied families separately. Furthermore, the function of the two gene variants was verified by an *in vitro* minigene assay and an NMD assay.

Materials and methods

Patients and ethical approval

Two unrelated non-consanguineous Chinese pedigrees involving 4 patients diagnosed with neurodevelopmental disorders were collected. The neurodevelopmental disorders of the studied patients were not caused by other clinical factors, e.g., perinatal brain injury, traumatic brain injury, and infections. In Family 1 (**Figure 1A**), the proband (III-2) and her mother (II-5) showed severe intellectual disability. Her young brother (III-4) displayed mild developmental delay, and her father exhibited hearing impairment and dysarthria. As an exception, her younger sister (III-3) was healthy. In Family 2 (**Figure 1B**), the proband presents showed the specific signs of language impairment and mental retardation, but his parents were healthy.

For both families, all the data and analyzed peripheral blood samples were collected after receiving the expressed consent from both the guardians and other participated family members. The study was approved by the Ethics Committee of the Xi'an Children's Hospital and complied with the Declaration of Helsinki declaration.

Genetic analysis

About 1 μg of genomic DNA was extracted from 200 μl of peripheral blood by using a Qiagen DNA Blood Midi/Mini

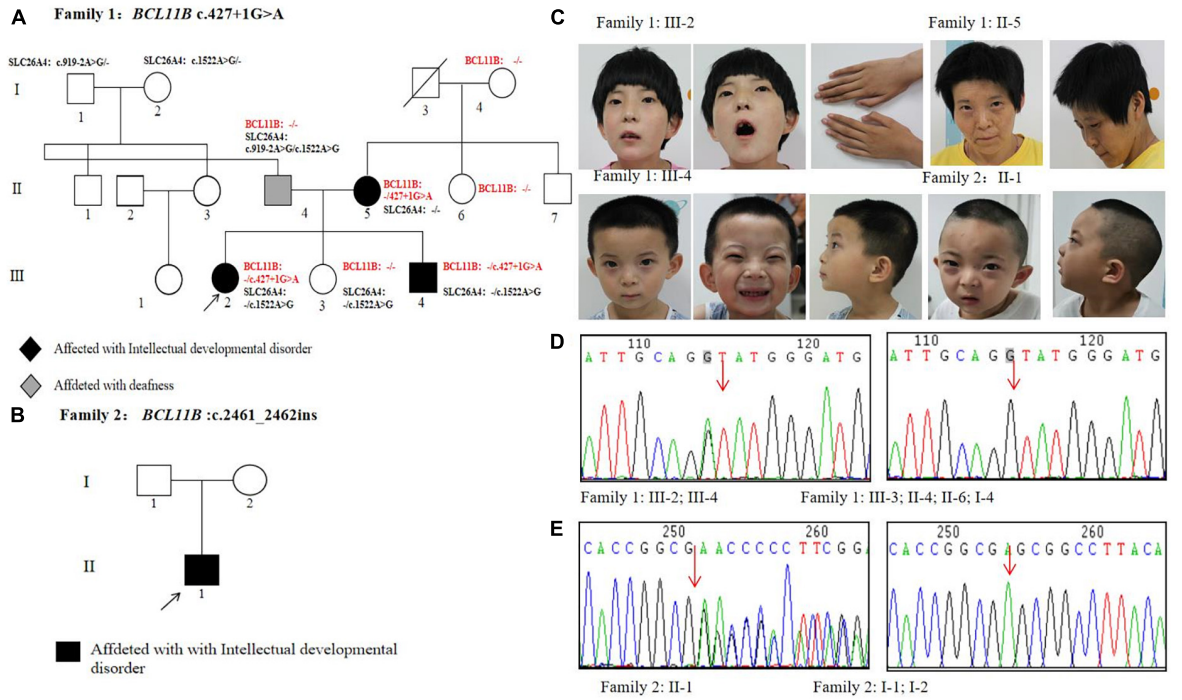

FIGURE 1
Pedigrees and genetic analysis of two families. **(A)** The pedigree of Family 1 carrying a splice variant c.427 + 1G > A in *BCL11B*. **(B)** The pedigree of Family 2 carrying a frameshift variant c.2461_2462insGAGCCACACCGGCG in *BCL11B*. **(C)** Images of patients with *BCL11B* variants. **(D)** The sanger sequencing of the c.427 + 1G > A variant in Family 1 members. **(E)** The sanger sequencing of the c.2461_2462insGAGCCACACCGGCG variant in Family 2 members.

kit (Qiagen GmbH, Hilden, Germany) and sheared into fragments. Then, they were hybridized by using the Nano WES Human Exome probe sequence capture kit (Berry Genomics Corporation, Beijing, China). Trio whole-exome sequencing (Trio-WES) was performed for both families. A Burrows-Wheeler Aligner tool was used to align the sequencing reads with the human reference genome (hg19/GRCh37). PCR duplicates were removed through the Verita Trekker® Variants Detection System (v1.57; Berry Genomics, Inc). The third-party software Genome Analysis Toolkit (GATK) was employed to carry out variant calling. Then, all variants were annotated and interpreted through multiple databases, including 1,000 Genomes Project, Exome Aggregation Consortium (ExAC), and Genome Aggregation Database (gnomAD). To better interpret the genetic variants, they were classified into five different categories according to the American College of Medical Genetics and Genomics (ACMG) guidelines (Richards et al., 2015). The suspected variants were subsequently validated through Sanger sequencing in the studied families.

Minigene splicing assay

The *in vitro* minigene assay was carried out to examine the target gene regions covering *BCL11B* exon1-3, intron 1, and intron 2, and they were amplified from gDNA of the proband in Family 1. Due to the large size of the introns 1 and 2 of the *BCL11B* gene, the two introns were split and constructed in plasmid (Figure 2). Three pairs of overlapping primers (P1F/1R, P2F/2R, P3F/3R) were developed to amplify the heterozygous c.427 + 1G > A mutation site from the gDNA fragment by seamless cloning (Vazyme Biotech Co., Ltd., Nanjing, China). Then, the amplified DNA products were recombined and cloned into the two digestion sites (*Xho*I/*Bam*HI) of the pMini-CopGFP vector (Hitrobio Biotechnology Co., Ltd., Beijing, China). Furthermore, the recombinant plasmids pMini-CopGFP-BCL11B-wt (wild type) and pMini-CopGFP-BCL11B-mt (c.427 + 1G > A) were validated through Sanger sequencing (P4F/4R). Subsequently, the plasmids were transfected into HEK293 cells. With total RNA extracted and reverse-transcribed into cDNA after 48 h of transfection, reverse transcription polymerase chain reaction (RT-PCR) was triggered by a primer pair of P5F/5R. Afterward, the cDNA products were examined using 1% agarose gel electrophoresis and further confirmed by means of Sanger sequencing. The length of wild-type cDNA products was determined as 711 bp.

To substantiate the conclusion drawn in this study, the assay was conducted repeatedly in another HepG2cell line by using the same experimental method as above.

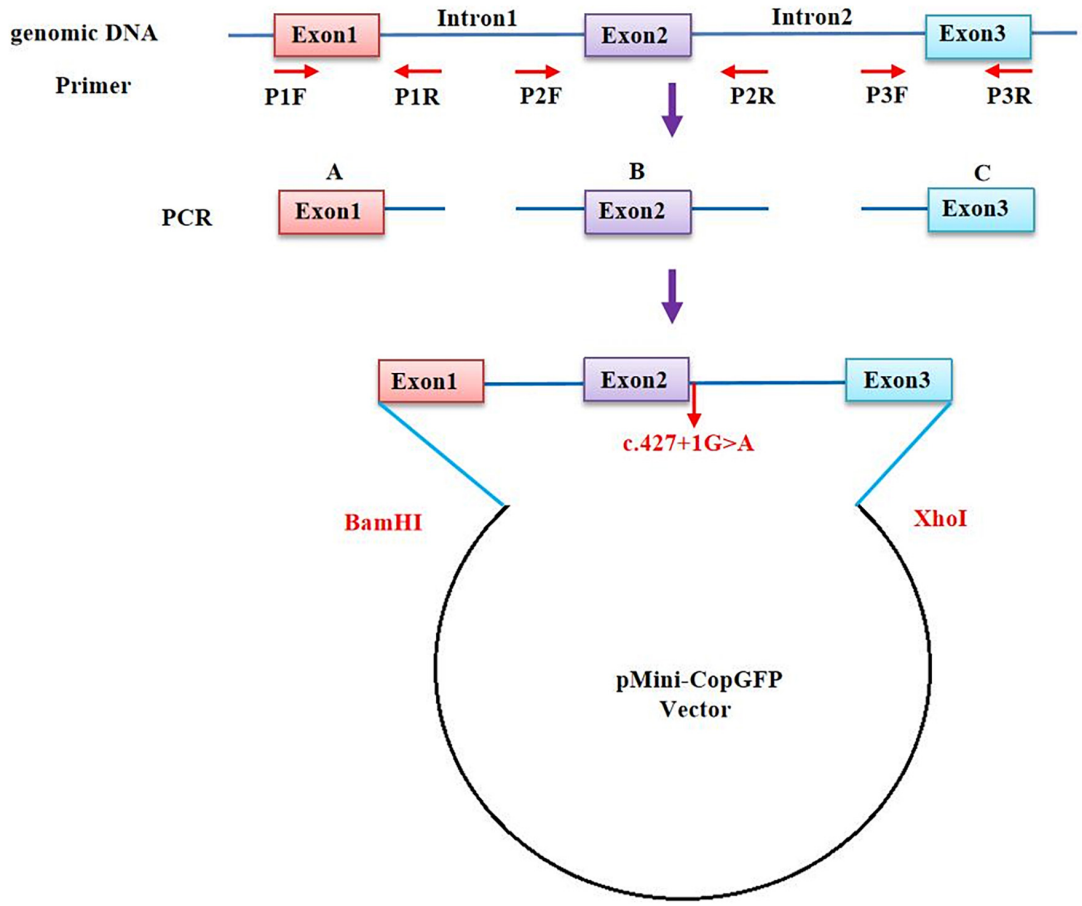

FIGURE 2
A schematic diagram of primer design for a minigene assay of the *BCL11B* gene. The upstream and the downstream of Intron 1 and Intron 2 were retained, respectively, and the intermediate sequences were removed (NG_027894.1: from g.5780 to g.18155 of Intron 1; from g.20001 to g.44443 of Intron 2).

Overexpression of recombinant plasmid carrying frameshift variant (p.Glu821Glyfs*28) of *BCL11B*

The full-length cDNA product of *BCL11B* was synthesized and cloned into the green-fluorescent pEGFP-C1 vector with two digestion sites (*Xho*I/*Bam*HI) so as to obtain a recombinant wild-type plasmid (pEGFP-C1-BCL11B-wt). Meanwhile, a pair of site-directed mutagenesis primers (P6F/6R) was developed to construct mutant plasmid pEGFP-C1-BCL11B-mt (c.2461_2462insGAGCCACACCGGCG) from pEGFP-C1-BCL11B-wt. Both wild-type and mutated plasmids were confirmed by bidirectional sequencing. As per the instruction of the manufacturer, the plasmids of pEGFP-C1-BCL11B-wt/mt (the wild-type group and the mutant group) and pEGFP-C1 (the control group) were separately transfected into HEK293T cells with the assistance of Lipofectamine^{TM} 2000 (Invitrogen, Thermo Fisher Scientific, United States). Each transfection group was replicated in 3 cell wells. After 48 h, total RNA was extracted from the transfected cells by using TRizol Reagent and then reverse-transcribed into cDNAs. Meanwhile, β-actin was treated as the housekeeping gene for processing in the same protocol. The primers for RT-PCR include P7F/7R and human-b-actin-F/R. The cell lysates in each group were collected to obtain total proteins, while the expression of targeted protein was analyzed through Western blotting, which was performed using Bcl-11B (D6F1) XP® Rabbit mAb (#12120, Cell Signaling Technology, United States). All the primers are detailed in **Supplementary Table 1**.

Results

Clinical features

The clinical features of 4 patients were summarized, as shown in **Table 1**. The phenotypes of the studied patients were consistent with the reported cases, showing psychomotor

retardation, the intellectual disability with speech and language impairment, but no obvious immune deficiency. Notably, the proband of Family 1 was able to sing nursery rhymes, recite ancient poems, and make simple communication before the age of 3. However, a significant regression in language and cognitive development manifested itself after Year 3. She also showed the signs of autism and the inability to speak and the lack of common attention and eye contact. In addition, she tended to feel anxious and frightened.

All these 4 patients exhibited the common signs of facial dysmorphism, such as thin eyebrows, long and smooth philtrum, thin upper lips, and micrognathia (**Figure 1C**). The proband in Family 1 was barely cooperative with IQ and autism tests due to poor recognition and adaptability. The proband in Family 2 scored 38.2 in total developmental quotient (DQ) against the Gesell developmental scale. To be specific, the proband scored 44.9 in adaptability, 46 in gross motor, 37 in fine motor, 30.7 in language, and 32 in personal-social ability. Laboratory investigation showed no abnormality among other patients in terms of blood ammonia, blood lactic acid, serum amino acids and urinary organic acids metabolic analysis, brain magnetic resonance imaging (MRI), hearing and vision examinations, except for the proband's mother (Family 1: II-5, who objected to any further clinical or laboratory investigations in this study). The electroencephalogram (EEG) results of two probands suggested occasional epileptiform discharges mainly in the bilateral temporal lobes, despite no experience of witnessing clinical seizures.

To evaluate the immunity level of the patients, flow cytometry investigation was conducted to indicate an abnormality in the absolute counts of the lymphocyte subset (**Table 2**). The ratio of CD4 + /CD8 + was significantly reduced not only in the proband (Family 1: III-2) and her young brother (Family 1: III-4) but also in the proband of Family 2 (Ding et al., 2018). As for the levels of immunoglobulins, IgA, IgG, and IgM, they fell within the normal range for the III-4 of Family 1 and the proband of Family 2. By contrast, there was a slight increase in the levels of IgM and IgA for the proband of Family 1, whose IgG level was normal (**Supplementary Table 2**).

Genetic findings

In Family 1, Trio-WES was performed to detect a novel matrilineal heterozygous splice variant NM_138576.4: c.427 + 1G > A in the *BCL11B* gene of the proband (III-2), as further verified by performing Sanger sequencing (P8F/8R) in other family members. The same gene variant was observed in the proband's brother (Family 1: III-4) rather than in her father (Family 1: II-4), younger sister (Family 1: III-3), her aunt (Family1: II-6), and maternal grandmother (Family 1: I-4) (**Figure 1D**). It indicates the occurrence of variant segregation in this family with the disorder. It was also shown in our study that the gene variant was non-existent in the ExAC, 1,000 Genomes Project and gnomAD. *In silico* prediction tools, Splice AI prediction was made that the c.427 + 1G > A variant could lead to the loss of the splice donor with a high score (0.99) and cause intron retention. In line with the ACMG guidelines, it was suggested that the gene variant should be classified as pathogenic (PVS1 + PP1 + PM2-Supporting). This variant has been submitted to the ClinVar database (Variation ID: 1292046). Besides, there were two other compound heterozygous variants of the *SLC26A4* gene detected as pathogenic gene variations in the proband's father: NM_000441.2: c.1522A > G (p.Thr508Ala) and c.919-2A > G.

In Family 2, Trio-WES was carried out to detect a *de novo* heterozygosis variant NM_138576.2: c.2461_2462 ins GAGCCACACCGGCG(p.Glu821Glyfs*28)of the *BCL11B* gene in the proband (Family 2: II-1), as confirmed by Sanger sequencing (P9F/9R) (**Figure 1E**). In addition, we confirmed that the proband of Family 2 (II-1) and his parents (I-1 and I-2) were first-degree relatives. The results are provided in **Supplementary Figure 1**. The gene variation was identified in the last exon of the *BCL11B* gene and then predicted to escape non-sense-mediated mRNA decay (NMD), which probably resulted in a truncated protein, given the loss of the last two C-terminal DNA-binding zinc-finger domains. This gene variant did not exist in the ExAC, 1,000 Genomes Project, and gnomAD, nor was it reported in literature. According to the ACMG guidelines, this variant could be classified as pathogenic (PVS1_Strong + PS2 + PM2-Supporting). This variant has been submitted to the ClinVar database (Variation ID: 1292051).

In vitro functional analysis

c.427 + 1G > A variant activates a cryptic splice site

For Family 1, an *in vitro* minigene splicing assay was performed to confirm whether the c.427 + 1G > A variant would affect normal splicing. The RT-PCR analysis of HEK-293T cells transfected with a mutant plasmid showed aberrant splicing in comparison with wild-type. As a result, the agarose gel electrophoresis of RT-PCR products displayed a single band (estimated 710 bp) from the wild type and a small band (estimated 420 bp) in the mutant type (**Figure 3A**). As revealed by the sequencing of the PCR fragment, the c.427 + 1G > A variant led to a shorter transcript with 286-bp deletion of downstream of Exon 2, which is attributed to the activation of a novel cryptic 5′donor splice site within Exon 2. Meanwhile, the 5′ donor splice site in Exon 3 was found normal, despite Exon 3 translation errors and premature termination. Represented as NM_138576.4: c.142_427del, the newly formed transcript was predicted to produce a prematurely truncated protein p.Val48Glyfs*14. A schematic diagram of the abnormal splice is shown in **Figure 3B**.

TABLE 1 Clinical features of the 4 patients with *BCL11B* variants.

Clinical features	Family 1			Family 2
General	III-2 (Proband)	III-4 (Young brother)	II-5 (Mother)	II-1 (Proband)
Perinatal conditions	Normal	Premature infant	Normal	Neonatal jaundice
Age at diagnosis	11 y	3 y 10 m	35 y	3 y 8 m
Gender	Female	Male	Female	Male
Degree of ID/DD	Severe	Mild	Severe	Moderate
Motor dealy	Mild	Mild	Mild	Mild
Walked unsupported	2 y	1 y 6 m	NA	1 y 6 m
Current speech	No words, high pitched voice	Short sentences	Short sentences, hoarse voice	3–4 words
Autistic features	+	–	–	–
Behavioral abnormalities	Stereotypic movements, sometimes aggression	No particular	Timid	Problems with changes
Neurology				
Muscle tension	Hypertonia	–	NA	Hypertonia
Serzures/Abnormal EEG	+	–	NA	+
Brain MRI	–	–	NA	–
Facial abnormalities				
Thin eyebrows	+	+	+	+
Hypertelorism	+	+	–	+
Long philtrum	+	+	+	+
pointed chin	+	+	+	+
Low-set ears	+	+	+	+
Prominent nose	+	+	–	+
Thin upper lip	+	+	+	+
Others				
Dental anomalies	Extensive caries	Extensive caries	–	Extensive caries
Feeding difficulties	–	–	–	+
Immune response	Frequent infections	Frequent infections	–	Allergies
***BCL11B* Variant**	c.427 + 1G > A	c.427 + 1G > A	c.427 + 1G > A	c.2461_2462ins

"+" Yes, "–" No, "NA," not available; y, year; m, month.

TABLE 2 T. B. NK lymphocyte immunophenotype of the patients of this study.

Cells	Family 1: III-2 (Proband)		Family 1: III-4 (young brother)		Family 2: Proband	
	Result	Reference range*	Result	Reference range*	Result	Reference range*
CD45 + (cells/μL)	**4,340**	2020–3,500	4,132	2,790–6,350	4,916	2,790∼6,350
CD3 + /CD45 + (%)	**86**	62–77	**81**	54–73	**74**	54∼73
CD3 + (cells/μL)	**3,720**	1,297–2,480	3,341	1,794–4,247	3,659	1,794∼4,247
CD3 + CD8 + /CD45 + (%)	**56**	23–32	**48**	19–33	30	19–33
CD3 + CD8 + (cells/μL)	**2,424**	509–1,050	**1,995**	580–1,735	1,483	580∼1,735
CD3 + CD4 + /CD45 + (%)	**23**	28–41	**23**	24–43	25	24–43
CD3 + CD4 + (cells/μL)	1,002	621–1,258	945	902–2,253	1,224	902–2,253
CD16 + 56 + /CD45 + (%)	**5**	8–23	8	7–21	10	7–21
CD16 + 56 + (cells/μL)	238	203–584	311	270–1,053	503	270–1,053
CD19 + /CD45 + (%)	**7**	9–18	**10**	13–26	13	13–26
CD19 + (cells/μL)	324	247–578	**398**	461–1,456	629	461–1,456
CD4 + /CD8 +	**0.413**	0.92–1.73	**0.47**	0.90–2.13	**0.8253**	0.90–2.13

Values higher or lower than the normal range were marked in bold. *The reference ranges suggested by previous publication (Ding et al., 2018).

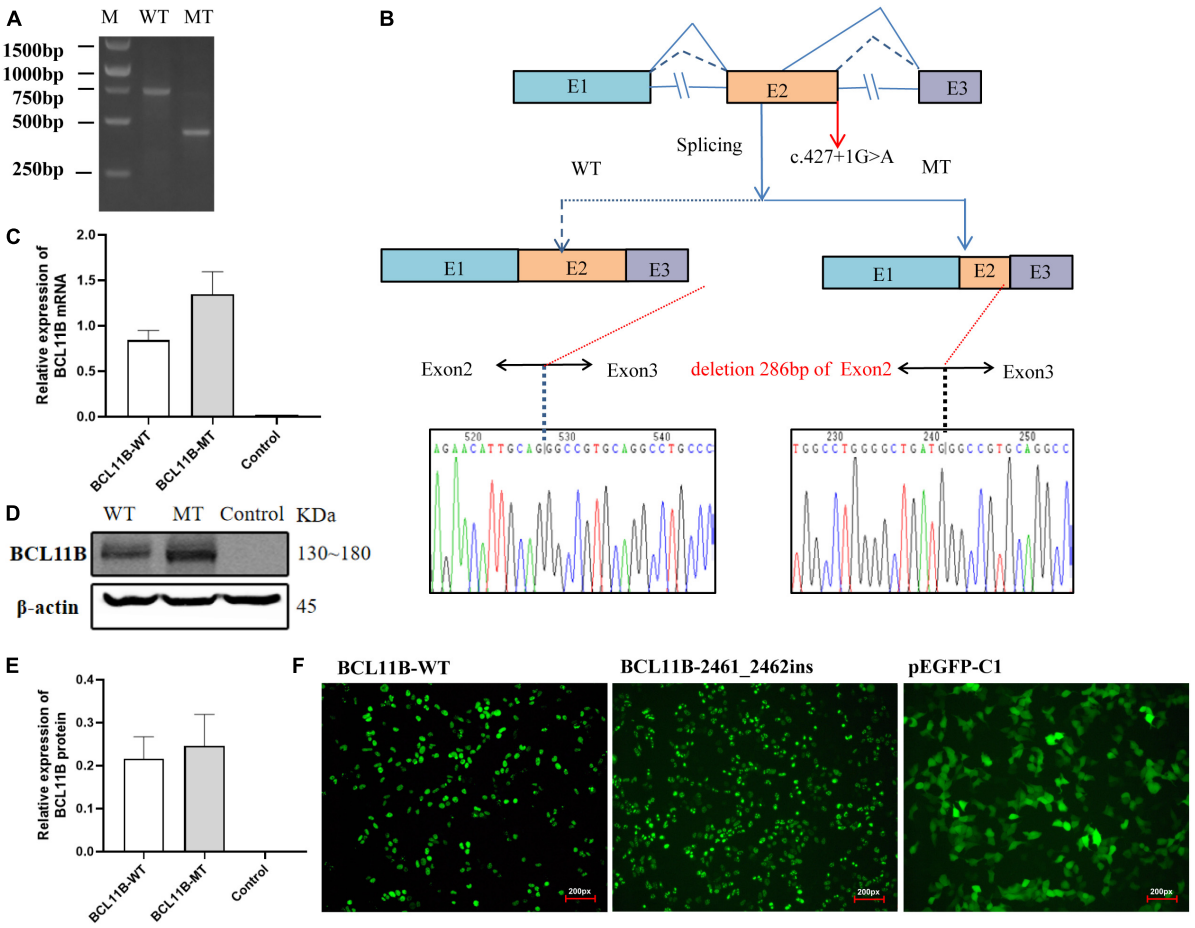

FIGURE 3
The *in vitro* minigene assay of the c.427 + 1G > A variant and the overexpression assay of the c.2461_2462insGAGCCACACCGGCG variant in HEK293T cells. **(A)** The identification of a shorter transcript with 286 bp deletion of the Exon 2 downstream, attributing to the activation of a novel cryptic 5′donor splice site in Exon 2. **(B)** A schematic diagram of the abnormal splice and Sanger sequencing of cDNA from transfected cells. **(C)** Quantitative analysis of mRNA expression of WT and frameshift mutant plasmids. **(D)** Western blot analysis of WT and frameshift mutant protein. **(E)** Quantitative analysis of protein expression of WT and frameshift mutant plasmids. **(F)** Fluorescent image (200px) of wild-type and mutant BCL11B-EGFP in HEK293T cells. Both wild-type and mutant types could be expressed, and there was no significant change in cell morphology and localization. M, DNA marker; WT, wild type; MT, mutant type.

We repeated the minigene splicing assay in HepG2 cells and found that the abnormal shear results caused by the c.427 + 1G > A variant were consistent with those in HEK 293T cells. Gel electrophoresis and Sanger sequencing results are provided in the Supplementary Material (Supplementary Figures 2–4).

p.Glu821Glyfs*28 variant escape non-sense-mediated mRNA decay

As for Family 2, the mutant and wild-type recombinant plasmids were constructed and transfected into the HEK293T cells so as to better observe the effect of frameshift variant on protein expression. There was no significant difference revealed by QPCR in the level of mRNA between the mutant and the wild type (Figure 3C). Three independent replicates of WB showed that the protein carrying the p.Gl821GlyFs *28 variant could be expressed, and there was no significant difference between the mutant and the wild type (Figures 3D,E). Moreover, after transfection of wild-type and mutant types of BCL11B plasmids into 293T cells, EGFP fluorescence imaging showed that the nuclear localization and cell morphology of the mutant cells did not change significantly compared with the wild type (Figure 3F), which confirms the escape of the p.Glu821Glyfs*28 variant from NMD. This finding is the same as expected because this variant introducing the premature stop codon is located in the last exon of *BCL11B* gene escape NMD-scanning.

Discussion

This study identified a new splice variant and a novel frameshift variant of the *BCL11B* gene in two

unrelated pedigrees, including 3 patients in Family 1 and 1 patient in Family 2 with neurodevelopmental disorders. According to the *in vitro* minigene assay, the splice variant could cause the abnormal splicing of the *BCL11B* gene. Meanwhile, the extended phenotype with developmental retardation was observed in the proband of Family 1, suggesting the clinical heterogeneity and complex biological mechanisms of the disease.

It is widely known that *BCL11B*-related disorder can lead to two phenotypes with common features, namely, type 49 immunodeficiency and intellectual development disorders with malformation, speech delay, and T-cell abnormalities. There were 19 patients reported to show delayed psychomotor development, of whom only one showed the severe combined immune deficiency caused by missense variants (Punwani et al., 2016). In addition to the common features shown by all patients, such as facial dysmorphism, it was also found in this study that the proband in Family 1 also showed regression in intellectual and language development, which has been unreported previously. Moreover, the clinical manifestations of the 3 patients in Family 1 varied significantly. The proband showed more typical features of the disorder than her mother and brother did, whereas the younger brother exhibited milder symptoms. This finding suggested phenotypic heterogeneity of the splice site variant in *BCL11B*-related disorder from this family-based study. There are various reasons for this phenotypic heterogeneity. It is suspected that the detected splice variation may lead to various sets of abnormal transcripts in different patients, which is associated with the significant variation in gene expression and function. Additionally, the other variants might be excluded from WES analysis, which is suspected to be a pathogenic factor located in non-coding regions or associated with complex structural rearrangements. For the proband's younger brother, the clinical phenotype showed changes due to aging. A follow-up survey or gene investigation could be conducted to clarify this.

At present, the diverse roles of *BCL11B* in T cell biology and Group 2 innate lymphoid cell (ILC2) development have been studied by many researchers (Walker et al., 2015; Yu et al., 2015, 2016; Xu et al., 2019). It was in 2016 that the first patient manifesting severe combined immunodeficiency (SCID) and multisystem anomalies was reported (Punwani et al., 2016), with nearly half of the reported patients displaying persistent infections, eosinophilia, allergy, and asthma. Consistently, it was discovered in our study that the proband and her younger brother in Family 1 exhibited persistent infections as well, and that the proband in Family 2 showed only allergy. Moreover, flow cytometric analysis was conducted to reveal that the ratio of CD4 + /CD8 + was the lowest in the proband and her younger brother of Family 1, but normal in the proband in Family 2. According to the study of Lessel et al. (2018) this is linked to the impairment of T cell immunity. Given a lack of definitive immune deficiency diagnosis, it is necessary to reveal the impact of *BCL11B* gene variation on the immune system through more clinical cases and pathogenic mechanism studies.

De novo cryptic splice variants contribute significantly to rare genetic disorders, especially intellectual disability and autism spectrum disorders (2015; Jaganathan et al., 2019). In this study, a minigene expression assay was performed to figure out the *in vitro* effects of the c.427 + 1G > A variant on gene function of *BLC11B*. By causing the absence of the splice donor on Intron 2 and the incidence of a novel cryptic donor splice site on Exon 2, the splice variant shortened Exon 2 and led to the generation of an abnormal pre-mRNA (c.142_427del). On the translation level, the abnormal pre-mRNA produced a prematurely truncated protein p.Val48Glyfs*14 but with no ZnF_C2H2 domains of the BCL11B protein. Given the involvement of ZnF2 and ZnF3 domains in DNA binding (Kominami, 2012), it is speculated that the c.427 + 1G > A gene variant could interfere with the recognition of BLC11B protein and DNA and the interaction between them. Besides, the abnormal truncated variant p.Val48Glyfs*14 is located in Exon 2, and it is thus predicted to trigger NMD and cause haploinsufficiency as a result. In summary, the genetic etiology of patients in Family 1 is closely associated with the splice variant c.427 + 1G > A of the *BCL11B* gene.

It is also known that *de novo* frameshift variants can result in severe intellectual disability and developmental delay (Kosmicki et al., 2017). For all the *BCL11B* variants associated with developmental delay and intellectual disability, frameshift variants account for 76% (13/17), with nearly all of them being *de novo*. However, there was only one frameshift variant p.Asp534Thrfs*29 reported as hereditary (Lessel et al., 2018). In our study, the proband in Family 2 carried a *de novo* frameshift variant p.Glu821Glyfs*28 in the *BCL11B* gene. As confirmed by the overexpression experiments, this variant could escape NMD to form a truncated protein, despite no significant difference observed in protein and RNA expression between the mutant plasmid and the wild-type plasmid. So far, the variant p. (Gly820Alafs*27) has been confirmed to result in a functional null allele and suppress progenitor cell proliferation in hippocampal of Bcl11b mutant mice. Also, it has been found to interfere with the expression of the BCL11B in dentate neurons (Lessel et al., 2018). As a neighboring variant, the p.Glu821Glyfs*28 truncated variant as identified in this study has a potential to produce a functional null allele, thus causing the disorder. By summarizing the phenotypes of all patients with a frameshift/non-sense variant (**Supplementary Table 3**), it can be found out that all the frameshift variants may cause the loss of the last two or three C-terminal ZnF_C2H2 domains, except for p.Ala891Profs *106 and p.Cys81Leufs*76 variants. As a result, NMD can be activated (Hamby et al., 2011). However, there was no significant correlation observed between the number of retained Zn finger domains and the severity of symptoms. Since the zinc finger domain, usually, must be connected in series for binding DNA (Avram et al., 2002), the loss of the zinc finger

domain may offset the physiological impact of BCL11B protein by affecting its transcription-regulatory activity.

Conclusion

In conclusion, a novel splicing variant of the *BCL11B* gene and a novel frameshift variant were identified in this study from two different families separately. The findings of this study expand the spectrum of gene variation associated with the disease. The genetic and clinical data used in the study provide evidence for a study to better understand the pathogenic mechanism and genetic etiology of the disease. *BCL11B*-related disorder is an intellectual development disorders characterized by malformation, speech delay, and T-cell abnormalities or immune deficiency. Genetic testing is conducive to improving the accuracy of a clinical diagnosis and providing firm evidence for gene counseling.

Data availability statement

The original contributions presented in this study are included in the article/**Supplementary material**, further inquiries can be directed to the corresponding author/s.

Ethics statement

The studies involving human participants were reviewed and approved by the Ethics Committee of the Xi'an Children's Hospital. Written informed consent to participate in this study was provided by the participants; legal guardian/next of kin. Written informed consent was obtained from the individual(s), and minor(s); legal guardian/next of kin, for the publication of any potentially identifiable images or data included in this article.

Author contributions

FC and YY contributed to conception and design of the study. XT and LZ collected the clinical data. FC and XT wrote the first draft of the manuscript. HL revised the manuscript, while XZ and MD coordinated and supervised data collection. All authors contributed to revising the manuscript and read through and approved the submitted version.

Funding

This work was supported by the Fundamental Research Funds for the Xi'an Jiaotong University (No. xzy012020053) and the Xi'an Children's Hospital Research Project (Nos. 2020A07 and 2021G15).

Acknowledgments

We would like to acknowledge all of the family members for their participation in this study, and to express gratitude to the Berry Genomics Co., for the technical support received.

Conflict of interest

The authors declare that the research was conducted in the absence of any commercial or financial relationships that could be construed as a potential conflict of interest.

Publisher's note

Supplementary material

The Supplementary Material for this article can be found online at: https://www.frontiersin.org/articles/10.3389/fnmol.2022.927357/full#supplementary-material

References

Arlotta, P., Molyneaux, B. J., Chen, J., Inoue, J., Kominami, R., and Macklis, J. D. (2005). Neuronal subtype-specific genes that control corticospinal motor neuron development in vivo. *Neuron* 45, 207–221. doi: 10.1016/j.neuron.2004.12.036

Avram, D., Fields, A., Senawong, T., Topark-Ngarm, A., and Leid, M. (2002). COUP-TF (chicken ovalbumin upstream promoter transcription factor)-interacting protein 1 (CTIP1) is a sequence-specific DNA binding protein. *Biochem. J.* 368, 555–563. doi: 10.1042/bj20020496

Daher, M. T., Bausero, P., Agbulut, O., Li, Z., and Parlakian, A. (2020). Bcl11b/Ctip2 in skin, tooth, and craniofacial system. *Front. Cell. Dev. Biol.* 8:581674. doi: 10.3389/fcell.2020.581674

Ding, Y., Zhou, L., Xia, Y., Wang, W., Wang, Y., Li, L., et al. (2018). Reference values for peripheral blood lymphocyte subsets of healthy children in China. *J. Allergy Clin. Immunol.* 142, 970–973.e8. doi: 10.1016/j.jaci.2018.04.022

Fang, D., Cui, K., Hu, G., Gurram, R. K., Zhong, C., Oler, A. J., et al. (2018). Bcl11b, a novel GATA3-interacting protein, suppresses Th1 while limiting Th2 cell differentiation. *J. Exp. Med.* 215, 1449–1462. doi: 10.1084/jem.20171127

Grabarczyk, P., Winkler, P., Delin, M., Sappa, P. K., Bekeschus, S., Hildebrandt, P., et al. (2018). The N-terminal CCHC Zinc finger motif mediates homodimerization of transcription factor BCL11B. *Mol. Cell. Biol.* 38:e00368-17. doi: 10.1128/mcb.00368-17

Hamby, S. E., Thomas, N. S., Cooper, D. N., and Chuzhanova, N. (2011). A meta-analysis of single base-pair substitutions in translational termination codons ('nonstop' mutations) that cause human inherited disease. *Hum. Genomics* 5, 241–264. doi: 10.1186/1479-7364-5-4-241

Jaganathan, K., Kyriazopoulou Panagiotopoulou, S., McRae, J. F., Darbandi, S. F., Knowles, D., Li, Y. I., et al. (2019). Predicting splicing from primary sequence with deep learning. *Cell* 176, 535–548.e24. doi: 10.1016/j.cell.2018.12.015

Kominami, R. (2012). Role of the transcription factor Bcl11b in development and lymphomagenesis. *Proc. Jpn. Acad. Ser. B Phys. Biol. Sci.* 88, 72–87. doi: 10.2183/pjab.88.72

Kosmicki, J. A., Samocha, K. E., Howrigan, D. P., Sanders, S. J., Slowikowski, K., Lek, M., et al. (2017). Refining the role of de novo protein-truncating variants in neurodevelopmental disorders by using population reference samples. *Nat. Genet.* 49, 504–510. doi: 10.1038/ng.3789

Lennon, M. J., Jones, S. P., Lovelace, M. D., Guillemin, G. J., and Brew, B. J. (2016). Bcl11b: A new piece to the complex puzzle of amyotrophic lateral sclerosis neuropathogenesis? *Neurotox Res.* 29, 201–207. doi: 10.1007/s12640-015-9573-5

Lessel, D., Gehbauer, C., Bramswig, N. C., Schluth-Bolard, C., Venkataramanappa, S., van Gassen, K. L. I., et al. (2018). BCL11B mutations in patients affected by a neurodevelopmental disorder with reduced type 2 innate lymphoid cells. *Brain* 141, 2299–2311. doi: 10.1093/brain/awy173

Li, L., Leid, M., and Rothenberg, E. V. (2010). An early T cell lineage commitment checkpoint dependent on the transcription factor Bcl11b. *Science* 329, 89–93. doi: 10.1126/science.1188989

Li, P., Burke, S., Wang, J., Chen, X., Ortiz, M., Lee, S. C., et al. (2010). Reprogramming of T cells to natural killer-like cells upon Bcl11b deletion. *Science* 329, 85–89. doi: 10.1126/science.1188063

Maia, N., Nabais Sá, M. J., Melo-Pires, M., de Brouwer, A. P. M., and Jorge, P. (2021). Intellectual disability genomics: Current state, pitfalls and future challenges. *BMC Genomics* 22:909. doi: 10.1186/s12864-021-08227-4

Prasad, M., Balci, T. B., Prasad, C., Andrews, J. D., Lee, R., Jurkiewicz, M. T., et al. (2020). BCL11B-related disorder in two Canadian children: Expanding the clinical phenotype. *Eur. J. Med. Genet.* 63:104007. doi: 10.1016/j.ejmg.2020.104007

Punwani, D., Zhang, Y., Yu, J., Cowan, M. J., Rana, S., Kwan, A., et al. (2016). Multisystem anomalies in severe combined immunodeficiency with mutant BCL11B. *N. Engl. J. Med.* 375, 2165–2176. doi: 10.1056/NEJMoa1509164

Qiao, F., Wang, C., Luo, C., Wang, Y., Shao, B., Tan, J., et al. (2019). A De Novo heterozygous frameshift mutation identified in BCL11B causes neurodevelopmental disorder by whole exome sequencing. *Mol. Genet. Genomic Med.* 7:e897. doi: 10.1002/mgg3.897

Richards, S., Aziz, N., Bale, S., Bick, D., Das, S., Gastier-Foster, J., et al. (2015). Standards and guidelines for the interpretation of sequence variants: A joint consensus recommendation of the American college of medical genetics and genomics and the association for molecular pathology. *Genet. Med.* 17, 405–424. doi: 10.1038/gim.2015.30

Simon, R., Baumann, L., Fischer, J., Seigfried, F. A., De Bruyckere, E., Liu, P., et al. (2016). Structure-function integrity of the adult hippocampus depends on the transcription factor Bcl11b/Ctip2. *Genes Brain Behav.* 15, 405–419. doi: 10.1111/gbb.12287

Simon, R., Wiegreffe, C., and Britsch, S. (2020). Bcl11 transcription factors regulate cortical development and function. *Front. Mol. Neurosci.* 13:51. doi: 10.3389/fnmol.2020.00051

Walker, J. A., Oliphant, C. J., Englezakis, A., Yu, Y., Clare, S., Rodewald, H. R., et al. (2015). Bcl11b is essential for group 2 innate lymphoid cell development. *J. Exp. Med.* 212, 875–882. doi: 10.1084/jem.20142224

Xu, W., Cherrier, D. E., Chea, S., Vosshenrich, C., Serafini, N., Petit, M., et al. (2019). An Id2(RFP)-reporter mouse redefines innate lymphoid cell precursor potentials. *Immunity* 50, 1054–1068.e3. doi: 10.1016/j.immuni.2019.02.022

Yan, S., Wei, Y. S., Yang, Q. Y., Yang, L., Zeng, T., Tang, X. M., et al. (2020). [A case report of BCL11B mutation induced neurodevelopmental disorder and literature review]. *Zhonghua Er Ke Za Zhi* 58, 223–227. doi: 10.3760/cma.j.issn.0578-1310.2020.03.012

Yang, S., Kang, Q., Hou, Y., Wang, L., Li, L., Liu, S., et al. (2020). Mutant BCL11B in a patient with a neurodevelopmental disorder and T-cell abnormalities. *Front. Pediatr.* 8:544894. doi: 10.3389/fped.2020.544894

Yu, Y., Tsang, J. C., Wang, C., Clare, S., Wang, J., Chen, X., et al. (2016). Single-cell RNA-seq identifies a PD-1(hi) ILC progenitor and defines its development pathway. *Nature* 539, 102–106. doi: 10.1038/nature20105

Yu, Y., Wang, C., Clare, S., Wang, J., Lee, S. C., Brandt, C., et al. (2015). The transcription factor Bcl11b is specifically expressed in group 2 innate lymphoid cells and is essential for their development. *J. Exp. Med.* 212, 865–874. doi: 10.1084/jem.20142318

frontiers | Frontiers in Molecular Neuroscience

TYPE Review
PUBLISHED 29 September 2022
DOI 10.3389/fnmol.2022.993671

OPEN ACCESS

EDITED BY
Melanie Grubisha,
University of Pittsburgh, United States

REVIEWED BY
Kazu Nakazawa,
Southern Research Institute,
United States
Daniel Fishman,
Stanford University, United States

*CORRESPONDENCE
Daniel Felipe Ariza-Salamanca
daniel.ariza@urosario.edu.co

SPECIALTY SECTION
This article was submitted to
Brain Disease Mechanisms,
a section of the journal
Frontiers in Molecular Neuroscience

RECEIVED 13 July 2022
ACCEPTED 31 August 2022
PUBLISHED 29 September 2022

CITATION
Ariza-Salamanca DF,
Corrales-Hernández MG,
Pachón-Londoño MJ and
Hernández-Duarte I (2022) Molecular
and cellular mechanisms leading to
catatonia: an integrative approach
from clinical and preclinical evidence.
Front. Mol. Neurosci. 15:993671.
doi: 10.3389/fnmol.2022.993671

Molecular and cellular mechanisms leading to catatonia: an integrative approach from clinical and preclinical evidence

Daniel Felipe Ariza-Salamanca[1,2]*,
María Gabriela Corrales-Hernández[2],
María José Pachón-Londoño[2] and
Isabella Hernández-Duarte[2]

[1]Medical and Health Sciences Education Research Group, School of Medicine and Health Sciences, Universidad del Rosario, Bogotá, Colombia, [2]Pharmacology Unit, Department of Biomedical Sciences, School of Medicine and Health Sciences, Universidad del Rosario, Bogotá, Colombia

This review aims to describe the clinical spectrum of catatonia, in order to carefully assess the involvement of astrocytes, neurons, oligodendrocytes, and microglia, and articulate the available preclinical and clinical evidence to achieve a translational understanding of the cellular and molecular mechanisms behind this disorder. Catatonia is highly common in psychiatric and acutely ill patients, with prevalence ranging from 7.6% to 38%. It is usually present in different psychiatric conditions such as mood and psychotic disorders; it is also a consequence of folate deficiency, autoimmunity, paraneoplastic disorders, and even autistic spectrum disorders. Few therapeutic options are available due to its complexity and poorly understood physiopathology. We briefly revisit the traditional treatments used in catatonia, such as antipsychotics, electroconvulsive therapy, and benzodiazepines, before assessing novel therapeutics which aim to modulate molecular pathways through different mechanisms, including NMDA antagonism and its allosteric modulation, and anti-inflammatory drugs to modulate microglia reaction and mitigate oxidative stress, such as lithium, vitamin B12, and NMDAr positive allosteric modulators.

KEYWORDS

catatonia, mechanism, neuroinflammation, oxidative stress, NMDA

Introduction

Catatonia is a complex neuropsychiatric syndrome and since its recognition, it was described as a symptom or consequence of schizophrenia (SCZ). A great body of neuroscientific evidence has thrown up interesting hypotheses around cellular and circuitry defects leading to catatonia. The clinical spectrum of catatonia is wide, mostly involving affective and motor control-related encephalic

areas (Walther and Strik, 2016). Its diverse clinical spectrum, which will be later discussed, makes an accurate diagnosis difficult. During the past three decades, therapeutics have remained relatively constant, with benzodiazepines being the first line of treatment; however, they are not always effective. The wide application of electroconvulsive therapy (ECT) in psychiatric disorders has shown great efficacy, including catatonia (Dhossche and Withane, 2019; Kellner et al., 2020). Nonetheless, a definitive, specific treatment is still to be elucidated.

The epidemiological data surrounding catatonia is variable and depends on the sample studied and the methods used to diagnose it (Stuivenga and Morrens, 2014). The establishment of catatonic symptomatology is frequently related to other psychiatric conditions and acutely ill patients. The most frequent association was first noticed with schizophrenia, with a prevalence of up to 50% depending on the study (Deister and Marneros, 1994; Bräunig et al., 1998; Ungvari et al., 2005); nonetheless, current data establishes, varying depending on the population, a coexistence of schizophrenia/catatonia between 9.8% and 20% (Stuivenga and Morrens, 2014; Rasmussen et al., 2016; Solmi et al., 2018). A systematic review presented by Solmi et al. (2018) studied the epidemiological heterogeneity regarding the coexistence between catatonia and schizophrenia, more than half of the 74 studies included presented a European population whereas a study performed by Zingela et al. (2022) reported a coexisting prevalence of 47.7% among South African population. Said statistical difference not only exemplifies changes in diagnostic tools and criteria throughout the years, but it also leaves a significant number of catatonic patients in whom no clear etiology is known thus encouraging further studies on the subject. Interestingly, a stronger association has been elucidated between catatonia and affective disorders, with the prevalence of up to 20% to 40% in depression and mania respectively (Bräunig et al., 1998; Solmi et al., 2018).

It is worth bearing in mind that catatonia can emerge with no prior psychiatric comorbidity or in the presence of medical and neurological illness, with an estimated prevalence of 20.6% (Solmi et al., 2018; Connell et al., 2021). As for autism, an early-onset neurodevelopmental disorder, its similar and sometimes overlapping clinical manifestations have led clinicians and investigators to study a possible correlation between these two entities (Wing and Shah, 2000). Many cases have clearly related autoimmunity to the onset of catatonia: anti-N-methyl-D-aspartate receptor (NMDAR) encephalitis, autoimmune thyroid disorders, multiple sclerosis, and systemic lupus erythematosus (Rogers et al., 2019; Durns et al., 2020). Other authors pinpointed alterations of the limbic system like lower volumes of the amygdala and the hypothalamus as the arise of the affective component of catatonia (Fritze et al., 2022). Furthermore, a widely known hypothesis is anomalies in dopamine and GABAergic circuitries result in deficits of top-down modulation (Northoff, 2002). This puzzle has forced researchers to formulate a comprehensive approach to the pathophysiology of catatonia beyond an alteration in neuron circuitry.

The mechanisms underlying catatonia onset have been broadly studied; however, there is no consensus on how or why this syndrome occurs. Current explanations involve dysfunctions in encephalic areas such as the supplementary motor area (SMA), orbitofrontal cortex (OFC), prefrontal cortex (PFC; Haroche et al., 2020), and gamma-Aminobutyric acid-A (GABA-A) and N-Methyl-D-Aspartate (NMDA) receptor dysfunction has been proposed as well (Moussa et al., 2019; Samra et al., 2020). Additionally, evidence of the role of glia in neuropsychiatric disorders is growing (González-Reyes et al., 2017; Vargas-Sánchez et al., 2018; Baracaldo-Santamaría et al., 2022), and when assessing preclinical evidence around catatonia, animal models inducing symptoms resembling catatonia have focused on the interactions between neurons and glia; moreover, they have tried to modulate glial activation with encouraging results (Hagemeyer et al., 2012). Therefore, it is crucial to elaborate on an integrative approach that includes the complex interactions between neurons, microglia, oligodendrocytes, and astrocytes.

In this review, we carefully assess clinical tools to diagnose catatonia and the preclinical evidence in experimental catatonic models, deeply emphasizing processes that alter microglia, astrocytes, and oligodendrocytes. We explore clinical evidence from an extensive analysis of reported cases and functional images in catatonic patients, as well as the best literature available for similar diseases, in order to help us frame the understanding of this complex syndrome. Furthermore, regarding the cellular and circuitry pathways, we will review and propose current and novel therapeutics that might help to treat catatonia.

Clinical spectrum and assessment of catatonia

Catatonia is a psychomotor syndrome and its diverse symptomatology can include motor, mental, behavioral, and vegetative manifestations (Madigand et al., 2016). Its broad clinical spectrum can be classified into the motor and psycho-affective symptoms. Motor manifestations encompass mutism, stupor, staring, grimacing, stereotypy, mannerisms, perseveration, withdrawal, impulsivity, combativeness, cessation of self-initiated movement, and mitgehen and/or gegenhalten reflexes. Psychoaffective symptoms include automatic obedience, verbigerations, echopraxia, repetitive speech, and refusal to eat and drink (Tandon et al., 2013).

One possible categorization of catatonia variants is the one proposed by Fink and Taylor, who argue this syndrome can occur in three forms: retarded, excited, and malignant (Fink and Taylor, 2009). The most recognized is the retarded form, characterized by immobility, posturing, mutism, stupor, and stereotypy. The excited form includes restless movements,

talkativeness, agitation, frenzy, and delirium. Lastly, and less commonly found, there is a malignant form, distinguished by autonomic excitement, abnormal blood pressure, tachycardia, and tachypnea (Mashayekhi and Ghayoumi, 2019). The latter resembles many aspects of the neuroleptic malignant syndrome (NMS) and must be strongly taken into account as it might result in death (Philbrick and Rummans, 1994; Ghaziuddin et al., 2017).

Clinical manifestations of catatonia are extremely heterogeneous, making its recognition challenging. There are many scales designed to diagnose catatonia that mainly focus on clinical symptoms. The DSM-V, BFCRS, Brauning, and Northoff scales are summarized and contrasted in **Table 1** (Northoff et al., 1999a; Sienaert et al., 2011; American Psychiatric Association, 2013; Aandi Subramaniyam et al., 2020). It is important to differentiate catatonia from other conditions such as nonpsychiatric stupor, encephalopathy, stroke, stiff-person syndrome, Parkinson's disease, locked-in syndrome, malignant hyperthermia, nonconvulsive status epilepticus, NMS, or autism (Ohry, 1990; Tormoehlen and Rusyniak, 2018; Apetauerova et al., 2021; Vaquerizo-Serrano et al., 2021). Underlying medical conditions might be the cause of catatonia and their treatment should resolve the catatonic syndrome.

Hallmarks of motor and psycho-affective neural circuits involved in catatonia

In this section, based on the clinical division of catatonia, we describe in detail the physiological functioning of neural circuits related to motor control and psycho-affective modulation.

Motor control pathways

As previously described, catatonia has a strong motor component, and, therefore, it is mandatory to understand the circuitry implicated in movement control and coordination and its dysfunction in this syndrome. Basal ganglia are collections of neuronal nuclei located in the brain that encompass structures such as the striatum, composed of the caudate nucleus (CN) and putamen, as well as the ventral striatum (VS), internal (iGP) and external globus pallidus (eGP), substantia nigra pars compacta (SNc) and reticulata (SNr), and the subthalamic nucleus (STN). Interconnectivity between these structures and the cerebral cortex, cerebellum, and thalamus is crucial for movement control. The direct and indirect pathways describe how basal ganglia either initiate or completely terminate movement (Graybiel et al., 1994; Lanciego et al., 2012; Bostan et al., 2018).

The direct pathway starts when the cerebral cortex sends projections to the striatum to initiate movement. This excitatory efference activates the GABAergic medium spiny neurons in the caudate and putamen, which project to the iGP and the SNr, resulting in the inhibition of both structures (Calabresi et al., 2014). Tonic inhibitory neurons arising from the iGP would inhibit the ventral lateral (VL) and the ventral anterior (VA) nuclei of the thalamus; however, as iGP activity ceased due to the previous inhibition by the striatum, it is unable to inhibit the VA/VL thalamic complex, leaving the thalamus activated and thus allowing the afference originally initiated in the cerebral cortex to finally reach the frontal cortex, translating these signals into movement (Báez-Mendoza and Schultz, 2013; Cui et al., 2013; Freeze et al., 2013).

On the other hand, the indirect pathway seeks to modulate the disinhibitory actions from the direct pathway. The activation of this pathway is marked by the integration of cortical afferences in the striatum, where spiny neurons coming from the striatum will synapse with the tonic inhibitory active neurons from the eGP, which will later project to the iGP and the STN (Smith et al., 1998). This interaction between the striatum and eGP inactivates the nucleus' ability to inhibit the STN. Consequently, the subthalamic nucleus neurons project and activate the iGP, which modulates the VL/VA thalamic nuclei, suppressing its activity and thus blocking the activation of the thalamus, leading to termination of movement.

Movement is also inhibited by the hyperdirect pathway, which starts with an excitatory efference arising from the cerebral cortex that projects to the STN. Once activated, the STN projects excitatory afferences to activate the iGP. As has been stated, when the iGP medium spiny neurons project to the VL and VA nuclei of the thalamus, the activation of the medium spiny neurons will inhibit the aforesaid nuclei, leaving them incapable of sending excitatory signals to the cortex, which translates into the inhibition of movement (Nambu et al., 2002).

Medium spiny neurons from the striatum project directly to the SNc, which also sends diffuse dopaminergic projections to the spiny neurons. The effects dopamine has over spiny neurons are complex and might just be an example of how the same neurotransmitter has a different effect depending on the type of receptor the postsynaptic neurons express. In this sense, the same nigral neurons might provide excitatory afferences to the medium spiny neurons projecting to the iGP, thus promoting movement (direct pathway); but at the same time, these neurons could also provide inhibitory afferences to the medium spiny neurons projecting to the eGP, hence inhibiting movement. The expression of dopamine type 1 receptors (D1R) on the medium spiny neurons in the direct pathway guarantees this excitatory effect, whereas the expression of the dopamine type 2 receptor (D2R) on the same kind of neurons in the indirect pathway has an inhibitory effect (Gerfen and Surmeier, 2011). **Figure 1A** illustrates these pathways.

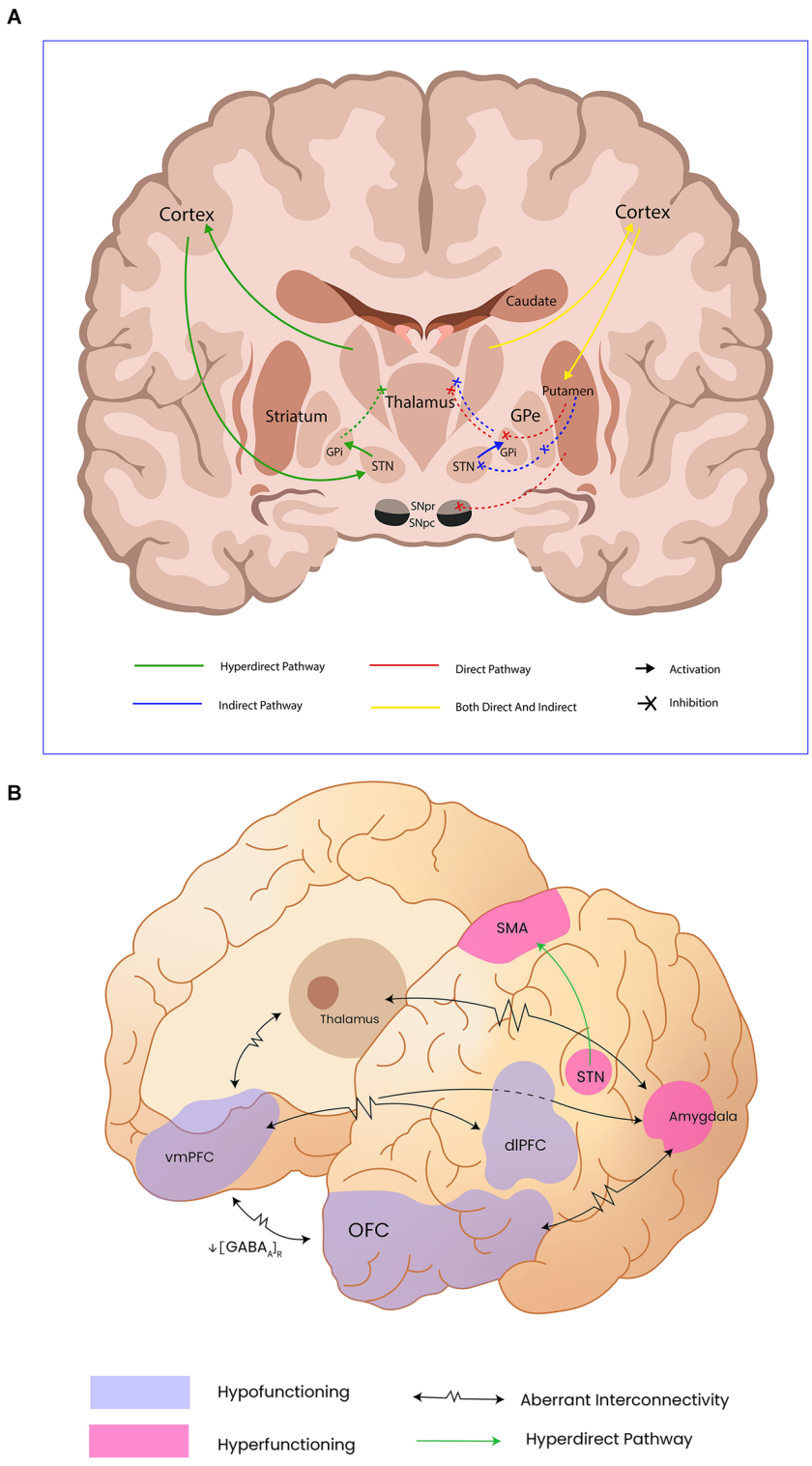

FIGURE 1
Panel **(A)** shows motor control pathways and the cortical and subcortical structures involved in movement control; Internal Globus pallidus (GPi), External Globus Pallidus (GPe), Subthalamic nucleus (STn). Panel **(B)** illustrates the abnormal functioning of cortical and subcortical structures reported by functional neuroimaging as well as the aberrant connectivity in catatonia; Orbitofrontal cortex (OFC), ventromedial prefrontal cortex (vmPFC), and dorsolateral prefrontral cortex (dlPFC) have been addressed as hypofunctioning, probable due to diminished GABAa receptor density. Subthalamic nucleus (STn), supplementary motor area (SMA), and the amygdala remain hyperfunctioning in catatonic patients, leading to motor inhibition.

TABLE 1 Diagnostic scales comparison: Bush–Francis Catatonia Rating Scale (BFCRS), Rogers Catatonia Scale (RCS), Braunig Catatonia Rating Scale (BCRS), Northoff Catatonia Rating Scale (NCRS).

Items	*BFCRS* (Bush et al., 1996)	*RCS* (Sienaert et al., 2011)	*BCRS* (Bräunig et al., 2000)	*NCRS* (Northoff et al., 1999a)
Excitement	X	X	X	X
Immobility/stupor	X	X	X	X
Mutism	X	X	X	X
Staring	X			X
Posturing/catalepsy	X	X	X	X
Grimacing	X		X	X
Echopraxia/echolalia	X	X	X	X
Stereotypy	X	X	X	X
Mannerisms	X	X	X	X
Verbigeration	X	X	X	X
Rigidity	X		X	X
Negativism	X	X	X	X
Waxy flexibility	X	X	X	X
Gegenhalten	X		X	X
Mitgehen/Mitmachen	X	X	X	X
Abnormal speech		X		X
Dyskinesia/parakinesia		X	X	X
Iterations		X	X	
Slowness/feebleness of spontaneous movements		X		
Simple abnormal posture		X		
Gait: reduced associated movements		X		
Gait: slow/shuffling		X		
Automatic obedience	X		X	X
Impulsivity	X		X	X
Grasp reflex/grasping	X		X	
Akinesia			X	X
Festination/jerky movements			X	X
Rituals			X	
Combativeness/aggression	X			X
Autism/withdrawal	X			X
Ambivalence/Ambitendency	X			X
Perseveration	X			X
Autonomic/vegetative abnormality	X			X
Agitation				X
Flaccidity/muscular hypotonus				X
Affect-related behavior				X
Affective latence				X
Flat affect				X
Anxiety				X
Athetotic Movements				X
Compulsive behavior				X
Compulsive emotions				X
Emotional lability				X
Sudden muscular tone alterations				X
Increased, compulsive-like speech				X
Loss of initiative				X
Magnetism			X	

Psycho-affective modulation circuits

Catatonia comprises not only motor but also affective and behavioral abnormalities. Therefore, in this section, we describe the neural substrate underlying emotional processing and the genesis of psychosis.

Regarding the neurobiological correlates of affective processing, it is crucial to understand catatonic affective symptoms by first explaining emotional regulation. Emotions can be defined as physiological responses to a given stimulus. The central processing of emotions is carried out by subcortical structures such as the amygdala, the striatum, the hypothalamus, the hippocampus, and the brain stem; cortical structures comprise the somatosensory cortex, cingulate cortex, and the motor cortex (Damasio and Carvalho, 2013). The amygdala is a key structure implicated in positive and negative emotional processing. Sensory inputs from the thalamus arrive at the lateral nucleus of the amygdala, connecting therefrom to the central nucleus, which in turn projects to the central gray region, and to the lateral and the paraventricular hypothalamus. Efferences to the autonomic and limbic systems result in an endocrine and motor output, usually evident as facial expressions, or more complex motor behaviors like freezing or running (Yang and Wang, 2017).

The genesis of psychosis has been tightly related to dopamine dysfunction. The classical dopaminergic theory stated there was an overactivity of the dopamine pathways due to enhanced neurotransmission or an increased sensibility to dopamine (Seeman and Seeman, 2014). Nonetheless, the role of dopamine in psychosis has evolved from a general

hyperdopaminergic state to a complex dysregulation, where there is greater activity of dopamine in the mesolimbic pathway and a lower dopaminergic activity in the mesocortical pathway (Kumakura et al., 2007; McCutcheon et al., 2020).

The increased sensibility to dopamine in the mesolimbic tract is thought to rely on different affinity states for agonism of D2R (Seeman et al., 1975; Seeman, 2013a). The different affinities are inter-convertible and depend on the coupling with G-proteins, where a coupled state is a high-affinity state (D2High) while the uncoupled state is a low-affinity state (D2low; Graff-Guerrero et al., 2009). Seeman et al. (2006) demonstrated that in schizophrenia there is an increase in D2High which is associated with a greater sensitivity to dopamine.

Our understanding of dopamine has evolved from its classical function as a reward neurotransmitter to having a more complex spectrum of functions including valuation, decision making, motivation behavior, awareness, and prediction of reward (Schultz et al., 1997; Fusar-Poli et al., 2010). Midbrain dopaminergic neurons and their interactions with other CNS structures have been postulated to mediate motivation, behavior, and valuation, and an aberrant circuitry function might be the substrate to aberrant behaviors (Montague et al., 2004). Furthermore, under normal conditions, dopamine is essential to make an accurate internal representation of an external stimulus. Thus, when altered, an incongruent representation and interpretation of the external stimulus results in psychosis (Howes and Kapur, 2009; Fusar-Poli et al., 2010; Howes et al., 2013). The *Aberrant Salience Theory* states complex diseases such as SCZ emerge from an incorrect adaptation process as a consequence of functional abnormalities in dopamine-related pathways (Roiser et al., 2013; Howes and Nour, 2016).

In brief, emotional regulation is performed by cortical and subcortical structures, and autonomic and motor responses are consequences of these processes. The genesis of psychosis is related to dopamine dysregulation, affecting the articulation of external vs. internal stimuli. The aforementioned structures and neurotransmitters juxtapose with those affected in catatonia. Furthermore, alterations in these circuits sometimes present with similar symptoms to those seen in catatonia.

Pathophysiology of catatonia

The role of neurotransmitters and circuitry dysfunction

In this section, we review and aim to elucidate catatonia's physiopathology by articulating functional imaging findings, preclinical data, current theories regarding neurotransmitter dysfunction, and successful pharmacological treatments reported in the literature. Understanding the aforementioned voluntary control movement, affective and behavioral neural substrates is crucial to correlate findings.

Recent systematic evidence (Haroche et al., 2020) gathers non-homogenous findings regarding structural imaging in patients diagnosed with catatonia. The most common cortical areas associated with catatonia are M1, the SMA, the parietal cortex, and the ventromedial prefrontal cortex (vmPFC). The frontal and parietal cortices are consistently found diminished, especially the right medial orbitofrontal cortex (OFC) and the superior left parietal gyrus (SPG). Disparate findings encompass fronto-parietal cortical sulcal enlargement, hyper gyrification of the anterior cingulate gyrus, medial OFC, right inferior temporal gyrus, and right insula, as well as hypo gyrification in the left superior temporal gyrus. Other important but not extensively studied structural findings are cerebellar vermis and brainstem atrophy and increased gray matter density in the cerebellum cortex (Wilcox, 1991; Northoff et al., 1999c).

The SMA is strongly related to the initiation, planning, learning, and programming of motor behavior, while the main synaptic outputs related to motor control encompass STN and parietal cortex stimulation. It is also associated with the integration of sequential elements into higher-order representations in complex processes like music, language, and working memory, implying that any required sequential process is structured by the SMA. In non-catatonic patients, SMA lesions manifest as slurred speech, perseverations, and repetitions. The radical cessation of self-initiated movement and sequence of movements are also observed (Ziegler et al., 1997).

Walther et al. (2017) found schizophrenic patients with catatonia had an increased cerebral blood flow to the SMA that directly correlates to catatonia severity. Moreover, they highlighted a diminished gray matter density in the insular and frontal cortices in these patients. A study performed by J. Scheuerecker found a normal medial motor loop (SMA, thalamus, and basal ganglia) activation in healthy control patients while performing self-initiated movements, but no activation in patients with catatonic schizophrenia (Scheuerecker et al., 2009). Additionally, regarding stimulation of the hyperdirect pathway, the VIIb cerebellar region projects to the STN, which in turn blocks movement by inhibiting M1 and the SMA (Walther et al., 2017). Taken together, the SMA integrates motor and cognitive information. Experimental and clinical SMA alterations in non-catatonic patients resemble motor and psychoactive symptoms observed in catatonia. The remarkable hyperperfusion of the SMA found on functional imaging in catatonic patients might correspond to compensation for insufficient or inhibitory basal ganglia output, and increased neural activity to override massive motor inhibition, probably coming from the cerebellum and the STN.

Another important finding using statistical functional imaging analysis is that catatonic patients present significant alterations in connections between the OFC and the vmPFC,

and between the ventromedial/dorsolateral PFC and the premotor/motor cortex. Moreover, functional imaging studies showed a decrease in cerebral blood flow in the right PFC and parietal cortex as well as a decrease in GABA-A receptor density and binding in the left sensorimotor cortex and right and left lower PFC (Northoff et al., 1999b). Northoff proposes a "top-down" modulation model in which he explains akinesia as a downregulation of the direct motor loop, emphasizing the fact that the source of this dysregulation does not come from the motor loop *per se* but rather from the GABAergic and cortico-cortical dysfunctions mediated by horizontal modulation in OFC and PFC. Vertical modulation understood as bidirectional interconnections between cortical and subcortical structures has also been suggested to explain motor symptom expression (Northoff, 2002; Hirjak et al., 2015).

Furthermore, vmPFC-thalamic connections are also crucial in cognitive behavioral control. Divergent projections from the vmPFC and dmPFC arrive at the mediodorsal thalamus and the ventromedial striatum, and apparently, these circuits maintain cognitive control tasks and guide a proper behavioral output by establishing a constant representation of a given task (de Kloet et al., 2021). The regulation and tracing of these interconnected projections are quite complex: there are at least four different circuits linking the vmPFC and dmPFC to the thalamus and striatum. Concerning catatonia, inhibitory corticostriatal projections arising from the mPFC to the striatum have been described; therefore, as seen in functional images, vmPFC and dmPFC hypofunction could activate striatum medium spiny neurons, resulting in behavior arrest (Lee et al., 2014).

Common associative areas are found when contrasting motor control, emotional regulation, and the genesis of psychosis. Subcortical structures like the basal ganglia circuits and the amygdala are involved in behavioral and emotional regulation, as well as cortical associative structures such as the primary motor cortex M1, SMA, PFC, OFC, thalamus, and the cerebellar-thalamo-cortical circuit (Walther et al., 2017). Functional MRI studies allow us to think of catatonic behavior as the result of a negative emotional processing, where a hyperactivation of the amygdala and in contrast a decreased activation of the OFC, supramarginal gyrus (SMG), mPFC, and cingulate anterior cortex (CAC) result in motor activity suppression, or tonic immobility as a response to fear (Northoff, 2002; Ellul and Choucha, 2015; Hirjak et al., 2019a).

Building on these ideas, Northoff and Hirkjak (Northoff et al., 2004; Hirjak et al., 2019b) both showed that a decreased activation and area of the OFC were related to behavioral and affective symptoms in catatonic patients, whereas motor abnormalities were linked to mPFC dysfunction. Catatonic patients have subjectively reported feeling overwhelmed with emotions, predominantly negative ones and specifically anxiety. Accordingly, depression can present as a prodrome of catatonia, while anxiety and psychotic symptoms can be present as well.

Additionally, catatonia might be considered as a fear syndrome, with cataplexy resembling a prey's freezing response while being hunted by a predator (Moskowitz, 2004). This behavior is related to an animal defense strategy named tonic immobility, which consists of sudden freezing when the animal is exposed to a dangerous stimulus (Lander et al., 2018). Environmental stimuli are conveyed in different brain areas that later project to the amygdala. After the information is sent to the amygdala, different cortical areas are activated. For example, connections between the OFC and the amygdala are assumed to be involved in emotional processing and control, especially when it comes to negative emotions. In consequence, decreased activation of the OFC impedes inhibition of the amygdala, thus leading to hyperactivation of the latter (Rempel-Clower, 2007; Ellul and Choucha, 2015). The vmPFC is a key area for fear generalization and perceiving emotions as well. Interesting evidence frames vmPFC interconnectivity between the amygdala and thalamus as a key regulator of fear and anxiety, so a reduced thickness or misfunction might lead to generalized anxiety (Arruda-Carvalho and Clem, 2014; Cha et al., 2014; Motzkin et al., 2015). Altogether, it is clear the OFC and vmPFC are key regulators of emotional and behavioral processing, and alterations seen in other pathologies help us shed light upon imaging findings in catatonia.

Symptoms such as echolalia and echopraxia are frequently present in catatonic patients. Previous studies have shown imitation behaviors might arise in response to lesions in the OFC. These echo-phenomena arise from the disinhibition of mirror neurons as a result of dysfunction in the GABAergic system within the OFC (Mehta et al., 2013; Ellul and Choucha, 2015).

The cellular and molecular mechanisms underlying the above-mentioned phenomena are scarce. Explanatory hypotheses are based on pathway dysfunction rather than a focal lesion in the central nervous system. The main neurotransmitters considered to play a critical role in catatonic pathophysiology are glutamate, GABA, and dopamine (Northoff et al., 1999b; Rasmussen et al., 2016). Akinetic catatonia, characterized by stupor, might be explained based on hypo functioning of GABAergic receptors, either by intrinsic dysfunction or by the overriding of said pathway generated by excess glutamate or NMDA receptor activity (Northoff et al., 1997; Carroll et al., 2007; Wijemanne and Jankovic, 2015). This hypothesis is supported by evidence showing catatonic responders to lorazepam developed hypokinetic movements, rather than hyperkinetic ones (Northoff et al., 1995). Serotonin plays a crucial role in indirect motoric control as the raphe nucleus directly modulates the activity of VTA and SN, and therefore less dopamine is released into the subcortical-cortical motor-related structures. In essence, the greater the activity of the raphe nucleus, the lower the activity of dopamine. This regulation is worth considering in psychiatric pathologies where catatonia might be present, as seen in bipolar disorder and

major depression, diseases where serotonin is augmented or diminished respectively (Conio et al., 2020; Martino et al., 2020; Northoff et al., 2021).

Interestingly, 72% of all autoimmune cases of catatonia are attributable to NMDAR encephalitis, a disease in which autoantibodies against the N1 subunit of NMDAR are internalized into the cells, leading to a decrease in the total number of receptors, increasing extracellular glutamate concentrations and interrupting synaptic connectivity (Rogers et al., 2019). It might seem counterintuitive that NMDA inhibition relieves catatonic symptoms when their internalization might produce them. Nonetheless, even when we can't pinpoint an exact cause of why anti-NMDA encephalitis produces catatonia, recent evidence helps us decipher this puzzle. Hare et al. (2020) administered ketamine and ketamine metabolites into the vmPFC of mice to assess their antidepressant actions. Amazingly, they found that the administration of these NMDA inhibitors increases vmPFC function in a dose-dependent manner. It is not clear why, but NMDA inhibitors probably modulate gene expression of calcium/calmodulin-dependent protein kinase II alpha (CaMK2A), a subunit intrinsically related to NMDA synaptic plasticity and long-potentiation. This allows us to infer that the administration of NMDA inhibitors, by modulating pyramidal CaMK2A-expressing neurons, can modify and reshape NMDA-dependent synapses in the vmPFC making them more active, nonetheless, more research needs to be done to verify this hypothesis. Catatonic patients who are not fully responsive to Benzodiazepines (BDZ) have shown positive response to treatment in combination with NMDA inhibitors such as amantadine and memantine (Babington and Spiegel, 2007; de Lucena et al., 2012; Ellul and Choucha, 2015). **Table 2** summarizes some cases reported in the literature using amantadine in combination with other medications resulting in positive clinical outcomes.

As for dopamine, the dopaminergic D2 blockade provided by first-generation antipsychotics has been commonly associated with Neuroleptic-Induced Catatonia. Neuroleptics induce a cataleptic state in rodents; this state is also called "animal catatonia", and it is used to measure propensity to extrapyramidal effects and in relation to D2 blockage (Lee, 2010; Ghaziuddin et al., 2017). As for dopaminergic signaling, the exact mechanism by which a dysregulation might cause catatonic signs is not clearly elucidated (Daniels, 2009). Treatment response, either improving symptoms or provoking them, shines a light as to which pathways and neurotransmitters are involved in catatonia.

Although current treatment regimens for catatonia will be discussed in Section "Revisiting current therapeutics", it is essential to examine the scenario of withdrawal catatonia. Few but consistently reported cases show that abrupt discontinuation of BDZs and antipsychotics, more often clozapine, is followed by catatonia (Brailey and Bastiampillai, 2020; Belteczki et al., 2021). These cases strengthen the evidence regarding the involvement of GABA receptors and dopamine circuit dysfunction in catatonia's physiopathology, but the question of how this happens remains. Some authors argue that the downregulation of GABA receptors due to long-term use of these medications might be the mechanism of withdrawal catatonia (Lander et al., 2018), which would concordantly relate to the aforementioned evidence. Nonetheless, it is worth considering that clozapine has unique mechanisms of action, is a D2 fast-off antipsychotic (Seeman, 2013b), an antagonist of 5HT2 and α2-adrenoceptor, and an indirect agonist of NMDAr, as it increases glycine synaptic availability by blocking the SNAT2 (Wenthur and Lindsley, 2013). In this regard, we would add to the underlying cause of catatonia onset shortly after abrupt cessation of clozapine the downregulation of D2 receptors, increased 5HT2A activity, and decreased NMDAr function.

Functional neuroimaging findings have been presented throughout this section, the main cerebral regions involved being the SMA, vmPFC, and OFC, and the current hypotheses involving neurotransmitter dysfunction have been discussed as well. Different authors have correlated these findings with the clinical spectrum of catatonia; however, the overlapping of motor and behavioral findings, added to the clinical heterogeneity, makes it difficult to come to a conclusive finding when it comes to the study of catatonia. As for the OFC, hyperactivation, and hypoactivation have been found in different studies: hyperactivation of the OFC correlated directly with negative emotional and affective processing in catatonic patients (Ellul and Choucha, 2015), while decreased activation of the OFC has been documented as well and has been associated with tonic immobility, one of the catatonia's pathophysiological theories (Northoff et al., 2004). Moreover, another key finding in catatonia is hypofunction of the vmPFC, which, as explained, has diverse projections to the amygdala, basal ganglia, and other subcortical structures related to fear extinction and behavioral control, and therefore its dysfunctions might be directly related to catatonic symptoms. On the other hand, SMA findings have been more homogeneous, indicating a directly proportional relationship between increased rCBF and clinical severity; however, discrepancies in blood flow have been seen depending on the clinical subtype of catatonia. For example, retarded-state catatonic patients were documented to have an overly activated SMA when compared to the excited subtype, linking increased neural activity to massive motor inhibition (Walther et al., 2017). Importantly, cortico-basal ganglia-thalamocortical loops related to motor, behavioral and emotional processing are the common substrate of a wide variety of symptoms present in catatonia. We consider that the disparity between objective findings in neuroimages relies on the diverse scenarios in which catatonia presents, and strengthens the theory that catatonia is the result of diffuse dysfunction rather than a focal lesion in the CNS. **Figure 1B** illustrates and contrasts with normal motor circuits and alterations evidenced in catatonic patients.

TABLE 2 Successful cases reported using amantadine, therapy regimen, and outcome.

Patient's diagnosis	Reference	Number of patients	Therapy regimen	Outcome
Bipolar disorder and catatonia	Ene-Stroescu et al. (2014a)	1	Amantadine (Dose notdisclosed) + Lorazepam + Carbamazepine	Full response after 72 h
Catatonia	Goetz et al. (2013)	1	ECT + Amantadine 250 mg/day	Discharged after 6 weeks. Full recovery
Catatoniain schizophrenia and schizo affective disorder	de Lucena et al. (2012)	5	Case 1: Clozapine + 400 mg of amantadine Case 2: Amantadine protocol Case 3: Amantadine protocol Case 4: Amantadine protocol Case 5: Amantadine protocol *Protocol: up to 600 mg of amantadine daily for 4 weeks	Case 1: Recovery on the 14th day with clozapine Case 2: Recovery by the 10th day Case 3: Recovery at the end of the protocol Case 4: Full recovery on the 8th day Case 5: Acceptable behavior by the 45th day
Catatonia and schizophrenia	Babington and Spiegel (2007)	1	Lorazepam+chlorpromazine+Amantadine 200 mgday	Fast recovery after 48 h of amantadine
Westphal variant Huntington disease and refractory catatonia	Merida-Puga et al. (2011)	1	Antipsychotics + ECT+L-dopa + Amantadine 300 mg/day	Not available
Catatonia and depressive disorder	Hervey et al. (2013)	1	Lorazepam + amantadine 200 mg/day	Recovery once amantadine was initiated
Catatonia, schizophrenia, and progressive diffuse cerebral atrophy	Ene-Stroescu et al. (2014b)	1	Clozapine+lorazepam+divalproex +amantadine (dose not specified)	Maximal response after 8 weeks of treatment
Catatonia in high-functioning ASD	Ellul et al. (2015)	1	Initial regimen of Zolpidem+lorazepamthen a 1-week washout followed by amantadine 200 mg/day	Maximal recovery after 2 weeks with amantadine
Akinetic catatonia	Northoff et al. (1997)	3	Case 1: Three IV infusions of amantadine 500 mg/dose Case 2: Two IV infusions of amantadine 500 mg/dose Case 3: Two IV infusions of amantadine 500 mg/dose	Case 1: Recovery after the third infusion of amantadine Case 2: Recovery after the second infusion Case 3: Recovery after the third infusion—needed lorazepam to treat aggressive and anxious behavior

Neuroinflammation in catatonia

In this section, we present the underlying cellular processes occurring during catatonia, especially focusing on the role of glia. Catatonia onset has been frequently associated with proinflammatory environments, whether as a trigger or comorbidity (Goforth, 2007; Quinn and Abbott, 2014). Inflammatory mechanisms leading to catatonia can only be hypothesized as current evidence is still insufficient to address causes. Nonetheless, we here present research evidence extracted from interesting animal models to help understand the roles of microglia, astrocytes, and oligodendrocytes in catatonia, and therefore how inflammation and oxidative stress could lead to this disease.

Microglia are CNS-resident immune cells actively involved in defense, pruning, and scar formation, and which are constantly interacting with other resident cells such as oligodendrocytes, astrocytes, and neurons (Liu et al., 2020). Early postnatal migration of microglia supports myelination and full synaptic functionality by inducing oligodendrocyte progenitor cell maturation through neurotrophic factor secretion when exposed to interleukins (IL) 4, 10, 13, and 33 (Butovsky et al., 2006; Banisadr et al., 2011; Miron et al., 2013). Microglia are also a key factor for remyelination: studies showed that an M2 (anti-inflammatory) rich environment prompts oligodendrocyte remyelination (Hagemeyer et al., 2017), while an M1 microglia (proinflammatory) rich environment enhances interleukin production, increasing antigen presentation and oxidative stress, and blocking M2 myelination properties (Miron et al., 2013). Moreover, the production of Tumour Necrosis Factor alpha (TNF alpha), nitric oxide (NO), and complement due to microglia activation are shown to induce oligodendrocyte death and phagocytosis (Greenhalgh et al., 2020).

2',3'-cyclic nucleotide 3'-phosphodiesterase (CNP) is an oligodendrocyte membrane enzyme protein. It has two isoforms, the first of which is related to RNA, tubulin, calmodulin and actin binding, ATP/GTP hydrolysis, and catalytic activity. These multiple functions are postulated to bridge the gap between the cytoskeleton and membrane, and are probably related to the transport of cargo along the axon, as well as the activation of second messenger (Raasakka and Kursula, 2020). The second isoform is found in mitochondria, and when activated it opens

the transition pore, leading to cellular apoptosis (Krestinina et al., 2015). CNP also oversees the catalysis of 2',3'-cyclic nucleotides and it is thought to prompt the expression of other structural myelin proteins in underdeveloped oligodendrocytes (Scherer et al., 1994; Myllykoski et al., 2012). Rodents null $^{(-/-)}$ for Cnp develop catatonia with aging, as soon as 8 weeks old (Janova et al., 2018). Cnp-heterozygous $^{(+/-)}$ rodents develop behavioral abnormalities that from a translational perspective resemble behaviors seen in schizophrenia and depression (Hagemeyer et al., 2012). Although evidence pinpointed Cnp as a feasible genetic mutation related to schizophrenia and catatonia, association studies did not support this correlation (Tang et al., 2007; Che et al., 2009). It is interesting that null and heterozygotic mice show behavior resembling the motor and affective symptoms characteristic in schizophrenia and catatonia. Furthermore, when Cnp-/- mice are exposed to PLX5622, a colony-stimulating factor inhibitor, and therefore a microglia suppressor, catatonia is ameliorated or prevented (Janova et al., 2018). These findings lead us to think microglia and oligodendrocytes play a role in catatonia.

When it comes to catatonia, evidence shows systemic pro-inflammatory environments trigger microglia, as well as metabolically stressful situations (Wolf et al., 2017). Even with subtle activation, a proinflammatory reaction of microglia can swell or damage the myelin sheet, generating a connectivity dysfunction (Poggi et al., 2016). We can infer the reaction of microglia in catatonia, as preclinical evidence has shown increased inflammation and myelin sheet swelling in the anterior corpus callosum and PFC, anatomical structures deeply correlated to affective and motor circuits, as described above (Hagemeyer et al., 2012; Janova et al., 2018). Although available preclinical evidence sheds light on catatonia development, the processes that determine the onset of this complex syndrome are not clear.

Astrocytes play a critical role in myelination, specifically through connexins that together form gap junctions: these proteins allow the diffusion of ions and molecules smaller than 1.5 kDa (Nagy and Rash, 2003; Orthmann-Murphy et al., 2008; Liang et al., 2020). In the CNS, astrocytes express connexins 26, 30, 46, and 47, and connect to oligodendrocytes through connexins 47/43, 47/30, 32/26, and 32/30. It is worth noticing that astrocytic connexin 47 is exclusive to the corpus callosum, striatum, cerebellum, and spinal cord. Astrocytes modulate myelination by providing oligodendrocytes with lipids and adjusting the structure and conduction velocity of myelin by modulating potassium homeostasis (Camargo et al., 2017; Sock and Wegner, 2019; Xia et al., 2020). Microglia directly modulate astrocyte function through the expression of IL-1B, IL-6, and TNF, turning them into a cytotoxic form characterized by loss of astrocytic gap junctions, increased glucose uptake, intracellular trafficking restriction, increased expression of complement, and poor stabilization and shaping of synapses (Prinz and Priller, 2014; Greenhalgh et al., 2020). Once astrocytes are turned into pro-inflammatory A1 type, astrogliosis is initiated and therefore neuroinflammation is perpetuated, thereby impeding normal synaptic connectivity. We consider astrocytes to play a role in catatonia, as Hagemeyer et al. (2012) showed high astrogliosis in the corpus callosum in CNP-heterozygous mice.

Oxidative stress in catatonia

Oxidative stress (OS) is a well-known consequence derived from an imbalance between the production of antioxidants and reactive species (RS), the latter group encompassing reactive oxygen (ROS) and nitrogen species (RNS). ROS include hydrogen peroxide (H_2O_2), peroxyl radicals (ROO·), the superoxide anion radical (O_2·(-)), singlet molecular oxygen (O_2^-), and the hydroxyl radical (OH·). RNS encompass peroxynitrite ($ONOO^-$) and NO (Sies, 2015). Naturally produced RS are buffered by potent antioxidants like superoxide dismutase (SOD) and glutathione (GSH). In pathological conditions, the increase in RS surpasses the production of antioxidants, and therefore RS are freed into the environment, reacting with membranes, damaging nuclear and mitochondrial DNA, and finally inducing cells to apoptosis (Qi and Dong, 2021). It is worth noting that the brain is particularly susceptible to OS, since for its physiological functioning it consumes as much as 20% of the body's oxygen supply, and is, in a great proportion, formed by lipids; therefore, in homeostatic environments, abundant RS are produced but they are naturally dampened by antioxidants produced by the mitochondria.

When it comes to catatonia, it is worth considering OS as a key factor, as the perphenazine-induced catatonia mice model has shown increased OS and depletion of antioxidant concentration when compared to controls. Interestingly, pretreatment with the cyclooxygenase-2 selective inhibitors rofecoxib and celecoxib decreased catatonic behavior, lipid peroxides, and brain nitrite (Gupta et al., 2009, 2011). Furthermore, it is widely known now that OS can directly activate multiple pathways related to inflammation. OS triggers the receptor for advanced glycation end-products (RAGE) and nuclear factor kappa-light-chain-enhancer of activated B cells (Nf-KB), leading to increased production of pro-inflammatory cytokines which will consequently create positive feedback between microglia and astrocyte activation (Kouidrat et al., 2013; Qin et al., 2013; Lingappan, 2018).

The glial syncytium in catatonia

The neurons, astrocytes, and oligodendrocytes connect through gap junctions, also known as the glial syncytium, thought to improve synaptic connection, calcium signaling, and regulate metabolism as well as cellular trafficking (Orthmann-

Murphy et al., 2008; Xia et al., 2020). Bearing in mind the specific roles of each cell in the prior sections, a dysfunction of any of them can cause a broader alteration of this syncytium.

We consider neuroinflammation as a key process underlying catatonia as acute ill patients diagnosed with autoimmune diseases or infections sporadically present with catatonic symptoms (Cawkwell et al., 2021; Zain et al., 2021; Sakhardande et al., 2022). Microglia and astrocytes are sensitive to inflammation, its morphological change to M1-A1 respectively is known to cause connexins to decouple, neurons and oligodendrocytes injury by activation of complement and oxidative stress, and thus generating weak synaptic transmission, myelin destabilization, and excitatory-inhibitory imbalance (Orthmann-Murphy et al., 2008; Verkhratsky et al., 2009; Verkhratsky, 2010). On the other hand, some cases reported using different medications, whether to treat psychosis, and immunomodulate, have been linked to the onset of catatonia (Bhangle et al., 2013; Lander et al., 2018; Durns et al., 2020). These clinical strengths the hypothesis that catatonia is predominantly an immune disease, and disturbing astrocytes and microglia directly interrupt movement control neural networks. Moreover, inflammation and OS directly damage the blood-brain barrier (BBB), creating a non-hermetic sealing of the brain and therefore allowing the leakage of plasma, proteins, and inflammatory cells to the brain parenchyma, affecting the homeostatic environment of the glial syncytium (Varatharaj and Galea, 2017).

Taken together, inflammation and OS are hallmarks of catatonia's physiopathology, as they form a positive feedback loop, creating a non-homeostatic environment in which microglia, astrocytes, oligodendrocytes, and neurons are disturbed, generating weak synaptic transmission. **Figure 2** illustrates glial syncytium and its dysregulation in catatonia.

Revisiting current therapeutics

Once catatonia is recognized, pharmacologic interventions and ECT can be used as they have shown the best clinical results so far (Denysenko et al., 2018). Currently, the first line of treatment are benzodiazepines (BDZ), due to their effect on GABA transmission by $GABA_A$ receptor agonism (Goodchild, 1993), especially lorazepam, which is the most widely used with a variable dosage ranging from 2 to 16 mg per day. For its part, ECT is effective in all forms of catatonia, even when BDZs have failed. Early intervention with this technique is recommended to avoid deterioration of the patient's medical condition; indeed acute severe and psychotic mood disorders have shown good therapeutic response to this therapy (Nolen and Zwaan, 1990; Luchini et al., 2015). Other medications such as dantrolene (Pennati et al., 1991), amantadine (Northoff et al., 1997; Hervey et al., 2012), and anticonvulsants (Rankel and Rankel, 1988) are reported as effective therapies in refractory catatonia. This section summarizes the current therapies used in catatonia from a mechanistic perspective.

Benzodiazepines (BDZ)

BDZs are $GABA_A$ allosteric modulators that enhance chloride conductance by binding to the BZ site of the receptor. Increasing the conductance of chloride ions is translated into an increasing frequency of channel opening. Congruently, BDZ efficacy is directly related to GABAergic enhancement (Walther et al., 2019). Some authors attribute the success of BDZ to an induced decreased activation of mPFC and OFC (Edinoff et al., 2021). We support this hypothesis and suggest that a GABAergic potentiation would decrease preSMA-SMA hyperactivation and, moreover, that BDZ could generate diffuse brain circuitry hyperpolarization.

A literature review by Rasmussen et al. (2016) recommends low-dose BDZ therapy (1–2 mg lorazepam SL or IV) followed by a repeated dose every 3 h until therapeutic effects are reached. Doses may be titrated depending on patient age and duration of symptoms, with chronic catatonia requiring higher doses for longer periods. In acute catatonia, 85% of patients had a positive response to treatment while 58.8% of patients recovered within three hours of a single dose of lorazepam. Treatment of the underlying condition must be ensured before discontinuing BDZ to prevent relapse (Rasmussen et al., 2016). Around 27% of patients experience only partial recovery, with poor response predictors being chronicity, increased age, and psychosis (Kritzinger and Jordaan, 2001; Walther et al., 2019).

Flunitrazepam, diazepam, and clonazepam are also viable options. Administration varies depending on the patient's health condition and collaboration: oral, intramuscular, and intravenous routes are available (Goodchild, 1993; Fink and Taylor, 2009; Pelzer et al., 2018). Recommended doses, titrations, and length of treatment vary among different authors. Reports with low-doses of lorazepam have shown fast responses and symptomatology improvement (Kritzinger and Jordaan, 2001; Sienaert et al., 2014; Rasmussen et al., 2016); however, longer treatments and higher doses have also been reported. A recent systematic review published by Zaman et al. (2019) compared BDZ use in catatonia vs. other drugs, placebo, and ECT, concluding there is not enough high-quality evidence to recommend specific treatment with BDZ, nonetheless BDZ, and regularly lorazepam, remain as the first-line treatment in catatonia, and therefore further research is needed in order to have a standardized regimen for this condition (Korkeila, 2016).

Antipsychotics

Second-generation antipsychotics are described as an alternative therapy for non-malignant catatonia, especially when

10.3389/fnmol.2022.993671

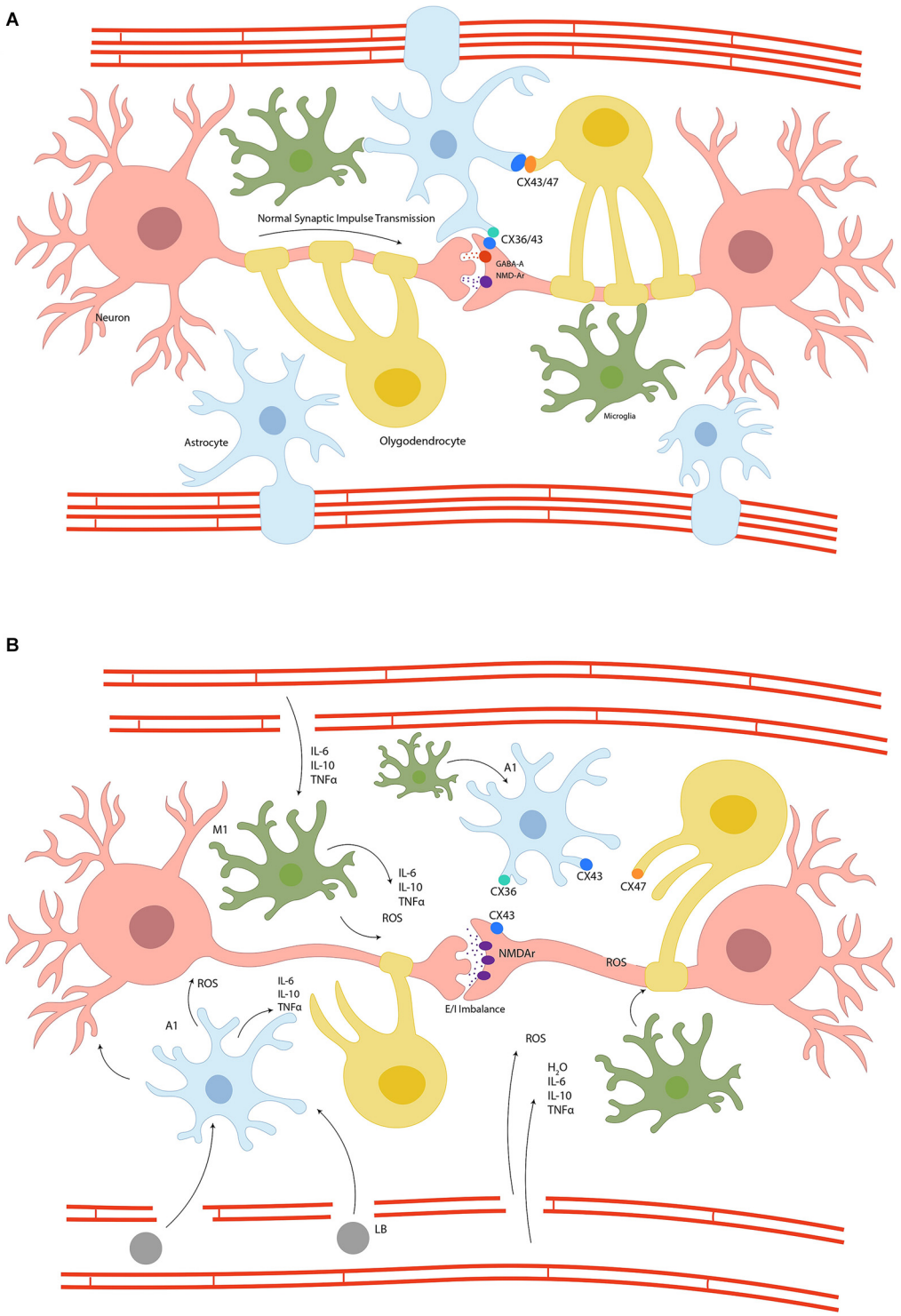

FIGURE 2
Panel **(A)** represents the glial syncytium, where astrocytes, oligodendrocytes, and neurons are coupled through connexins to stabilize the synapsis and the blood-brain barrier, preserving homeostasis and therefore a normal synaptic impulse transmission. Panel **(B)** schematizes the disruption of glial syncytium due to inflammation and metabolic dyshomeostasis. The switch of glial cells to proinflammatory phenotype results in connexins uncoupling, impedes synaptic stability and an excitatory/inhibitory imbalance, the leaking of blood-brain barrier and therefore migration of systemic inflammatory cells, increase oxidative stress, and the activation of apoptotic cascades ending in cellular death; Connexins (CX), N-methyl-D-Aspartate Receptor (NMDAr), Gamma-Aminobutyric acid-A (GABA-A), lymphocyte B (LB), Interleukin (IL), Tumour Necrosis Factor-alpha (TNFα) reactive oxygen species (ROS), proinflammatory astrocyte (A1), proinflammatory microglia (M1), water (H_2O).

a psychotic disorder is suspected as the underlying cause of catatonia. Second- generation antipsychotics block 5HT2A and D2 receptors, which may in turn increase relative dopamine activity in the mesocortical pathway. It is proposed that they may work in catatonia through the treatment of the underlying condition (Sienaert et al., 2019). Even though second-generation antipsychotics might show beneficial effects in catatonia with underlying psychiatric illness, they should be used with caution due to possibility of NMS and other motor side effects.

First-generation antipsychotics are generally not recommended due to the risk of worsening the condition. Several authors suggested that first-generation antipsychotics may aggravate non-malignant and malignant catatonia (Philbrick and Rummans, 1994; Ghaziuddin et al., 2017; Sienaert et al., 2019). Malignant catatonia is diagnosed when there are clear signs of autonomic alteration and hyperthermia, and it must be considered as it is highly lethal (Philbrick and Rummans, 1994). Not to be confused with NMS, which onset is directly related to antipsychotic use.

Beach et al. (2017) performed a systematic review of alternative treatments in catatonia in which aripiprazole, clozapine, olanzapine, risperidone, and ziprasidone were used individually in a total of 33 cases. Most patients recovered in a few days, though recovery was linked to pre-existing schizophrenia. In this study, two patients under clozapine developed catatonia after its withdrawal, which makes its use in this disease controversial. Paparrigopoulos et al. (2009) also described a clozapine-induced neuroleptic malignant syndrome in a patient with catatonia.

A case series described three cases in which intramuscular (IM) aripiprazole was successful in the treatment of catatonia. As an example, the first patient was a 61-year-old male with schizophrenia in his 72nd admission to the mental unit. Acute symptoms were treated with first-generation antipsychotics and BDZ, and his usual PO therapy with clozapine, aripiprazole, and valproic acid was continued. Three days later, catatonic symptoms were evident with a BFCRS score of 52. Iatrogenic catatonia was presumed. Symptoms resolved on the third day of IM aripiprazole at a dose of 10 mg × 3 days (Voros et al., 2009).

Even though success with second-generation antipsychotics is closely linked to pre-existing schizophrenia, it remains elusive whether antipsychotics work by directly resolving the catatonic syndrome or by treating the underlying psychotic disorder associated with catatonia. Stronger evidence is needed to clarify the safety and to standardize a regimen for antipsychotic prescription in patients diagnosed with schizophrenia and catatonia.

Electroconvulsive therapy (ECT)

ECT is employed in major psychiatric and medical disorders that are refractory to first-line treatments such as mood disorders, Parkinson's disease, post-stroke depression, schizophrenia, and catatonia. Even though it has been used for decades, the exact mechanism of action through which it is therapeutic is still unknown (Kaliora et al., 2018).

Therapy consists of inducing a controlled seizure under proper sedation. The classical approach includes both temporal lobes, although variations of electrode positions has been reported. In the first session, the initial seizure threshold (IST) is calculated either by administrating a low dose and titrating until a seizure threshold is obtained, or by giving a standard dose and adjusting it depending on the patient's tolerance considering age, sex, body mass, and co-treatment factors such as the chosen anesthesia (Jeong et al., 2019). Side effects include headaches, myalgias, and memory deficits, which typically resolve within weeks, but may last beyond 6 months in some patients (Lloyd et al., 2020).

ECT is currently the definitive treatment for catatonic syndromes. This complex motor syndrome, as discussed previously, is a potentially life-threatening condition and since ECT's introduction, the mortality associated with catatonia has decreased. Even though ECT has shown encouraging results in case series studies, there is a lack of high-quality randomized controlled trials to standardize ECT implementation in catatonia, and further research must therefore be carried out to potentiate the benefits of this therapy (Weiner and Reti, 2017). Nonetheless, its broad application with tremendous results, especially those associated with a GABAergic deficit in the orbitofrontal cortex and therefore the top-down catatonia type described by Northoff, has encouraged the use of ECT in catatonia (Northoff, 2002; Luchini et al., 2015).

The mechanisms underlying the success of ECT in catatonia are not elucidated. A neuroendocrine hypothesis has been proposed, but ECT might as well be treating the underlying etiology of catatonia, e.g., bipolar disorder and major depression (Dierckx et al., 2012; Perugi et al., 2017). ECT is thought to act principally in the diencephalon, especially in the hypothalamus where it "restores" endocrine function with the release of various hormones such as adrenocorticotropic and thyroid-stimulating hormones into the systemic circulation and cerebrospinal fluid (Haskett, 2014). Several hypothalamic functions such as sleep, appetite, menstrual cycle, circadian rhythm, and libido are restored after ECT (Fink and Ottosson, 1980; Bodnar et al., 2016; Weiner and Reti, 2017).

Furthermore, ECT has proven to be a safe therapy with positive responses ranging from 80 to 100%, nonetheless, unsuccessful results do not rule out catatonia (Hermida et al., 2018). The mortality rate is 1 in 10,000 patients and it can be increased by medical comorbidities including cardiovascular dysfunction, cerebral disease, and respiratory disease. Though elderly patients may have a higher comorbidity

rate, age alone is not considered to increase mortality (Meyer et al., 2018).

Amantadine and NMDAr antagonists

Amantadine is a synthetic tricyclic amine; it was initially used as an antiviral drug with specificity to inhibit replication of the Influenza A virus acting on the M2 protein, preventing viral uncoating and thus its replication (Aoki and Sitar, 1988). Its use as an antiviral drug is no longer recommended. Other uses of amantadine in clinical practice have been Parkinson's disease, drug-induced extrapyramidal syndromes, multiple sclerosis, and catatonia. The most common adverse reactions reported in the literature are cardiovascular, such as orthostatic hypotension, presyncope, syncope, and peripheral edema, with an incidence of >10%. Neurological side effects such as dizziness, hallucinations, delusions, and paranoia are common too. Ataxia, confusion, fatigue, dyschromia, and suicidal ideation have been reported with less frequency (Babington and Spiegel, 2007; Pahwa, 2021).

Recently it has been noted that amantadine might have other significant mechanisms of action with direct and indirect effects on dopamine neurons such as inhibition of dopamine uptake and increased affinity of dopamine for D2 receptors, thereby increasing the release of dopamine, noradrenaline, and serotonin in the amygdala and hippocampus (de Lucena et al., 2012).

As previously described, catatonia might be due to hyper-excitability of PFC, SMA, thalamus, and limbic system, as well as an increased oxidative stress and neuroinflammation. Amantadine acts as a weak antagonist of NMDA receptors, and accelerates channel closure, thereby reducing excitotoxicity and hyper-excitability arising from calcium entry to the cell, and preventing mitochondrial stress. This diminishes RS production, avoiding cellular apoptosis and dysfunction (de Lucena et al., 2012; Fryml et al., 2017). Furthermore, by reducing excitotoxicity, it can in turn compensate $GABA_A$ hypofunction at the mesostriatal circuit and reduce dopamine uptake at the synaptic cleft (Northoff et al., 1997; Roy et al., 2016).

Table 2 summarizes amantadine regimens used in catatonic patients and their clinical outcomes. Based on encouraging results reported in the literature, considering BDZs are not always effective, that amantadine has a longer time to treatment when compared to BDZs, and ECT is not widely available, we consider that clinical trials must be carried out to establish a therapeutic schedule to set amantadine as a first or common approach to patients with catatonia.

There are few reported cases where memantine was successfully used to treat catatonia, these cases were frequently associated with schizophrenia, also named catatonic schizophrenia (Thomas et al., 2005; Carpenter et al., 2006; Mukai et al., 2011; Obregon et al., 2011; Roy et al., 2016). Memantine is an antagonist of NMDAr, and it is a derivate from amantadine, therefore its mechanism of action is thought to be very similar to the one exposed earlier in this section. Memantine might be used when pro-dopaminergic effects of amantadine want to be avoided, but it must be carefully considered as its adverse effects include psychosis and seizures (Carpenter et al., 2006).

Minocycline is a tetracyclic-derived antibiotic that has come to our attention as there is evidence it reduces excitotoxicity and microglia activation, therefore attenuating neuroinflammation, OS, and apoptosis (Tikka et al., 2001). It is under study in many neurological pathologies (Cruz et al., 2020; Yang et al., 2020; Baracaldo-Santamaría et al., 2022). Regarding catatonia, Miyaoka et al. (2007) published a case series where minocycline successfully treated catatonia in concurrence with schizophrenia. As we stated earlier, microglia's activation is a hallmark of catatonia. It was proven minocycline attenuates microglia's reaction; thus, it is congruous to consider this antibiotic for the treatment of catatonia.

Novel therapies

Repetitive transmagnetic stimulation

A case report published by Di Michele and Bolino described a patient diagnosed with bipolar type I disorder with a psychotic depressive episode and catatonia, and who was refractory to most common treatments (Di Michele and Bolino, 2006). Interestingly, an improvement in motor behavior was achieved by using Repetitive Transmagnetic Stimulation (rTMS; 10 sessions, 20 Hz) in the left dorsolateral prefrontal cortex with no other drugs administered. Encouraging evidence has triggered the application of rTMS in diverse psychiatric disorders with fruitful results (McClintock et al., 2018; Ocampo et al., 2022). rTMS is a non-invasive brain stimulation technique and aims to either increase or decrease cortical activity by applying different electrical frequency protocols (Begemann et al., 2020). When considered in catatonia, it might be useful as its mechanism of action, although not clearly elucidated, resembles that of ECT therapy, and might act by treating catatonia itself, or the underlying condition (Spampinato et al., 2013). Modulation of GABAergic transmission might be the mechanism of action of rTMS, and we speculate rTMS might work well when ECT is not available. Nonetheless, more research is needed to support its implementation (Trojak et al., 2014).

Lithium therapy

A prospective study performed by Lee (1998) assessed lithium levels in catatonic patients, finding that a great

proportion of these patients had low levels of lithium. In consequence, repletion therapy was started and, interestingly, its administration successfully treated catatonia. Similar cases are reported in the literature (Padhy et al., 2011; Sugawara et al., 2021). Even though there is no clear mechanism of action for lithium, it appears to stabilize the excitatory/inhibitory disbalance, that can be either generated by catatonia or the underlying disease beneath. It has been clearly stated that SMA hyperactivation and OFC/vmPFC hypofunction are common findings in catatonia, so reestablishing balance among circuitries is a clear solution to the disorder. Moreover, lithium has a protective role as it prompts homeostasis, and modulates OS and inflammatory cascades (Forlenza et al., 2014). Altogether, lithium is a promising therapy in catatonia as it acts in diverse pathological processes, as described earlier. Caution must be taken when prescribing lithium: important adverse effects are not common but when established they might have a great impact on the patients' health (Thippaiah et al., 2021).

Positive allosteric modulation of N-methyl-D-aspartate

Section "Amantadine and NMDAr antagonists" describes the mechanism of action of amantadine and other antagonists of NMDAr and its success in catatonia; additionally, Section "The role of neurotransmitters and circuitry dysfunction" demonstrates functional reconstitution of vmPFC mediated by NMDA blockers. In this section, we encourage considering NMDAR-positive allosteric modulators such as rapastinel and spermine to treat catatonia with psychoaffective predominance, as they can target both catatonia and psychiatric disease. Interestingly, rapastinel is a positive allosteric modulator whose mechanism of action resembles that of ketamine but without adverse effects such as cognitive impairment and psychomimetic symptoms (Kato and Duman, 2020). Rapastinel has shown encouraging results in patients with treatment-resistant major depressive disorder (Donello et al., 2019; Ragguett et al., 2019; Naurex, Inc, an affiliate of Allergan plc., 2020). By modulating NMDAR action, rapastinel could reverse hyperactivity of SMA, restore the inhibitory wave from basal ganglia and induce CaMK2A expression to improve NMDA-dependent synaptic plasticity. NMDA-positive allosteric modulators have a broad clinical application and have shown good safety and efficacy profile in many neurological disorders (Baracaldo-Santamaría et al., 2022; Geoffroy et al., 2022). Nonetheless, it is essential to consider that NMDA modulators have different targets, as the dynamic endogenous configuration of NMDAR is complex, and different brain areas express different NMDARs. We consider that rapastinel and spermine might have a positive impact in patients with catatonia (Velloso et al., 2009; Geoffroy et al., 2022).

Cyclooxygenase-2 selective (COX-2) inhibitors—nonsteroidal anti-inflammatories

Taking into consideration that OS is a consequence of sustained metabolic stress and inflammation, while also bearing in mind the evidence provided by preclinical studies (Gupta et al., 2011), we consider COX-2 selective inhibitors might be regarded as a reasonable parallel therapeutic strategy to mitigate OS and inflammation, decreasing cellular damage and thus avoiding long-term consequences arising from catatonia. Even though there are no cases reported in the literature, rofecoxib and 1-(Phenyl)-5-(4-methylsulfonylphenyl)-2-ethylthioimidazole were used successfully in preclinical models (Gupta et al., 2009; Fathi-Moghaddam et al., 2010). The mechanisms by which COX-2 inhibitors might reduce catatonia vary from scavenger increase to enhancement of dopaminergic transmission at the striatum.

Vitamin B12/cobalamin

B12 or Cobalamin is an essential water-soluble vitamin which plays an important role in maintaining physiological functions in the hematopoietic and central nervous systems; however, when deficient, B12 might cause demyelination of peripheral and central neurons (Green et al., 2017; Calderón-Ospina and Nava-Mesa, 2020). In a case reported by Bram et al. (2015), a 60-year-old woman diagnosed with Biermer's disease was receiving a monthly IM dose of 1,000 μg/month of cyanocobalamin to treat her underlying condition. During admission, she started to present slow speech, apathy, minimal changes of facial expression, anxiety, a perplexed look, flat affect, poor spontaneous movements, waxy flexibility, and facial and manual stereotypies. Throughout time, consistently low levels of B12 were found, so finally the catatonic syndrome was resolved using 12 mg of lorazepam daily and cyanocobalamin injections every 3 weeks, the latter titrated to achieve B12 plasma concentrations of no less than 200 pg/ml. Few, but encouraging, cases report successful treatment of catatonia using cyanocobalamin injections (Berry et al., 2003). Whether deficiency of vitamin B12 is a cause, or a consequence of catatonia remains elusive; nonetheless, it is clear that vitamin B12 has an important antioxidant effect. The oxidative stress regulation mechanism encompasses scavenging of ROS, preservation of GSH, regulation of cytokine and growth factor production, reduction of homocysteine-induced OS, and diminishment of OS produced by advanced glycation end products (van de Lagemaat et al., 2019).

As it is well known, neither humans nor plants can produce cobalamin by themselves, said vitamin is exclusively obtained exogenously as a product of certain microorganisms,

especially anaerobes. Different model organisms have been studied for the biosynthesis of cobalamin, among which are *P. freudenreichii*, an organism used in the commercial production of vitamin B12, and more recently *Lactobacillus reuteri* CRL1098. The latter lactic acid bacteria has shown to produce a compound which closely resembles cobalamin which has led investigators to believe the use of said bacteria during food production might be a natural way to increase vitamin B12 levels avoiding side effects coming from chemically synthesized products (Taranto et al., 2003; LeBlanc et al., 2013). As previously mentioned, vitamin B12 deficiency's role in catatonia is yet to be further studied, however, as will be discussed in Section "Microbiota-gut-brain axis", maintaining a healthy and appropriate gut microbiota, especially *Lactobacillus reuteri* CRL1098, might be a pivotal aspect in preventing catatonia and the inflammatory consequences that it entails.

Microbiota-gut-brain axis

In recent decades, diverse studies have been carried out seeking to characterize and define the human microbiota. Today, microbiota are defined as a set of microorganisms that cohabit within humans (Lloyd-Price et al., 2016; Heintz-Buschart and Wilmes, 2018; Das and Nair, 2019). Microbiota contribute to body homeostasis through the regulation of metabolic processes, digestion and absorption of nutrients, regulation of gene expression, and modulation of proinflammatory and anti-inflammatory cytokines (Schirmer et al., 2016; Al Bander et al., 2020). Regarding CNS, the production of essential neurotransmitters and stabilization of BBB are worth noting as key functions of microbiota. Furthermore, a strong communication between the brain and gut has been proposed: the gut-brain axis. These systems are thought to be connected through the vagus nerve, and the lymphatic and circulatory systems. In this complex interaction, abnormalities at either end of the axis could therefore affect the other.

Considering the influence of microbiota on neurotransmitter production, and its modulation of BBB permeability and neuroinflammation, it is worth considering microbiota as a therapeutic target in CNS pathologies. Abundant literature describing the role of microbiota in autism spectrum disorders and SCZ, among others, has emerged (Jaskiw et al., 2019; Dong et al., 2022; Padhi et al., 2022). As described above, immune dysregulation is a hallmark in catatonia; in consequence, we consider that introducing prebiotics and probiotics could be promising as concurrent therapies in catatonia to help modulate BBB permeability, inflammation, and OS. An individualized characterization and posterior prescription of specific prebiotics and probiotics, or microbiota transfer therapy, can enhance microorganisms such as *F. prausnitzii, Acinetobacter spp., Bacteroides fragilis*, and *Proteobacteria*, which would stimulate short chain fatty acid production and in consequence could help to regulate systemic inflammation and therefore neuroinflammation (Blander et al., 2017). Nonetheless, as it is a new field of research, much speculation surrounds the literature, and careful assessment of each individual case must be carried out before initiating this therapy.

Conclusions

In conclusion, this review has described and assessed the broad literature surrounding catatonia and similar conditions to frame a translational explanation of the mechanisms underlying catatonia's etiology. The mechanisms underlying the onset of this syndrome are complex and involve variable aspects including the patient's condition and comorbidities. A relatively high frequency of catatonic syndrome is observed in patients with psychiatric conditions, with mood disorders being the most frequent, followed by psychotic syndrome and acute illness. Available evidence from clinical, neuroimaging, and preclinical research encourage us to list catatonia's hallmarks as inhibitory/excitatory imbalance, neuroinflammation, and OS. Additionally, the interactions between astrocytes, neurons, oligodendrocytes, and microglia determine the onset and progression of catatonia. Nonetheless, what exactly triggers catatonic symptoms is yet to be elucidated. When it comes to treatment, evidence suggests clinicians should always aim to treat the underlying condition first as it has been proven to be the most effective therapy. Current therapeutics such as BDZ and ECT are usually enough to resolve the syndrome when available, while other drugs such as amantadine and lithium are available and have shown consistent results to treat this condition. Bearing in mind the molecular and cellular mechanisms described and the lack of evidence around them, we encourage further research of other treatments like vitamin B12, COX inhibitors, microbiota reestablishment, and positive allosteric modulation of NMDAR to control OS and inflammation, as well as to reestablish the excitatory/inhibitory balance. Finally, encouraging research has been made on this disorder, nonetheless, there is still much more research to be done to fill the remaining voids.

Author contributions

DA-S: conceptualization, writing—review and editing, and **Figure 2** construction. DA-S, MC-H, and MP-L: writing—original draft preparation. MC-H and DA-S: **Figure 1** construction. IH-D: **Table 1** construction. MP-L: **Table 2**

construction. All authors contributed to the article and approved the submitted version.

Funding

This project was supported by the Universidad del Rosario.

Acknowledgments

We deeply thank Dr. Carlos Calderon-Ospina for his support throughout the time of this research. We thank Tim Hilley for his support in English proofreading and editing. We thank Laura Arango for illustrating the figures.

Conflict of interest

The authors declare that the research was conducted in the absence of any commercial or financial relationships that could be construed as a potential conflict of interest.

Publisher's note

References

Aandi Subramaniyam, B., Muliyala, K. P., Suchandra, H. H., and Reddi, V. S. K. (2020). Diagnosing catatonia and its dimensions: cluster analysis and factor solution using the Bush Francis Catatonia Rating Scale (BFCRS). *Asian J. Psychiatr.* 52:102002. doi: 10.1016/j.ajp.2020.102002

Al Bander, Z., Nitert, M. D., Mousa, A., and Naderpoor, N. (2020). The gut microbiota and inflammation: an overview. *Int. J. Environ. Res. Public Health* 17:E7618. doi: 10.3390/ijerph17207618

American Psychiatric Association (2013). *Diagnostic and Statistical Manual of Mental Disorders: DSM-5.* 5th ed. Washington, DC: American Psychiatric Association.

Aoki, F. Y., and Sitar, D. S. (1988). Clinical pharmacokinetics of amantadine hydrochloride. *Clin. Pharmacokinet.* 14, 35–51. doi: 10.2165/00003088-198814010-00003

Apetauerova, D., Patel, P. A., Burns, J. D., and Lerner, D. P. (2021). Movement disorder emergencies. *Neurol. Clin.* 39, 615–630. doi: 10.1016/j.ncl.2021.01.005

Arruda-Carvalho, M., and Clem, R. L. (2014). Pathway-selective adjustment of prefrontal-amygdala transmission during fear encoding. *J. Neurosci.* 34, 15601–15609. doi: 10.1523/JNEUROSCI.2664-14.2014

Babington, P. W., and Spiegel, D. R. (2007). Treatment of catatonia with olanzapine and amantadine. *Psychosomatics* 48, 534–536. doi: 10.1176/appi.psy.48.6.534

Báez-Mendoza, R., and Schultz, W. (2013). The role of the striatum in social behavior. *Front. Neurosci.* 7:233. doi: 10.3389/fnins.2013.00233

Banisadr, G., Frederick, T. J., Freitag, C., Ren, D., Jung, H., Miller, S. D., et al. (2011). The role of CXCR4 signaling in the migration of transplanted oligodendrocyte progenitors into the cerebral white matter. *Neurobiol. Dis.* 44, 19–27. doi: 10.1016/j.nbd.2011.05.019

Baracaldo-Santamaría, D., Ariza-Salamanca, D. F., Corrales-Hernández, M. G., Pachón-Londoño, M. J., Hernandez-Duarte, I., and Calderon-Ospina, C.-A. (2022). Revisiting excitotoxicity in traumatic brain injury: from bench to bedside. *Pharmaceutics* 14:152. doi: 10.3390/pharmaceutics14010152

Beach, S. R., Gomez-Bernal, F., Huffman, J. C., and Fricchione, G. L. (2017). Alternative treatment strategies for catatonia: a systematic review. *Gen. Hosp. Psychiatry* 48, 1–19. doi: 10.1016/j.genhosppsych.2017.06.011

Begemann, M. J., Brand, B. A., Ćurčić-Blake, B., Aleman, A., and Sommer, I. E. (2020). Efficacy of non-invasive brain stimulation on cognitive functioning in brain disorders: a meta-analysis. *Psychol. Med.* 50, 2465–2486. doi: 10.1017/S0033291720003670

Belteczki, Z., Ujvari, J., and Dome, P. (2021). Clozapine withdrawal-induced malignant catatonia or neuroleptic malignant syndrome: a case report and a brief review of the literature. *Clin. Neuropharmacol.* 44, 148–153. doi: 10.1097/WNF.0000000000000462

Berry, N., Sagar, R., and Tripathi, B. (2003). Catatonia and other psychiatric symptoms with vitamin B. *Acta Psychiatr. Scand.* 108, 156–159. doi: 10.1034/j.1600-0447.2003.00089.x

Bhangle, S. D., Kramer, N., and Rosenstein, E. D. (2013). Corticosteroid-induced neuropsychiatric disorders: review and contrast with neuropsychiatric lupus. *Rheumatol. Int.* 33, 1923–1932. doi: 10.1007/s00296-013-2750-z

Blander, J. M., Longman, R. S., Iliev, I. D., Sonnenberg, G. F., and Artis, D. (2017). Regulation of inflammation by microbiota interactions with the host. *Nat. Immunol.* 18, 851–860. doi: 10.1038/ni.3780

Bodnar, A., Krzywotulski, M., Lewandowska, A., Chlopocka-Wozniak, M., Bartkowska-Sniatkowska, A., Michalak, M., et al. (2016). Electroconvulsive therapy and cognitive functions in treatment-resistant depression. *World J. Biol. Psychiatry* 17, 159–164. doi: 10.3109/15622975.2015.1091501

Bostan, A. C., Dum, R. P., and Strick, P. L. (2018). Functional anatomy of basal ganglia circuits with the cerebral cortex and the cerebellum. *Prog. Neurol. Surg.* 33, 50–61. doi: 10.1159/000480748

Brailey, J., and Bastiampillai, T. (2020). Clozapine withdrawal malignant catatonia in a medical intensive care unit setting. *Asian J. Psychiatr.* 52:102043. doi: 10.1016/j.ajp.2020.102043

Bram, D., Bubrovszky, M., Durand, J.-P., Lefevre, G., Morell-Dubois, S., and Vaiva, G. (2015). Pernicious anemia presenting as catatonia: correlating vitamin B12 levels and catatonic symptoms. *Gen. Hosp. Psychiatry* 37, 273.e5–277.e5. doi: 10.1016/j.genhosppsych.2015.02.003

Bräunig, P., Krüger, S., and Shugar, G. (1998). Prevalence and clinical significance of catatonic symptoms in mania. *Compr. Psychiatry* 39, 35–46. doi: 10.1016/s0010-440x(98)90030-x

Bräunig, P., Krüger, S., Shugar, G., Höffler, J., and Börner, I. (2000). The catatonia rating scale I—Development, reliability and use. *Compr. Psychiatry* 41, 147–158. doi: 10.1016/s0010-440x(00)90148-2

Bush, G., Fink, M., Petrides, G., Dowling, F., and Francis, A. (1996). Catatonia. I. rating scale and standardized examination. *Acta Psychiatr. Scand.* 93, 129–136. doi: 10.1111/j.1600-0447.1996.tb09814.x

Butovsky, O., Ziv, Y., Schwartz, A., Landa, G., Talpalar, A. E., Pluchino, S., et al. (2006). Microglia activated by IL-4 or IFN-γ differentially induce neurogenesis and oligodendrogenesis from adult stem/progenitor cells. *Mol. Cell. Neurosci.* 31, 149–160. doi: 10.1016/j.mcn.2005.10.006

Calabresi, P., Picconi, B., Tozzi, A., Ghiglieri, V., and Di Filippo, M. (2014). Direct and indirect pathways of basal ganglia: a critical reappraisal. *Nat. Neurosci.* 17, 1022–1030. doi: 10.1038/nn.3743

Calderón-Ospina, C. A., and Nava-Mesa, M. O. (2020). B Vitamins in the nervous system: current knowledge of the biochemical modes of action and synergies of thiamine, pyridoxine and cobalamin. *CNS Neurosci. Ther.* 26, 5–13. doi: 10.1111/cns.13207

Camargo, N., Goudriaan, A., van Deijk, A.-L. F., Otte, W. M., Brouwers, J. F., Lodder, H., et al. (2017). Oligodendroglial myelination requires astrocyte-derived lipids. *PLoS Biol.* 15:e1002605. doi: 10.1371/journal.pbio.1002605

Carpenter, S. S., Hatchett, A. D., and Fuller, M. A. (2006). Catatonic schizophrenia and the use of memantine. *Ann. Pharmacother.* 40, 344–346. doi: 10.1345/aph.1G297

Carroll, B. T., Goforth, H. W., Thomas, C., Ahuja, N., McDaniel, W. W., Kraus, M. F., et al. (2007). Review of adjunctive glutamate antagonist therapy in the treatment of catatonic syndromes. *J. Neuropsychiatry Clin. Neurosci.* 19, 406–412. doi: 10.1176/jnp.2007.19.4.406

Cawkwell, P. B., Mayor, I. D., and Shaw, R. J. (2021). Catatonia in a 6-year-old patient following disseminated group A streptococcus infection. *Innov. Clin. Neurosci.* 18, 17–20. doi: 10.3389/fpsyt.2021.673166

Cha, J., Greenberg, T., Carlson, J. M., DeDora, D. J., Hajcak, G., and Mujica-Parodi, L. R. (2014). Circuit-wide structural and functional measures predict ventromedial prefrontal cortex fear generalization: implications for generalized anxiety disorder. *J. Neurosci.* 34, 4043–4053. doi: 10.1523/JNEUROSCI.3372-13.2014

Che, R., Tang, W., Zhang, J., Wei, Z., Zhang, Z., Huang, K., et al. (2009). No relationship between 2',3'-cyclic nucleotide 3'-phosphodiesterase and schizophrenia in the Chinese Han population: an expression study and meta-analysis. *BMC Med. Genet.* 10:31. doi: 10.1186/1471-2350-10-31

Conio, B., Martino, M., Magioncalda, P., Escelsior, A., Inglese, M., Amore, M., et al. (2020). Opposite effects of dopamine and serotonin on resting-state networks: review and implications for psychiatric disorders. *Mol. Psychiatry* 25, 82–93. doi: 10.1038/s41380-019-0406-4

Connell, J., Kim, A., Brummel, N. E., Patel, M. B., Vandekar, S. N., Pandharipande, P., et al. (2021). Advanced age is associated with catatonia in critical illness: results from the delirium and catatonia prospective cohort investigation. *Front. Psychiatry* 12:673166. doi: 10.3389/fpsyt.2021.673166

Cruz, S. L., Armenta-Reséndiz, M., Carranza-Aguilar, C. J., and Galván, E. J. (2020). Minocycline prevents neuronal hyperexcitability and neuroinflammation in medial prefrontal cortex, as well as memory impairment caused by repeated toluene inhalation in adolescent rats. *Toxicol. Appl. Pharmacol.* 395:114980. doi: 10.1016/j.taap.2020.114980

Cui, G., Jun, S. B., Jin, X., Pham, M. D., Vogel, S. S., Lovinger, D. M., et al. (2013). Concurrent activation of striatal direct and indirect pathways during action initiation. *Nature* 494, 238–242. doi: 10.1038/nature11846

Damasio, A., and Carvalho, G. B. (2013). The nature of feelings: evolutionary and neurobiological origins. *Nat. Rev. Neurosci.* 14, 143–152. doi: 10.1038/nrn3403

Daniels, J. (2009). Catatonia: clinical aspects and neurobiological correlates. *J. Neuropsychiatry Clin. Neurosci.* 21, 371–380. doi: 10.1176/jnp.2009.21.4.371

Das, B., and Nair, G. B. (2019). Homeostasis and dysbiosis of the gut microbiome in health and disease. *J. Biosci.* 44:117. doi: 10.1007/s12038-019-9926-y

de Kloet, S. F., Bruinsma, B., Terra, H., Heistek, T. S., Passchier, E. M. J., van den Berg, A. R., et al. (2021). Bi-directional regulation of cognitive control by distinct prefrontal cortical output neurons to thalamus and striatum. *Nat. Commun.* 12:1994. doi: 10.1038/s41467-021-22260-7

de Lucena, D. F., Pinto, J. P., Hallak, J. E., Crippa, J. A., and Gama, C. S. (2012). Short-term treatment of catatonia with amantadine in schizophrenia and schizoaffective disorder. *J. Clin. Psychopharmacol.* 32, 569–572. doi: 10.1097/JCP.0b013e31825ebf6e

Deister, A., and Marneros, A. (1994). Prognostic value of initial subtype in schizophrenic disorders. *Schizophr. Res.* 12, 145–157. doi: 10.1016/0920-9964(94)90072-8

Denysenko, L., Sica, N., Penders, T. M., Philbrick, K. L., Walker, A., Shaffer, S., et al. (2018). Catatonia in the medically ill: Etiology, diagnosis and treatment. The academy of consultation-liaison psychiatry evidence-based medicine subcommittee monograph. *Ann. Clin. Psychiatry* 30, 140–155.

Dhossche, D. M., and Withane, N. (2019). Electroconvulsive therapy for catatonia in children and adolescents. *Child Adolesc. Psychiatr. Clin. N. Am.* 28, 111–120. doi: 10.1016/j.chc.2018.07.007

Di Michele, V., and Bolino, F. (2006). A novel treatment option of bipolar depression with psychotic and catatonic features. *Gen. Hosp. Psychiatry* 28, 364–365. doi: 10.1016/j.genhosppsych.2006.05.003

Dierckx, B., Heijnen, W. T., van den Broek, W. W., and Birkenhäger, T. K. (2012). Efficacy of electroconvulsive therapy in bipolar versus unipolar major depression: a meta-analysis. *Bipolar Disord.* 14, 146–150. doi: 10.1111/j.1399-5618.2012.00997.x

Donello, J. E., Banerjee, P., Li, Y.-X., Guo, Y.-X., Yoshitake, T., Zhang, X.-L., et al. (2019). Positive N-Methyl-D-Aspartate receptor modulation by rapastinel promotes rapid and sustained antidepressant-like effects. *Int. J. Neuropsychopharmacol.* 22, 247–259. doi: 10.1093/ijnp/pyy101

Dong, L., Zheng, Q., Cheng, Y., Zhou, M., Wang, M., Xu, J., et al. (2022). Gut microbial characteristics of adult patients with epilepsy. *Front. Neurosci.* 16:803538. doi: 10.3389/fnins.2022.803538

Durns, T., Rich, B., Benson, C., Mickey, B., and Weischedel, K. (2020). A case of biopharmaceutical-induced catatonia and the implication of a novel mechanism. *J. ECT* 36, e29–e30. doi: 10.1097/YCT.0000000000000650

Edinoff, A. N., Kaufman, S. E., Hollier, J. W., Virgen, C. G., Karam, C. A., Malone, G. W., et al. (2021). Catatonia: clinical overview of the diagnosis, treatment and clinical challenges. *Neurol. Int.* 13, 570–586. doi: 10.3390/neurolint13040057

Ellul, P., and Choucha, W. (2015). Neurobiological approach of catatonia and treatment perspectives. *Front. Psychiatry* 6:182. doi: 10.3389/fpsyt.2015.00182

Ellul, P., Rotgé, J. Y., and Choucha, W. (2015). Resistant catatonia in a high-functioning autism spectrum disorder patient successfully treated with amantadine. *J. Child Adolesc. Psychopharmacol.* 25:726. doi: 10.1089/cap.2015.0064

Ene-Stroescu, V., Nguyen, T., and Waiblinger, B. E. (2014a). Excellent response to amantadine in a patient with bipolar disorder and catatonia. *J. Neuropsychiatry Clin. Neurosci.* 26:E43. doi: 10.1176/appi.neuropsych.13020038

Ene-Stroescu, V., Nguyen, T., and Waiblinger, B. E. (2014b). Successful treatment of catatonia in a young man with schizophrenia and progressive diffuse cerebral atrophy. *J. Neuropsychiatry Clin. Neurosci.* 26, E21–E22. doi: 10.1176/appi.neuropsych.13010007

Fathi-Moghaddam, H., Shafiee Ardestani, M., Saffari, M., Jabbari Arabzadeh, A., and Elmi, M. (2010). The selective cyclooxygenase-2 inhibitor, the compound 11b improves haloperidol induced catatonia by enhancing the striatum dopaminergic neurotransmission. *Iran. J. Pharm. Res.* 9, 387–393.

Fink, M., and Ottosson, J.-O. (1980). A theory of convulsive therapy in endogenous depression: significance of hypothalamic functions. *Psychiatry Res.* 2, 49–61. doi: 10.1016/0165-1781(80)90006-2

Fink, M., and Taylor, M. A. (2009). The catatonia syndrome: forgotten but not gone. *Arch. Gen. Psychiatry* 66, 1173–1177. doi: 10.1001/archgenpsychiatry.2009.141

Forlenza, O. V., De-Paula, V. J. R., and Diniz, B. S. O. (2014). Neuroprotective effects of lithium: implications for the treatment of Alzheimer's disease and related neurodegenerative disorders. *ACS Chem. Neurosci.* 5, 443–450. doi: 10.1021/cn5000309

Freeze, B. S., Kravitz, A. V., Hammack, N., Berke, J. D., and Kreitzer, A. C. (2013). Control of basal ganglia output by direct and indirect pathway projection neurons. *J. Neurosci.* 33, 18531–18539. doi: 10.1523/JNEUROSCI.1278-13.2013

Fritze, S., Brandt, G. A., Kubera, K. M., Schmitgen, M. M., Northoff, G., Geiger-Primo, L. S., et al. (2022). Structural alterations of amygdala and hypothalamus contribute to catatonia. *Schizophr. Res.* S0920-9964(22)00165-7. doi: 10.1016/j.schres.2022.05.003[Online ahead of print]

Fryml, L. D., Williams, K. R., Pelic, C. G., Fox, J., Sahlem, G., Robert, S., et al. (2017). The role of amantadine withdrawal in 3 cases of treatment-refractory altered mental status. *J. Psychiatr. Pract.* 23, 191–199. doi: 10.1097/PRA.0000000000000237

Fusar-Poli, P., Howes, O. D., Allen, P., Broome, M., Valli, I., Asselin, M.-C., et al. (2010). Abnormal frontostriatal interactions in people with prodromal signs of psychosis: a multimodal imaging study. *Arch. Gen. Psychiatry* 67, 683–691. doi: 10.1001/archgenpsychiatry.2010.77

Geoffroy, C., Paoletti, P., and Mony, L. (2022). Positive allosteric modulation of NMDA receptors: mechanisms, physiological impact and therapeutic potential. *J. Physiol.* 600, 233–259. doi: 10.1113/JP280875

Gerfen, C. R., and Surmeier, D. J. (2011). Modulation of striatal projection systems by dopamine. *Annu. Rev. Neurosci.* 34, 441–466. doi: 10.1146/annurev-neuro-061010-113641

Ghaziuddin, N., Hendriks, M., Patel, P., Wachtel, L. E., and Dhossche, D. M. (2017). Neuroleptic malignant syndrome/malignant catatonia in child psychiatry: literature review and a case series. *J. Child Adolesc. Psychopharmacol.* 27, 359–365. doi: 10.1089/cap.2016.0180

Goetz, M., Kitzlerova, E., Hrdlicka, M., and Dhossche, D. (2013). Combined use of electroconvulsive therapy and amantadine in adolescent catatonia precipitated by cyber-bullying. *J. Child Adolesc. Psychopharmacol.* 23, 228–231. doi: 10.1089/cap.2012.0045

Goforth, H. (2007). Amantadine in catatonia due to major depressive disorder in a medically ill patient. *J. Neuropsychiatry Clin. Neurosci.* 19, 480–481. doi: 10.1176/jnp.2007.19.4.480

González-Reyes, R. E., Nava-Mesa, M. O., Vargas-Sánchez, K., Ariza-Salamanca, D., and Mora-Muñoz, L. (2017). Involvement of astrocytes in Alzheimer's disease from a neuroinflammatory and oxidative stress perspective. *Front. Mol. Neurosci.* 10:427. doi: 10.3389/fnmol.2017.00427

Goodchild, C. S. (1993). GABA receptors and benzodiazepines. *Br. J. Anaesth.* 71, 127–133. doi: 10.1093/bja/71.1.127

Graff-Guerrero, A., Mizrahi, R., Agid, O., Marcon, H., Barsoum, P., Rusjan, P., et al. (2009). The dopamine D2 receptors in high-affinity state and D3 receptors in schizophrenia: a clinical [^{11}C]-(+)-PHNO PET study. *Neuropsychopharmacology* 34, 1078–1086. doi: 10.1038/npp.2008.199

Graybiel, A. M., Aosaki, T., Flaherty, A. W., and Kimura, M. (1994). The basal ganglia and adaptive motor control. *Science* 265, 1826–1831. doi: 10.1126/science.8091209

Green, R., Allen, L. H., Bjørke-Monsen, A.-L., Brito, A., Guéant, J.-L., Miller, J. W., et al. (2017). Vitamin B_{12} deficiency. *Nat. Rev. Dis. Primers* 3:17040. doi: 10.1038/nrdp.2017.40

Greenhalgh, A. D., David, S., and Bennett, F. C. (2020). Immune cell regulation of glia during CNS injury and disease. *Nat. Rev. Neurosci.* 21, 139–152. doi: 10.1038/s41583-020-0263-9

Gupta, A., Dhir, A., Kumar, A., and Kulkarni, S. K. (2009). Protective effect of cyclooxygenase (COX)-inhibitors against drug-induced catatonia and MPTP-induced striatal lesions in rats. *Pharmacol. Biochem. Behav.* 94, 219–226. doi: 10.1016/j.pbb.2009.07.018

Gupta, A., Kumar, A., and Kulkarni, S. K. (2011). Targeting oxidative stress, mitochondrial dysfunction and neuroinflammatory signaling by selective cyclooxygenase (COX)-2 inhibitors mitigates MPTP-induced neurotoxicity in mice. *Prog. Neuropsychopharmacol. Biol. Psychiatry* 35, 974–981. doi: 10.1016/j.pnpbp.2011.01.017

Hagemeyer, N., Goebbels, S., Papiol, S., Kästner, A., Hofer, S., Begemann, M., et al. (2012). A myelin gene causative of a catatonia-depression syndrome upon aging. *EMBO Mol. Med.* 4, 528–539. doi: 10.1002/emmm.201200230

Hagemeyer, N., Hanft, K.-M., Akriditou, M.-A., Unger, N., Park, E. S., Stanley, E. R., et al. (2017). Microglia contribute to normal myelinogenesis and to oligodendrocyte progenitor maintenance during adulthood. *Acta Neuropathol.* 134, 441–458. doi: 10.1007/s00401-017-1747-1

Hare, B. D., Pothula, S., DiLeone, R. J., and Duman, R. S. (2020). Ketamine increases vmPFC activity: effects of (R)- and (S)-stereoisomers and (2R,6R)-hydroxynorketamine metabolite. *Neuropharmacology* 166:107947. doi: 10.1016/j.neuropharm.2020.107947

Haroche, A., Rogers, J., Plaze, M., Gaillard, R., Williams, S. C., Thomas, P., et al. (2020). Brain imaging in catatonia: systematic review and directions for future research. *Psychol. Med.* 50, 1585–1597. doi: 10.1017/S0033291720001853

Haskett, R. F. (2014). Electroconvulsive therapy's mechanism of action: neuroendocrine hypotheses. *J. ECT* 30, 107–110. doi: 10.1097/YCT.0000000000000143

Heintz-Buschart, A., and Wilmes, P. (2018). Human gut microbiome: function matters. *Trends Microbiol.* 26, 563–574. doi: 10.1016/j.tim.2017.11.002

Hermida, A. P., Glass, O. M., Shafi, H., and McDonald, W. M. (2018). Electroconvulsive therapy in depression: current practice and future direction. *Psychiatr. Clin. North Am.* 41, 341–353. doi: 10.1016/j.psc.2018.04.001

Hervey, W. M., Stewart, J. T., and Catalano, G. (2012). Treatment of catatonia with amantadine. *Clin. Neuropharmacol.* 35, 86–87. doi: 10.1097/WNF.0b013e318246ad34

Hervey, W. M., Stewart, J. T., and Catalano, G. (2013). Diagnosis and management of periodic catatonia. *J. Psychiatry Neurosci.* 38, E7–E8. doi: 10.1503/jpn.120249

Hirjak, D., Kubera, K. M., Northoff, G., Fritze, S., Bertolino, A. L., Topor, C. E., et al. (2019a). Cortical contributions to distinct symptom dimensions of catatonia. *Schizophr. Bull.* 45, 1184–1194. doi: 10.1093/schbul/sby192

Hirjak, D., Wolf, R. C., and Northoff, G. (2019b). GABA and negative affect—catatonia as model of RDoC-based investigation in psychiatry. *Schizophr. Bull.* 45, 1168–1169. doi: 10.1093/schbul/sbz088

Hirjak, D., Thomann, P. A., Kubera, K. M., Wolf, N. D., Sambataro, F., and Wolf, R. C. (2015). Motor dysfunction within the schizophrenia-spectrum: a dimensional step towards an underappreciated domain. *Schizophr. Res.* 169, 217–233. doi: 10.1016/j.schres.2015.10.022

Howes, O. D., and Kapur, S. (2009). The dopamine hypothesis of schizophrenia: version III–the final common pathway. *Schizophr. Bull.* 35, 549–562. doi: 10.1093/schbul/sbp006

Howes, O. D., and Nour, M. M. (2016). Dopamine and the aberrant salience hypothesis of schizophrenia. *World Psychiatry* 15, 3–4. doi: 10.1002/wps.20276

Howes, O. D., Williams, M., Ibrahim, K., Leung, G., Egerton, A., McGuire, P. K., et al. (2013). Midbrain dopamine function in schizophrenia and depression: a post-mortem and positron emission tomographic imaging study. *Brain* 136, 3242–3251. doi: 10.1093/brain/awt264

Janova, H., Arinrad, S., Balmuth, E., Mitjans, M., Hertel, J., Habes, M., et al. (2018). Microglia ablation alleviates myelin-associated catatonic signs in mice. *J. Clin. Investig.* 128, 734–745. doi: 10.1172/JCI97032

Jaskiw, G. E., Obrenovich, M. E., and Donskey, C. J. (2019). The phenolic interactome and gut microbiota: opportunities and challenges in developing applications for schizophrenia and autism. *Psychopharmacology (Berl)* 236, 1471–1489. doi: 10.1007/s00213-019-05267-3

Jeong, S. H., Youn, T., Lee, Y., Jang, J. H., Jeong, Y. W., Kim, Y. S., et al. (2019). Initial seizure threshold in brief-pulse bilateral electroconvulsive therapy in patients with schizophrenia or schizoaffective disorder. *Psychiatry Investig.* 16, 704–712. doi: 10.30773/pi.2019.06.20.2

Kaliora, S. C., Zervas, I. M., and Papadimitriou, G. N. (2018). [Electroconvulsive therapy: 80 years of use in psychiatry]. *Psychiatriki* 29, 291–302. doi: 10.22365/jpsych.2018.294.291

Kato, T., and Duman, R. S. (2020). Rapastinel, a novel glutamatergic agent with ketamine-like antidepressant actions: convergent mechanisms. *Pharmacol. Biochem. Behav.* 188:172827. doi: 10.1016/j.pbb.2019.172827

Kellner, C. H., Obbels, J., and Sienaert, P. (2020). When to consider electroconvulsive therapy (ECT). *Acta Psychiatr. Scand.* 141, 304–315. doi: 10.1111/acps.13134

Korkeila, J. (2016). Catatonia. *Duodecim* 132, 1321–1327.

Kouidrat, Y., Amad, A., Desailloud, R., Diouf, M., Fertout, E., Scoury, D., et al. (2013). Increased advanced glycation end-products (AGEs) assessed by skin autofluorescence in schizophrenia. *J. Psychiatr. Res.* 47, 1044–1048. doi: 10.1016/j.jpsychires.2013.03.016

Krestinina, O., Azarashvili, T., Baburina, Y., Galvita, A., Grachev, D., Stricker, R., et al. (2015). In aging, the vulnerability of rat brain mitochondria is enhanced due to reduced level of 2',3'-cyclic nucleotide-3'-phosphodiesterase (CNP) and subsequently increased permeability transition in brain mitochondria in old animals. *Neurochem. Int.* 80, 41–50. doi: 10.1016/j.neuint.2014.09.008

Kritzinger, P. R., and Jordaan, G. P. (2001). Catatonia: an open prospective series with carbamazepine. *Int. J. Neuropsychopharmacol.* 4, 251–257. doi: 10.1017/S1461145701002486

Kumakura, Y., Cumming, P., Vernaleken, I., Buchholz, H.-G., Siessmeier, T., Heinz, A., et al. (2007). Elevated [^{18}F]fluorodopamine turnover in brain of patients with schizophrenia: an [^{18}F]fluorodopa/positron emission tomography study. *J. Neurosci.* 27, 8080–8087. doi: 10.1523/JNEUROSCI.0805-07.2007

Lanciego, J. L., Luquin, N., and Obeso, J. A. (2012). Functional neuroanatomy of the basal ganglia. *Cold Spring Harb. Perspect. Med.* 2:a009621. doi: 10.1101/cshperspect.a009621

Lander, M., Bastiampillai, T., and Sareen, J. (2018). Review of withdrawal catatonia: what does this reveal about clozapine? *Transl. Psychiatry* 8:139. doi: 10.1038/s41398-018-0192-9

LeBlanc, J. G., Milani, C., de Giori, G. S., Sesma, F., van Sinderen, D., and Ventura, M. (2013). Bacteria as vitamin suppliers to their host: a gut microbiota perspective. *Curr. Opin. Biotechnol.* 24, 160–168. doi: 10.1016/j.copbio.2012.08.005

Lee, J. W. (1998). Serum iron in catatonia and neuroleptic malignant syndrome. *Biol. Psychiatry* 44, 499–507. doi: 10.1016/s0006-3223(98)00109-7

Lee, J. W. Y. (2010). Neuroleptic-induced catatonia: clinical presentation, response to benzodiazepines and relationship to neuroleptic malignant syndrome. *J. Clin. Psychopharmacol.* 30, 3–10. doi: 10.1097/JCP.0b013e3181c9bfe6

Lee, A. T., Vogt, D., Rubenstein, J. L., and Sohal, V. S. (2014). A class of GABAergic neurons in the prefrontal cortex sends long-range projections to the nucleus accumbens and elicits acute avoidance behavior. *J. Neurosci.* 34, 11519–11525. doi: 10.1523/JNEUROSCI.1157-14.2014

Liang, Z., Wang, X., Hao, Y., Qiu, L., Lou, Y., Zhang, Y., et al. (2020). The multifaceted role of astrocyte connexin 43 in ischemic stroke through forming hemichannels and gap junctions. *Front. Neurol.* 11:703. doi: 10.3389/fneur.2020.00703

Lingappan, K. (2018). NF-κB in oxidative stress. *Curr. Opin. Toxicol.* 7, 81–86. doi: 10.1016/j.cotox.2017.11.002

Liu, L.-R., Liu, J.-C., Bao, J.-S., Bai, Q.-Q., and Wang, G.-Q. (2020). Interaction of microglia and astrocytes in the neurovascular unit. *Front. Immunol.* 11:1024. doi: 10.3389/fimmu.2020.01024

Lloyd, J. R., Silverman, E. R., Kugler, J. L., and Cooper, J. J. (2020). Electroconvulsive therapy for patients with catatonia: current perspectives. *Neuropsychiatr. Dis. Treat.* 16, 2191–2208. doi: 10.2147/NDT.S231573

Lloyd-Price, J., Abu-Ali, G., and Huttenhower, C. (2016). The healthy human microbiome. *Genome Med.* 8:51. doi: 10.1186/s13073-016-0307-y

Luchini, F., Medda, P., Mariani, M. G., Mauri, M., Toni, C., and Perugi, G. (2015). Electroconvulsive therapy in catatonic patients: Efficacy and predictors of response. *World J. Psychiatry* 5, 182–192. doi: 10.5498/wjp.v5.i2.182

Madigand, J., Lebain, P., Callery, G., and Dollfus, S. (2016). Catatonic syndrome: from detection to therapy. *Encephale* 42, 340–345. doi: 10.1016/j.encep.2015.09.008

Martino, M., Magioncalda, P., Conio, B., Capobianco, L., Russo, D., Adavastro, G., et al. (2020). Abnormal functional relationship of sensorimotor network with neurotransmitter-related nuclei *via* subcortical-cortical loops in manic and depressive phases of bipolar disorder. *Schizophr. Bull.* 46, 163–174. doi: 10.1093/schbul/sbz035

Mashayekhi, A., and Ghayoumi, A. (2019). Catatonia development in a patient with bipolar disorder following electroconvulsive therapy: a case report. *Iran. J. Psychiatry* 14, 109–112. doi: 10.18502/ijps.v14i1.429

McClintock, S. M., Reti, I. M., Carpenter, L. L., McDonald, W. M., Dubin, M., Taylor, S. F., et al. (2018). Consensus recommendations for the clinical application of repetitive transcranial magnetic stimulation (rTMS) in the treatment of depression. *J. Clin. Psychiatry* 79:16cs10905. doi: 10.4088/JCP.16cs10905

McCutcheon, R. A., Reis Marques, T., and Howes, O. D. (2020). Schizophrenia-an overview. *JAMA Psychiatry* 77, 201–210. doi: 10.1001/jamapsychiatry.2019.3360

Mehta, U. M., Basavaraju, R., and Thirthalli, J. (2013). Mirror neuron disinhibition may be linked with catatonic echo-phenomena: a single case TMS study. *Brain Stimul.* 6, 705–707. doi: 10.1016/j.brs.2012.12.002

Merida-Puga, J., Ramirez-Bermudez, J., Aguilar-Venegas, L. C., Fricchione, G. L., and Espinola-Nadurille, M. (2011). Westphal variant Huntington disease and refractory catatonia: a case report. *Cogn. Behav. Neurol.* 24, 204–208. doi: 10.1097/WNN.0b013e318240080d

Meyer, J. P., Swetter, S. K., and Kellner, C. H. (2018). Electroconvulsive therapy in geriatric psychiatry: a selective review. *Psychiatr. Clin. North Am.* 41, 79–93. doi: 10.1016/j.psc.2017.10.007

Miron, V. E., Boyd, A., Zhao, J.-W., Yuen, T. J., Ruckh, J. M., Shadrach, J. L., et al. (2013). M2 microglia and macrophages drive oligodendrocyte differentiation during CNS remyelination. *Nat. Neurosci.* 16, 1211–1218. doi: 10.1038/nn.3469

Miyaoka, T., Yasukawa, R., Yasuda, H., Hayashida, M., Inagaki, T., and Horiguchi, J. (2007). Possible antipsychotic effects of minocycline in patients with schizophrenia. *Prog. Neuropsychopharmacol. Biol. Psychiatry* 31, 304–307. doi: 10.1016/j.pnpbp.2006.08.013

Montague, P. R., Hyman, S. E., and Cohen, J. D. (2004). Computational roles for dopamine in behavioural control. *Nature* 431, 760–767. doi: 10.1038/nature03015

Moskowitz, A. K. (2004). "Scared stiff": catatonia as an evolutionary-based fear response. *Psychol. Rev.* 111, 984–1002. doi: 10.1037/0033-295X.111.4.984

Motzkin, J. C., Philippi, C. L., Wolf, R. C., Baskaya, M. K., and Koenigs, M. (2015). Ventromedial prefrontal cortex is critical for the regulation of amygdala activity in humans. *Biol. Psychiatry* 77, 276–284. doi: 10.1016/j.biopsych.2014.02.014

Moussa, T., Afzal, K., Cooper, J., Rosenberger, R., Gerstle, K., and Wagner-Weiner, L. (2019). Pediatric anti-NMDA receptor encephalitis with catatonia: treatment with electroconvulsive therapy. *Pediatr. Rheumatol. Online J.* 17:8. doi: 10.1186/s12969-019-0310-0

Mukai, Y., Two, A., and Jean-Baptiste, M. (2011). Chronic catatonia with obsessive compulsive disorder symptoms treated with lorazepam, memantine, aripiprazole, fluvoxamine and neurosurgery. *BMJ Case Rep.* 2011:bcr0220113858. doi: 10.1136/bcr.02.2011.3858

Myllykoski, M., Raasakka, A., Han, H., and Kursula, P. (2012). Myelin 2′,3′-cyclic nucleotide 3′-phosphodiesterase: active-site ligand binding and molecular conformation. *PLoS One* 7:e32336. doi: 10.1371/journal.pone.0032336

Nagy, J. I., and Rash, J. E. (2003). Astrocyte and oligodendrocyte connexins of the glial syncytium in relation to astrocyte anatomical domains and spatial buffering. *Cell Commun. Adhes.* 10, 401–406. doi: 10.1080/15419060390263191

Nambu, A., Tokuno, H., and Takada, M. (2002). Functional significance of the cortico-subthalamo-pallidal "hyperdirect" pathway. *Neurosci. Res.* 43, 111–117. doi: 10.1016/s0168-0102(02)00027-5

Naurex, Inc, an affiliate of Allergan plc. (2020). A randomized, double-blind, placebo-controlled, multicenter study of rapastinel as adjunctive therapy in the prevention of relapse in patients with major depressive disorder. Available online at: https://clinicaltrials.gov/ct2/show/NCT02951988. Accessed March 28, 2022.

Nolen, W. A., and Zwaan, W. A. (1990). Treatment of lethal catatonia with electroconvulsive therapy and dantrolene sodium: a case report. *Acta Psychiatr. Scand.* 82, 90–92. doi: 10.1111/j.1600-0447.1990.tb01364.x

Northoff, G. (2002). What catatonia can tell us about "top-down modulation": a neuropsychiatric hypothesis. *Behav. Brain Sci.* 25, 555–577. doi: 10.1017/s0140525x02000109

Northoff, G., Eckert, J., and Fritze, J. (1997). Glutamatergic dysfunction in catatonia? Successful treatment of three acute akinetic catatonic patients with the NMDA antagonist amantadine. *J. Neurol. Neurosurg. Psychiatry* 62, 404–406. doi: 10.1136/jnnp.62.4.404

Northoff, G., Hirjak, D., Wolf, R. C., Magioncalda, P., and Martino, M. (2021). All roads lead to the motor cortex: psychomotor mechanisms and their biochemical modulation in psychiatric disorders. *Mol. Psychiatry* 26, 92–102. doi: 10.1038/s41380-020-0814-5

Northoff, G., Koch, A., Wenke, J., Eckert, J., Böker, H., Pflug, B., et al. (1999a). Catatonia as a psychomotor syndrome: a rating scale and extrapyramidal motor symptoms. *Mov. Disord.* 14, 404–416. doi: 10.1002/1531-8257(199905)14:3<404::aid-mds1004>3.0.co;2-5

Northoff, G., Steinke, R., Czcervenka, C., Krause, R., Ulrich, S., Danos, P., et al. (1999b). Decreased density of GABA-A receptors in the left sensorimotor cortex in akinetic catatonia: investigation of *in vivo* benzodiazepine receptor binding. *J. Neurol. Neurosurg. Psychiatry* 67, 445–450. doi: 10.1136/jnnp.67.4.445

Northoff, G., Waters, H., Mooren, I., Schlüter, U., Diekmann, S., Falkai, P., et al. (1999c). Cortical sulcal enlargement in catatonic schizophrenia: a planimetric CT study. *Psychiatry Res.* 91, 45–54. doi: 10.1016/s0925-4927(99)00024-4

Northoff, G., Kötter, R., Baumgart, F., Danos, P., Boeker, H., Kaulisch, T., et al. (2004). Orbitofrontal cortical dysfunction in akinetic catatonia: a functional magnetic resonance imaging study during negative emotional stimulation. *Schizophr. Bull.* 30, 405–427. doi: 10.1093/oxfordjournals.schbul.a007088

Northoff, G., Wenke, J., Demisch, L., Eckert, J., Gille, B., and Pflug, B. (1995). Catatonia: short-term response to lorazepam and dopaminergic metabolism. *Psychopharmacology (Berl)* 122, 182–186. doi: 10.1007/BF02246093

Obregon, D. F., Velasco, R. M., Wuerz, T. P., Catalano, M. C., Catalano, G., and Kahn, D. (2011). Memantine and catatonia: a case report and literature review. *J. Psychiatr. Pract.* 17, 292–299. doi: 10.1097/01.pra.0000400268.60537.5e

Ocampo, F. F., Matic, A. E., Cruz, M. G., and Damian, L. F. (2022). Treatment of stuporous catatonia with repetitive transcranial magnetic stimulation (rTMS) therapy in a Filipino adult patient: a case report. *Asian J. Psychiatr.* 67:102946. doi: 10.1016/j.ajp.2021.102946

Ohry, A. (1990). The locked-in syndrome and related states. *Paraplegia* 28, 73–75. doi: 10.1038/sc.1990.8

Orthmann-Murphy, J. L., Abrams, C. K., and Scherer, S. S. (2008). Gap junctions couple astrocytes and oligodendrocytes. *J. Mol. Neurosci.* 35, 101–116. doi: 10.1007/s12031-007-9027-5

Padhi, P., Worth, C., Zenitsky, G., Jin, H., Sambamurti, K., Anantharam, V., et al. (2022). Mechanistic insights into gut microbiome dysbiosis-mediated neuroimmune dysregulation and protein misfolding and clearance in the pathogenesis of chronic neurodegenerative disorders. *Front. Neurosci.* 16:836605. doi: 10.3389/fnins.2022.836605

Padhy, S. K., Subodh, B., Bharadwaj, R., Arun Kumar, K., Kumar, S., and Srivastava, M. (2011). Recurrent catatonia treated with lithium and carbamazepine: a series of 2 cases. *Prim. Care Companion CNS Disord.* 13:PCC.10l00992. doi: 10.4088/PCC.10l00992

Pahwa, R. (2021). Amantadine: an old drug reborn. *Lancet Neurol.* 20, 975–977. doi: 10.1016/S1474-4422(21)00356-2

Paparrigopoulos, T., Tzavellas, E., Ferentinos, P., Mourikis, I., and Liappas, J. (2009). Catatonia as a risk factor for the development of neuroleptic malignant syndrome: report of a case following treatment with clozapine. *World J. Biol. Psychiatry* 10, 70–73. doi: 10.1080/15622970701287369

Pelzer, A. C., van der Heijden, F. M., and den Boer, E. (2018). Systematic review of catatonia treatment. *Neuropsychiatr. Dis. Treat.* 14, 317–326. doi: 10.2147/NDT.S147897

Pennati, A., Sacchetti, E., and Calzeroni, A. (1991). Dantrolene in lethal catatonia. *Am. J. Psychiatry* 148:268.

Perugi, G., Medda, P., Toni, C., Mariani, M. G., Socci, C., and Mauri, M. (2017). The role of electroconvulsive therapy (ECT) in bipolar disorder: effectiveness in

522 patients with bipolar depression, mixed-state, mania and catatonic features. *Curr. Neuropharmacol.* 15, 359–371. doi: 10.2174/1570159X14666161017233642

Philbrick, K. L., and Rummans, T. A. (1994). Malignant catatonia. *J. Neuropsychiatry Clin. Neurosci.* 6, 1–13. doi: 10.1176/jnp.6.1.1

Poggi, G., Boretius, S., Möbius, W., Moschny, N., Baudewig, J., Ruhwedel, T., et al. (2016). Cortical network dysfunction caused by a subtle defect of myelination. *Glia* 64, 2025–2040. doi: 10.1002/glia.23039

Prinz, M., and Priller, J. (2014). Microglia and brain macrophages in the molecular age: from origin to neuropsychiatric disease. *Nat. Rev. Neurosci.* 15, 300–312. doi: 10.1038/nrn3722

Qi, J.-H., and Dong, F.-X. (2021). The relevant targets of anti-oxidative stress: a review. *J. Drug Target.* 29, 677–686. doi: 10.1080/1061186X.2020.1870987

Qin, L., Liu, Y., Hong, J.-S., and Crews, F. T. (2013). NADPH oxidase and aging drive microglial activation, oxidative stress and dopaminergic neurodegeneration following systemic LPS administration. *Glia* 61, 855–868. doi: 10.1002/glia.22479

Quinn, D. K., and Abbott, C. C. (2014). Catatonia after cerebral hypoxia: do the usual treatments apply? *Psychosomatics* 55, 525–535. doi: 10.1016/j.psym.2014.03.010

Raasakka, A., and Kursula, P. (2020). Flexible players within the sheaths: the intrinsically disordered proteins of myelin in health and disease. *Cells* 9:470. doi: 10.3390/cells9020470

Ragguett, R.-M., Rong, C., Kratiuk, K., and McIntyre, R. S. (2019). Rapastinel - an investigational NMDA-R modulator for major depressive disorder: evidence to date. *Expert Opin. Investig. Drugs* 28, 113–119. doi: 10.1080/13543784.2019.1559295

Rankel, H. W., and Rankel, L. E. (1988). Carbamazepine in the treatment of catatonia. *Am. J. Psychiatry* 145, 361–362. doi: 10.1176/ajp.145.3.361

Rasmussen, S. A., Mazurek, M. F., and Rosebush, P. I. (2016). Catatonia: our current understanding of its diagnosis, treatment and pathophysiology. *World J. Psychiatry* 6, 391–398. doi: 10.5498/wjp.v6.i4.391

Rempel-Clower, N. L. (2007). Role of orbitofrontal cortex connections in emotion. *Ann. N. Y. Acad. Sci.* 1121, 72–86. doi: 10.1196/annals.1401.026

Rogers, J. P., Pollak, T. A., Blackman, G., and David, A. S. (2019). Catatonia and the immune system: a review. *Lancet Psychiatry* 6, 620–630. doi: 10.1016/S2215-0366(19)30190-7

Roiser, J. P., Howes, O. D., Chaddock, C. A., Joyce, E. M., and McGuire, P. (2013). Neural and behavioral correlates of aberrant salience in individuals at risk for psychosis. *Schizophr. Bull.* 39, 1328–1336. doi: 10.1093/schbul/sbs147

Roy, K., Warnick, S. J., and Balon, R. (2016). Catatonia Delirium: 3 Cases Treated With Memantine. *Psychosomatics* 57, 645–650. doi: 10.1016/j.psym.2016.08.001

Sakhardande, K. A., Pathak, H., Mahadevan, J., Muliyala, K. P., Moirangthem, S., and Reddi, V. S. K. (2022). Concurrent catatonia and COVID-19 infection - an experiential account of challenges and management of cases from a tertiary care psychiatric hospital in India. *Asian J. Psychiatr.* 69:103004. doi: 10.1016/j.ajp.2022.103004

Samra, K., Rogers, J., Mahdi-Rogers, M., and Stanton, B. (2020). Catatonia with GABAA receptor antibodies. *Pract. Neurol.* 20, 139–143. doi: 10.1136/practneurol-2019-002388

Scherer, S. S., Braun, P. E., Grinspan, J., Collarini, E., Wang, D. -y., Kamholz, J., et al. (1994). Differential regulation of the 2′,3′-cyclic nucleotide 3′-phosphodiesterase gene during oligodendrocyte development. *Neuron* 12, 1363–1375. doi: 10.1016/0896-6273(94)90451-0

Scheuerecker, J., Ufer, S., Käpernick, M., Wiesmann, M., Brückmann, H., Kraft, E., et al. (2009). Cerebral network deficits in post-acute catatonic schizophrenic patients measured by fMRI. *J. Psychiatr. Res.* 43, 607–614. doi: 10.1016/j.jpsychires.2008.08.005

Schirmer, M., Smeekens, S. P., Vlamakis, H., Jaeger, M., Oosting, M., Franzosa, E. A., et al. (2016). Linking the human gut microbiome to inflammatory cytokine production capacity. *Cell* 167, 1125–1136.e8. doi: 10.1016/j.cell.2016.10.020

Schultz, W., Dayan, P., and Montague, P. R. (1997). A neural substrate of prediction and reward. *Science* 275, 1593–1599. doi: 10.1126/science.275.5306.1593

Seeman, P. (2013a). Schizophrenia and dopamine receptors. *Eur. Neuropsychopharmacol.* 23, 999–1009. doi: 10.1016/j.euroneuro.2013.06.005

Seeman, P. (2013b). Clozapine, a fast-Off-D2 antipsychotic. *ACS Chem. Neurosci.* 5, 24–29. doi: 10.1021/cn400189s

Seeman, P., Chau-Wong, M., Tedesco, J., and Wong, K. (1975). Brain receptors for antipsychotic drugs and dopamine: direct binding assays. *Proc. Natl. Acad. Sci. U S A* 72, 4376–4380. doi: 10.1073/pnas.72.11.4376

Seeman, P., Schwarz, J., Chen, J.-F., Szechtman, H., Perreault, M., McKnight, G. S., et al. (2006). Psychosis pathways converge via $D2^{high}$ dopamine receptors. *Synapse* 60, 319–346. doi: 10.1002/syn.20303

Seeman, M. V., and Seeman, P. (2014). Is schizophrenia a dopamine supersensitivity psychotic reaction? *Prog. Neuropsychopharmacol. Biol. Psychiatry* 48, 155–160. doi: 10.1016/j.pnpbp.2013.10.003

Sienaert, P., Dhossche, D. M., Vancampfort, D., De Hert, M., and Gazdag, G. (2014). A clinical review of the treatment of catatonia. *Front. Psychiatry* 5:181. doi: 10.3389/fpsyt.2014.00181

Sienaert, P., Rooseleer, J., and De Fruyt, J. (2011). Measuring catatonia: a systematic review of rating scales. *J. Affect. Disord.* 135, 1–9. doi: 10.1016/j.jad.2011.02.012

Sienaert, P., van Harten, P., and Rhebergen, D. (2019). The psychopharmacology of catatonia, neuroleptic malignant syndrome, akathisia, tardive dyskinesia and dystonia. *Handb. Clin. Neurol.* 165, 415–428. doi: 10.1016/B978-0-444-64012-3.00025-3

Sies, H. (2015). Oxidative stress: a concept in redox biology and medicine. *Redox Biol.* 4, 180–183. doi: 10.1016/j.redox.2015.01.002

Smith, Y., Bevan, M. D., Shink, E., and Bolam, J. P. (1998). Microcircuitry of the direct and indirect pathways of the basal ganglia. *Neuroscience* 86, 353–387. doi: 10.1016/s0306-4522(98)00004-9

Sock, E., and Wegner, M. (2019). Transcriptional control of myelination and remyelination. *Glia* 67, 2153–2165. doi: 10.1002/glia.23636

Solmi, M., Pigato, G. G., Roiter, B., Guaglianone, A., Martini, L., Fornaro, M., et al. (2018). Prevalence of catatonia and its moderators in clinical samples: results from a meta-analysis and meta-regression analysis. *Schizophr. Bull.* 44, 1133–1150. doi: 10.1093/schbul/sbx157

Spampinato, C., Aguglia, E., Concerto, C., Pennisi, M., Lanza, G., Bella, R., et al. (2013). Transcranial magnetic stimulation in the assessment of motor cortex excitability and treatment of drug-resistant major depression. *IEEE Trans. Neural Syst. Rehabil. Eng.* 21, 391–403. doi: 10.1109/TNSRE.2013.2256432

Stuivenga, M., and Morrens, M. (2014). Prevalence of the catatonic syndrome in an acute inpatient sample. *Front. Psychiatry* 5:174. doi: 10.3389/fpsyt.2014.00174

Sugawara, H., Takamatsu, J., Hashimoto, M., and Ikeda, M. (2021). Catatonia associated with late-life psychosis successfully treated with lithium: a case report. *Ann. Gen. Psychiatry* 20:14. doi: 10.1186/s12991-021-00336-4

Tandon, R., Heckers, S., Bustillo, J., Barch, D. M., Gaebel, W., Gur, R. E., et al. (2013). Catatonia in DSM-5. *Schizophr. Res.* 150, 26–30. doi: 10.1016/j.schres.2013.04.034

Tang, F., Qu, M., Wang, L., Ruan, Y., Lu, T., Zhang, H., et al. (2007). Case-control association study of the 2′,3′-cyclic nucleotide 3′-phosphodiesterase (CNP) gene and schizophrenia in the Han Chinese population. *Neurosci. Lett.* 416, 113–116. doi: 10.1016/j.neulet.2007.01.054

Taranto, M. P., Vera, J. L., Hugenholtz, J., De Valdez, G. F., and Sesma, F. (2003). Lactobacillus reuteri CRL1098 produces cobalamin. *J. Bacteriol.* 185, 5643–5647. doi: 10.1128/JB.185.18.5643-5647.2003

Thippaiah, S. M., Fargason, R. E., Gude, J. G., Muralidhara, S. N., and Birur, B. (2021). Lithium-associated hyperparathyroidism followed by catatonia. *AACE Clin. Case Rep.* 7, 189–191. doi: 10.1016/j.aace.2020.12.010

Thomas, C., Carroll, B. T., Maley, R. T., Jayanti, K., and Koduri, A. (2005). Memantine and catatonic schizophrenia. *Am. J. Psychiatry* 162:626. doi: 10.1176/appi.ajp.162.3.626

Tikka, T., Fiebich, B. L., Goldsteins, G., Keinänen, R., and Koistinaho, J. (2001). Minocycline, a tetracycline derivative, is neuroprotective against excitotoxicity by inhibiting activation and proliferation of microglia. *J. Neurosci.* 21, 2580–2588. doi: 10.1523/JNEUROSCI.21-08-02580.2001

Tormoehlen, L. M., and Rusyniak, D. E. (2018). Neuroleptic malignant syndrome and serotonin syndrome. *Handb. Clin. Neurol.* 157, 663–675. doi: 10.1016/B978-0-444-64074-1.00039-2

Trojak, B., Meille, V., Bonin, B., and Chauvet-Geliner, J.-C. (2014). Repetitive transcranial magnetic stimulation for the treatment of catatonia: an alternative treatment to electroconvulsive therapy? *J. Neuropsychiatry Clin. Neurosci.* 26, E42–E43. doi: 10.1176/appi.neuropsych.13050102

Ungvari, G. S., Leung, S. K., Ng, F. S., Cheung, H.-K., and Leung, T. (2005). Schizophrenia with prominent catatonic features ('catatonic schizophrenia'): i. Demographic and clinical correlates in the chronic phase. *Prog. Neuropsychopharmacol. Biol. Psychiatry* 29, 27–38. doi: 10.1016/j.pnpbp.2004.08.007

van de Lagemaat, E. E., de Groot, L. C. P. G. M., and van den Heuvel, E. G. H. M. (2019). Vitamin B12 in relation to oxidative stress: a systematic review. *Nutrients* 11:E482. doi: 10.3390/nu11020482

Vaquerizo-Serrano, J., Salazar De Pablo, G., Singh, J., and Santosh, P. (2021). Catatonia in autism spectrum disorders: a systematic review and meta-analysis. *Eur. Psychiatry* 65:e4. doi: 10.1192/j.eurpsy.2021.2259

Varatharaj, A., and Galea, I. (2017). The blood-brain barrier in systemic inflammation. *Brain Behav. Immun.* 60, 1–12. doi: 10.1016/j.bbi.2016.03.010

Vargas-Sánchez, K., Mogilevskaya, M., Rodríguez-Pérez, J., Rubiano, M. G., Javela, J. J., González-Reyes, R. E., et al. (2018). Astroglial role in the pathophysiology of status epilepticus: an overview. *Oncotarget* 9, 26954–26976. doi: 10.18632/oncotarget.25485

Velloso, N. A., Dalmolin, G. D., Gomes, G. M., Rubin, M. A., Canas, P. M., Cunha, R. A., et al. (2009). Spermine improves recognition memory deficit in a rodent model of Huntington's disease. *Neurobiol. Learn. Mem.* 92, 574–580. doi: 10.1016/j.nlm.2009.07.006

Verkhratsky, A. (2010). Physiology of neuronal-glial networking. *Neurochem. Int.* 57, 332–343. doi: 10.1016/j.neuint.2010.02.002

Verkhratsky, A., Anderova, M., and Chvatal, A. (2009). Differential calcium signalling in neuronal-glial networks. *Front. Biosci. (Landmark Ed)* 14, 2004–2016. doi: 10.2741/3359

Voros, V., Kovacs, A., Herold, R., Osvath, P., Simon, M., Fekete, S., et al. (2009). Effectiveness of intramuscular aripiprazole injection in patients with catatonia: report on three cases. *Pharmacopsychiatry* 42, 286–287. doi: 10.1055/s-0029-1224185

Walther, S., Schäppi, L., Federspiel, A., Bohlhalter, S., Wiest, R., Strik, W., et al. (2017). Resting-state hyperperfusion of the supplementary motor area in catatonia. *Schizophr. Bull.* 43, 972–981. doi: 10.1093/schbul/sbw140

Walther, S., Stegmayer, K., Wilson, J. E., and Heckers, S. (2019). Structure and neural mechanisms of catatonia. *Lancet Psychiatry* 6, 610–619. doi: 10.1016/S2215-0366(18)30474-7

Walther, S., and Strik, W. (2016). Catatonia. *CNS Spectr.* 21, 341–348. doi: 10.1017/S1092852916000274

Weiner, R. D., and Reti, I. M. (2017). Key updates in the clinical application of electroconvulsive therapy. *Int. Rev. Psychiatry* 29, 54–62. doi: 10.1080/09540261.2017.1309362

Wenthur, C. J., and Lindsley, C. W. (2013). Classics in chemical neuroscience: clozapine. *ACS Chem. Neurosci.* 4, 1018–1025. doi: 10.1021/cn400121z

Wijemanne, S., and Jankovic, J. (2015). Movement disorders in catatonia. *J. Neurol. Neurosurg. Psychiatry* 86, 825–832. doi: 10.1136/jnnp-2014-309098

Wilcox, J. A. (1991). Cerebellar atrophy and catatonia. *Biol. Psychiatry* 29, 733–734. doi: 10.1016/0006-3223(91)9152-c

Wing, L., and Shah, A. (2000). Catatonia in autistic spectrum disorders. *Br. J. Psychiatry* 176, 357–362. doi: 10.1192/bjp.176.4.357

Wolf, S. A., Boddeke, H. W. G. M., and Kettenmann, H. (2017). Microglia in physiology and disease. *Annu. Rev. Physiol.* 79, 619–643. doi: 10.1146/annurev-physiol-022516-034406

Xia, C.-Y., Xu, J.-K., Pan, C.-H., Lian, W.-W., Yan, Y., Ma, B.-Z., et al. (2020). Connexins in oligodendrocytes and astrocytes: possible factors for demyelination in multiple sclerosis. *Neurochem. Int.* 136:104731. doi: 10.1016/j.neuint.2020.104731

Yang, Q., Luo, L., Sun, T., Yang, L., Cheng, L.-F., Wang, Y., et al. (2020). Chronic minocycline treatment exerts antidepressant effect, inhibits neuroinflammation and modulates gut microbiota in mice. *Psychopharmacology (Berl)* 237, 3201–3213. doi: 10.1007/s00213-020-05604-x

Yang, Y., and Wang, J.-Z. (2017). From structure to behavior in basolateral amygdala-hippocampus circuits. *Front. Neural Circuits* 11:86. doi: 10.3389/fncir.2017.00086

Zain, S. M., Muthukanagaraj, P., and Rahman, N. (2021). Excited catatonia - a delayed neuropsychiatric complication of COVID-19 infection. *Cureus* 13:e13891. doi: 10.7759/cureus.13891

Zaman, H., Gibson, R. C., and Walcott, G. (2019). Benzodiazepines for catatonia in people with schizophrenia or other serious mental illnesses. *Cochrane Database Syst. Rev.* 8:CD006570. doi: 10.1002/14651858.CD006570.pub3

Ziegler, W., Kilian, B., and Deger, K. (1997). The role of the left mesial frontal cortex in fluent speech: evidence from a case of left supplementary motor area hemorrhage. *Neuropsychologia* 35, 1197–1208. doi: 10.1016/s0028-3932(97)00040-7

Zingela, Z., Stroud, L., Cronje, J., Fink, M., and Van Wyk, S. (2022). A prospective descriptive study on prevalence of catatonia and correlates in an acute mental health unit in Nelson Mandela Bay, South Africa. *PLoS One* 17:e0264944. doi: 10.1371/journal.pone.0264944

Glossary

NMDAr	N-methyl-D-Aspartate Receptor
SMA	Supplementary Motor Area
OFC	Orbitofrontal Cortex
PFc	Prefrontal Cortex
GABA-A	Gamma-Aminobutyric acid-A
NMDA	N-Methyl-D-Aspartate
CN	Caudate Nucleus
VS	Putamen and Ventral Striatum
iGP	Internal Globus Pallidus
eGP	ExternalGlobus Pallidus
SNc	Substantia Nigra Pars Compacta
SNr	Substantia Nigra Pars Reticulata
STN	Subthalamic Nucleus
VL	Ventral Lateral Nuclei of the Thalamus
VA	Ventral Anterior Nuclei of theThalamus
D1R	Dopamine Type 1 Receptor
D2R	Dopamine Type 2 Receptor
SCZ	Schizophrenia
vmPFC	Ventromedial Prefrontal Cortex
SPG	Superior Left Parietal Gyrus
SMG	Supramarginal Gyrus
MPF	Medial Prefrontal Cortex
CAC	Cingulate Anterior Cortex
NIC	Neuroleptic-Induced Catatonia
TNF alpha	Tumour Necrosis Factoralpha
NO	Nitric Oxide
Cnp	2',3'- cyclic nucleotide 3'-phosphodiesterase
OS	Oxidative Stress
RS	Reactive Species
ROS	Reactive Oxygen Species
RNS	Reactive Nitrogen Species
H_2O_2	HydrogenPeroxide
ROO	Peroxyl Radicals
$O_2^- O_2^-$	Superoxide Anion Radical
OH	Hydroxyl Radical
ONOO-	Peroxynitrite
O_2^-	Single Molecular Oxygen
SOD	Superoxide Dismutase
GSH	Glutathione
RAGE	Receptor for Advanced Glycation End-Products
Nf-KB	Nuclear factor kappa-light-chain-enhancer ofactivated B cells
BBB	Blood-Brain Barrier
BZD	Benzodiazepines
ECT	Electroconvulsive Therapy
IM	Intramuscular
IST	Initial Seizure Threshold
rTMS	Repetitive Transmagnetic Stimulation
NMS	Neuroleptic Malignant Syndrome
CNS	Central Nervous System

frontiers | Frontiers in Molecular Neuroscience

TYPE Original Research
PUBLISHED 10 October 2022
DOI 10.3389/fnmol.2022.965697

OPEN ACCESS

EDITED BY
Mónica Isa Moreira-Rodrigues,
Universidade Do Porto, Portugal

REVIEWED BY
Pei Zhang,
Huazhong University of Science and Technology, China
You-Dong Wei,
First Affiliated Hospital of Chongqing Medical University, China
Alexander Kulikov,
Russian Academy of Sciences (RAS), Russia

*CORRESPONDENCE
Meixue Dong
dong_meixue@whu.edu.cn
Jiabao Hou
bohrhou@whu.edu.cn
Benhong Zhou
benhongzhou@163.com

†These authors have contributed equally to this work

SPECIALTY SECTION
This article was submitted to Brain Disease Mechanisms, a section of the journal Frontiers in Molecular Neuroscience

RECEIVED 10 June 2022
ACCEPTED 14 September 2022
PUBLISHED 10 October 2022

CITATION
Chen G, Zhou S, Chen Q, Liu M, Dong M, Hou J and Zhou B (2022) Tryptophan-5-HT pathway disorder was uncovered in the olfactory bulb of a depression mice model by metabolomic analysis. *Front. Mol. Neurosci.* 15:965697. doi: 10.3389/fnmol.2022.965697

Tryptophan-5-HT pathway disorder was uncovered in the olfactory bulb of a depression mice model by metabolomic analysis

Guanghui Chen[1†], Siqi Zhou[2†], Qiang Chen[3], Mengmeng Liu[1], Meixue Dong[4*], Jiabao Hou[5*] and Benhong Zhou[1*]

[1]Department of Pharmacy, Renmin Hospital of Wuhan University, Wuhan, China, [2]Department of Orthopedics, Renmin Hospital of Wuhan University, Wuhan, China, [3]Department of Pharmacy, Liyuan Hospital, Tongji Medical College, Huazhong University of Science and Technology, Wuhan, China, [4]Department of Neurology, Renmin Hospital of Wuhan University, Wuhan, China, [5]Department of Anesthesiology, Renmin Hospital of Wuhan University, Wuhan, China

Major depression (MD) is a severe mental illness that creates a heavy social burden, and the potential molecular mechanisms remain largely unknown. Lots of research demonstrate that the olfactory bulb is associated with MD. Recently, gas chromatography-mass spectrometry-based metabolomic studies on depressive rats indicated that metabolisms of purine and lipids were disordered in the olfactory bulb. With various physicochemical properties and extensive concentration ranges, a single analytical technique could not completely cover all metabolites, hence it is necessary to adopt another metabolomic technique to seek new biomarkers or molecular mechanisms for depression. Therefore, we adopted a liquid chromatography-mass spectrometry metabonomic technique in the chronic mild stress (CMS) model to investigate significant metabolic changes in the olfactory bulb of the mice. We discovered and identified 16 differential metabolites in the olfactory bulb of the CMS treatments. *Metabolic pathway analysis by MetaboAnalyst 5.0* was generated according to the differential metabolites, which indicated that the tryptophan metabolism pathway was the core pathogenesis in the olfactory bulb of the CMS depression model. Further, the expressions of tryptophan hydroxylase (TpH) and aromatic amino acid decarboxylase (AAAD) were detected by western blotting and immunofluorescence staining. The expression of TpH was increased after CMS treatment, and the level of AAAD was unaltered. These results revealed that abnormal metabolism of the tryptophan pathway in the olfactory bulb mediated the occurrence of MD.

KEYWORDS

major depression, metabolomic, olfactory bulb, tryptophan hydroxylase, chronic mild stress

Introduction

Major depression (MD) is a severe mental illness that creates a heavy social burden. The disease influences exceeding 300 million people yearly, which is an important reason for disability worldwide (Hamel et al., 2019). The human brain is so complicated that depressive pathogenesis is still largely unknown, although much effort has been made (Robinson, 2018). Current antidepressant therapy carries out lots of side effects in most depressed patients (Cipriani et al., 2018). Therefore, it is emergent to find a new way to study the pathogenesis of depression and seek new targets for antidepressants.

Metabolomics employs liquid chromatography-mass spectrometry (LC-MS), gas chromatography (GC)-MS, and so on to analyze micromolecule of biological samples qualitatively and quantitatively for exploring the pathophysiological mechanism of life process (Ding and Mohan, 2016; Wishart, 2016). Metabolomics has been widely used to study the pathogenesis of depression (Ling-Hu et al., 2021; Pu et al., 2021). An increasing body of evidence suggests that olfactory bulb dysfunction is closely associated with depression. The olfactory bulb volume and olfactory sensitivity in MD patients are reduced (Negoias et al., 2010). Olfactory bulb volume could predict the therapeutic outcome of MD patients (Negoias et al., 2016), and the lowered olfactory sensitivity could partly be predicted by high depression scores (Pause et al., 2001). The reduced neurogenesis and olfactory receptor neurons, and increased apoptosis in the olfactory bulb were discovered in the rodent model of depression (Yang et al., 2011a,b; Li et al., 2015; Cheng et al., 2016). Recently, a GC-MS-based metabolomic study on the olfactory bulb of depressive rats indicates that purine and lipid metabolism are disordered (He et al., 2020). As various physicochemical properties and extensive concentration range, a single analytical technique could not completely cover all metabolites (Williams et al., 2006), so it is necessary to adopt other metabolomic techniques to seek new biomarkers or molecular mechanisms for depression. This complementation was vital to seek biomarkers and study pathogenesis in MD (Zheng et al., 2013a,b).

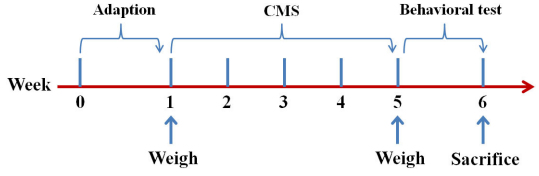

FIGURE 1
Time schedule for the CMS procedure and behavior tests. CMS, chronic mild stress.

Therefore, based on previous GC-MS research, we adopted LC-MS metabonomic method to explore meaningful metabolic changes in the olfactory bulb of chronic mild stress (CMS) depression mice model (Huang et al., 2020). Further, the probable abnormal metabolism of the tryptophan pathway was confirmed. The main purpose of this research is to discover several novel metabolic changes in the olfactory bulb of depression model mice and search for new mechanisms and therapeutic targets for depression.

Materials and methods

Animals

Thirty C57BL/6J mice (male; weight, about 22 g; age: 8 weeks) were obtained from Beijing Vital River Laboratory Animal Technology Co., Ltd. The mice were kept in a standard environment for feeding. Before the experiment begins, the mice were fed adaptively for 1 week. Then, the mice were weighed and randomly divided into the CMS group ($n = 15$) and Control (CON) group ($n = 15$). The schedule of CMS was according to the previous research with few alterations (Crowley et al., 2004; Xie et al., 2022). All experimental procedures were ratified by the Institutional Animal Care and Use Committee of Wuhan University (IACUC Issue No. WDRM20210123) and carried out based on the Declaration of the Health Guide for Care and Use of Laboratory Animals formulated by Wuhan University.

CMS treatment

As shown in Figure 1, the mice were exposed to CMS for 4 weeks before the behavioral tests. Stressors mainly include food deprivation (24 h), water deprivation (1 day), wet bedding (1 day), inversion of dark/light cycle (12 h), cage tilting (45°, 1 day), tail pinching (2 min), and shaking cage (horizontal, 5 min). The CMS mice were given a stressor every day randomly and 2 days in a row without the same stressor.

Forced swimming test (FST)

FST was conducted based on previous research (Xie et al., 2022). In general, the mice were separately placed in glass cylinders (height, 25 cm; diameter, 12 cm) full of 18 cm of water (25°C) for testing. The mice were put in the cylinder for 6 min, and the duration of immobility was calculated in the last 4 min. Immobility was defined as floating or remaining motionless, which means the absence of all movement except motions required to maintain the head above the water.

Tail suspension test (TST)

The TST was conducted to assess behavioral despair of mice as previously described (Crowley et al., 2004). The mouse's tail was held in place with tape and its head 30 cm above the ground. The immobile time was recorded by video system in the 6 min experimental process. The state that the mice were motionless without any struggle was defined as immobility.

Open field test (OFT)

Locomotor activity and exploratory behavior were evaluated by OFT based on previous research (Xie et al., 2022). In general, the mice were separately placed in the apparatus (transparent plastic square: 45 cm × 45 cm). The mice were put in the open field center and recorded for 5 min after the beginning of the experiment. The whole activity of the animal was monitored by a video system. The video system was used to calculate the total distance and rearing frequency.

Sample collection and preparation

Isoflurane was used to anesthetize mice when the behavioral experiments were finished. Once the righting reflexes of mice disappeared, they were rapidly sacrificed and the olfactory bulb was collected.

LC/MS analysis

We adopted an LC/MS metabolomic method to conduct this research and the specific procedure was described in previous studies (Dong et al., 2018; Chen et al., 2019; Xie et al., 2022). The detailed information was described in the Supplementary materials.

Histological and immunofluorescence analysis

The olfactory bulbs were embedded in paraffin after 4% paraformaldehyde solution overnight.

Hematoxylin–eosin was used to stain the slices. Every 5th section of them was preserved and taken photos by an Olympus light microscope. The maximal cross-sectional areas and diameter of the olfactory bulb were calculated, which were estimated by the Photo Imaging System according to the sections.

For immunofluorescence analysis, the olfactory bulb slices were dewaxed and potched by phosphate buffer saline (PBS). The olfactory bulb tissue slices were blocked for 30 min in bovine serum albumin (BSA) (3%) and fetal bovine serum (2 in 0.2% Triton X-100/PBS) after antigen retrieval, and incubated with a primary antibody (4°C, overnight) for tryptophan hydroxylase (TpH) (abcam 52,954; dilution, 1:300) and aromatic amino acid decarboxylase (AAAD) (abcam 142,497; dilution, 1:500). Then, the slices were incubated in a biotinylated secondary antibody and an avidin-biotinylated horseradish peroxidase complex solution, ordinally. 4,6-diamidino-2-phenylindole (DAPI) (1:500, 5 min) was used to stain nuclei. Negative controls were conducted by omitting the primary antibody and presented with negligible background fluorescence. At last, peroxidase activity was detected by a diaminobenzidine staining kit and observed in the Photo Imaging System (five fields of different samples).

Western blot assay

BCA Protein Assay Kit was adopted to detect the total protein concentration of the olfactory bulb. Then, the proteins were separated by sodium dodecyl sulfate–polyacrylamide gel electrophoresis and transferred to polyvinylidene fluoride membranes, furtherly. The membranes were incubated with the primary antibodies (overnight, 4°C): TpH (dilution, 1:2,000), AAAD (dilution, 1:1,500), and glyceraldehyde 3-phosphate dehydrogenase (GAPDH) (dilution, 1:2,000). Then, the membranes were washed by TBST (3 times/10 min) and reacted with horseradish peroxidase-conjugated secondary antibodies (1:15,000) (room temperature, 1 h). The ChemiDoc XRS + System was used to detect the immunoreactive bands. The protein expression was normalized by GAPDH.

Statistical analysis

SPSS 18.0 was adopted to analyze the data. Means ± S.E.M. was used to convey quantitative data. Student's *t*-tests were adopted to process the data of behavior test and protein expression, and $P < 0.05$ was regarded as statistical significance. *MetaboAnalyst 5.0* was adopted to achieve the significant pathways for capturing the disturbed metabolic pathway ($P < 0.05$).

Results

CMS model establishments

We employed the indicators (body weight, OFT, FST, and TST) to evaluate the quality of the CMS model. The

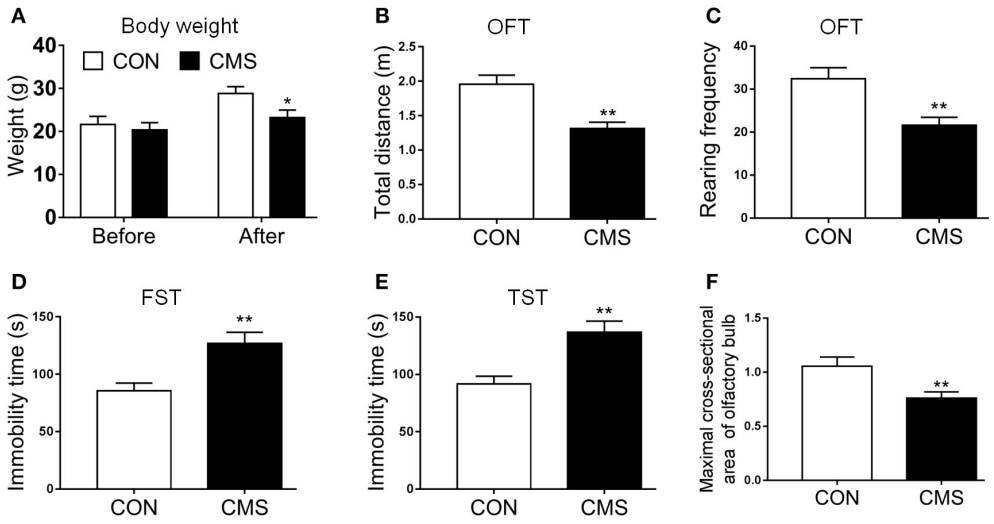

FIGURE 2
Evaluating the results of the CMS depression model. **(A)** Body weight before and after the CMS; **(B,C)** Total distance of central zone and rearing frequency in OFT; **(D,E)** The immobile time in FST and TST; **(F)** Olfactory bulb maximal cross-sectional area and diameter. Data are expressed as means ± S.E.M. *$P < 0.05$, **$P < 0.01$ as compared with control group. CMS, chronic mild stress; OFT, open field test; TST, tail suspension test; FST, forced swimming test. $n = 15$ for weight and behavior test and $n = 3$ for olfactory bulb maximal cross-sectional areas and diameter.

body weight of CMS mice was less than CON mice after CMS, while no significant differences were discovered between them at baseline [Figure 2A, $t(10) = 1.56$, $P < 0.05$]. In OFT, the number of locomotor and rearing activities in mice subjected to CMS for 4 weeks was decreased significantly compared to CON mice [Figures 2B,C, $t(10) = 5.81$, $P < 0.01$, $t(10) = 3.26$, $P < 0.01$]. Regarding FST and TST, the immobility time in CMS mice was increased compared to CON mice [Figures 2D,E, $t(10) = 3.28$, $P < 0.01$, $t(10) = 4.56$, $P < 0.01$]. In addition, we found the maximum cross-section area of the olfactory bulb in CMS mice was reduced compared to CON mice [Figure 2F, $t(4) = 2.89$, $P < 0.01$].

Metabolomic analysis and differential metabolite identification

The data acquired through LC-MS were subjected to multivariate analyses (including negative ionization and positive ionization). The clear differences were shown by PCA scores plot in CMS and CON groups (Figure 3A). Further, statistical difference was indicated by OPLS–DA score plots between CMS mice and CON mice ($R^2X = 0.866$, $R^2Y = 0.821$, and $Q^2 = 0.913$) (Figure 3B). At last, a total of 16 differential metabolites were identified between them (Table 1). CMS mice were characterized by an increased level of uric acid (UA), methacholine, sorbitol, inosine, taurine, acetone, ribitol, and metanephrine compared with controls, as well as a reduced level of phosphatidylcholine (PC) O-34:2, PC[20:0/22:1(13Z)], tryptophan, 5-hydroxytryptamine (5-HT), 5-hydroxy-L-tryptophan (5-HTP), fructose-6-phosphate, spermidine, and glucose.

Metabolic pathway analysis by metabo analyst 5.0 and verification

We used *Metabo Analyst 5.0* to analyze the metabolic profiling and found that all metabolites of CMS mice and CON mice were shown in the hierarchical clustering heatmap (Figure 3C). Then, we used *Metabo Analyst 5.0* to perform metabolic pathway analysis according to the 16 differential metabolites. Three differentially metabolic pathways are discovered (Figure 3D, $P < 0.05$): (1) Tryptophan metabolism (impact = 0.38, $P < 0.05$), (2) Linoleic acid metabolism (impact = 0.43, $P < 0.05$), and (3) Taurine and hypotaurine metabolism (impact = 0.19, $P < 0.05$). The results indicated that the tryptophan metabolism pathway of the olfactory bulb was involved in the underlying pathogenesis of depression. In general, tryptophan formates indoleamine, which produces 5-HTP by TpH and 5-HT by AAAD (Maffei, 2020). At last, we adopted immunofluorescence and western blot to detect the expressions of TpH and by AAAD for verification. We discovered that the protein expression of TpH was increased in the olfactory bulb of CMS mice compared with CON mice, while the protein expression of AAAD was unchanged [Figures 4A–E, $t(4) = 1.55$, $P < 0.05$, $t(4) = 4.69$, $P < 0.01$].

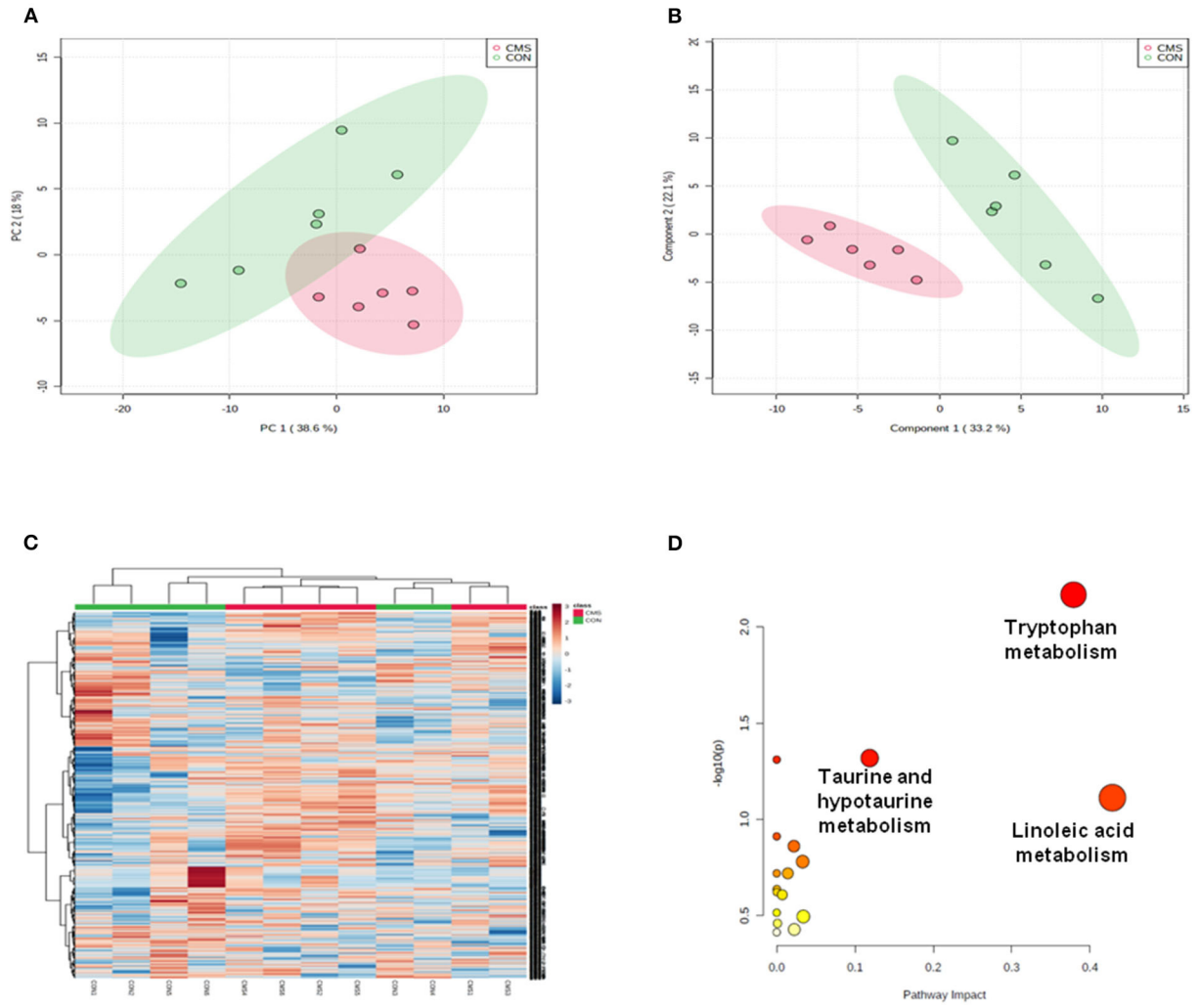

FIGURE 3
Multivariate statistical analysis and metabolic pathway analysis. **(A)** Principal component analysis (PCA) scores plot derived from LC/MS of the chronic mild stress (CMS) and healthy control (CON) groups. **(B)** Pair-wise orthogonal projections to latent structures discriminant (OPLS–DA) scores plot derived from LC/MS of the CMS and CON groups. **(C)** Clustering analysis for the differential metabolites. **(D)** Pathway analysis; a, tryptophan metabolism; b: linoleic acid metabolism; c: taurine and hypotaurine metabolism. $n = 6$.

Discussion

The main findings of this study

Lots of evidence suggest that olfactory bulb dysfunction is associated with depression. Olfactory bulb volume in MD patient was reduced and recovered after antidepressant treatment (Negoias et al., 2010, 2016). In this research, we first discovered the maximum cross-section area of the olfactory bulb in CMS mice was reduced. Then, we used LC/MS (metabolomics techniques) to study the metabolic alterations of the olfactory bulb. We discovered 16 metabolites categorized into three influenced pathways by OPLS-DA analysis and *MetaboAnalyst*. The metabolic disturbance of olfactory (including tryptophan metabolism, linoleic acid metabolism, and taurine and hypotaurine metabolism) was regarded as the main pathway that mediated the onset of depression. Eight differential metabolites were increased and 8 were decreased, which may be therapeutic targets of depression. The previous metabolomic study of the olfactory bulb by GC-MS found that 19 metabolites were altered in CMS rats compared to CON rats (He et al., 2020). These metabolites were highly associated with the disturbances of purine and lipids metabolism.

Three influenced metabolic pathways were relevant to differential metabolites. Our results indicated that disturbance of these metabolites may refer to promoting depressive-like phenotypes and olfactory bulb disorder in CMS mice. The

TABLE 1 List of differential metabolites between CMS group and CON group.

Number	Differential metabolites	VIP	Abundance		*t*(10)	*P*
			CMS	CON		
1	Uric acid	2.06	3.54 ± 0.18	2.06 ± 0.16	4.91	**
2	Methacholine	1.87	8.64 ± 0.63	6.67 ± 0.87	1.53	*
3	Sorbitol	1.97	2.75 ± 0.15	2.21 ± 0.15	2.69	**
4	Inosine	2.08	2.06 ± 0.16	1.39 ± 0.087	6.45	**
5	Taurine	1.74	10.75 ± 1.38	8.76 ± 0.83	1.61	*
6	Acetone	2.53	15.34 ± 1.37	4.06 ± 0.36	5.52	**
7	Ribitol	1.97	0.46 ± 0.024	0.22 ± 0.015	3.56	**
8	Metanephrine	1.65	1.21 ± 0.13	0.24 ± 0.018	3.12	**
9	PC O-34:2	2.08	21.87 ± 1.26	27.6 ± 1.97	2.68	**
10	PC(20:0/22:1(13Z))	1.92	23.34 ± 1.48	33.35 ± 2.86	2.08	**
11	Tryptophan	1.67	1.57 ± 0.12	2.88 ± 0.23	4.36	**
12	5-HT	2.53	4.08 ± 0.58	5.7 ± 0.61	1.39	*
13	5-HTP	1.75	26.98 ± 1.56	33.24 ± 2.86	7.67	**
14	Fructose-6-phosphate	2.54	0.21 ± 0.017	1.05 ± 0.13	6.28	**
15	Spermidine	2.17	0.68 ± 0.033	1.28 ± 0.11	3.86	**
16	Glucose	1.79	4.98 ± 0.69	7.27 ± 0.86	1.26	*

CMS, chronic mild stress; CON, control; PC, phosphatidylcholine; 5-HT, 5-hydroxytryptamine; 5-HTP, 5-hydroxy-L-tryptophan; *P < 0.05; **P < 0.01.

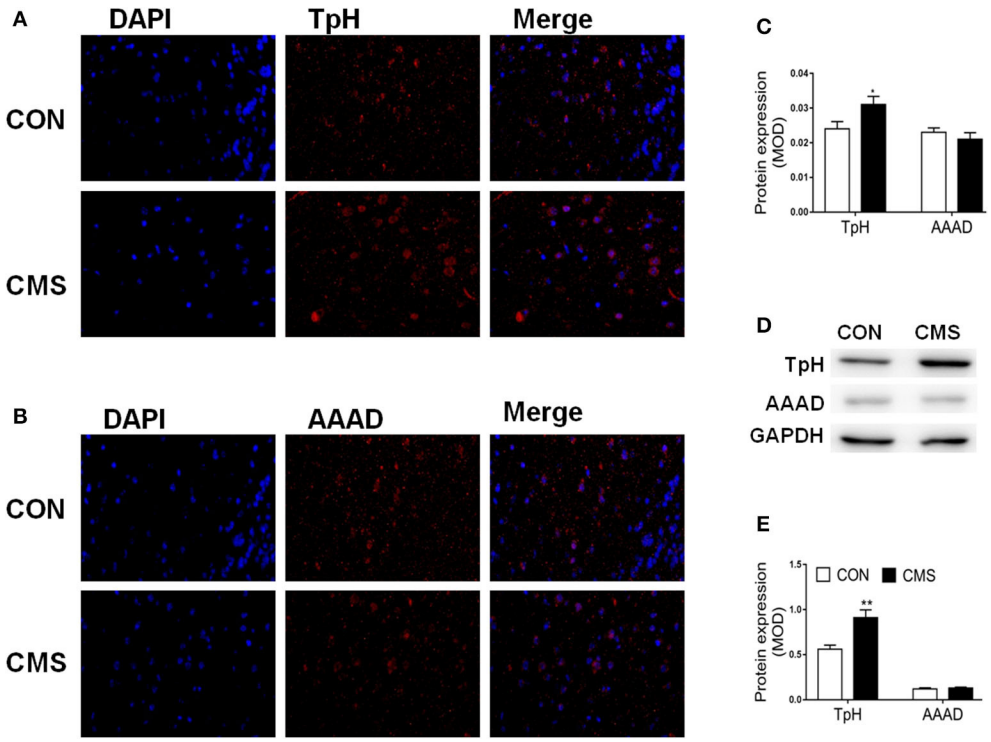

FIGURE 4
The protein expression of tryptophan hydroxylase (TpH) and aromatic amino acid decarboxylase (AAAD) in the olfactory bulb of chronic mild stress mice. **(A–C)** The protein level of TpH and AAAD by immunofluorescence; **(D, E)** The protein level of TpH and AAAD by Western blot. $n = 3$.

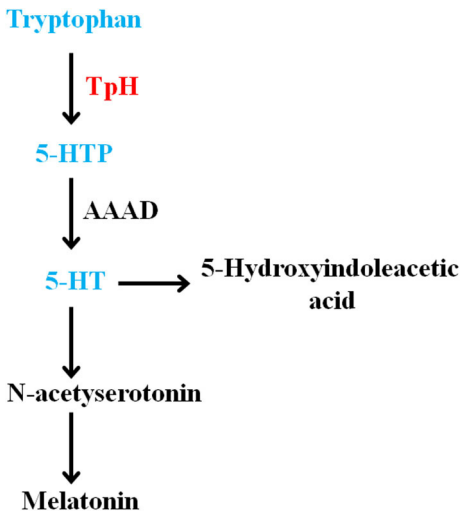

FIGURE 5
Summary of the olfactory bulb metabolites involved in the disturbance of tryptophan-5-HT pathway in chronic mild stress mice. 5-HT, 5-hydroxytryptamine; 5-HTP, 5-hydroxy-L-tryptophan.

abnormal tryptophan metabolism has been reported to associate with MD and depression model (Wang et al., 2021; Tian et al., 2022). What's more, we first found that linoleic acid metabolism and taurine and hypotaurine metabolism mediated the onset of depression.

Tryptophan-5-HT pathway

Tryptophan is an essential acid used for synthesizing proteins. It is also the precursor of the neurotransmitter serotonin (Slominski et al., 2002). The monoamine neurotransmitters (including 5-HT) can modulate mood, cognition, and so on (Young, 2007). In general, tryptophan formates indoleamine, which produces 5-hydroxytryptophan by TpH and 5-HT by AAAD (Maffei, 2020). The detailed metabolic steps of the tryptophan-5-HT pathway are summarized in Figure 5.

The metabolic disturbance of tryptophan and 5-HT was vital for MD. Plasma tryptophan levels in depression (including MD, suicidal MD patients, and depression model rats) were reduced (Messaoud et al., 2019, 2021; Li et al., 2020), and reversed after antidepressant treatment (Ciocan et al., 2021). In addition, tryptophan supplementation could improve symptoms of depression in MD patients (Gonzalez et al., 2021). The decreased 5-HT transporter availability was observed in depressed patients (Staley et al., 2006). The plasma 5-HT level was reduced in depression patients and increased after antidepressant administration (Blardi et al., 2002), and the plasma 5-HT level of responders was increased compared to nonresponders (Celada et al., 1992). The 5-HT level of the prefrontal cortex and hippocampus was downregulated in the acute and chronic stress-induced depression model (Jia et al., 2017; Zhang et al., 2018). In this study, we discovered that the levels of metabolites (including tryptophan, 5-HTP, and 5-HT) were reduced in the olfactory bulb of CMS mice. Then, we discovered that the protein expression of TpH was increased and AAAD was unchanged in the olfactory bulb of CMS mice. These results suggested that TpH may be an intervention target for olfactory bulb metabolism abnormality mediating depression.

PC

PC, a kind of phospholipids, is the main component of biomembrane and synthesizes choline. Clinical research indicated that plasma PC concentrations of depression patients were associated with the severity of depression (Demirkan et al., 2013). Plasma PC levels showed a positive correlation with depression status in postmenopausal women (Huang et al., 2021). Serum PC in the olfactory bulbectomy-induced depression model was increased, (Yan et al., 2021) while some PCs [PC (32:1), PC (37:4) and its like] in plasma of depressed rats were reduced (Chen et al., 2014). These differences may be due to the difference between the depression model and depressive phenotype. PC supplementation efficiently reversed the disorder of hippocampal neurogenesis by inhibiting circulating TNF-α levels (Tokés et al., 2011). The neuroplasticity of neural stem cells was damaged by inflammatory stress and could be restored by PC (Magaquian et al., 2021). The neurogenesis of the olfactory bulb was reduced (Yang et al., 2011a). Therefore, the reduced PC level of olfactory bulb mediated neurogenesis disorder in CMS mice.

UA

The levels of serum and plasma UA in patients with depression and CMS rats were lower than in control, which was a depression biomarker (Peng et al., 2016; Xiong et al., 2016; Meng et al., 2020; Yuan et al., 2021; Ceresa et al., 2022). Plasma UA-adjusted mean levels were lower in current major depressive disorder compared to remitted disorders and controls (Black et al., 2018). The plasma UA levels showed a negative correlation with the risk of depression in patients and antidepressant use (Wium-Andersen et al., 2017). The plasma UA levels of comorbid unipolar depression were increased compared with the unipolar depression and healthy control (Ozten et al., 2015). The research indicates that increased serum UA levels in depressed patients have a positive correlation with hypomanic episodes or subsequent manic (Dos Santos Oliveira et al., 2019). The rates of hyperuricemia and serum UA levels in bipolar were

significantly increased compared with the control (Albert et al., 2015). Therefore, the reduced UA level of the olfactory bulb may be a biomarker for CMS mice.

Conclusion

We employed LC/MS metabolomics techniques to achieve metabolic profiling in the olfactory bulb of CMS mice. We discovered that tryptophan-5-HT pathway metabolism was disordered in the olfactory bulb of depression mice and TpH may be an intervention and treatment target for depression. Futher, we first discovered that linoleic acid metabolism and taurine and hypotaurine metabolism mediated the onset of depression.

Data availability statement

The raw data supporting the conclusions of this article will be made available by the authors, without undue reservation.

Ethics statement

The animal study was reviewed and approved by the Institutional Animal Care and Use Committee of Wuhan University. Written informed consent was obtained from the owners for the participation of their animals in this study.

Author contributions

BZ performed the research. QC and SZ designed the research study. GC, ML, and MD analyzed the data and wrote the article. GC and JH revised the article. All authors contributed to the article and approved the submitted version.

Funding

This research was funded by the National Natural Science Foundation of China (No. 82104312, No. 82001119), the National Natural Science Foundation of Hubei Province (No. 2020CFB258), and the Fundamental Research Funds for the Central Universities (No. 2042020kf0044).

Conflict of interest

The authors declare that the research was conducted in the absence of any commercial or financial relationships that could be construed as a potential conflict of interest.

The reviewer PZ declared a shared affiliation with the author QC to the handling editor at the time of review.

Publisher's note

All claims expressed in this article are solely those of the authors and do not necessarily represent those of their affiliated organizations, or those of the publisher, the editors and the reviewers. Any product that may be evaluated in this article, or claim that may be made by its manufacturer, is not guaranteed or endorsed by the publisher.

Supplementary material

The Supplementary Material for this article can be found online at: https://www.frontiersin.org/articles/10.3389/fnmol.2022.965697/full#supplementary-material

References

Albert, U., De Cori, D., Aguglia, A., Barbaro, F., Bogetto, F., and Maina, G. (2015). Increased uric acid levels in bipolar disorder subjects during different phases of illness. *J. Affect. Disord.* 173, 170–175. doi: 10.1016/j.jad.2014.11.005

Black, C. N., Bot, M., Scheffer, P. G., Snieder, H., and Penninx, B. (2018). Uric acid in major depressive and anxiety disorders. *J. Affect. Disord.* 225, 684–690. doi: 10.1016/j.jad.2017.09.003

Blardi, P., De Lalla, A., Leo, A., Auteri, A., Iapichino, S., Di Muro, A., et al. (2002). Serotonin and fluoxetine levels in plasma and platelets after fluoxetine treatment in depressive patients. *J. Clin. Psychopharmacol.* 22, 131–136. doi: 10.1097/00004714-200204000-00005

Celada, P., Pérez, J., Alvarez, E., and Artigas, F. (1992). Monoamine oxidase inhibitors phenelzine and brofaromine increase plasma serotonin and decrease 5-hydroxyindoleacetic acid in patients with major depression: relationship to clinical improvement. *J. Clin. Psychopharmacol.* 12, 309–315.

Ceresa, A., Esposito, C. M., Surace, T., Legnani, F., Cirella, L., Cetti, D., et al. (2022). Gender differences in clinical and biochemical parameters of patients consecutively hospitalized for unipolar depression. *Psychiatry Res.* 310, 114476. doi: 10.1016/j.psychres.2022.114476

Chen, G., Xiao, H., Zhang, J., Zhang, H., Li, B., Jiang, T., et al. (2019). Prenatal dexamethasone exposure-induced a gender-difference and sustainable multi-organ damage in offspring rats *via* serum metabolic profile analysis. *Toxicol. Lett.* 316, 136–146. doi: 10.1016/j.toxlet.2019.09.007

Chen, S., Wei, C., Gao, P., Kong, H., Jia, Z., Hu, C., et al. (2014). Effect of Allium macrostemon on a rat model of depression studied by using plasma lipid and acylcarnitine profiles from liquid chromatography/mass spectrometry. *J. Pharm. Biomed. Anal.* 89, 122–129. doi: 10.1016/j.jpba.2013.10.045

Cheng, K., Li, J., Yang, D., Yang, Y., Rao, C., Zhang, S., et al. (2016). 2D-gel based proteomics unravels neurogenesis and energetic metabolism dysfunction of the olfactory bulb in CUMS rat model. *Behav. Brain Res.* 313, 302–309. doi: 10.1016/j.bbr.2016.05.026

Ciocan, D., Cassard, A. M., Becquemont, L., Verstuyft, C., Voican, C. S., El Asmar, K., et al. (2021). Blood microbiota and metabolomic signature of major

depression before and after antidepressant treatment: a prospective case-control study. *J. Psychiatry Neurosci.* 46, E358–e38. doi: 10.1503/jpn.200159

Cipriani, A., Furukawa, T. A., Salanti, G., Chaimani, A., Atkinson, L. Z., Ogawa, Y., et al. (2018). Comparative efficacy and acceptability of 21 antidepressant drugs for the acute treatment of adults with major depressive disorder: a systematic review and network meta-analysis. *Lancet* 391, 1357–1366. doi: 10.1016/S0140-6736(17)32802-7

Crowley, J. J., Jones, M. D., O'leary, O. F., and Lucki, I. (2004). Automated tests for measuring the effects of antidepressants in mice. *Pharmacol. Biochem. Behav.* 78, 269–274. doi: 10.1016/j.pbb.2004.03.014

Demirkan, A., Isaacs, A., Ugocsai, P., Liebisch, G., Struchalin, M., Rudan, I., et al. (2013). Plasma phosphatidylcholine and sphingomyelin concentrations are associated with depression and anxiety symptoms in a Dutch family-based lipidomics study. *J. Psychiatr. Res.* 47, 357–362. doi: 10.1016/j.jpsychires.2012.11.001

Ding, H., and Mohan, C. (2016). Connective tissue diseases: promises and challenges of metabolomics in SLE. *Nat. Rev. Rheumatol.* 12, 627–628. doi: 10.1038/nrrheum.2016.163

Dong, M. X., Feng, X., Xu, X. M., Hu, L., Liu, Y., Jia, S. Y., et al. (2018). Integrated analysis reveals altered lipid and glucose metabolism and identifies NOTCH2 as a biomarker for parkinson's disease related depression. *Front. Mol. Neurosci.* 11, 257. doi: 10.3389/fnmol.2018.00257

Dos Santos Oliveira, P. M., Santos, V., Coroa, M., Ribeiro, J., and Madeira, N. (2019). Serum uric acid as a predictor of bipolarity in individuals with a major depressive episode. *Bipolar Disord.* 21, 235–243. doi: 10.1111/bdi.12708

Gonzalez, I., Polvillo, R., Ruiz-Galdon, M., Reyes-Engel, A., and Royo, J. L. (2021). MAOB rs3027452 modifies mood improvement after tryptophan supplementation. *Int. J. Gen. Med.* 14, 1751–1756. doi: 10.2147/IJGM.S305443

Hamel, C., Lang, E., Morissette, K., Beck, A., Stevens, A., Skidmore, B., et al. (2019). Screening for depression in women during pregnancy or the first year postpartum and in the general adult population: a protocol for two systematic reviews to update a guideline of the Canadian task force on preventive health care. *Syst. Rev.* 8, 27. doi: 10.1186/s13643-018-0930-3

He, Y., Wang, Y., Wu, Z., Lan, T., Tian, Y., Chen, X., et al. (2020). Metabolomic abnormalities of purine and lipids implicated olfactory bulb dysfunction of CUMS depressive rats. *Metab. Brain Dis.* 35, 649–659. doi: 10.1007/s11011-020-00557-8

Huang, T., Balasubramanian, R., Yao, Y., and Clish, C. B. (2021). Associations of depression status with plasma levels of candidate lipid and amino acid metabolites: a meta-analysis of individual data from three independent samples of US postmenopausal women. *Mol. Psychiatry* 26, 3315–3327. doi: 10.1038/s41380-020-00870-9

Huang, X., Fei, G. Q., Liu, W. J., Ding, J., Wang, Y., Wang, H., et al. (2020). Adipose-derived mesenchymal stem cells protect against CMS-induced depression-like behaviors in mice *via* regulating the Nrf2/HO-1 and TLR4/NF-κB signaling pathways. *Acta Pharmacol. Sin.* 41, 612–619. doi: 10.1038/s41401-019-0317-6

Jia, M., Li, C., Zheng, Y., Ding, X., Chen, M., et al. (2017). Leonurine exerts antidepressant-like effects in the chronic mild stress-induced depression model in mice by inhibiting neuroinflammation. *Int. J. Neuropsychopharmacol.* 20, 886–895. doi: 10.1093/ijnp/pyx062

Li, C. C., Jiang, N., Gan, L., Zhao, M. J., Chang, Q., Liu, M., et al. (2020). Peripheral and cerebral abnormalities of the tryptophan metabolism in the depression-like rats induced by chronic unpredicted mild stress. *Neurochem. Int.* 138, 104771. doi: 10.1016/j.neuint.2020.104771

Li, Q., Yang, D., Wang, J., Liu, L., Feng, G., Li, J., et al. (2015). Reduced amount of olfactory receptor neurons in the rat model of depression. *Neurosci. Lett.* 603, 48–54. doi: 10.1016/j.neulet.2015.07.007

Ling-Hu, T., Liu, S. B., Gao, Y., and Tian, J. S. (2021). Stable isotope-resolved metabolomics reveals the abnormal brain glucose catabolism in depression based on chronic unpredictable mild stress rats. *J. Proteome Res.* 20, 3549–3558. doi: 10.1021/acs.jproteome.1c00155

Maffei, M. E. (2020). 5-Hydroxytryptophan (5-HTP): natural occurrence, analysis, biosynthesis, biotechnology, physiology and toxicology. *Int. J. Mol. Sci.* 22, 181. doi: 10.3390/ijms22010181

Magaquian, D., Delgado Ocaña, and Banchio, C. (2021). Phosphatidylcholine restores neuronal plasticity of neural stem cells under inflammatory stress. *Sci. Rep.* 11, 22891. doi: 10.1038/s41598-021-02361-5

Meng, X., Huang, X., Deng, W., Li, J., and Li, T. (2020). Serum uric acid a depression biomarker. *PLoS ONE* 15, e0229626. doi: 10.1371/journal.pone.0229626

Messaoud, A., Mensi, R., Douki, W., Neffati, F., Najjar, M. F., Gobbi, G., et al. (2019). Reduced peripheral availability of tryptophan and increased activation of the kynurenine pathway and cortisol correlate with major depression and suicide. *World J. Biol. Psychiatry* 20, 703–711. doi: 10.1080/15622975.2018.1468031

Messaoud, A., Rym, M., Wahiba, D., Neffati, F., Najjar, M. F., Gobbi, G., et al. (2021). Investigation of the relationship among cortisol, pro-inflammatory cytokines, and the degradation of tryptophan into kynurenine in patients with major depression and suicidal behavior. *Curr. Top. Med. Chem.* doi: 10.2174/1568026621666210909160210. [Epub ahead of print].

Negoias, S., Croy, I., Gerber, J., Puschmann, S., Petrowski, K., Joraschky, P., et al. (2010). Reduced olfactory bulb volume and olfactory sensitivity in patients with acute major depression. *Neuroscience* 169, 415–421. doi: 10.1016/j.neuroscience.2010.05.012

Negoias, S., Hummel, T., Symmank, A., Schellong, J., Joraschky, P., and Croy, I. (2016). Olfactory bulb volume predicts therapeutic outcome in major depression disorder. *Brain Imag. Behav.* 10, 367–372. doi: 10.1007/s11682-015-9400-x

Ozten, E., Kesebir, S., Eryilmaz, G., Tarhan, N., and Karamustafalioglu, O. (2015). Are uric acid plasma levels different between unipolar depression with and without adult attention deficit hyperactivity disorder? *J. Affect. Disord.* 177, 114–117. doi: 10.1016/j.jad.2015.01.047

Pause, B. M., Miranda, A., Göder, R., Aldenhoff, J. B., and Ferstl, R. (2001). Reduced olfactory performance in patients with major depression. *J. Psychiatr. Res.* 35, 271–277. doi: 10.1016/S0022-3956(01)00029-2

Peng, Y. F., Xiang, Y., and Wei, Y. S. (2016). The significance of routine biochemical markers in patients with major depressive disorder. *Sci. Rep.* 6, 34402. doi: 10.1038/srep34402

Pu, J., Liu, Y., Gui, S., Tian, L., Yu, Y., Song, X., et al. (2021). Metabolomic changes in animal models of depression: a systematic analysis. *Mol. Psychiatry* 26, 7328–7336. doi: 10.1038/s41380-021-01269-w

Robinson, E. S. J. (2018). Translational new approaches for investigating mood disorders in rodents and what they may reveal about the underlying neurobiology of major depressive disorder. *Philos. Trans. R. Soc. Lond. B Biol. Sci.* 373, 36. doi: 10.1098/rstb.2017.0036

Slominski, A., Semak, I., Pisarchik, A., Sweatman, T., Szczesniewski, A., and Wortsman, J. (2002). Conversion of L-tryptophan to serotonin and melatonin in human melanoma cells. *FEBS Lett.* 511, 102–106. doi: 10.1016/S0014-5793(01)03319-1

Staley, J. K., Sanacora, G., Tamagnan, G., Maciejewski, P. K., Malison, R. T., Berman, R. M., et al. (2006). Sex differences in diencephalon serotonin transporter availability in major depression. *Biol. Psychiatry* 59, 40-47. doi: 10.1016/j.biopsych.2005.06.012

Tian, P., Chen, Y., Zhu, H., Wang, L., Qian, X., et al. (2022). Bifidobacterium breve CCFM1025 attenuates major depression disorder *via* regulating gut microbiome and tryptophan metabolism: a randomized clinical trial. *Brain Behav. Immun.* 100, 233-241. doi: 10.1016/j.bbi.2021.11.023

Tokés, T., Eros, G., Bebes, A., Hartmann, P., Várszegi, S., Varga, G., et al. (2011). Protective effects of a phosphatidylcholine-enriched diet in lipopolysaccharide-induced experimental neuroinflammation in the rat. *Shock* 36, 458–465. doi: 10.1097/SHK.0b013e31822f36b0

Wang, Q. S., Yan, K., Li, K. D., Gao, L. N., Wang, X., Liu, H., et al. (2021). Targeting hippocampal phospholipid and tryptophan metabolism for antidepressant-like effects of albiflorin. *Phytomedicine* 92, 153735. doi: 10.1016/j.phymed.2021.153735

Williams, R., Lenz, E. M., Wilson, A. J., Granger, J., Wilson, I. D., Major, H., et al. (2006). A multi-analytical platform approach to the metabonomic analysis of plasma from normal and Zucker (fa/fa) obese rats. *Mol. Biosyst.* 2, 174–183. doi: 10.1039/b516356k

Wishart, D. S. (2016). Emerging applications of metabolomics in drug discovery and precision medicine. *Nat. Rev. Drug Discov.* 15, 473–484. doi: 10.1038/nrd.2016.32

Wium-Andersen, M. K., Kobylecki, C. J., Afzal, S., and Nordestgaard, B. G. (2017). Association between the antioxidant uric acid and depression and antidepressant medication use in 96,989 individuals. *Acta Psychiatr. Scand.* 136, 424–433. doi: 10.1111/acps.12793

Xie, J., Wang, Y., Zhong, Q., Bai, S. J., Zhou, C. J., Tian, T., et al. (2022). Associations between disordered microbial metabolites and changes of neurotransmitters in depressed mice. *Front. Cell Infect. Microbiol.* 12, 906303. doi: 10.3389/fcimb.2022.906303

Xiong, Z., Yang, J., Huang, Y., Zhang, K., Bo, Y., Lu, X., et al. (2016). Serum metabonomics study of anti-depressive effect of Xiao–Chai–Hu–Tang on rat model of chronic unpredictable mild stress. *J. Chromatogr. B Anal. Technol. Biomed. Life Sci.* 1029–1030, 28–35. doi: 10.1016/j.jchromb.2016.06.044

Yan, L., Gu, M. Q., Yang, Z. Y., Xia, J., Li, P., Vasar, E., et al. (2021). Endogenous n-3 PUFAs attenuated olfactory bulbectomy-induced behavioral and

metabolomic abnormalities in fat-1 mice. *Brain Behav. Immun.* 96, 143–153. doi: 10.1016/j.bbi.2021.05.024

Yang, D., Li, Q., Fang, L., Cheng, K., Zhang, R., Zheng, P., et al. (2011a). Reduced neurogenesis and pre-synaptic dysfunction in the olfactory bulb of a rat model of depression. *Neuroscience* 192, 609–618. doi: 10.1016/j.neuroscience.2011.06.043

Yang, D., Liu, X., Zhang, R., Cheng, K., Mu, J., Fang, L., et al. (2011b). Increased apoptosis and different regulation of pro-apoptosis protein bax and anti-apoptosis protein bcl-2 in the olfactory bulb of a rat model of depression. *Neurosci. Lett.* 504, 18–22. doi: 10.1016/j.neulet.2011.08.046

Young, S. N. (2007). How to increase serotonin in the human brain without drugs. *J. Psychiatry Neurosci.* 32, 394–399.

Yuan, D., Kuan, T., Ling, H., Wang, H., Feng, L., and Zhao, Q., et al. (2021). Serum metabolomics of end-stage renal disease patients with depression: potential biomarkers for diagnosis. *Ren. Fail* 43, 1479–1491. doi: 10.1080/0886022X.2021.1994995

Zhang, Y., Fan, K., Liu, Y., Liu, G., Yang, X., and Ma, J. (2018). Cathepsin C aggravates neuroinflammation involved in disturbances of behaviour and neurochemistry in acute and chronic stress-induced murine model of depression. *Neurochem. Res.* 43, 89–100. doi: 10.1007/s11064-017-2320-y

Zheng, P., Chen, J. J., Huang, T., Wang, M. J., Wang, Y., Dong, M. X., et al. (2013a). A novel urinary metabolite signature for diagnosing major depressive disorder. *J. Proteome Res.* 12, 5904–5911. doi: 10.1021/pr400939q

Zheng, P., Wang, Y., Chen, L., Yang, D., Meng, H., Zhou, D., et al. (2013b). Identification and validation of urinary metabolite biomarkers for major depressive disorder. *Mol. Cell Proteom.* 12, 207–214. doi: 10.1074/mcp.M112.021816

frontiers | Frontiers in Molecular Neuroscience

TYPE Original Research
PUBLISHED 01 December 2022
DOI 10.3389/fnmol.2022.994513

OPEN ACCESS

EDITED BY
Tilmann Achsel,
Université de Lausanne, Switzerland

REVIEWED BY
Nicolas Gervasi,
Institut National de la Santé et de la Recherche Médicale (INSERM), France
David Bartolome-Martin,
University of La Laguna, Spain

*CORRESPONDENCE
Peter Penzes
P-penzes@northwestern.edu

†These authors have contributed equally to this work and share first authorship

SPECIALTY SECTION
This article was submitted to Brain Disease Mechanisms, a section of the journal Frontiers in Molecular Neuroscience

RECEIVED 14 July 2022
ACCEPTED 28 September 2022
PUBLISHED 01 December 2022

CITATION
Parnell E, Voorn RA, Martin-de-Saavedra MD, Loizzo DD, Dos Santos M and Penzes P (2022) A developmental delay linked missense mutation in Kalirin-7 disrupts protein function and neuronal morphology. *Front. Mol. Neurosci.* 15:994513. doi: 10.3389/fnmol.2022.994513

A developmental delay linked missense mutation in Kalirin-7 disrupts protein function and neuronal morphology

Euan Parnell[1†], Roos A. Voorn[1†], M. Dolores Martin-de-Saavedra[2], Daniel D. Loizzo[1], Marc Dos Santos[1] and Peter Penzes[1,3,4*]

[1]Department of Neuroscience, Feinberg School of Medicine, Northwestern University, Chicago, IL, United States, [2]Department of Biochemistry and Molecular Biology, School of Pharmacy, Instituto Universitario de Investigación en Neuroquímica, Complutense University of Madrid, Madrid, Spain, [3]Department of Neurology, Feinberg School of Medicine, Northwestern University, Chicago, IL, United States, [4]Centre for Autism and Neurodevelopment, Feinberg School of Medicine, Northwestern University, Chicago, IL, United States

The Rac1 guanine exchange factor Kalirin-7 is a key regulator of dendritic spine morphology, LTP and dendritic arborization. Kalirin-7 dysfunction and genetic variation has been extensively linked to various neurodevelopmental and neurodegenerative disorders. Here we characterize a Kalirin-7 missense mutation, glu1577lys (E1577K), identified in a patient with severe developmental delay. The E1577K point mutation is located within the catalytic domain of Kalirin-7, and results in a robust reduction in Kalirin-7 Rac1 Guanosine exchange factor activity. In contrast to wild type Kalirin-7, the E1577K mutant failed to drive dendritic arborization, spine density, NMDAr targeting to, and activity within, spines. Together these results indicate that reduced Rac1-GEF activity as result of E1577K mutation impairs neuroarchitecture, connectivity and NMDAr activity, and is a likely contributor to impaired neurodevelopment in a patient with developmental delay.

KEYWORDS

developmental delay, neuron, spine, NMDAr, neurodevelopment

Introduction

Neuronal network function is highly dependent on the dendritic morphology of neurons, which harbor the synaptic connections through which input is received, processed and integrated (Harris and Kater, 1994; Hausser et al., 2000; Alvarez and Sabatini, 2007). Most excitatory synapses are located on dendritic spines: membranous and protein dense protrusions of dendrites (Harris, 1999; Carlisle and Kennedy, 2005; Alvarez and Sabatini, 2007). The formation, stabilization and maintenance of dendritic structure are required for synaptic development and plasticity. Synaptic activity drives morphological changes and can induce long-term potentiation (LTP) and long-term

depression (LTD) of synaptic junctions, processes essential to learning and memory (Harris and Kater, 1994; Yuste and Bonhoeffer, 2001). Many developmental and psychiatric disorders display affected structural and functional plasticity, resulting in deficiencies in neural connectivity (Forrest et al., 2018).

Rho family guanosine nucleotide exchange factors (GEFs) are key regulators of dendrite and spine morphogenesis, being highly important in the remodeling of the actin cytoskeleton to drive spine growth and formation (Nakayama et al., 2000; Jaffe and Hall, 2005; Tada and Sheng, 2006; Tolias et al., 2011). GEFs interact with small GTPases to drive GDP for GTP exchange, inducing an active GTP-bound state (Rossman et al., 2005; Bai et al., 2015). This active state is temporally controlled by intrinsic Rho GTPase activity that cleaves GTP to GDP, returning the GTPase to the inactive state. The GTPases Rac1, Cdc42, and RhoA are important factors in shaping the dendritic arbor (Threadgill et al., 1997; Nakayama et al., 2000); Rac1 and Cdc42 promote dendritic branching and the formation, enlargement and maintenance of spines, whereas RhoA decreases and apposes these processes. Kalirin-7, a GEF for Rac1 has been found to be a key player in driving dendritic arborization and dendritic spine morphogenesis through Rac1.

Kalirin-7 has been found to localize to the post synaptic density (PSD) of dendritic spines, and to contribute to spine formation, maturation, LTP and LTD, and dendritic arborization (Parnell et al., 2021). Kalirin-7 activates Rac1, facilitating the interaction and relocalization of downstream effectors, including P21–activated kinase (PAK) that activates remodeling of the actin cytoskeleton and contributes to the formation of spines and dendritic arborization (Johnson et al., 2000; Penzes et al., 2001a,b; Penzes and Remmers, 2012).

The Rac-GEF catalytic domain of Kalirin is composed of a typical Dbl homology (DH)- pleckstrin homology (PH) module (Parnell et al., 2021). Whereas the DH domain directly interacts with Rac1 to drive activity, the PH auxiliary domain has varying function in related GEFs—it can tether enzyme activity to membrane regions via lipid interactions, regulate Rac-GEF activity (Liu et al., 1998; Chhatriwala et al., 2007), and couple with regulatory partners to provide intermolecular regulation of GEF activity (Chakrabarti et al., 2005; Kiraly et al., 2011). Indeed, the Rac1-GEF domain of Kalirin-7 has been shown to directly interact with the NR2B subunit of the NMDAr, via the PH domain (Kiraly et al., 2011; Lemtiri-Chlieh et al., 2011). Kalirin-7 plays a critical role in NMDAr dependent structural plasticity and LTP, by regulating synaptic levels of the NMDAr as well as the α-amino-3-hydroxy-5-methyl-4-isoxazolepropionic acid receptor (AMPAr) (Xie et al., 2007; Ma et al., 2008; Lemtiri-Chlieh et al., 2011; Herring and Nicoll, 2016). Thus, there appears to be an intimate relationship between the Rac1-GEF domain of Kalirin, and NMDAr activity and trafficking, linked not only to Rac1 activation, but Kalirin-7/NR2B interactions.

Recent exome sequencing studies [reviewed in Parnell et al. (2021)] have isolated a range of mutations that disrupt Kalirin expression or function and potentially contribute to neurodevelopmental disorder risk, such as ASD (Leblond et al., 2019; Satterstrom et al., 2020), schizophrenia (Kushima et al., 2012; Purcell et al., 2014; Howrigan et al., 2020), and developmental delay/ID (Makrythanasis et al., 2016; Deciphering Developmental Disorders Study, 2017). Moreover, many of these mutations have been predicted or found to disrupt Rac1-GEF activity (Russell et al., 2014), suggesting an integral role for Kalirin Rac1-GEF activity in normal neurodevelopment. A recent, uncharacterized point mutation (DDD4K.02292) 4729G > A, within the Rac1-GEF domain of Kalirin was found in an individual with severe developmental delay (Deciphering Developmental Disorders Study, 2017). This mutation, encoding a single nucleotide polymorphism resulting in glu1577lys substitution (E1577K) within the PH sub-domain, was predicted to be highly deleterious. However, the precise mechanisms through which E1577K impaired Kalirin function was unclear, due to its position distal to the catalytic site (**Figure 1**). We therefore set out to characterize the functional effects of E1577K mutation on Kalirin function, focusing on the known roles of the PH domain; NMDAr interaction and Rac11-GEF regulation.

E1577K mutation was found to impair the ability of Kalirin-7 to drive dendritic arborization, spine formation and NMDAr-dependent calcium influx within dendritic spines. Interestingly, despite being distal to the catalytic site of Kalirin-7's Rac1-GEF domain, E1577K mutation was found to ablate Rac1 activation, suggesting an integral role of the auxiliary PH domain in regulating Rac-GEF activity. Moreover, this mutation was found to drastically impair NR2B surface expression and NMDAr activity, suggesting that Rac1-GEF activity may be required for Kalirin-mediated NR2B trafficking. These results suggest a key role for the PH domain in regulating RAC1-GEF activity

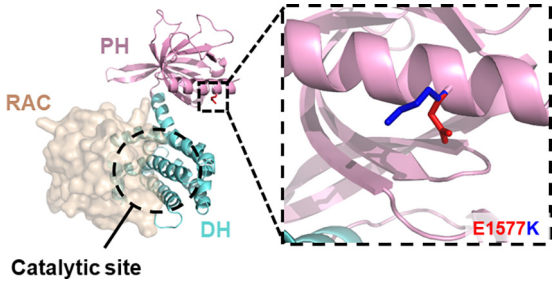

FIGURE 1
E1577 lies distal to the catalytic GEF site. Homology model of the Kalirin DH- (cyan) PH (pink) in complex with Rac11 (tan, surface) reveals the surface exposed position of glutamate 1577 (inset, blue) and the predicted position of lysine (red) mutant at this site. Note, E1577 lies distal to the catalytic site suggesting indirect modulation of Kalirin GEF activity.

and provide insight into Kalirin-7-dependent mechanisms contributing to developmental delay.

Materials and methods

Homology modeling

Kalirin DHPH model was generated using the Kalirin-7 DH domain (5O33, unpublished) and trio DHPH (6D8Z, Bandekar et al., 2019) crystal structures as templates using Modeler (SaliLab, Webb and Sali, 2021). 5O33 was used to orient Rac relative to the GEF domain of Kalirin-7. All images generated with Pymol2 (Schrodinger).

Recombinant DNA

PCS2Flag-hKalirin-7 was generated by PCR amplification of human KALRN-7 cDNA (F - GATGAT GATAAGAATATGACGGACCGC/R-TCGAGAGGCCAACTT AACTAAACGTAAGTTGG) and inserted into EcoR1-cut pCS2Flag backbone via ligation independent cloning (Takara Biosciences). The pCS2Flag-hKalirin-7-E1577K construct was generated via site directed mutagenesis, using Quikchange Lightning kit according to manufacturer's instruction (Agilent), using complementary probes of the sequence; GGAGTGGATCAAGAACATTCGAAAAGTGATTCAAGAAA GGATCATTCACC. pEYFP-NR1a and pEGFP-NR2B were gifts from Stefano Vicini (Addgene plasmids #17928, #17925). pAAV.Syn.GCaMP6f.WPRE.SV40 was a gift from Douglas Kim & GENIE Project (Addgene plasmid # 100837[1]; RRID:Addgene_100837). pEGFP-N2 and 1pmCherry-C1 plasmid was purchased from Clontech (Mountain View, CA, USA). pCS2FLAG was a gift from Peter Klein (Addgene plasmid # 16331[2]; RRID:Addgene_16331).

Primary neuron culture

Primary cortical cultures were prepared from E18 embryonic Sprague-Dawley rats. Cortices were dissected and homogenized, and cells were dissociated mechanically in papain solution (DNAseI, L-cysteine, EDTA). Cells were strained, counted and plated on poly-D-lysine (PDL) (Sigma-Aldrich) coated 1.5 mm thick, 180 mm diameter coverslips (0.25 μg/coverslip, 2 h) at 2,50,000–3,50,000 cells per coverslip. Neurons were maintained for 1 h in NeuralBasal medium (NBM) (Life Technologies) + 1% B27 (Gibco) + 0.5 mM glutamine + 5% fetal calf serum, before complete media change to growth media; NBM + 1% B27 + 0.5 mM glutamine + 1% Penicillin/Streptomycin. After 4 days in culture, 200 μM D-2-amino-5-phosphonovaleric acid (*D*-APV) was added to growth media. Following maintenance for 3 weeks *in vitro* (WIV), rat neurons were transfected using Lipofectamine 2,000 (Thermo Fisher Scientific) as per the manufacturer's instructions with indicated constructs.

Fixation and immunocytochemistry

Neurons were fixed in 3.7% formaldehyde, 4% sucrose in phosphate buffered saline (PBS) at room temperature for 10 min, and washed 3x in PBS at 4°C. For surface staining, anti-NR2B was added directly to live cells and incubated for 30 min before 3x PBS wash and fixation. Coverslips were permeabilized and blocked in PBS + 4% normal goat serum + 0.4% bovine serum albumin + 0.1% TritonX for 30 min, after which all steps were performed in PBS + 2% NGS. Coverslips were incubated with primary antibodies overnight at 4°C, washed 3 times and incubated with secondary antibodies for 1 h at room temperature. Antibodies were diluted in in PBS + 2% NGS. After washing, coverslips were mounted using Prolong Gold (Invitrogen). Antibodies used were against PSD95 (NeuroMab #75028), N2RB (NeuroMab #75-097), vGlut (Synaptic systems #135304) and Kalirin-7 (Penzes et al., 2000).

Co-immunoprecipitation

Human embryonic kidney 293 cells (Hek293 cells) were grown to confluency in dMEM + 10% FBS in 10 cm dishes. Transfection and co-immunoprecipitation were performed by adjusted protocol (based on Kiraly et al., 2011); Hek293 cells were transfected with Lipofectamine 2000 (Thermo Fisher Scientific), in a ratio of 1 NR1: 3 NR2B: 1.5 KALRN-7/E1577K, with a total amount of 10 μg DNA per 10 cm dish. After transfection, cells were lysed in lysis buffer (50 mM Tris, 100 mM NaCl, 0.1% TritonX100) + complete protease inhibitors (Sigma-Aldrich) by passage through a 28-gauge needle 8 times, followed by centrifugation at 10,000 rpm for 10 min. Equilibrated M2 Flag beads (Sigma) were added to Co-IP samples and incubated for binding overnight at 4°C. After, samples were pelleted and washed 3 times with lysis buffer. Bound proteins were eluted by boiling into Laemmli buffer (1X) for 5 min at 95°C, alongside input samples. Proteins were separated by SDS PAGE, immobilized on PVDF by Western blot, and visualized [Flag M2 (Sigma #F1804), NR2B (Novus Biologicals, #NB100-74475), Kalirin-spectrin (Sigma #02122)].

Imaging and analysis

Images for morphological dendrite analysis were acquired using a TI2 wide field microscope with CMOS detector (Nikon)

1 http://n2t.net/addgene:100837

2 http://n2t.net/addgene:16331

at a magnification of 40x (NA 1.00). Large field images were generated from 4 stitched images. Two microgram Z stack images were extracted and were used for the tracing of the arbor in Fiji. Axons were not traced and sholl analysis was performed at a radius of 10 μm on the dendritic arbor.

Images for spine analysis were acquired using a Nikon C2 confocal microscope with C2-DUS PMT detection, at 63× magnification (NA 1.40). Z stacks were acquired spanning the Z depth of the dendritic arbor. Approximately 100 μm of the secondary dendrite was traced for spine analyses. Deconvolution was performed using the deconvolute stack function (NIS elements). Surface NR2B quantification was performed by generating an ROI using GFP channel. This ROI was expanded by 0.5 microns and area measured for normalization purposes. NR2B signal outside of this ROI was cleared, threshold applied and "analyze puncta" was employed to detect puncta larger than 0.2 microns. The same threshold was employed for all images within matched replicates. The number of puncta detected was divided by total dendrite area to control for variation in dendrite area analyzed.

Live cell imaging was performed using a Nikon C2 confocal microscope with Zyla cMOS camera (Andor) at a magnification of 63× at 488 nm, 10 frames per second. For each cell a Z-stack was taken prior to GCAMP6 imaging, to allow tracing of dendritic spines labeled with mCherry cell-fill. Coverslips were transferred to artificial cerebrospinal fluid (aCSF containing in mM: NaCl 125, KCl 2.5, CaCl2 2, glucose 11, NaHCO3 26.2, NaH2PO4 1, HEPES 10, pH 7.4) supplemented with NBQX (5 μM) and TTX (500 nM) to inhibit AMPAr and sodium channels, respectively, allowing visualization of NMDAr-specific calcium influx. Analysis was performed by generating Z scored stacks in FIJI (average intensity *Z*-projection subtracted from each image in stack, and then divided by the standard deviation *Z*-projection) and regions of interest (ROI) were drawn over dendritic spines using the cell-fill red channel. ROI intensity was calculated at each frame and analyzed using custom MATLAB scripts. In brief, a rolling average was employed to reduce photobleaching effects and "find peaks" was employed with a 3x standard deviation filter to identify calcium events within spines. Kalirin-7 overexpression increased baseline noise (**Figure 5D**), irrespective of baseline fluorescence, suggestive of noise induced by enhanced surface expression (**Figure 4A**) and relieved magnesium block, resulting in spontaneous opening of NR2B. 3x standard deviation resulted in peak detection of only high amplitude peaks above noise, likely resulting from glutamate release. Spines with no events were omitted and averages per cell were generated based on the calcium event duration, frequency and amplitude.

Active-Rac1 pulldown assay

HEK-293T in 10 cm^2 plates were transfected with Kalirin-7 or E1577K (10 μg) using Lipofectamine 2000 (10 μL), as per manufacturers recommendation. 24 h after transfection, growth medium was replaced with serum-free DMEM for 4 h. Lysis and active Rac1 pulldown was achieved using Peirce Active-Rac1 pulldown kit as per manufacturers instruction; in brief, cells were lysed in 500 μL "lysis/pulldown" buffer with protease inhibitor. Nuclear material was removed by 15-min centrifugation at 15,000xG. Positive and negative samples were prepared by incubation with EDTA (10 mM) and GTP-γ-S (0.1 mM) and GDP (1 mM), respectively, for 30 min, 37°C, before addition of $MgCl_2$ (final concentration, 60 mM) to terminate loading. Glutathione Sepharose beads (50 μL slurry per sample), were washed 3x in "Lysis buffer" and coated with GST-PBD (7 μL per sample). Input samples were taken, and 450 μL lysate was applied to PBD-beads, and rotated gently for 1 h at 4°C. Beads were pelleted at 500xG, 30 s, homogenate removed, washed with 500 μL lysis buffer. This was repeated 3 times before addition of 20 μL 2x sample loading buffer, vigorous vortexing and elution of sample at 500xG for 1 min.

Statistical analyses

Data were analyzed by two-way ANOVA using GraphPad Prism 8 (GraphPad Software Inc.), followed by Tukey's multiple comparisons post-test for conditions with three independent variables. All experiments were subject to three biological replicates unless otherwise indicated, and cell numbers are indicated in figure legends. Statistical significance $p < 0.05$ (*), $p < 0.01$ (**), $p < 0.005$ (***) is indicated.

Results

E1577K mutation ablates Kalirin-7 mediated dendritic arborization

To assess the functional significance of E1577K mutation, overexpression of mCherry control, mCherry + Kalirin-7 and mCherry + Kalirin-7-E1577K (E1577K) was performed in primary rat cortical cultured neurons. Observations of Kalirin-7 activity have revealed strong alterations in dendritic arborization and spine density/morphology (Russell et al., 2014, 2018; Herring and Nicoll, 2016; Paskus et al., 2019; Grubisha et al., 2021). Neuronal morphology was assessed after 36 h overexpression, after cultures were fixed, stained and dendritic arbors traced (**Figure 2A**). Sholl analyses revealed a significant increase in proximal dendrite arborization following Kalirin-7 overexpression. However, Kalirin-7-E1577K failed to recapitulate these effects on neuroarchitecture, and arborization was unchanged relative to control neurons (**Figure 2B**). Overall dendritic length was found to be increased following overexpression of Kalirin-7 (2,387 μm ± 86.1 vs. 2,857 μm ± 188.6, $P = 0.044$), consistent with previous reports (Grubisha et al., 2021) and opposing the effects of Kalirin-7 knockdown

(Xie et al., 2010). E1577K failed to induce changes to dendritic outgrowth observed for Kalirin-7 (Figure 2C, 2,857 μm ± 188.6 vs. 2,376 μm ± 115.1, $p = 0.028$).

E1577K mutation blocks Kalirin-7 mediated dendritic spine formation, but not growth

Spine density and morphological changes have been observed to occur following overexpression of Kalirin-7 (Russell et al., 2014, 2018; Herring and Nicoll, 2016; Paskus et al., 2019; Grubisha et al., 2021). In order to characterize the functional effects on dendritic spine density and morphology, mCherry control, Kalirin-7 WT and E1577K constructs were transfected into cultured rat neurons and ∼100 μm sections of secondary dendrite were imaged for spine assessment (Figure 3A). Kalirin-7 WT produced a robust increase in spine density (0.57 spines/μm ±0.024 vs. 0.77 spines/μm ± 0.033, $P < 0.0001$). However, E1577K failed to induce this effect, with spine density indistinguishable from control conditions and significantly reduced as compared to Kalirin-7 overexpression

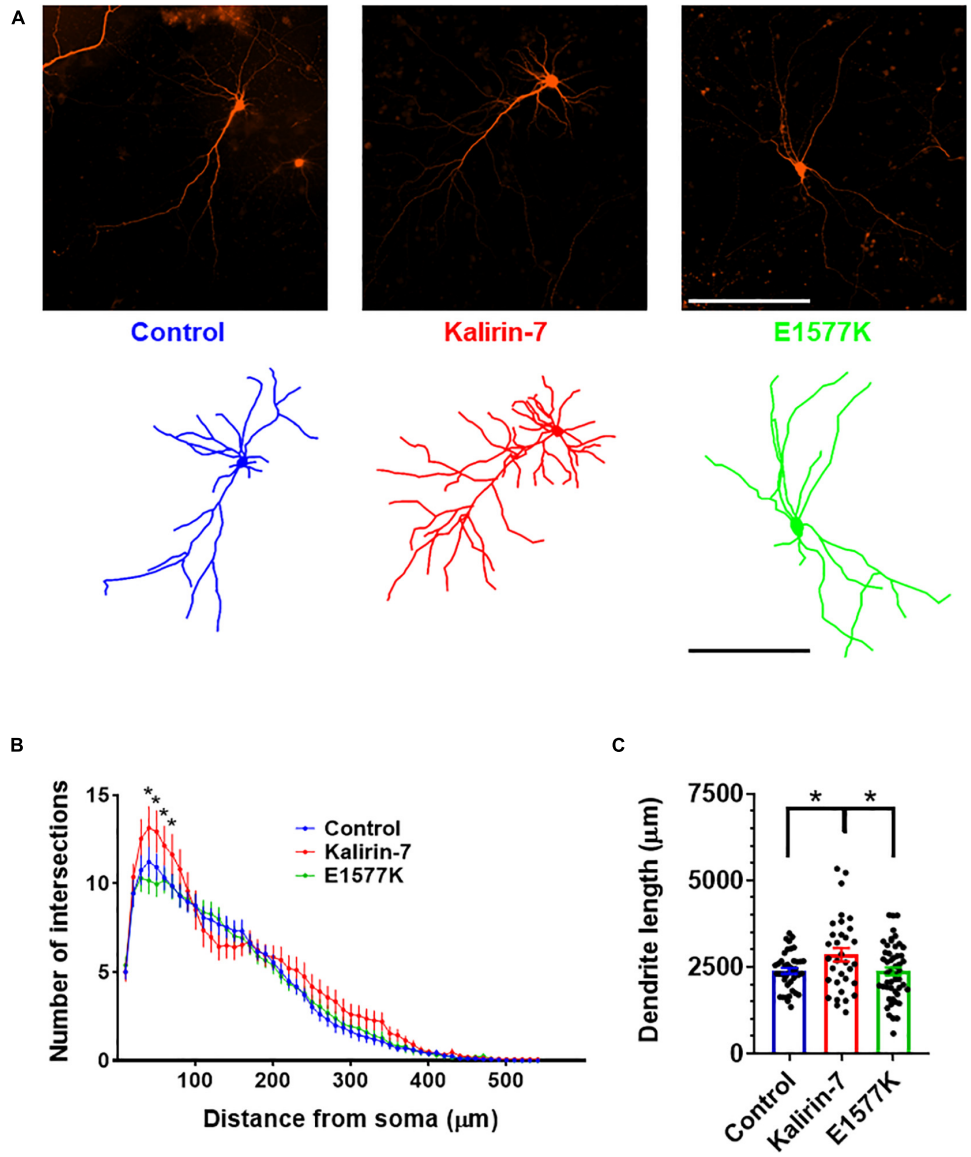

FIGURE 2
E1577K is deficient in driving dendritic arborization. **(A)** Representative images (Top) and dendritic traces of control (mCherry), Kalirin-7 and Kalirin-7-E1577K (E1577K) transfected rat cultured cortical neurons. Scale bar -200 μm. **(B)** Sholl analysis of dendritic arbors of indicated conditions. **(C)** Average total length of dendritic arbors of indicated conditions. Data points represent average ± SEM, *$p < 0.05$. $n = 10–15$ neurons per replicate, $N = 3$.

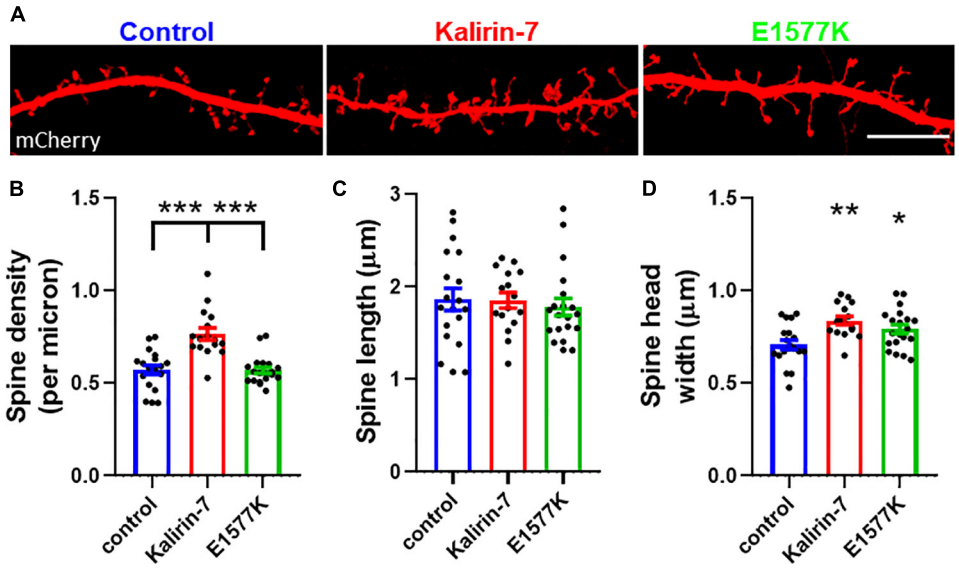

FIGURE 3
E1577K fails to drive spine formation, but increases spine size. **(A)** Representative regions of mCherry labeled secondary dendrites. Scale bar = 10 μm. **(B)** quantification of spine density per micron of secondary dendrite. Quantification of spine length **(C)** and head width **(D)** per neuron. Data points represent average ± SEM, *$p < 0.05$. **$p < 0.01$. ***$p < 0.005$. n = 5–8 neurons per replicate, N = 3.

(Figure 3B, 0.77 spines/μm ± 0.033 vs. 0.57 spines/μm ± 0.017, $P < 0.0001$). Neither Kalirin-7 nor E1577K altered dendritic spine length (Figure 3C), however Kalirin-7 overexpression induced a robust alteration in dendritic spine width (0.71 μm ± 0.025 vs. 0.84 μm ± 0.022 microns, $P = 0.0014$) supporting the development of larger, more mature spines. Interestingly, E1577K recapitulated this effect, producing a significant increase in dendritic spine width compared to control (Figure 3D, 0.71 μm ± 0.025 vs. 0.79 μm ± 0.024, $P = 0.037$). Together these results demonstrate that E1577K is unable to drive spinogenesis but retains functionality in driving spine maturation.

E1577K mutation blocks Kalirin-7 mediated NMDAr surface trafficking

Kalirin-7 has been found to directly interact with and regulate the surface expression of NMDAr receptors, via the NR2B subunit (Kiraly et al., 2011; Lemtiri-Chlieh et al., 2011). As E1577K lies within the PH domain that was found to be the site of NR2B interaction (Kiraly et al., 2011), we set out to assess the effect of Kalirin-7 and E1577K on NR2B trafficking. Neurons were transfected with Kalirin-7 and E1577K, and surface expression of the NR2B receptor was validated (Supplementary Figure 3) and assessed (Figure 4A). Interestingly, Kalirin-7 overexpression resulted in a dramatic increase in the number (Figure 4B, normalized puncta number—0.088 ± 0.13 vs. 0.228 ± 0.21, $P < 0.0001$) and size (Figure 4C, normalized puncta size—0.455 ± 0.028 vs. 0.645 ± 0.061, $P = 0.0213$) of NR2B puncta within transfected neurons, although average NR2B puncta intensity was unchanged (Figure 4D). E1577K expression failed to recapitulate these effects and puncta number and size were significantly reduced compared to Kalirin-7 (normalized puncta number—0.228 ± 0.21 vs. 0.138 ± 0.016, $P = 0.0018$. Average puncta area—0.645 ± 0.061 vs. 0.479 ± 0.037, $P = 0.0309$). No significant difference was observed between control and E1577K for either parameter.

These results suggest that Kalirin-7, but not E1577K, can drive surface expression of NR2B. In order to assess whether this alteration in NR2B trafficking was due to altered localization of mutant Kalirin-7, neurons were stained for total NR2B and Kalirin-7 to assess their subcellular distribution. Both Kalirin-7 and E1577K proteins were found to localize to dendritic spines, colocalizing with PSD95 and with NR2B (Figure 4E), and juxtaposed vGlut (Supplementary Figure 1). These results suggest that both Kalirin-7 and E1577K are directed to the dendritic spine, though E1577K is robustly impaired in its ability to direct NR2B to the surface.

E1577K mutation blocks Kalirin-7 mediated NMDAr potentiation

In order to prove the functional implications of enhanced NR2B surface expression, we set out to image NMDAr channel activity following overexpression of mCherry control, Kalirin-7-WT and E1577K. Primary cortical neurons were cotransfected with mCherry, GcamP6 (Chen et al., 2013) and either Kalirin-7

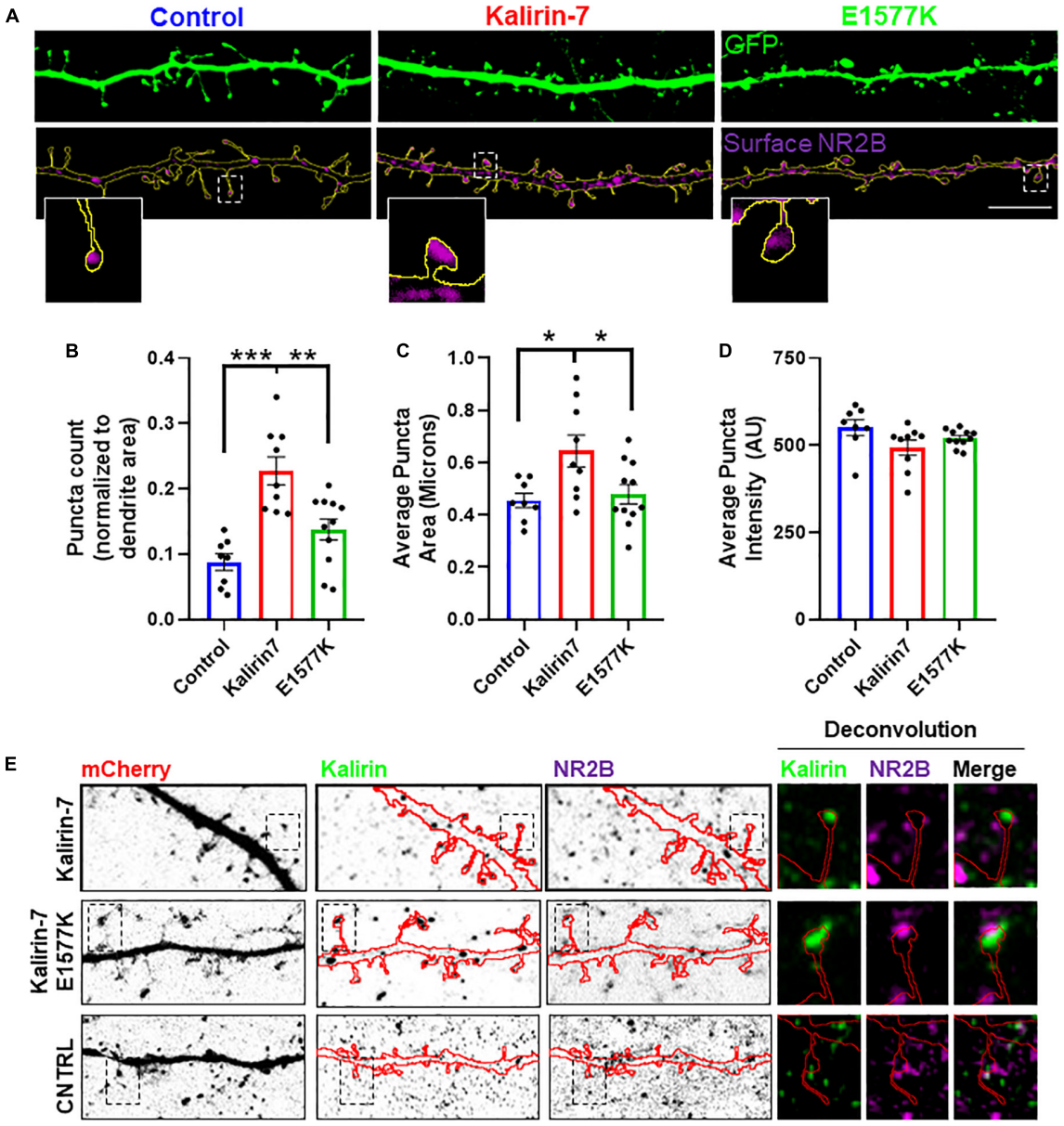

FIGURE 4
E1577K impairs surface expression of NR2B. **(A)** Representative regions of secondary dendrites with GFP-cell fill and NR2B surface stain. Insets show a single spine from each condition. Scale bar -10 μm. **(B)** Number of NR2B surface puncta normalized to total dendrite (GFP) area measured. **(C)** Average surface NR2B puncta size. **(D)** Average intensity of NR2B surface puncta. *N* = 2, 5 cells per replicate. **(E)** Regions of dendrites stained with Kalirin-7 and total NR2B to assess colocalization following overexpression of indicated constructs. Deconvoluted insets indicate Kalirin-7 and NR2B puncta adjacent within indicated spines. *$p < 0.05$. **$p < 0.01$. ***$p < 0.005$.

or E1577K mutant constructs. Neurons were transferred to artificial cerebrospinal fluid (aCSF) containing NBQX and TTX to inhibit AMPAr and sodium channels, respectively. Thus calcium entry is blocked through calcium-permeable AMPAr, and depolarization is inhibited, blocking calcium entry through voltage gated calcium channels. Together these interventions facilitate the observation of calcium events mediated by NMDAr (**Supplementary Videos 1–3**). In addition, magnesium was retracted, allowing NMDAr calcium influx independently of depolarization (**Figure 5A**). ROIs were drawn over individual spines using the mCherry channel, and Z-scored GcamP6 signal was measured at each frame within the ROI, as previously reported (Walker et al., 2017; **Figure 5B**). Importantly, neuronal activity was blocked completely with *D*-APV (**Supplementary Figures 2A,B**) and application of NMDA resulted in a robust influx of calcium

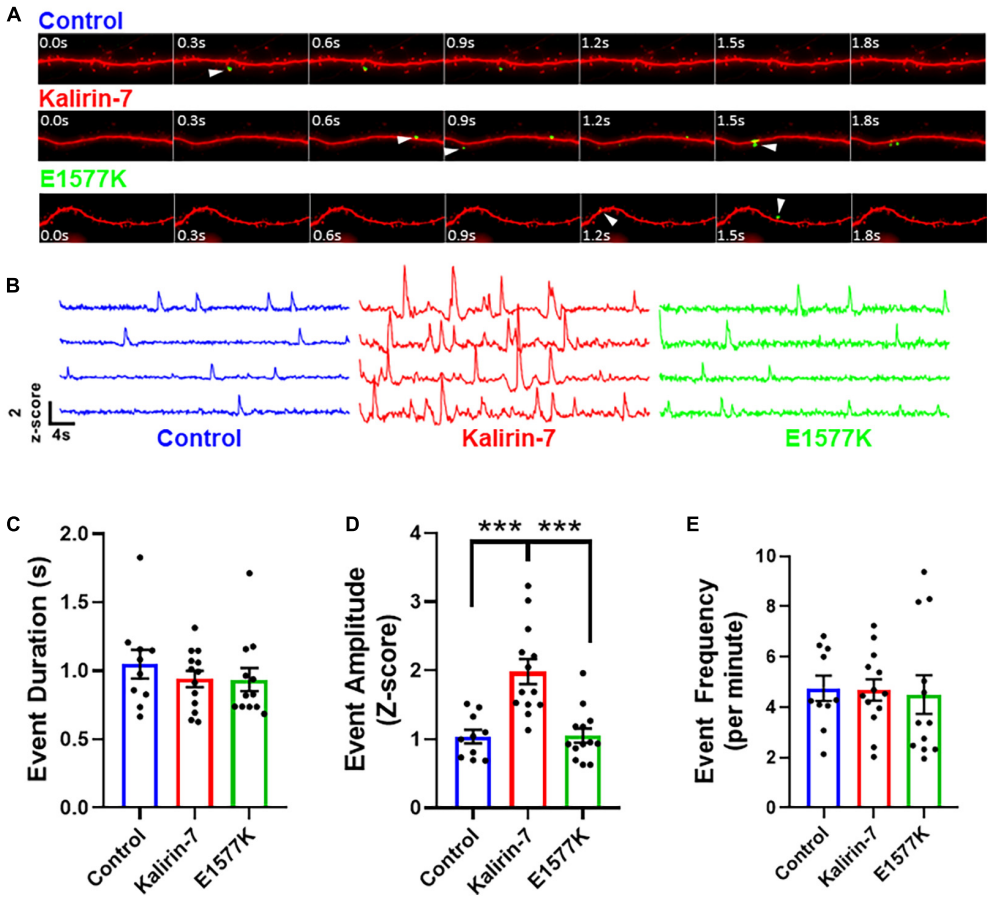

FIGURE 5
E1577K fails to drive NMDAr-dependent calcium influx. **(A)** 4 s time course of GCamP6 Z-scored live imaging of dendrite with mCherry cell fill (red). Calcium events within spines (white arrowhead) indicate calcium entry through NMDAr channels for each indicated overexpression condition. **(B)** Representative GCamP6 Z-score traces of individual dendrite spines under each overexpression condition (control—blue, Kalirin-7—red, E1577K—green). Quantification of duration **(C)**, amplitude **(D)** and frequency **(E)** of GcamP6 events per individual spine, averaged per cell over 1 min imaging (n = 3–4 neurons per replicate, N = 3). ***$p < 0.005$.

(Supplementary Figures 2C,D), confirming that NMDAr channel activity specifically was observed. Overexpression of Kalirin-7 and E1577K had no effect on the duration of calcium influx events (Figure 5C), however, Kalirin-7 had a robust effect on the amplitude of NMDAr calcium events (Figure 5B, Z-score amplitude—1.037 ± 0.099 vs. 1.983 ± 0.181, $P = 0.0001$) supporting increased NMDAr content within spines, consistent with surface staining (Figure 4). Despite colocalization with NR2B within dendritic spines, E1577K failed to recapitulate this enhancement with NMDAr event amplitude significantly reduced as compared to Kalirin-7 (Z-score amplitude—1.983 ± 0.181 vs. 1.052 ± 0.103, $P = < 0.0001$). No alteration in calcium event frequency was observed for either Kalirin-7 or E1577K overexpression conditions (Figure 5E) as expected, as presynaptic release probability is unlikely to be altered following post-synaptic alterations in Kalirin-7 signaling. These results indicate that Kalirin-7 drives NMDAr surface expression at excitatory synapses to promote their activity within dendritic spines, and that E1577K mutation blocks these effects. Importantly, impaired NMDAr content and activity during neurodevelopment may play a powerful role in the presentation of developmental delay in the affected patient by impairing NMDAr-mediated synaptic plasticity.

Mutation at E1577 ablates Rac1-GEF catalytic activity

E1577K failed to recapitulate the effects of Kalirin-7 on dendritic arborization, spinogenesis and NMDAr activity within dendritic spines. Kalirin-7 is known to directly interact with NR2B, providing a potential mechanism underlying the observed deficit in E1577K-mediated NMDAr trafficking and activity. We therefore set out to assess the interaction strength between Kalirin-7/E1577K by heterologous co-immunoprecipitation. HEK293T were co-transfected with

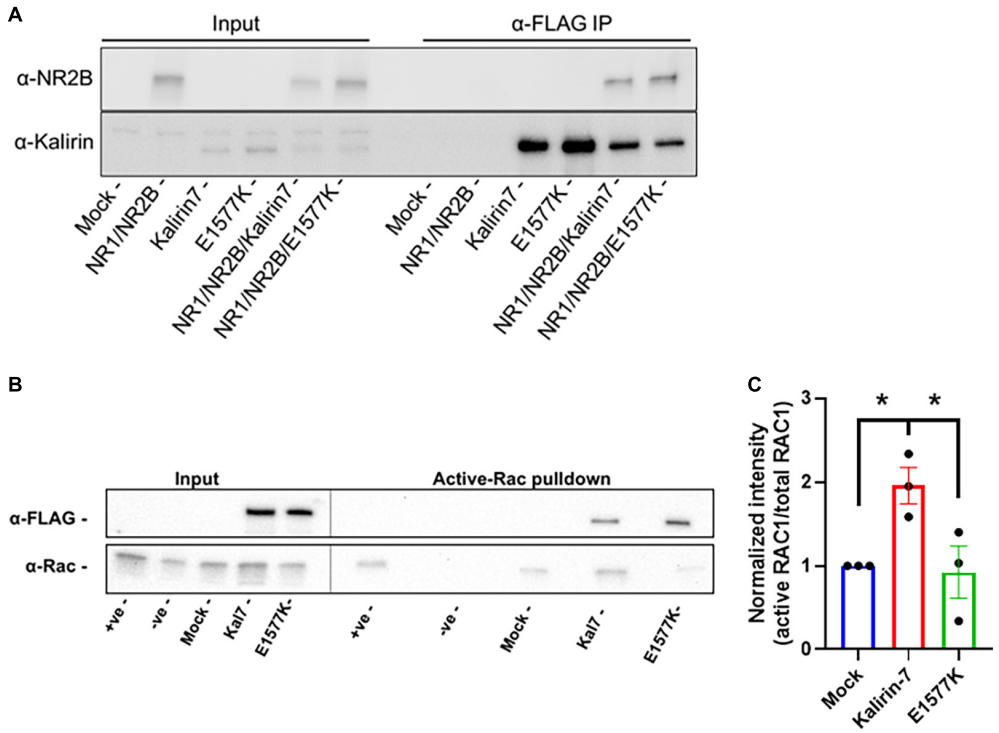

FIGURE 6
E1577K shows impaired Rac1-GEF activity. **(A)** Western Blot of anti-FLAG pulldown of Kalirin-7 and E1577K from HEK293T, with co-immunoprecipitation of transfected NR2B (Mock = non-transfected). **(B)** HEK293T cells were transfected with the indicated conditions and active-Rac1 was pulled down from lysates with PAK-PBD coated Sepharose beads. Positive (+ ve) and Negative (-ve) samples indicate Mock transfected lysates Loaded with GTP-γ-S and GDP, respectively. Blots were probed with anti-FLAG and anti-Rac1. **(C)** Quantification of Active-RAC1 pulldown under the indicated conditions. *$p < 0.05$.

YFP-NR1, GFP-NR2B (Luo et al., 2002) and either Kalirin-7 or E1577K and anti-FLAG pulldown targeting Kalirin-7 recapitulated previous reports of direct Kalirin-7 interaction with NR2B (**Figure 6A**). The interaction with NR2B was not affected by E1577K mutation, suggesting that other mechanisms may underly the observed deficits in NMDAr trafficking and activity imparted by E1577K mutation. The location of E1577 is distal to the catalytic site (**Figure 1**) but within the overall catalytic DH-PH domain. Therefore, we hypothesized that E1577K mutation may impair catalytic activity. We therefore assessed Kalirin-7 and E1577K Rac1-GEF activity by heterologous active-Rac1 pulldown. HEK293T were transfected with GFP control, Kalirin-7 and E1577K, before serum starvation and lysis. Active-Rac1 was pulled down with PAK-PBD conjugated to GST-sepharose beads, alongside positive and negative controls (mock transfected cells incubated with GDP or the non-hydrolysable GTP analog, GTP-γ-S, see materials and methods). Kalirin-7 induced a robust increase in the levels of active Rac1 as compared to mock transfection (**Figures 6B,C**, + 95.8% ± 22%, $P = 0.0485$). However, E1577K failed to raise active-Rac1 levels above baseline, and showed significantly decreased Rac1 activation compared to that of Kalirin-7 WT (-103% ± 31%, $P = 0.361\%$), indicating that E1577K is catalytically inactive. Thus, loss of Rac1-GEF activity is impairs the ability of Kalirin-7 to drive NMDAr surface expression and activity, likely contributing to the patient's observed developmental delay.

Discussion

The KALRN gene has been linked to neurodevelopmental disorder risk, with mutations in KALRN implicated in schizophrenia (Kushima et al., 2012; Purcell et al., 2014; Russell et al., 2014, 2018; Howrigan et al., 2020), ASD (Leblond et al., 2019; Satterstrom et al., 2020), developmental delay (Deciphering Developmental Disorders Study, 2017), and intellectual disability linked to hereditary homozygous loss of KALRN-expression (Makrythanasis et al., 2016). Here we show that a single point mutation within the Rac1-GEF PH domain of KALRN, found in a patient with developmental delay, results in loss of catalytic activity. Indeed, although Kalirin-7 was able to drive dendritic arborization/growth, spine formation, NMDAr surface expression and activity as previously reported (Penzes et al., 2001a,b; Xie et al., 2007; Lemtiri-Chlieh et al., 2011; Russell et al., 2014; Herring and Nicoll, 2016), the E1577K mutant was

deficient in all these functional outcomes of Rac1-GEF activity. These results suggest that Kalirin-7 GEF activity is required for the trafficking and surface expression of NMDAr. It is therefore likely that loss of Kalirin-7 GEF activity in patients harboring the E1577K mutation is a contributing factor to impaired neurodevelopment. Indeed, impaired surface expression and NMDAr activity is likely to have profound impact on activity-dependent synaptic plasticity, supporting KALRN expression and activity as vital to normal neurodevelopment.

Interestingly, the E1577K mutant retained the ability to drive spine morphological changes, with overexpression of the mutant resulting in an increase in spine size similar to wild type. This observation is consistent with loss of Rac1-GEF activity, as the N-terminal region of Kalirin was found to drive spine size increases following truncation of the Rac1-GEF domain (Ma et al., 2014), likely by acting as a scaffold for post-synaptic density and cell adhesion molecules, such as Neuroligan-1 (Paskus et al., 2019).

The observation of a point mutation in the auxiliary PH domain blocking GEF activity supports a role for the auxiliary PH domain in DH-mediated Rac1-GEF activity, as previously reported for related GEF proteins (Liu et al., 1998; Das et al., 2000). Interestingly, phosphorylation at T1590 by CDK5, proximal to the E1577 mutation site, has been shown to drive NMDAr to dendritic spines (Li et al., 2019), suggesting that this region of Kalirin-7 is involved in the regulation NMDAr surface expression. It is tempting to hypothesize that T1590 phosphorylation may act as a regulatory switch, altering Rac1-GEF activity essential to the normal trafficking of NMDAr to the membrane. E1577K, imparting a net negative to positive charge opposite to phosphorylation, may result in an abrogation or blockade of this regulatory mechanism, resulting in the observed lack of GEF activity. Together, these results suggest that mutations with the Rac1-GEF domain of Kalirin likely contribute to developmental delay via impairment of dendritic arborization, dendritic spine formation, NMDAr surface expression and activity.

Data availability statement

The original contributions presented in this study are included in the article/**Supplementary material**, further inquiries can be directed to the corresponding author.

Author contributions

EP and RV wrote the manuscript and carried out all experiments. EP devised the project. MM-d-S, DL, and MD assisted with experimental procedures and analysis. PP oversaw and funded the project. All authors contributed to the article and approved the submitted version.

Funding

This work was funded by NIH-NIMH-5R01MH071316-15 and NIMH-2R56MH071316-16 awarded to PP.

Conflict of interest

The authors declare that the research was conducted in the absence of any commercial or financial relationships that could be construed as a potential conflict of interest.

Publisher's note

Supplementary material

The Supplementary Material for this article can be found online at: https://www.frontiersin.org/articles/10.3389/fnmol.2022.994513/full#supplementary-material

SUPPLEMENTARY FIGURE 1
Kalirin-7 and E1577K localize to PSD-95/V-Glut positive synaptic sites within dendritic spines. Scale bar = 2 μm.

SUPPLEMENTARY FIGURE 2
D-APV and NMDA block and induce GCamP6 signaling, respectively. **(A)** Standard deviation Z-projections of 30 seconds before and after D-APV (100 μM) application. Spines showing variation associated with calcium influx are indicated (arrowhead). **(B)** Representative dendritic spine Z-scored traces of calcium events before and after application of D-APV (arrowhead) indicate all calcium events are blocked by NMDAr inhibition. **(C)** 1.5 second timecourse of GCamP6 imaging after application of NMDA (100 μM). **(D)** Representative GCamp6 Z-score traces of individual spine ROIs with application of NMDA (arrowhead). Scale bars = 50 μm.

SUPPLEMENTARY FIGURE 3
NR2B surface stain validation. Neurons were transfected with GFP-NR2B and surface stained with anti-NR2B. Overlap indicates surface GFP-NR2B. Scale bar = 10 μm.

SUPPLEMENTARY VIDEO 1
Representative videos of GCamP6 spine minis. Z-scored signal (green) with cell fill (red), after transfection with mCherry control.

SUPPLEMENTARY VIDEO 2
Representative videos of GCamP6 spine minis. Z-scored signal (green) with cell fill (red), after transfection with Kalirin-7.

SUPPLEMENTARY VIDEO 3
Representative videos of GCamP6 spine minis. Z-scored signal (green) with cell fill (red), after transfection with E1577K.

References

Alvarez, V. A., and Sabatini, B. L. (2007). Anatomical and physiological plasticity of dendritic spines. *Annu. Rev. Neurosci.* 30, 79–97. doi: 10.1146/annurev.neuro.30.051606.094222

Bai, Y., Xiang, X., Liang, C., and Shi, L. (2015). Regulating Rac in the nervous system: Molecular function and disease implication of Rac GEFs and GAPs. *Biomed Res. Int.* 2015:632450. doi: 10.1155/2015/632450

Bandekar, S. J., Arang, N., Tully, E. S., Tang, B. A., Barton, B. L., Li, S., et al. (2019). Structure of the C-terminal guanine nucleotide exchange factor module of Trio in an autoinhibited conformation reveals its oncogenic potential. *Sci. Signal.* 12:eaav2449. doi: 10.1126/scisignal.aav2449

Carlisle, H. J., and Kennedy, M. B. (2005). Spine architecture and synaptic plasticity. *Trends Neurosci.* 28, 182–187. doi: 10.1016/j.tins.2005.01.008

Chakrabarti, K., Lin, R., Schiller, N. I., Wang, Y., Koubi, D., Fan, Y. X., et al. (2005). Critical role for Kalirin in nerve growth factor signaling through TrkA. *Mol. Cell. Biol.* 25, 5106–5118. doi: 10.1128/MCB.25.12.5106-5118.2005

Chen, T. W., Wardill, T. J., Sun, Y., Pulver, S. R., Renninger, S. L., Baohan, A., et al. (2013). Ultrasensitive fluorescent proteins for imaging neuronal activity. *Nature* 499, 295–300. doi: 10.1038/nature12354

Chhatriwala, M. K., Betts, L., Worthylake, D. K., and Sondek, J. (2007). The DH and PH domains of Trio coordinately engage Rho GTPases for their efficient activation. *J. Mol. Biol.* 368, 1307–1320. doi: 10.1016/j.jmb.2007.02.060

Das, B., Shu, X., Day, G. J., Han, J., Krishna, U. M., Falck, J. R., et al. (2000). Control of intramolecular interactions between the pleckstrin homology and Dbl homology domains of Vav and Sos1 regulates Rac binding. *J. Biol. Chem.* 275, 15074–15081. doi: 10.1074/jbc.M907269199

Deciphering Developmental Disorders Study (2017). Prevalence and architecture of de novo mutations in developmental disorders. *Nature* 542, 433–438. doi: 10.1038/nature21062

Forrest, M. P., Parnell, E., and Penzes, P. (2018). Dendritic structural plasticity and neuropsychiatric disease. *Nat. Rev. Neurosci.* 19, 215–234. doi: 10.1038/nrn.2018.16

Grubisha, M. J., Sun, T., Eisenman, L., Erickson, S. L., Chou, S. Y., Helmer, C. D., et al. (2021). A Kalirin missense mutation enhances dendritic RhoA signaling and leads to regression of cortical dendritic arbors across development. *Proc. Natl. Acad. Sci. U.S.A.* 118:e2022546118. doi: 10.1073/pnas.2022546118

Harris, K. M. (1999). Structure, development, and plasticity of dendritic spines. *Curr. Opin. Neurobiol.* 9, 343–348. doi: 10.1016/S0959-4388(99)80050-6

Harris, K. M., and Kater, S. B. (1994). Dendritic spines: Cellular specializations imparting both stability and flexibility to synaptic function. *Annu. Rev. Neurosci.* 17, 341–371. doi: 10.1146/annurev.ne.17.030194.002013

Hausser, M., Spruston, N., and Stuart, G. J. (2000). Diversity and dynamics of dendritic signaling. *Science* 290, 739–744. doi: 10.1126/science.290.5492.739

Herring, B. E., and Nicoll, R. A. (2016). Kalirin and Trio proteins serve critical roles in excitatory synaptic transmission and LTP. *Proc. Natl. Acad. Sci. U.S.A.* 113, 2264–2269. doi: 10.1073/pnas.1600179113

Howrigan, D. P., Rose, S. A., Samocha, K. E., Fromer, M., Cerrato, F., Chen, W. J., et al. (2020). Exome sequencing in schizophrenia-affected parent-offspring trios reveals risk conferred by protein-coding de novo mutations. *Nat. Neurosci.* 23, 185–193. doi: 10.1038/s41593-019-0564-3

Jaffe, A. B., and Hall, A. (2005). Rho GTPases: Biochemistry and biology. *Annu. Rev. Cell Dev. Biol.* 21, 247–269. doi: 10.1146/annurev.cellbio.21.020604.150721

Johnson, R. C., Penzes, P., Eipper, B. A., and Mains, R. E. (2000). Isoforms of kalirin, a neuronal Dbl family member, generated through use of different 5'- and 3'-ends along with an internal translational initiation site. *J. Biol. Chem.* 275, 19324–19333. doi: 10.1074/jbc.M000676200

Kiraly, D. D., Lemtiri-Chlieh, F., Levine, E. S., Mains, R. E., and Eipper, B. A. (2011). Kalirin binds the NR2B subunit of the NMDA receptor, altering its synaptic localization and function. *J. Neurosci.* 31, 12554–12565. doi: 10.1523/JNEUROSCI.3143-11.2011

Kushima, I., Nakamura, Y., Aleksic, B., Ikeda, M., Ito, Y., Shiino, T., et al. (2012). Resequencing and association analysis of the KALRN and EPHB1 genes and their contribution to schizophrenia susceptibility. *Schizophr. Bull.* 38, 552–560. doi: 10.1093/schbul/sbq118

Leblond, C. S., Cliquet, F., Carton, C., Huguet, G., Mathieu, A., Kergrohen, T., et al. (2019). Both rare and common genetic variants contribute to autism in the Faroe Islands. *NPJ Genom. Med.* 4:1. doi: 10.1038/s41525-018-0075-2

Lemtiri-Chlieh, F., Zhao, L., Kiraly, D. D., Eipper, B. A., Mains, R. E., and Levine, E. S. (2011). Kalirin-7 is necessary for normal NMDA receptor-dependent synaptic plasticity. *BMC Neurosci.* 12:126. doi: 10.1186/1471-2202-12-126

Li, M. X., Qiao, H., Zhang, M., and Ma, X. M. (2019). Role of Cdk5 in Kalirin7-mediated formation of dendritic spines. *Neurochem. Res.* 44, 1243–1251. doi: 10.1007/s11064-019-02771-y

Liu, X., Wang, H., Eberstadt, M., Schnuchel, A., Olejniczak, E. T., Meadows, R. P., et al. (1998). NMR structure and mutagenesis of the N-terminal Dbl homology domain of the nucleotide exchange factor Trio. *Cell* 95, 269–277. doi: 10.1016/S0092-8674(00)81757-2

Luo, J. H., Fu, Z. Y., Losi, G., Kim, B. G., Prybylowski, K., Vissel, B., et al. (2002). Functional expression of distinct NMDA channel subunits tagged with green fluorescent protein in hippocampal neurons in culture. *Neuropharmacology* 42, 306–318. doi: 10.1016/S0028-3908(01)00188-5

Ma, X. M., Kiraly, D. D., Gaier, E. D., Wang, Y., Kim, E. J., Levine, E. S., et al. (2008). Kalirin-7 is required for synaptic structure and function. *J. Neurosci.* 28, 12368–12382. doi: 10.1523/JNEUROSCI.4269-08.2008

Ma, X. M., Miller, M. B., Vishwanatha, K. S., Gross, M. J., Wang, Y., Abbott, T., et al. (2014). Nonenzymatic domains of Kalirin7 contribute to spine morphogenesis through interactions with phosphoinositides and Abl. *Mol. Biol. Cell.* 25, 1458–1471. doi: 10.1091/mbc.e13-04-0215

Makrythanasis, P., Guipponi, M., Santoni, F. A., Zaki, M., Issa, M. Y., Ansar, M., et al. (2016). Exome sequencing discloses KALRN homozygous variant as likely cause of intellectual disability and short stature in a consanguineous pedigree. *Hum. Genomics.* 10:26. doi: 10.1186/s40246-016-0082-2

Nakayama, A. Y., Harms, M. B., and Luo, L. (2000). Small GTPases Rac and Rho in the maintenance of dendritic spines and branches in hippocampal pyramidal neurons. *J. Neurosci.* 20, 5329–5338. doi: 10.1523/JNEUROSCI.20-14-05329.2000

Parnell, E., Shapiro, L. P., Voorn, R. A., Forrest, M. P., Jalloul, H. A., Loizzo, D. D., et al. (2021). KALRN: A central regulator of synaptic function and synaptopathies. *Gene* 768:145306. doi: 10.1016/j.gene.2020.145306

Paskus, J. D., Tian, C., Fingleton, E., Shen, C., Chen, X., Li, Y., et al. (2019). Synaptic Kalirin-7 and Trio Interactomes reveal a GEF protein-dependent neuroligin-1 mechanism of action. *Cell Rep.* 29, 2944–2952.e5. doi: 10.1016/j.celrep.2019.10.115

Penzes, P., and Remmers, C. (2012). Kalirin signaling: Implications for synaptic pathology. *Mol. Neurobiol.* 45, 109–118. doi: 10.1007/s12035-011-8223-z

Penzes, P., Johnson, R. C., Alam, M. R., Kambampati, V., Mains, R. E., and Eipper, B. A. (2000). An isoform of kalirin, a brain-specific GDP/GTP exchange factor, is enriched in the postsynaptic density fraction. *J. Biol. Chem.* 275, 6395–6403. doi: 10.1074/jbc.275.9.6395

Penzes, P., Johnson, R. C., Kambampati, V., Mains, R. E., and Eipper, B. A. (2001a). Distinct roles for the two Rho GDP/GTP exchange factor domains of Kalirin in regulation of neurite growth and neuronal morphology. *J. Neurosci.* 21, 8426–8434. doi: 10.1523/JNEUROSCI.21-21-08426.2001

Penzes, P., Johnson, R. C., Sattler, R., Zhang, X., Huganir, R. L., Kambampati, V., et al. (2001b). The neuronal Rho-GEF Kalirin-7 interacts with PDZ domain-containing proteins and regulates dendritic morphogenesis. *Neuron* 29, 229–242. doi: 10.1016/S0896-6273(01)00193-3

Purcell, S. M., Moran, J. L., Fromer, M., Ruderfer, D., Solovieff, N., Roussos, P., et al. (2014). A polygenic burden of rare disruptive mutations in schizophrenia. *Nature* 506, 185–190. doi: 10.1038/nature12975

Rossman, K. L., Der, C. J., and Sondek, J. (2005). GEF means go: Turning on Rho GTPases with guanine nucleotide-exchange factors. *Nat. Rev. Mol. Cell Bio.* 6, 167–180. doi: 10.1038/nrm1587

Russell, T. A., Blizinsky, K. D., Cobia, D. J., Cahill, M. E., Xie, Z., Sweet, R. A., et al. (2014). A sequence variant in human KALRN impairs protein function and coincides with reduced cortical thickness. *Nat. Commun.* 5:4858. doi: 10.1038/ncomms5858

Russell, T. A., Grubisha, M. J., Remmers, C. L., Kang, S. K., Forrest, M. P., Smith, K. R., et al. (2018). A schizophrenia-linked KALRN coding variant alters neuron morphology, protein function, and transcript stability. *Biol. Psychiatry* 83, 499–508. doi: 10.1016/j.biopsych.2017.10.024

Satterstrom, F. K., Kosmicki, J. A., Wang, J., Breen, M. S., De Rubeis, S., An, J. Y., et al. (2020). Large-scale exome sequencing study implicates both developmental and functional changes in the neurobiology of autism. *Cell* 180, 568–584.e23. doi: 10.1016/j.cell.2019.12.036

Tada, T., and Sheng, M. (2006). Molecular mechanisms of dendritic spine morphogenesis. *Curr. Opin. Neurobiol.* 16, 95–101. doi: 10.1016/j.conb.2005.12.001

Threadgill, R., Bobb, K., and Ghosh, A. (1997). Regulation of dendritic growth and remodeling by Rho, Rac, and Cdc42. *Neuron* 19, 625–634. doi: 10.1016/S0896-6273(00)80376-1

Tolias, K. F., Duman, J. G., and Um, K. (2011). Control of synapse development and plasticity by Rho GTPase regulatory proteins. *Prog. Neurobiol.* 94, 133–148.

Walker, A. S., Neves, G., Grillo, F., Jackson, R. E., Rigby, M., O'Donnell, C., et al. (2017). Distance-dependent gradient in NMDAR-driven spine calcium signals along tapering dendrites. *Proc. Natl. Acad. Sci. U.S.A.* 114, E1986–E1995. doi: 10.1073/pnas.1607462114

Webb, B., and Sali, A. (2021). Protein structure modeling with MODELLER. *Methods Mol. Biol.* 2199, 239–255. doi: 10.1007/978-1-0716-0892-0_14

Xie, Z., Cahill, M. E., and Penzes, P. (2010). Kalirin loss results in cortical morphological alterations. *Mol. Cell. Neurosci.* 43, 81–89. doi: 10.1016/j.mcn.2009.09.006

Xie, Z., Srivastava, D. P., Photowala, H., Kai, L., Cahill, M. E., Woolfrey, K. M., et al. (2007). Kalirin-7 controls activity-dependent structural and functional plasticity of dendritic spines. *Neuron* 56, 640–656.doi: 10.1016/j.neuron.2007.10.005

Yuste, R., and Bonhoeffer, T. (2001). Morphological changes in dendritic spines associated with long-term synaptic plasticity. *Annu. Rev. Neurosci.* 24, 1071–1089. doi: 10.1146/annurev.neuro.24.1.1071

Frontiers in
Molecular Neuroscience

Leading research into the brain's molecular structure, design and function

Part of the most cited neuroscience series, this journal explores and identifies key molecules underlying the structure, design and function of the brain across all levels.

Discover the latest Research Topics

See more →

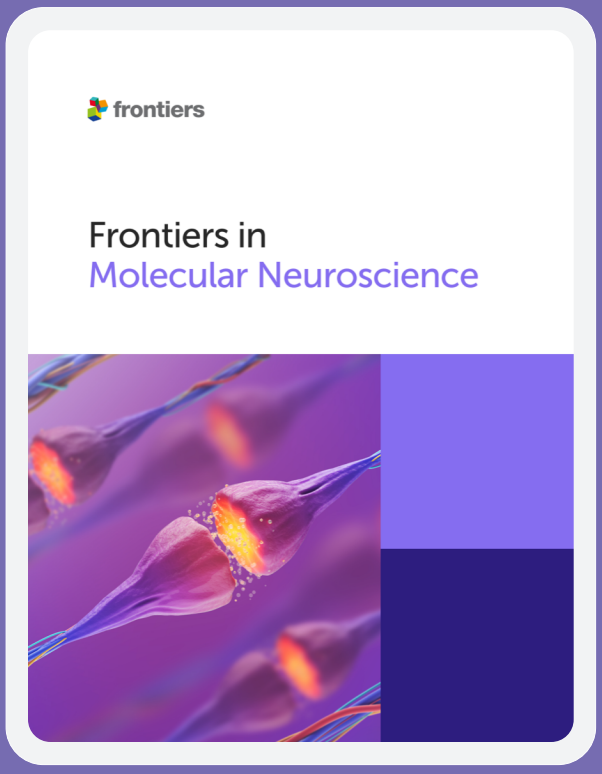

Frontiers

Avenue du Tribunal-Fédéral 34
1005 Lausanne, Switzerland
frontiersin.org

Contact us

+41 (0)21 510 17 00
frontiersin.org/about/contact